

# Dissertation

## Structure, thermodynamics and phase behavior of a polydisperse colloidal mixture

ausgeführt zum Zwecke der Erlangung des akademischen  
Grades eines Doktors der technischen Wissenschaften unter der Leitung  
von

Univ.Doz. Ass.Prof. Dipl.-Ing. Dr. Gerhard Kahl  
Institut für theoretische Physik

eingereicht an der technischen Universität Wien  
Fakultät für technische Naturwissenschaften und Informatik

von  
Dipl.-Ing. Sabine Leroch  
9226250  
Bendlgasse 24/3, 1120 Wien

August 4, 2005

---



## Zusammenfassung

In dieser Arbeit haben wir die thermodynamischen Eigenschaften und das Phasenverhalten einfacher polydisperser Flüssigkeiten untersucht, wobei wir uns hierbei nur auf die fluide Phase beschränken. Wir haben polydisperse Flüssigkeiten als  $n$ -Komponenten Mischung im Grenzwert  $n \rightarrow \infty$  betrachtet in dem die Teilchendurchmesser kontinuierlich in einem Bereich  $[\sigma_{min}, \sigma_{max}]$  variieren und die Konzentrationen der Teilchenarten durch eine kontinuierliche Verteilungsfunktion  $f(\sigma)$  ersetzt werden. Die Teilchen wechselwirken über effektive Paar-Potentiale, deren repulsiver Anteil aus einer hard sphere Wechselwirkung besteht und die anziehenden Anteile in einem Fall durch ein square-well und im zweiten Fall durch ein Yukawa Potential gegeben sind, zusätzlich haben wir eine van der Waals Flüssigkeit untersucht.

Um die Ornstein Zernike Gleichungen zu lösen, haben wir eine thermodynamische Störungstheorie - die optimized random phase approximation (ORPA) - angewandt. Im ersten Teil dieser Arbeit haben wir die ORPA Ausdrücke für die thermodynamischen Größen verwendet und den Einfluß der Polydispersität auf die thermodynamischen Größen untersucht.

Um Phasenübergänge zu berechnen, haben wir uns auf Systeme mit einfacheren freien Energien als jenen aus der ORPA beschränkt, sie werden als sogenannten ‘truncatable’ freie Energien bezeichnet. Das Wort truncatable bedeutet, daß es sich hierbei um freie Energien handelt, die nur von einem endlichen Satz von verallgemeinerten Momenten der Verteilungsfunktion  $f(\sigma)$  und der mittleren Teilchendichte des Systems abhängen. Für Systeme mit truncatable freier Energie können wir daher polydisperse Phasenübergänge ähnlich wie bei  $n$ -komponentigen Mischungen mit der üblichen Tangentenkonstruktion in einem endlich dimensionalen Momenten-Raum berechnen. Wir haben den Einfluß der (Größen- und Amplituden-) Polydispersität auf den Phasenübergang für drei verschiedene Modelle von truncatable freien Energien (für die van der Waals, die hard-sphere square-well und die hard-sphere Yukawa freie Energie) untersucht und dadurch zahlreiche Einsichten über das Phasenverhalten polydisperser Systeme gewonnen. Die Polydispersität führt unter anderem zu neuen Phänomenen im Bezug auf das Phasenverhalten, das bei den entsprechenden monodispersen Systemen nicht auftritt.



## Abstract

In this work we have studied the thermodynamic properties and the phase transitions of simple polydisperse systems, where we direct our attention on the fluid phases only. In our study we have treated a polydisperse system as a  $n$ -component mixture in the limit  $n \rightarrow \infty$  where the particle diameters are distributed continuously within a range  $[\sigma_{min}, \sigma_{max}]$  and the concentrations of the various particle types are replaced by a distribution function  $f(\sigma)$ . The particles interact via effective potentials which are given by a hard sphere repulsion with attractive tail. The attractions are in one case given by a square-well and in the second case by a Yukawa potential. In addition we have studied a polydisperse van der Waals system.

To calculate the structure and thermodynamic properties of the polydisperse system we have used a thermodynamic perturbation theory - the optimized random phase approximation (ORPA). In the first part of this work the ORPA expressions for the thermodynamic properties were used to study the influence of polydispersity on the thermodynamic properties.

For the calculation of phase transitions we have limited ourselves to approaches that lead to free energies that are simpler than the ones obtained from the ORPA; they are commonly referred to as ‘truncatable’ free energies i.e. the expressions for the free energy depend only on a finite set of generalized moments of the distribution function  $f(\sigma)$  and on the number density of the system. For systems of truncatable free energies we can calculate phase equilibria via the usual common tangent construction in a finite dimensional moment-space as for  $n$ -component mixtures. We have studied the influence of (size or amplitude) polydispersity on the phase transition process for three different truncatable free energy models (a van der Waals, a hard sphere square-well and a hard sphere Yukawa free energy) and have gained new insight into the phase behavior of polydisperse fluids in comparison to the corresponding monodisperse phase transition.



For my grandparents  
Aloisia and Johann Rauter

This thesis is based on the following original papers:

**Section 4.2.3**

S. Leroch, G. Kahl and F. Lado  
Thermodynamic perturbation theory for polydisperse colloidal suspensions using orthogonal polynomial expansions  
*Phys. Rev. E* **59**, 6937 (1999)

**Section 6.2**

S. Leroch, D. Gottwald, G. Kahl  
Thermodynamic properties of polydisperse fluid mixtures  
*J. Phys. Condensed Matter* **7**, 301 (2004)

# Contents

<b>1</b>	<b>Introduction</b>	<b>3</b>
<b>2</b>	<b>The system</b>	<b>9</b>
2.1	Definition of a polydisperse liquid . . . . .	9
2.1.1	Random systems of hard spheres with attractive tail . . . . .	10
2.1.1.1	Mathematical description . . . . .	11
2.1.1.2	Generalization to the polydisperse case . . . . .	12
2.2	Interatomic potentials . . . . .	13
2.2.1	Hard-sphere potential . . . . .	13
2.2.2	Square-well potential . . . . .	15
2.2.3	Hard-sphere Yukawa potential . . . . .	15
<b>3</b>	<b>Basics of liquid state theory</b>	<b>17</b>
3.1	Static structure functions . . . . .	17
3.2	Thermodynamic properties . . . . .	21
3.2.1	Internal energy $U$ . . . . .	21
3.2.2	Virial pressure $p^v$ . . . . .	22
3.2.3	Helmholtz free energy $A$ . . . . .	23
3.2.4	Chemical potential $\mu(\sigma)$ . . . . .	23
3.2.5	Isothermal compressibility $\chi_T$ . . . . .	24
3.3	Thermodynamic inconsistency . . . . .	25
<b>4</b>	<b>Theoretical concepts</b>	<b>27</b>
4.1	Van der Waals approach . . . . .	27
4.2	Thermodynamic perturbation theories . . . . .	29
4.2.1	The $\lambda$ -expansion . . . . .	30
4.2.2	The $\gamma$ -expansion . . . . .	31
4.2.3	ORPA, mean spherical approximation for a polydisperse system . . . . .	33
4.2.3.1	Structure of a polydisperse system . . . . .	34
4.2.3.2	Thermodynamics of a polydisperse system . . . . .	37
4.2.4	HS Reference system . . . . .	45
4.3	Integral equations . . . . .	48

<b>5</b>	<b>Phase equilibria of a polydisperse system</b>	<b>51</b>
5.1	Phase coexistence conditions . . . . .	52
5.1.1	Binodals . . . . .	52
5.1.2	Cloud point and shadow . . . . .	53
5.2	Thermodynamic stability conditions . . . . .	55
5.2.1	Spinodals and critical states . . . . .	55
5.3	Methods . . . . .	57
5.3.1	Truncatable free energy method . . . . .	57
5.3.2	Moment free energy method . . . . .	57
5.3.3	Binning and pseudo-components . . . . .	59
5.4	Phase coexistence for truncatable free energy method . . . . .	59
5.4.1	Binodals . . . . .	60
5.4.2	CPC and SC . . . . .	62
5.4.3	Spinodals and ordinary critical points . . . . .	62
5.4.4	Van der Waals fluid . . . . .	66
5.4.5	HS fluid with attractive tail . . . . .	70
5.4.5.1	Square-well fluid . . . . .	73
5.4.5.2	Yukawa fluid . . . . .	75
<b>6</b>	<b>Results</b>	<b>77</b>
6.1	Parent phase distribution . . . . .	77
6.2	Thermodynamics . . . . .	78
6.2.1	Square-well fluid . . . . .	79
6.2.2	Yukawa fluid . . . . .	90
6.3	Phase Diagrams . . . . .	100
6.3.1	Van der Waals fluid . . . . .	101
6.3.1.1	Size polydispersity only . . . . .	101
6.3.1.2	Amplitude polydispersity only . . . . .	107
6.3.2	Square-well fluid . . . . .	112
6.3.2.1	Size polydispersity . . . . .	112
6.3.2.2	Size and amplitude polydispersity . . . . .	116
6.3.3	Yukawa fluid . . . . .	123
6.3.3.1	Size polydispersity . . . . .	123
6.3.3.2	Size and amplitude polydispersity . . . . .	127
	<b>Conclusion</b>	<b>137</b>
<b>A</b>		<b>141</b>
A.1	Abbreviations . . . . .	141
<b>B</b>		<b>143</b>
B.1	Numerical methods . . . . .	143
B.1.1	Numerical solution of the ORPA . . . . .	143
B.1.2	Numerical solution of the phase equilibrium conditions . . . . .	145
B.1.2.1	Globally convergent Newton-Raphson Algorithm . . . . .	145

---

<b>C</b>	<b>149</b>
C.1 Mathematical Expressions . . . . .	149
C.1.1 Trace of a symmetric matrix . . . . .	149
<b>Bibliography</b>	<b>151</b>
<b>Acknowledgment</b>	<b>155</b>
<b>Curriculum Vitae</b>	<b>157</b>

---



# Chapter 1

## Introduction

Colloidal suspensions consist of mesoscopic particles (with mean diameters typically from  $1nm$  to  $1\mu m$ ) that are dispersed in a suspending microscopic fluid. The fact that such colloids are practically ubiquitous in our everyday lives (ranging from industrial products such as paints, glues or lubricants to basics such as food or pharmaceuticals) is one reason why increasing attention has been dedicated to these systems. (For an overview see, for instance, [1].) On the other hand, for a liquid state physicist such systems are very attractive in that they represent mesoscopic realizations of simple atomic liquids. Surprising analogies between the statistical behavior of such systems and that of simple atomic systems can be observed, and in some cases analogous experiments can be carried out much more easily for colloids than for atomic systems. To describe these suspensions, one usually integrates out (at least conceptually) the molecular degrees of freedom of the microscopic suspending fluid, and employs effective potentials acting directly between the mesoscopic particles that are rather simple: a harsh repulsion at short distances followed by an attraction at larger distances. In some cases, these interactions can even be tailored by suitable production techniques, while in atomic liquids one is simply stuck with the interaction dictated by the electronic structure.

Statistical mechanics was originally developed for the study of large systems of identical particles such as atoms and small molecules. However, many materials of industrial and commercial importance do not fit into this framework: due to their production process, the colloidal particles are never precisely identical to each other, but have a range of radii (and possibly surface charges, shapes etc.), meaning that they are *polydisperse*. A polydisperse liquid can be considered as a mixture with an infinite number of components, characterized, for instance, by the particle diameter  $\sigma$ , that is now a continuous rather than a discrete variable.

The first attempts to treat such systems date back to the late 1970s [2, 3], when a model of polydisperse hard spheres was investigated within the Percus-Yevick approximation.

---

In later years the concept of polydispersity was cast in a mathematically rigorous form by Salacuse and Stell [4] and by Briano and Glandt [5]. In these formulations,  $\sigma$  is the realization of some random variable  $\Sigma$  distributed according to a probability distribution  $f_{\Sigma}(\sigma)$ , which replaces the finite set of concentrations of the discrete components of a mixture. Meanwhile, the formalism has been extended systematically to more refined and more sophisticated hard-core model systems [6, 7]. The first step toward numerically solving such general (i.e., continuous) systems was carried out by D'Aguzzo and Klein [8], who applied well-known integral equation approaches of liquid state theory to the polydisperse case. This was achieved by replacing the continuous distribution  $f_{\Sigma}(\sigma)$  with a histogram for a finite set of  $n$  well-chosen diameters, thus mapping the polydisperse system back onto a  $n$ -component mixture. Recently this approach was modified by Lado [9] by joining the orthogonal polynomial technique with classical liquid state integral equation theory. In this procedure, all  $\sigma$ -dependent functions (in particular, the correlation functions) are expanded in terms of orthogonal polynomials  $p_i(\sigma)$  associated with the distribution function  $f_{\Sigma}(\sigma)$ . This expansion technique avoids the rapid increase in computational cost with the number of components  $n$  in the D'Aguzzo-Klein mixtures-method, while fully retaining the advantages and numerical accuracy of Gaussian quadrature based on the distribution function  $f_{\Sigma}(\sigma)$ . The same technique can further be applied to a much wider range of problems dealing with internal and external degrees of freedom in fluid systems [10, 11].

In my diploma thesis [12], we merged the orthogonal polynomial expansion method with a thermodynamic perturbation theory, the optimized random phase approximation (ORPA). The same formalism was used in this work to calculate structure and thermodynamic properties of a polydisperse system. The ORPA was introduced in the 1970s [13, 14], and turned out to be a very successful liquid state theory, favored by practitioners over a considerable period of time until - because of new, more efficient numerical algorithms - it was overtaken by integral equations in the 1980s. In the ORPA, the pair potential is split into a harshly repulsive reference term (the optimum choice is of course a hard sphere interaction) and a perturbation term; the Ornstein-Zernike equations are then solved along with a mean-spherical-type-closure relation which guarantees in addition that the pair distribution function vanishes in the region that is not accessible due to the strong repulsion ('core region'). It can be shown that the solution of the resulting integral equation is equivalent to the minimization problem of a suitably chosen functional of the direct correlation function. This makes the ORPA very attractive, since it is sometimes more convenient (and numerically more stable) to solve the minimization problem than to solve an integral equation. Thermodynamic and structural properties are calculated via perturbation expressions. In recent years - in particular due to the work

---

of Pastore and co-workers [15, 16] - the ORPA has been rediscovered: new numerical tools and the rapid development of computers have brought this liquid state method back into the race. Preliminary calculations for simple square-well systems have shown that in some cases the ORPA can in fact be applied over a larger range of system parameters than integral equation approaches [17]. In addition, the ORPA shows a remarkable degree of thermodynamic consistency without the necessity of introducing an additional parameter, as required in applications of parameterized integral equations theories that enforce some thermodynamic consistency.

In [18] we have presented results of a polydisperse hard-sphere square-well system obtained via the ORPA. As shown there the structure functions obtained via the random phase approximation (RPA), a liquid state theory where the pair distribution functions do not necessarily vanish within the core region, differs significantly from the ones calculated within the ORPA. Moreover we have shown that the thermodynamic quantities of a polydisperse liquid differ only slightly from the corresponding monodisperse properties and are almost independent from the choice of the truncation level within the Gaussian quadrature. In this work we have studied the influence of polydispersity on the thermodynamic properties calculated within the framework of the ORPA. As sample applications we have chosen again the square-well fluid and in addition the Yukawa fluid. These are rather simple systems that nevertheless capture all essential features of a typical potential of atomic liquids or colloidal suspensions. In these formulations, the potential parameters of the polydisperse systems (hard-core diameter  $\sigma$ , well width  $\lambda$  and well depth  $\varepsilon$  for the square-well fluid; inverse screening length  $\kappa$  and contact value  $\gamma$  for the Yukawa fluid) can be varied independently; i.e. they can be distributed according to three independent distribution functions for each potential  $f_{\Sigma}(\sigma)$ ,  $f_{\Lambda}(\sigma)$  and  $f_E(\sigma)$  (for the square-well potential) and  $f_{\Sigma}(\sigma)$ ,  $f_{\kappa}(\sigma)$  and  $f_{\Gamma}(\sigma)$  (for the Yukawa potential).

Apart from the calculation of structure and thermodynamics of a polydisperse system we have examined the influence of polydispersity on a phase separation process. In the study of polydisperse phase equilibria, one is interested to examine under which conditions of pressure and temperature a polydisperse system will be stable against demixing, how many phases will result if it does demix, and what their properties are, where the emphasis of this work will be on the problem of predicting such phase behavior theoretically. We will concentrate exclusively on bulk phase equilibria. In addition, we will only discuss the case of fixed polydispersity, where the polydisperse attribute (in this work the particle diameters) of each particle remains fixed once and for all.

The theoretical study of phase separations in polydisperse systems is faced with rather hard technical problems (mainly due to the infinite number of components). While for a  $n$ -component system the phase coexistences can be calculated from the free energy via

---

the common tangent construction in a  $n$ -dimensional density space (where each axis corresponds to the density  $\rho_i$  of the  $i$ th particle type), for a polydisperse system this becomes an impossible task as the free energy depends in general on a continuous density distribution function  $\rho(\sigma)$ . That means the free energy is now a functional of  $\rho(\sigma) = \rho f_\Sigma(\sigma)$  (with  $\rho$  the number density of the polydisperse system) and one has to make the common tangent construction in an infinite dimensional space. To calculate phase splits of polydisperse systems we have therefore to look for methods which can be used to reduce the dimensionality of the occurring equations. One of the most conventional possibilities is to use the ‘truncatable’ free energy method [19, 20], because it is an exact method. The expression truncatable means that along with this method the excess free energy can be expressed as a function of a finite set of moments of the distribution function  $f_\Sigma(\sigma)$  and of the number density  $\rho$  only. So we can reduce the problem to finite dimensionality given through the  $k$ -dimensional moment-space (where  $k$  stands for an arbitrary finite number). However the number of systems with a truncatable free energy is limited (for an overview see [20]). To calculate phase transitions of polydisperse systems that do not belong to this class (the free energy calculated via the ORPA for example) one is therefore forced to use approximations. The most straightforward way is to discretize the equations that define the phase coexistences and to map the polydisperse system onto a finite  $n$ -component mixture. The advantage of this approximation is that it can be applied to all systems irrespective of their dependence on the distribution function  $f_\Sigma(\sigma)$ ; the drawback of this approach is that the method of discretization is very sensitive to systematic and numerical errors and that it is high in computational cost (because  $n$  has to be rather large to minimize the occurring errors). Other more suitable methods to calculate the phase equilibrium in polydisperse systems is for instant the so called moment free energy method introduced in [21] and [22]. These approximate methods lead in contrast to the truncatable free energy method, to approximations for the phase coexistence curves; that means one can only define regions in the  $\rho$ - $T$  plane characterized by the so called ‘cloud’ and ‘shadow’ curves which provide envelopes for the phase coexistence curves - the binodals.

In our calculation of phase-equilibria via truncatable free moment models we have considered the simplest possible phase separation, namely the fluid-fluid phase separation. To calculate the phase transition we have chosen either a van der Waals fluid or a hard sphere fluid with attractive tail given by a square-well or a Yukawa potential.

The polydisperse phase diagrams show aspects which cannot be observed at the monodisperse ones: While for monodisperse systems there exists only one binodal for polydisperse systems one can calculate an arbitrary number of binodals - one for each choice of parent number density (corresponding to the number density of the initial phase)  $\rho^{(0)}$  -, where

only the binodal calculated for  $\rho^{(0)} = \rho_{crit}$  approaches the critical point; all other binodals are truncated at a certain temperature below or above the critical point. The cloud point curve with incipient shadow curve are special cases of binodals which can be obtained if we let the composition of the initial or parent phase unaltered and calculate the phase coexistence between this parent phase (where the equilibrium number densities are identical to  $\rho^{(0)}$ ) and the incipient minority-phase which is present in infinitesimal amounts only.

Also for the critical point an evident difference between monodisperse and polydisperse system can be observed: while the critical point in the monodisperse case is always situated at the maximum of binodal or spinodal, in the polydisperse case it can be obtained from the intersection of cloud point curve and shadow curve which have in general no common maximum (only for special choices of potential parameters). In most cases the maxima of cloud point curve and shadow curve are at temperature  $t_m$  above the critical point; this allows for a re-entrant behavior of the high or low density phase. Where with re-entrant behavior we mean that also for the case of two phase coexistence there can occur phase coexistences above the critical point (at least for special choices of  $\rho^{(0)}$ ).

We have studied the influence of the so called size polydispersity, the amplitude polydispersity and the combination of size and amplitude polydispersity on the phase transition process. With size polydispersity we mean that the amplitude of the attractions is constant for all particle type interactions, while for amplitude polydispersity it depends on the diameters  $\sigma$  of the interacting particles. The size or (and) amplitude polydispersity of the potential can be adjusted by the special choice of the potential parameters ( $z$  for the square-well model and  $a$  for the Yukawa model).

For the size polydisperse van der Waals and square-well system the cloud point and shadow curves have a common maximum which is identical to the critical point, while for the size polydisperse Yukawa system the cloud curve is slightly shifted to higher densities so that the maxima of shadow- and cloud point- curve never coincide and the critical point is lying at their intersection. In the size and amplitude polydisperse van der Waals and square-well system the shadow curve is shifted to higher densities and moves partly out of the interior of the cloud point curve whereas the size and amplitude polydisperse Yukawa fluid shows for moderate values of  $a$  ( $a = 1$ ) a similar behavior with respect to the shadow and cloud point curves as the size polydisperse Yukawa model.

While for the size polydisperse square-well system the phase coexistence region does not shift to lower temperatures as compared to the corresponding monodisperse case the size polydispersity has big influence on the phase coexistence regions of the van der Waals and Yukawa system. Size polydispersity is not favorable for the phase transition process, where with not favorable we mean that with increasing size polydispersity the critical

temperature moves to lower values and the high density phase on the cloud point curve is shifted towards lower densities. The last statement can also be written as follows: If we start at a certain temperature  $T$  above the critical point of the monodisperse system we have a stable fluid phase by reducing the temperature first the monodisperse system approaches its critical point and for further decrease of the temperature finally also the size polydisperse system splits off in two or more phases.

When the system is in addition to the size polydispersity also polydisperse in amplitude then we can observe for the square-well model that even for small values of  $z$  ( $z = 0.1$ ) (weak amplitude polydispersity) the phase coexistence region is shifted to higher temperatures as compared to the monodisperse case while in the Yukawa fluid the effects of the amplitude polydispersity dominates over the one of the size polydispersity only for potential parameters  $a \geq 2$  what means the critical region is shifted to higher temperatures with respect to the one of the corresponding monodisperse system. From that we can summarize that the amplitude polydispersity is favorable to the phase separation process, i.e. the critical temperature is shifted to higher values and the high density phase on the cloud point curve moves to higher densities with increasing amplitude polydispersity.

The work is organized as follows. In chapter 2 we give a definition for a polydisperse system including the mathematical description of so called ‘random systems’ given by Salacuse [24] and present the chosen interaction potentials. In chapter 3 we define the Ornstein Zernike (OZ) equation of a polydisperse fluid and discuss the correlation functions as well as the thermodynamic properties calculated within the framework of statistical mechanics. In chapter 4 we present the different liquid state methods which can be used to solve the OZ equations for a polydisperse system, where we finally use one of this liquid state-theories - a perturbation theory (ORPA) - to obtain general expressions for structure and thermodynamics of a polydisperse liquid. We have done this by introducing orthogonal polynomial expansions for all  $\sigma$  dependent functions. In chapter 5 we define the phase equilibrium conditions of the studied systems by use of the truncated free energy method. In chapter 6 finally we show the results and discuss occurring problems.

---

# Chapter 2

## The system

Most substances appearing in nature like Ar, Ne, Fe, C etc. are perfectly monodisperse, that means all particles of the considered system are equal in size (charge etc.) and interact via the same potentials with each other. To the contrary industrially produced colloidal suspensions always contain macromolecules with a range of particle diameters (charges etc.); they often consist of a large number of different molecular species best described as having continuously varying properties across each family of molecules. All these materials are therefore polydisperse: they contain particles with properties depending continuously on one or several parameters.

### 2.1 Definition of a polydisperse liquid

In this thesis we regard polydisperse colloidal suspensions. These consist of mesoscopic particles characterized, i.e., each by different diameters, charges etc., that are dispersed in a microscopic solvent. The polydisperse colloidal suspension will for further considerations be called polydisperse liquid and the mesoscopic particles are designated simply as particles. A polydisperse liquid can be considered as a system, where the particles are characterized by a random variable  $X$ , which is distributed by a continuous function  $f(X)$ . In this thesis the variable  $X$  is chosen to be the diameter  $\sigma$  of the particles. The function  $f$  has the interpretation, that  $f(\sigma_0)d\sigma_0$  represents the fraction of particles in the system characterized by a  $\sigma$  value in the range  $[\sigma_0, \sigma_0 + d\sigma_0]$ . Thus  $f(\sigma)$  is positive and integrates to one and hence may be interpreted as a probability density function (pdf)

$$f(\sigma) > 0, \quad \int_0^{\infty} f(\sigma)d\sigma = 1. \quad (2.1)$$

Thermodynamic properties of a polydisperse system can be obtained by generalizing from a mixture with a finite number of components to the polydisperse case. This procedure

is characterized by the rules [4]

$$\begin{aligned} c_i &= \frac{N_i}{N} \rightarrow f(\sigma)d\sigma \\ \sum_{i=1}^{\infty} c_i x_i &\rightarrow \int_0^{\infty} d\sigma f(\sigma)x(\sigma), \end{aligned} \quad (2.2)$$

where  $N_i$  represents the number of particles,  $c_i$  the concentrations and  $x_i$  a characteristic quantity of species  $i$  in the case of a mixture with a finite number of components consisting of  $N$  particles. The above generalization may be thought of as allowing the index  $i$  to take a continuum of values, while the probability of finding a particle of type  $i$ ,  $\frac{N_i}{N}$ , goes into  $f(\sigma)d\sigma$ . In addition, the summations over  $i$  become integrations over  $\sigma$ . The above described rules (2.2) can be justified if we regard the conception of ‘binning’. With binning we mean that we regard a system, where the  $\sigma$  values for which  $f(\sigma)$  is defined have been partitioned into  $n$  subdivisions (bins) and demanded that within the chosen interval  $\Delta\sigma$  all particles have the same diameter  $\sigma$ , which means they are indistinguishable. In this way, one obtains a  $n$  component mixture. If the number  $n$  of components (bins) goes to infinity the bins become infinitesimally small and all  $\sigma$  dependent variables become continuous functions in  $\sigma$ , which means that the discrete system becomes polydisperse in the limit  $n \rightarrow \infty$ .

In an alternative derivation of the polydisperse limit, one can assume from the start that all particles are genuinely different, with  $\sigma$  sampled randomly from the normalized distribution function  $f(\sigma)$ , so that the number of distinct species is always  $N$  (every particle represents a component too) and is taken to infinity together with the system size. The two procedures give equivalent results [24]. The second procedure proposed by Salacuse [24] is physically more plausible for colloid materials treated in this thesis in which no two particles present are exactly alike, even in a sample of macroscopic size [20]. For this reason we shortly describe the concept of so called random systems defined by Salacuse in the following section.

### 2.1.1 Random systems of hard spheres with attractive tail

Consider a reservoir of particles with diameters distributed via pdf  $H(\sigma)$ , where  $H(\sigma)$  can be a continuous or discrete pdf. We then form a system of  $N$  particles by random selections from this population. Salacuse defined the ensemble of systems constructed in this manner as an  $N$ -particle random system of particles and any particular such system is a realization of the  $N$ -particle random system. A particular realization will yield a set of values  $(\sigma_1, \sigma_2, \dots, \sigma_N)$ . Different realizations give different sets, where the sphere diameters  $\sigma_i$  are associated with random variables, because we are not knowing which

---

realization member one is dealing with. This means that random systems of particles are inherently probabilistic in character; every sphere diameter is given with a certain probability (depending on the random selection) within one realization. If we let the particle number  $N$  within one realization go to infinity, we can show, that the probability of finding a particle of certain diameter in this realization converges towards the probability of finding a particle of the same diameter in the reservoir. The distribution of particle diameters in the reservoir can also be obtained by averaging over the contributions given by the whole set of  $N$ -particle realizations.

### 2.1.1.1 Mathematical description

To bring the above qualitative conclusions in mathematical form [24], it is often convenient to associate an underlying space  $\Omega$  with the random variable  $\sigma_i(\omega)$ . In describing a random system of particles it is convenient to use the infinite dimensional space  $R^{+\infty}$  as underlying space  $\Omega$ . Each  $\omega$  belonging to  $\Omega$  is an infinite sequence of real numbers,  $\omega = (\omega_1, \omega_2, \dots)$  and represents an outcome of the random experiment of making a countable infinity of independent selections of spheres from a reservoir. We define the  $\sigma_i$  as  $\sigma_i : \Omega \rightarrow \sigma$ , where  $\sigma$  represents the set of real numbers, such that  $\sigma_i(\omega) = \omega_i$  for  $i = 1, 2, \dots, N$  (where we take later the limit  $N \rightarrow \infty$  to see the equivalence between random system and polydisperse system). Thus  $\sigma_1(\omega), \sigma_2(\omega), \dots$  are independent, identically distributed random variables having common pdf  $H(\sigma)$  with  $\sigma_i(\omega)$  representing the diameter of the  $i$ th sphere selected in the outcome  $\omega$ . The random vector  $[\sigma_1(\omega), \sigma_2(\omega), \dots, \sigma_N(\omega)]$  is a  $N$ -particle random system of spheres characterized by pdf  $H(\sigma)$ . For fixed  $\omega$  this vector is a  $N$ -tuple of real numbers representing a realization of the  $N$ -particle random system. The notation,  $\sigma_j(\omega)$ , is particularly convenient since it allows one to vary  $j$  and fix  $\omega$ , hence vary over the diameters of a particular realization, or alternatively fix  $j$  and vary  $\omega$ , thus consider the  $j$ th diameter over different realizations.

The random variables  $\sigma_1^k(\omega), \sigma_2^k(\omega), \dots$  are independent and identically distributed with first moment  $m_k$ , the  $k$ th moment of  $H(\sigma)$  which is assumed to exist. The law of large numbers gives

$$\frac{1}{N} \sum_{i=1}^N \sigma_i^k(\omega) \rightarrow m_k, \quad \text{with probability one as } N \rightarrow \infty \quad (2.3)$$

Thus almost every countable infinite selection of spheres yields an  $\omega$  such that

$$\sigma_1(\omega), \sigma_2(\omega), \dots$$

satisfies (2.3).

We consider now how the distribution of sphere diameters in a given realization of a random system approximates the distribution of spheres in the reservoir. For a  $N$ -particle realization  $[\sigma_1(\omega), \sigma_2(\omega), \dots, \sigma_N(\omega)]$ , we define the function  $H_N(\omega, \sigma)$  to be a right continuous step-like function with steps of height  $\frac{1}{N}$  at  $\sigma$  values  $\sigma_i(\omega)$ ,  $i = 1, \dots, N$ . The  $H_N(\omega, \sigma)$ , often called empirical distribution functions satisfy the following relations

$$E[H_N(\omega, \sigma)] = H(\sigma), \quad (2.4)$$

with  $E[\ ]$  representing the expected value and,

$$H_N(\omega, \sigma) \rightarrow H(\sigma) \text{ as } N \rightarrow \infty \quad (2.5)$$

for all  $\sigma$  and uniformly in  $\sigma$ . Result (2.4) (proof [24]) simply notes that although for a given  $N$ ,  $H_N(\omega, \sigma)$  varies from one realization to another, where averaging over all such realizations yields  $H(\sigma)$ . Result (2.5) states that almost every selection  $\omega$  yields an  $N$ -particle realization such that  $H_N(\omega, \sigma)$  converges to  $H(\sigma)$  if we take the limit  $N \rightarrow \infty$ .

Now we can summarize as follows: A  $N$ -particle random system of particles is characterized by the random vector  $[\sigma_1(\omega), \dots, \sigma_N(\omega)]$  where the  $\sigma_i$  are independent random variables which are identically distributed according to the pdf  $H(\sigma)$  and are defined on the common underlying space  $\Omega$ . A particular  $\omega \in \Omega$  yields a realization of the random system. The composition of a  $N$ -particle realization, characterized by  $H_N(\omega, \sigma)$ , varies over the ensemble of realizations, while the expected composition (ensemble average) is given by  $H(\sigma)$ . As  $N$  increases, the composition of ensemble members becomes more similar and in the limit  $N \rightarrow \infty$ , the composition of essentially all realizations is  $H(\sigma)$ .

Finally we have to remark that if we restrict ourselves to continuous pdfs it is obvious that a typical realization of a random system contains no spheres of the same diameter [24]. Comparison of two or, in general, a countable number of typical realizations yields no sphere of common diameter. This holds for  $N$ -particle realizations and also for the limiting case  $N \rightarrow \infty$ .

### 2.1.1.2 Generalization to the polydisperse case

A polydisperse system is a system with composition given by a continuous pdf, which has been denoted by  $f(\sigma)$ . As is the case for random systems with continuous pdf a typical polydisperse realization contains no sphere of common diameter, the same is valid if we compare two or in general a countable number of  $N$ -particle realizations. This means that every particle is also a distinct component. Further, random systems are directly related to polydisperse systems by expression (2.5) which shows that as  $N \rightarrow \infty$  almost every realization of a  $N$ -particle random system becomes polydisperse in that its composition is described by pdf  $f(\sigma)$  of the entire ensemble. Hence, essentially every realization of

$[\sigma_1(\omega), \sigma_2(\omega), \dots, \sigma_N(\omega)]$  with the  $\sigma_i(\omega)$  representing independent random variables identically distributed according to pdf  $f_N(\sigma)$  represents a polydisperse realization of particles with composition given by  $f_N(\sigma)$ , where  $f_N(\sigma)$  gives the pdf of an ensemble member ( $N$ -particle realization) of the polydisperse system.

Since a polydisperse system is a  $N$ -particle random system in the limit  $N \rightarrow \infty$  the results (2.4) and (2.5) apply to such systems, thus almost every polydisperse realization satisfies (2.3).

## 2.2 Interatomic potentials

As already defined above a colloidal suspension consists of mesoscopic particles dispersed in a microscopic solvent. At the calculation of the potential the influence of the solvent is taken into account only through an effective interaction mediated between the colloidal particles within the suspension. This effective interactions are rather simple: a harsh repulsion at short distances followed by attraction at larger distances. In some cases one is even able to tailor a suitable effective potential (see [25]), where one not depends at the calculation on the electronic structure like it is the case for atomic liquids. In an exact calculation of the effective potential we would have to take into account all contributions of  $n$ -body interactions (with  $n$  up to order  $N$  where  $N$  gives the number of the particles in the regarded system), what means the potential measured at a point within the suspension is given by a sum of all pair-, triplet-, and all higher order particle interactions [25]. For most liquid state theories it is sufficient to restrict oneself to effective pair potentials [26], which simplifies the calculations.

In this chapter we give an overview over the effective pair potentials used in this thesis. The liquid and the gas phases are homogenous and isotropic, hence at every space point within the fluid the number density  $\rho$  is constant. The particles of the regarded systems interact via radially symmetric pair-potentials  $\phi(r, \sigma_i, \sigma_j)$ , where the interaction depends on the distances  $r$  between two particles characterized by diameters  $\sigma_i$  and  $\sigma_j$ .

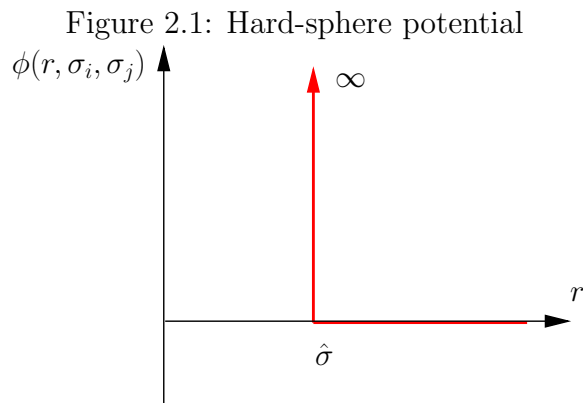
### 2.2.1 Hard-sphere potential

The partial hard-sphere (HS) potential is defined via

$$\phi(r, \sigma_i, \sigma_j) = \begin{cases} \infty & r < \hat{\sigma} \\ 0 & r \geq \hat{\sigma} \end{cases} . \quad (2.6)$$

We assume additivity of the diameters, i.e.,

$$\hat{\sigma} = \frac{\sigma_i + \sigma_j}{2} . \quad (2.7)$$



For many years, the HS system was a very useful, but rather academic model system. A purely hard potential does not materialize in atomic systems. However, with the advance of colloidal science, it became possible to prepare samples, which are extremely close in their behavior to an ideal HS system. By index matching colloidal particles with the surrounding solvent, the van der Waals attraction can be drastically reduced (see [25]), and the interaction between the colloids is then dominated by the repulsive core [27, 28, 29]. The HS system is without doubt the best examined system in liquid state theory; its structural and thermodynamic properties have been studied thoroughly. The HS potential plays an important role as a reference system in perturbation theories, since it captures the main features of the repulsive part of a typical interatomic potential. For the HS potential the Percus-Yevick (PY) approximation is analytically solvable. Percus and Yevick found the solution for the monodisperse HS fluid [30], which was then extended to the binary fluid by Lebowitz [31] and finally to the polydisperse fluid by Blum and Stell [3]. However, it has turned out that the solution of the PY approximation is not able to reproduce the results for structure or thermodynamic properties from computer simulations, in particular for high packing fractions. The empirical Carnahan-Starling [32] equation, developed for the one component fluid (which is based on the PY expressions for the thermodynamic properties), leads to an improved agreement of the thermodynamic properties of the fluid with results from simulation. To improve the agreement for the structure, Verlet and Weis [33] and also Henderson and Grundke [34] proposed a semiempirical parameterization of the correlation functions. Both the Carnahan-Starling and the Verlet Weis formalism can be extended to the multicomponent case [36, 35] and finally to the polydisperse case [12].

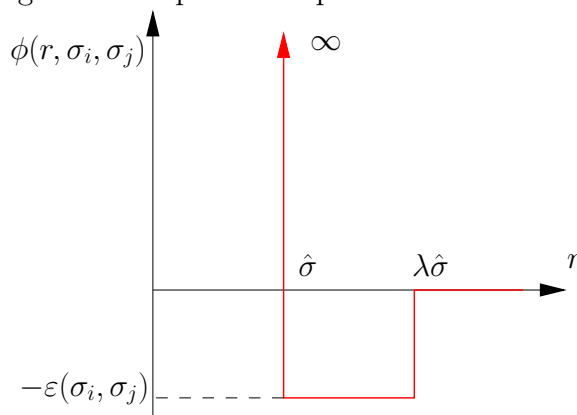
### 2.2.2 Square-well potential

The square-well (SW) potential is given by a HS core and an adjacent perturbation in form of a well. We use the following definition

$$\phi(r, \sigma_i, \sigma_j) = \begin{cases} \infty & r < \hat{\sigma} \\ -\varepsilon(\sigma_i, \sigma_j) & \hat{\sigma} \leq r \leq \hat{\sigma}\lambda(\sigma_i, \sigma_j) \\ 0 & r > \hat{\sigma}\lambda(\sigma_i, \sigma_j) \end{cases}, \quad (2.8)$$

where  $\lambda(\sigma_i, \sigma_j)$  is the perturbation width. Again the diameters  $\sigma_i$  are assumed to be additive. Although this potential seems rather academic, it captures (to a certain extent) the

Figure 2.2: Square-well potential with  $\lambda = 2$



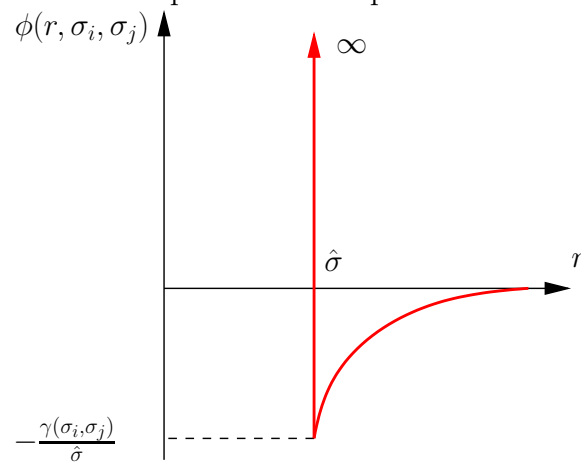
behavior of mesoscopic spherical particles (interacting via a hard-sphere-like interaction) in a microscopic solvent (assuming that the mesoscopic particles and the particles of the solvent have no or only very weak interactions). The SW potential models the effective potential between the particles of colloid-polymer mixtures or between particles of atomic systems with van der Waals attractions.

### 2.2.3 Hard-sphere Yukawa potential

The hard-sphere Yukawa (HSY) potential is given by an additive HS core and an adjacent perturbation in form of a Yukawa potential. We use the following definition

$$\phi(r, \sigma_i, \sigma_j) = \begin{cases} \infty & r < \hat{\sigma} \\ -\gamma(\sigma_i, \sigma_j) \frac{1}{r} e^{-\kappa(\sigma_i, \sigma_j)(r-\hat{\sigma})} & r \geq \hat{\sigma} \end{cases}, \quad (2.9)$$

where  $\kappa(\sigma_i, \sigma_j)$  is the so called inverse screening length and  $\gamma(\sigma_i, \sigma_j)$  is the measure for the electric charge multiplied with a length. The HSY potential is the effective potential of charge-stabilized colloidal suspensions [37]: such suspensions are created by putting mesoscopic particles with surface radicals into a polar solvent like water. Most of the charged surface groups dissociate into the solvent and form counter-ions carrying one

Figure 2.3: Hard-sphere Yukawa potential with  $\kappa = 2.3$ 

or two elementary charges. Consequently, the colloidal particles become highly charged and may be called macro-ions (they carry typically 100-10000 elementary charges). Since the counter-ion distribution is diffuse due to their finite temperature, the screening of the macro-ions is imperfect and a screened Coulomb repulsion between the macro-ions is the result. The van der Waals attractions between the colloidal particles together with the screened Coulomb repulsion which includes the influence of the solvent (where in this calculation the solvent is regarded as continuous dielectric medium with dielectric constant  $\epsilon$ ) lead then to the HSY potential which models the effective interaction potential between the macro-ions. In order to get a net attraction, the van der Waals contribution must dominate over the screened Coulomb repulsion.

# Chapter 3

## Basics of liquid state theory

### 3.1 Static structure functions

The Ornstein Zernike (OZ) equation is the central equation in liquid state theory. In the homogenous, isotropic polydisperse fluid it is an integral equation coupling the total correlation function  $h(r, \sigma_i, \sigma_j)$  to the direct correlation function  $c(r, \sigma_i, \sigma_j)$ , where the particle diameters  $\sigma_i$  and  $\sigma_j$  of two interacting particles, separated by distance  $r$  from each other, are distributed by a continuous distribution function  $f(\sigma)$ . The OZ equation for a homogeneous, isotropic polydisperse fluid is given by [9]

$$h(r, \sigma_i, \sigma_j) = c(r, \sigma_i, \sigma_j) + \rho \int_0^\infty f(\sigma_l) d\sigma_l \int c(|\vec{r} - \vec{r}'|, \sigma_i, \sigma_l) h(r', \sigma_l, \sigma_j) d^3r'. \quad (3.1)$$

As we can see from (3.1) the OZ equation consists of a convolution integral, so we can write the OZ equation in Fourier space as

$$\tilde{h}(k, \sigma_i, \sigma_j) = \tilde{c}(k, \sigma_i, \sigma_j) + \rho \int_0^\infty f(\sigma_l) d\sigma_l \tilde{c}(k, \sigma_i, \sigma_l) \tilde{h}(k, \sigma_l, \sigma_j). \quad (3.2)$$

To solve the OZ equations, one requires a further (functional) relation between the correlation functions and the pair potentials, known in the literature as closure relations (we will discuss closure relations in the next chapter). Such relations can be derived from exact statistical mechanical diagrammatic expansions [26], introducing simplifying approximations.

By starting from the direct correlation functions  $c(r, \sigma_i, \sigma_j)$ , the total correlation functions  $h(r, \sigma_i, \sigma_j)$  can be formally defined through the OZ equation (3.1). The meaning of the direct correlation functions is usefully illustrated by a representation of the OZ equation, which follows by iterative substitution of  $h(r, \sigma_i, \sigma_j)$  inside the kernel of (3.1). One easily obtains an infinite series of convolution integrals

$$\begin{aligned}
h(r, \sigma_i, \sigma_j) &= c(r, \sigma_i, \sigma_j) + \rho \int_0^\infty d\sigma_k f(\sigma_k) \int c(|\vec{r} - \vec{r}'|, \sigma_i, \sigma_k) c(r', \sigma_k, \sigma_j) d^3r' + \\
&\rho^2 \int_0^\infty d\sigma_k f(\sigma_k) \int d^3r' c(|\vec{r} - \vec{r}'|, \sigma_i, \sigma_k) \int_0^\infty d\sigma_l f(\sigma_l) \times \\
&\int d^3r'' c(|\vec{r}' - \vec{r}''|, \sigma_k, \sigma_l) c(r'', \sigma_l, \sigma_j) + \dots,
\end{aligned}$$

here truncated at the second iteration. The chain structure of this equation shows that the OZ equation amounts to describing the total correlation function between a pair of particles as a sum of different contributions, the first of which being given by a ‘direct’ term,  $c(r, \sigma_i, \sigma_j)$ , and the rest amounting to indirect correlations mediated by the same  $c(r, \sigma_i, \sigma_j)$  through many-body integrals over other particles in the fluid. The direct correlation functions  $c(r, \sigma_i, \sigma_j)$  are short range functions, even when correlations between density fluctuations tend to develop long-range algebraic tails, as it happens when the system approaches criticality or the associated ‘spinodal-line’. From diagrammatic expansions (see [26]) we can deduce that the range of  $c(r, \sigma_i, \sigma_j)$  is roughly the same as the range of the potential. To lowest order in density,  $c(r, \sigma_i, \sigma_j) \simeq f(r, \sigma_i, \sigma_j)$ , where  $f(r, \sigma_i, \sigma_j) = e^{-\beta\phi(r, \sigma_i, \sigma_j)} - 1$  is the Mayer function, or at large distances,  $c(r, \sigma_i, \sigma_j) \simeq -\beta\phi(r, \sigma_i, \sigma_j)$  with  $\beta = \frac{1}{k_B T}$ ;  $k_B$  the Boltzmann constant and  $T$  the temperature of the system.

In the following, we will introduce the  $N$ -particle density distribution functions  $\rho^{(N)}(r_1, \dots, r_N; \sigma_1, \dots, \sigma_N)$ . In particular we define the one-particle and two-particle density distribution function. For the one-particle density distribution function  $\rho^{(1)}(r, \sigma)$ , concerning particles of diameter  $\sigma$  at position  $\vec{r}$ , it follows [5, 9]

$$\rho^{(1)}(\vec{r}, \sigma) = \left\langle \sum_{i=1}^N \delta(\vec{r} - \vec{r}_i) \delta(\sigma - \sigma_i) \right\rangle, \quad (3.3)$$

where  $\vec{r}_i$  is the location of particle  $i$  and  $\sigma_i$  its diameter; the brackets denote an ensemble average. The one-particle density distribution function  $\rho^{(1)}(\vec{r}, \sigma)$  is defined so, that  $\rho^{(1)}(\vec{r}, \sigma) d^3r d\sigma$  is the probability of finding a particle with size  $\sigma \in [\sigma, \sigma + d\sigma]$  in the volume  $d^3r$  at  $\vec{r}$ . For a spatially homogeneous fluid,  $\rho^{(1)}(\vec{r}, \sigma) = \rho(\sigma)$  is independent of  $\vec{r}$  and is separable into  $\rho(\sigma) = \rho f(\sigma)$ , where the number density is defined as

$$\rho = \int_0^\infty \rho f(\sigma) d\sigma.$$

For the corresponding Fourier transforms  $\tilde{\rho}(\vec{k}, \sigma)$ , we obtain

$$\begin{aligned}\tilde{\rho}(\vec{k}, \sigma) &= \sum_{l=1}^N \delta(\sigma - \sigma_l) e^{-i\vec{k}\vec{r}_l} \\ \langle \tilde{\rho}(\vec{k}, \sigma) \rangle &= \int d^3r e^{-i\vec{k}\vec{r}} \left\langle \sum_{i=1}^N \delta(\sigma - \sigma_i) \delta(\vec{r}_i - \vec{r}) \right\rangle.\end{aligned}\quad (3.4)$$

In the homogenous, isotropic fluid the one-particle density distribution function in  $k$  space  $\langle \rho(k, \sigma) \rangle = (2\pi)^3 \rho f(\sigma) \delta(k)$ , which means that, it has only a contribution for  $k = 0$ . This can be explained by the homogeneity of the fluid, where the one-particle density distribution function  $\rho(\sigma)$  in  $r$ -space is independent of  $r$ .

The two-particle density distribution function  $\rho^{(2)}(\vec{r}, \vec{r}', \sigma, \sigma')$  is defined as [5, 9]

$$\begin{aligned}\rho^{(2)}(\vec{r}, \vec{r}', \sigma, \sigma') &= \rho^{(1)}(\vec{r}, \sigma) \rho^{(1)}(\vec{r}', \sigma') g(\vec{r}, \vec{r}', \sigma, \sigma') \\ &= \left\langle \sum_{i=1}^N \sum_{j \neq i}^N \delta(\vec{r} - \vec{r}_i) \delta(\sigma - \sigma_i) \delta(\vec{r}' - \vec{r}_j) \delta(\sigma' - \sigma_j) \right\rangle,\end{aligned}\quad (3.5)$$

where  $\vec{r}_i$  and  $\vec{r}_j$  are the locations of particle  $i$  and  $j$  with diameters  $\sigma_i$  and  $\sigma_j$ ; the brackets denote an ensemble average. The function  $g(\vec{r}, \vec{r}', \sigma, \sigma')$ , introduced above, is the pair distribution function, which will be discussed below. The two-particle density distribution function is defined so, that  $\rho^{(2)}(\vec{r}, \vec{r}', \sigma, \sigma') d^3r d^3r' d\sigma d\sigma'$  is the probability of simultaneously finding a particle with size  $\sigma \in [\sigma, \sigma + d\sigma]$  in a volume  $d^3r$  at  $\vec{r}$  and another of size  $\sigma' \in [\sigma', \sigma' + d\sigma']$  in a volume  $d^3r'$  at  $\vec{r}'$ . If we take the average in the canonical ensemble, the two-particle density distribution function  $\rho^{(2)}(\vec{r}, \vec{r}', \sigma, \sigma')$  can be defined as a functional derivative of the configurational integral  $Z_N(V, T)$  with respect to the pair potential

$$\begin{aligned}\rho^{(2)}(\vec{r}, \vec{r}', \sigma, \sigma') &= \rho^{(1)}(\vec{r}, \sigma) \rho^{(1)}(\vec{r}', \sigma') g(\vec{r}, \vec{r}', \sigma, \sigma') \\ &= \frac{N(N-1)}{Z_N(V, T)} \int_{x_3} \dots \int_{x_N} e^{-\beta V_N(\vec{x}, \vec{x}', \vec{x}_3, \dots, \vec{x}_N)} d^4x_3 \dots d^4x_N \\ &= -2 \frac{\delta \ln Z_N(V, T)}{\delta \beta \phi(\vec{r}, \vec{r}', \sigma, \sigma')}\end{aligned}\quad (3.6)$$

with

$$Z_N(V, T) = \int_{x_1} \dots \int_{x_N} e^{-\beta V_N(\vec{x}_1, \vec{x}_2, \dots, \vec{x}_N)} d^4x_1 \dots d^4x_N.$$

We assume pairwise additivity hence

$$V_N(\vec{x}_1, \dots, \vec{x}_N) = V_N(\vec{r}_1, \dots, \vec{r}_N; \sigma_1, \dots, \sigma_N) = \frac{1}{2} \sum_{i=1}^N \sum_{j \neq i}^N \phi(\vec{r}_i, \vec{r}_j, \sigma_i, \sigma_j), \quad (3.7)$$

where the vector  $d^4x = d^3r d\sigma$ ,  $V$  is the volume and  $V_N$  is the potential energy of the system. In a homogeneous system the two particle density distribution function becomes

a function of the distance between the particles, i.e.  $\rho^{(2)}(r, \sigma, \sigma') = \rho^2 f(\sigma) f(\sigma') g(r, \sigma, \sigma')$ , where  $g(r, \sigma, \sigma')$  is the radial pair distribution function. The radial pair distribution function  $g(r, \sigma_i, \sigma_j) = h(r, \sigma_i, \sigma_j) + 1$  is proportional to the probability density, that given a particle of identity  $\sigma_i$  in a volume  $d^3r$  at the origin, a particle of identity  $\sigma_j$  is found in a volume  $d^3r$  a distance  $r$  apart. If the distances between the particles tends to infinity, the radial pair distribution functions  $g(r, \sigma_i, \sigma_j) \rightarrow 1$ , a limiting value, which expresses the loss of correlations between particles at large distances. One can show [5], that the radial pair distribution function behaves as  $e^{-\beta\phi(r, \sigma_i, \sigma_j)}$  as  $\rho \rightarrow 0$ , in the same limit,  $h(r, \sigma_i, \sigma_j)$  behaves as  $f(r, \sigma_i, \sigma_j)$ .

The Fourier transforms of the radial pair distribution functions are directly related to the structure factor  $S^M(k)$ , a quantity experimentally measurable, for instance, through scattering techniques. The structure factor  $S^M(k)$  depends on the form factors  $\tilde{b}(k, \sigma)$  for spherical particles of diameter  $\sigma$  and is defined as [9, 12]

$$\begin{aligned} S^M(k) &= 1 + \rho \frac{\int d\sigma f(\sigma) \int d\sigma' f(\sigma') \tilde{b}(k, \sigma) \tilde{b}(k, \sigma') \int d^3r e^{-ikr} [g(r, \sigma, \sigma') - 1]}{\int d\sigma f(\sigma) \tilde{b}^2(k, \sigma)} \\ &= 1 + \rho \frac{\int d\sigma f(\sigma) \int d\sigma' f(\sigma') \tilde{b}(k, \sigma) \tilde{b}(k, \sigma') \tilde{h}(k, \sigma, \sigma')}{\int d\sigma f(\sigma) \tilde{b}^2(k, \sigma)} \end{aligned}$$

where  $\tilde{h}(k, \sigma_i, \sigma_j)$  is the Fourier transform of the total correlation function

$$\tilde{h}(k, \sigma_i, \sigma_j) = \int h(r, \sigma_i, \sigma_j) e^{-ikr} d^3r.$$

Because the structure factor  $S^M(k)$  depends on the form factors  $\tilde{b}(k, \sigma)$ , measuring of its peaks gives no information about the density distribution, respectively about the positions of the particles within the fluid [8]. For this reason, one defines the so called number-number structure factor  $S_{NN}(k)$ , which gives information about the density fluctuations. By starting from the basic definition of  $S_{NN}(k)$  as the autocorrelation function of the Fourier components of the density fluctuations [38], one can show that

$$S_{NN}(k) = \int d\sigma_i \int d\sigma_j \sqrt{f(\sigma_i) f(\sigma_j)} S(k, \sigma_i, \sigma_j) \quad (3.8)$$

with the partial structure factors  $S(k, \sigma_i, \sigma_j)$

$$\begin{aligned} S(k, \sigma_i, \sigma_j) &= \frac{1}{N \sqrt{f(\sigma_i) f(\sigma_j)}} \langle \delta \tilde{\rho}_k^{(\sigma_i)} \delta \tilde{\rho}_{-k}^{(\sigma_j)} \rangle \\ &= \frac{\langle \tilde{\rho}(k, \sigma_i) \tilde{\rho}(-k, \sigma_j) \rangle - \langle \tilde{\rho}(k, \sigma_i) \rangle \langle \tilde{\rho}(-k, \sigma_j) \rangle}{N \sqrt{f(\sigma_i) f(\sigma_j)}} \\ &= \delta(\sigma_i - \sigma_j) + \rho \sqrt{f(\sigma_i) f(\sigma_j)} \int d^3r [g(r, \sigma_i, \sigma_j) - 1] e^{-ikr}, \quad (3.9) \end{aligned}$$

where we have used equation (3.4) to calculate the density fluctuations in the partial structure factor, and the brackets denote an ensemble average. The total correlation functions have a Fourier representation in terms of  $S(k, \sigma_i, \sigma_j)$

$$\rho \sqrt{f(\sigma_i)f(\sigma_j)} h(r, \sigma_i, \sigma_j) = \frac{1}{(2\pi)^3} \int d^3k e^{ikr} [S(k, \sigma_i, \sigma_j) - \delta(\sigma_i - \sigma_j)].$$

Inserting (3.9) into (3.8), we can write for the number-number structure factor

$$S_{NN}(k) = S(k) = 1 + \rho \int d\sigma_i f(\sigma_i) \int d\sigma_j f(\sigma_j) \tilde{h}(k, \sigma_i, \sigma_j), \quad (3.10)$$

where we skip the subindex  $NN$  for further considerations.

## 3.2 Thermodynamic properties

Once the structure functions are known, they can be used to obtain the thermodynamic properties of the system. Because of the various Maxwell relations, thermodynamic provides different routes to calculate the thermodynamic properties. Here we will discuss three of them, the energy-, the virial- and compressibility-route. It is convenient to split thermodynamic quantities into two contributions:

- The ideal part ('id') describes the corresponding thermodynamic property for an ideal gas; here all these quantities can be calculated analytically.
- the contribution to a thermodynamic property arising from the (pair)interactions is the excess part ('ex') and has to be calculated - in general - numerically.

### 3.2.1 Internal energy $U$

The ideal part of the internal energy is given by [26]

$$U_{id} = \frac{3}{2} N k_B T.$$

For the excess internal energy it follows [9]

$$\begin{aligned} U_{ex} &= \frac{1}{Z_N(V, T)} \int e^{-\beta V_N(x_1, \dots, x_N)} V_N(x_1, \dots, x_N) \prod_{i=1}^N d^4x_i \\ &= \frac{1}{Z_N(V, T)} \int e^{-\beta V_N(x_1, \dots, x_N)} \left( \frac{1}{2} \sum_{l=1}^N \sum_{k \neq l}^N \phi(r_{lk}, \sigma_l, \sigma_k) \right) \prod_{i=1}^N d^4x_i \\ &= \frac{1}{2} \int_{x_1} \int_{x_2} \phi(r_{12}, \sigma_1, \sigma_2) \left( \frac{N(N-1)}{Z_N(V, T)} \int \dots \int e^{-\beta V_N(x_1, \dots, x_N)} \prod_{i=3}^N d^4x_i \right) d^4x_1 d^4x_2 \\ &= \frac{1}{2} \frac{N^2}{V} \int_0^\infty f(\sigma_1) d\sigma_1 \int_0^\infty f(\sigma_2) d\sigma_2 \int \phi(r, \sigma_1, \sigma_2) g(r, \sigma_1, \sigma_2) d^3r, \end{aligned}$$

where we have used the homogeneous version of equation (3.6) for the last manipulation. This result is called the energy equation. Hence we obtain for the internal energy

$$U = U_{id} + U_{ex} = \frac{N}{\beta} \left( \frac{3}{2} + \frac{\rho}{2} \int_0^\infty d\sigma f(\sigma) \int_0^\infty d\sigma' f(\sigma') \int d^3r g(r, \sigma, \sigma') \beta \phi(r, \sigma, \sigma') \right). \quad (3.11)$$

### 3.2.2 Virial pressure $p^v$

In the virial route we derive a relation between the pressure and the radial pair distribution function  $g(r, \sigma_i, \sigma_j)$  which corresponds to the homogeneous version of (3.6). The pressure can be split into the ideal part [26]

$$p_{id} = k_B T \frac{N}{V}$$

and the excess part, which is given by the ensemble average [9]

$$\begin{aligned} p_{ex} &= - \frac{\rho}{3N Z_N(V, T)} \int e^{-\beta V_N(x_1, \dots, x_N)} \sum_{l=1}^N \vec{r}_l \vec{\nabla}_l \left( \sum_{k \neq l}^N \phi(r_{lk}, \sigma_i, \sigma_j) \right) \prod_{i=1}^N d^4 x_i \\ &= - \frac{\rho}{3N} \frac{1}{2} \sum_{l=1}^N \sum_{k \neq l}^N \frac{1}{Z_N(V, T)} \int e^{-\beta V_N(x_1, \dots, x_N)} \vec{r}_{lk} \vec{\nabla}_{lk} \phi(r_{lk}, \sigma_i, \sigma_j) \prod_{i=1}^N d^4 x_i \\ &= - \frac{\rho}{6N} \int d^4 x_1 \int d^4 x_2 r_{12} \phi'(r_{12}, \sigma_i, \sigma_j) \left( \frac{N(N-1)}{Z_N(V, T)} \int e^{-\beta V_N(x_1, \dots, x_N)} \prod_{i=3}^N d^4 x_i \right) \\ &= - \frac{\rho^2}{6} \int_0^\infty d\sigma_i f(\sigma_i) \int_0^\infty d\sigma_j f(\sigma_j) \int r \phi'(r, \sigma_i, \sigma_j) g(r, \sigma_i, \sigma_j) d^3 r, \end{aligned}$$

where  $\phi'(r, \sigma_i, \sigma_j) = \frac{d\phi(r, \sigma_i, \sigma_j)}{dr}$ . The virial pressure  $p^v$  of the system is then given as

$$p^v = k_B T \frac{N}{V} - \frac{2\pi\rho^2}{3} \int_0^\infty d\sigma f(\sigma) \int_0^\infty d\sigma' f(\sigma') \int r^3 \frac{d\phi(r, \sigma, \sigma')}{dr} g(r, \sigma, \sigma') dr. \quad (3.12)$$

Equation (3.12) is called the virial equation. Because this relation involves the derivative of pair potentials, it has to be treated with special care in the case of hard core systems. The problem can be overcome by rewriting the equation in terms of the function  $y(r, \sigma, \sigma') = e^{\beta\phi(r, \sigma, \sigma')} g(r, \sigma, \sigma')$ . The function  $y(r, \sigma, \sigma')$  is a continuous function of  $r$ , even if both  $\phi(r, \sigma, \sigma')$  and  $g(r, \sigma, \sigma')$  have discontinuities [26]. On introducing  $y(r, \sigma, \sigma')$  into equation (3.12), we find that

$$\begin{aligned} \frac{\beta p^v}{\rho} &= 1 - \frac{2}{3} \pi \beta \rho \int d\sigma f(\sigma) \int d\sigma' f(\sigma') \int_0^\infty \phi'(r, \sigma, \sigma') y(r, \sigma, \sigma') e^{-\beta\phi(r, \sigma, \sigma')} r^3 dr \\ &= 1 - \frac{2}{3} \pi \rho \int_0^\infty d\sigma f(\sigma) \int_0^\infty d\sigma' f(\sigma') \int_0^\infty y(r, \sigma, \sigma') r^3 \frac{d}{dr} e^{-\beta\phi(r, \sigma, \sigma')} dr. \quad (3.13) \end{aligned}$$

### 3.2.3 Helmholtz free energy $A$

The ideal part of the Helmholtz free energy,  $A_{id}$ , is given by [26]

$$\frac{\beta A_{id}}{N} = \int d\sigma f(\sigma) (\ln [\rho f(\sigma) \Lambda^3(\sigma)] - 1),$$

where  $\Lambda(\sigma)$  is the de Broglie thermal wavelength

$$\Lambda(\sigma) = \sqrt{\frac{2\pi\beta\hbar^2}{m(\sigma)}},$$

$m(\sigma)$  is the mass of a particle with diameter  $\sigma$  and  $\hbar$  is Plank's constant, while the excess free energy is given as [26]

$$A_{ex} = -k_B T \ln \frac{Z_N(V, T)}{V^N}. \quad (3.14)$$

The free energy  $A = A^{id} + A^{ex}$  can be calculated from known thermodynamic quantities like pressure or internal energy via Maxwell relations, such as

$$U = A + TS = A - T \left( \frac{\partial A}{\partial T} \right)_{V, T} \quad (3.15)$$

$$p = - \left( \frac{\partial A}{\partial V} \right)_{T, N}. \quad (3.16)$$

Hence  $A$  can be obtained from the pressure  $p$  via thermodynamic integration along isotherms:

$$\begin{aligned} A_{ex}(V, T) &= A_{ex}(0, T) - \int_0^V dV' p_{ex}(V') \\ A_{ex}(\rho, T) &= A_{ex}(0, T) + N \int_0^\rho d\rho' \frac{p_{ex}(\rho')}{\rho'^2}, \end{aligned} \quad (3.17)$$

or from  $U$  along isochores:

$$\frac{A_{ex}(V, T_1)}{T_1} = \frac{A_{ex}(V, T_0)}{T_0} + \int_{\frac{1}{T_0}}^{\frac{1}{T_1}} d' \frac{1}{T} U_{ex}(T). \quad (3.18)$$

### 3.2.4 Chemical potential $\mu(\sigma)$

The chemical potential is a measure for the change in free energy by adding a particle of diameter  $\sigma$  to a mixture of  $N$  particles, while temperature and volume are kept fixed. The chemical potential  $\mu(\sigma)$  can be obtained via functional derivation of  $A$  with respect to the particle number distribution function  $N(\sigma) = Nf(\sigma)$  [4]

$$\mu(\sigma_i) = \left( \frac{\delta A}{\delta N f(\sigma_i)} \right)_{T, V, N f(\sigma_j)} = \frac{1}{\beta} \left( \frac{\delta A^+}{\delta \rho f(\sigma_i)} \right)_{T, V, \rho f(\sigma_j)}, \quad (3.19)$$

where all values of the particle number distribution function  $Nf(\sigma_j)$ , and all one-particle density distribution functions  $\rho f(\sigma_j)$ , at  $\sigma_j \neq \sigma_i$  must also be kept constant and  $A^+ = \frac{\beta A}{V}$  is the energy density. The ideal part  $\mu_{id}(\sigma)$  is given by

$$\mu_{id}(\sigma_i) = \left( \frac{\delta A_{id}}{\delta Nf(\sigma_i)} \right)_{T,V,Nf(\sigma_j)} \quad (3.20)$$

$$= k_B T \ln [\rho f(\sigma_i) \Lambda^3(\sigma_i)]. \quad (3.21)$$

### 3.2.5 Isothermal compressibility $\chi_T$

The isothermal compressibility is defined as

$$\chi_T = -\frac{1}{V} \left( \frac{\partial V}{\partial p} \right)_T = \frac{1}{\rho} \left( \frac{\partial \rho}{\partial p} \right)_T.$$

For the ideal gas one finds [26]

$$\chi_{Tid} = \frac{1}{\rho k_B T}.$$

One can show [9], that the isothermal compressibility can be calculated from the direct correlation functions via

$$\begin{aligned} \frac{1}{\rho k_B T \chi_T} &= 1 - \rho \int d^3r \int_0^\infty d\sigma_i f(\sigma_i) \int_0^\infty d\sigma_j f(\sigma_j) c(r, \sigma_i, \sigma_j) \\ &= 1 - \rho \int_0^\infty d\sigma_i f(\sigma_i) \int_0^\infty d\sigma_j f(\sigma_j) \tilde{c}(0, \sigma_i, \sigma_j). \end{aligned} \quad (3.22)$$

The pressure can be obtained from (3.22) via thermodynamic integration

$$p(\rho) = p(0) + k_B T \int_0^\rho d\rho' \left[ 1 - \int_0^\infty d\sigma_i f(\sigma_i) \int_0^\infty d\sigma_j f(\sigma_j) \rho' \tilde{c}(0, \sigma_i, \sigma_j; \rho') \right] = p^c \quad (3.23)$$

and will be denoted as the compressibility pressure,  $p^c$ . If we insert this pressure into equation (3.17), we get

$$A_{ex}(\rho) - A_{ex}(0) = -\frac{N}{\beta} \int_0^\rho d\rho' \frac{1}{\rho'^2} \int_0^{\rho'} d\rho'' \rho'' \int_0^\infty d\sigma_i f(\sigma_i) \int_0^\infty d\sigma_j f(\sigma_j) \tilde{c}(0, \sigma_i, \sigma_j; \rho').$$

With  $A_{ex}(0) = 0$  (ideal gas) and partial integration we get [40]

$$\begin{aligned} A_{ex}(\rho) &= -\frac{N}{\beta} \left\{ - \left[ \frac{1}{\rho'} \int_0^{\rho'} d\rho'' \rho'' \int_0^\infty d\sigma_i f(\sigma_i) \int_0^\infty d\sigma_j f(\sigma_j) \tilde{c}(0, \sigma_i, \sigma_j; \rho'') \right]_0^\rho \right. \\ &\quad \left. + \int_0^\rho d\rho' \int_0^\infty d\sigma_i f(\sigma_i) \int_0^\infty d\sigma_j f(\sigma_j) \tilde{c}(0, \sigma_i, \sigma_j; \rho') \right\} \\ A_{ex}^+ &= \int_0^\rho d\rho' (\rho' - \rho) \int_0^\infty d\sigma_i f(\sigma_i) \int_0^\infty d\sigma_j f(\sigma_j) \tilde{c}(0, \sigma_i, \sigma_j; \rho') \\ &= - \int_0^\rho d\rho' \int_0^{\rho'} d\rho'' \int_0^\infty d\sigma_i f(\sigma_i) \int_0^\infty d\sigma_j f(\sigma_j) \tilde{c}(0, \sigma_i, \sigma_j; \rho'') = A_{ex}^c. \end{aligned} \quad (3.24)$$

### 3.3 Thermodynamic inconsistency

In the last subsections we have derived the formulae needed to calculate the thermodynamic properties of a polydisperse system from its structure. Further, we have shown, that one thermodynamic quantity (as, for example, the pressure) can be calculated via different routes (corresponding to different thermodynamic relations). If we knew the exact structure functions (i.e. without approximation), then all these different routes would yield the same results for one thermodynamic quantity. However, due to the various simplifications and approximations (discussed later) made in the concepts of liquid state theory the value of a certain thermodynamic quantity will depend on the thermodynamic path one has chosen. This deficiency is also known in the literature as thermodynamic inconsistency. To minimize these deficiencies, so called self-consistent liquid state theories have been developed during the past years. For instance Verlet and Weis [33] have proposed a semi-empirical parameterization for the structure functions of a monodisperse HS fluid, which leads to thermodynamically self-consistent results; their ideas can be generalized to the polydisperse case [12]. For the case of one component and binary systems several (at least partly) self-consistent approaches have been proposed during the past years (for an overview see e. g. Caccamo [38]). Some of these approaches have been generalized to the polydisperse case [9]. The method used in this thesis, the optimized random phase approximation (see next chapter), shows a rather high degree of self-consistency [17].

---



# Chapter 4

## Theoretical concepts

In this chapter we will describe the various theoretical concepts that can be used to obtain the thermodynamic properties and the structure functions (radial pair distribution functions and direct correlation functions) of a homogenous isotropic polydisperse fluid.

We start with a rather simple system, the van der Waals fluid, for which only thermodynamic properties have to be calculated. Then we discuss in detail the methods of thermodynamic perturbation theory, where we concentrate here mainly on the (optimized) random phase approximation. Within this method we have calculated structure functions and obtained closed expressions for the thermodynamic quantities of a polydisperse system. Finally we give a short insight to integral equation theories, which can easily be applied to polydisperse fluids.

### 4.1 Van der Waals approach

The idea of representing a liquid as a system of HS moving in a uniform, attractive potential tail or sea is an old one, providing as it does the physical basis for the van der Waals (vdW) equation [26]. The hard repulsion, arising from the strong Pauli exclusions of the core electrons in, e.g., the noble gas elements, are taken into account by an excluded volume term, while the attractions are averaged over the whole volume of the system, to obtain a uniform attractive potential. The uniform potential comes physically from spontaneously fluctuating electric dipoles that tend to align themselves giving rise to the so called ‘dispersion forces’. The vdW model is simple enough to allow a clear explication and yet complex enough to illustrate fundamental calculational problems (concerning for example later calculated phase diagrams). Within the vdW theory no structural functions are calculated. The vdW approach starts directly with an approximation for the Helmholtz free energy, other thermodynamic quantities can be deduced via appropriate Maxwell relations.

For a polydisperse fluid the vdW free energy density reads [19]

$$A^+[f] = \int_0^\infty d\sigma \rho f(\sigma) \left\{ \ln \left( \frac{\Lambda^3(\sigma) \rho f(\sigma)}{E[f]} \right) - 1 \right\} + \frac{1}{2} \beta \int_0^\infty d\sigma \int_0^\infty d\sigma' \varphi(\sigma, \sigma') \rho f(\sigma) \rho f(\sigma'), \quad (4.1)$$

where  $[f]$  indicates a functional dependence on the distribution function  $f(\sigma)$ . The hard repulsion between the particles in (4.1) can be taken into account via the vdW excluded volume correction

$$\begin{aligned} E[f] &= 1 - \int d\sigma V(\sigma) \rho f(\sigma) = 1 - \frac{4\pi}{3} \int d\sigma \left( \frac{\sigma}{2} \right)^3 \rho f(\sigma) \\ &= 1 - \rho \frac{\pi}{6} \int d\sigma f(\sigma) \sigma^3 = 1 - \eta, \end{aligned} \quad (4.2)$$

$V(\sigma) = \frac{\pi}{6} \sigma^3$  being the volume of a particle with diameter  $\sigma$  and  $\eta$  the packing fraction. The second term of (4.1) gives, in the vdW mean field approximation, the cohesive energy resulting from the interparticle attractions, described by the pair potentials  $\phi(r, \sigma, \sigma')$

$$\varphi(\sigma, \sigma') = \int d^3r \phi(r, \sigma, \sigma'). \quad (4.3)$$

If equation (2.7) denotes the contact distance between two particles of species  $\sigma$  and  $\sigma'$ , we have  $\phi(r, \sigma, \sigma') = 0$  when  $r < \hat{\sigma}$ , so that the last equation can always be rewritten

$$\varphi(\sigma, \sigma') = -\nu(\sigma, \sigma') \frac{4\pi}{3} \hat{\sigma}^3, \quad (4.4)$$

where  $\nu(\sigma, \sigma') > 0$  characterizes the amplitude of the attractions.

From equations (4.1) and (3.19) we obtain for the chemical potential within the vdW approximation [19]

$$\beta\mu(\sigma, [f]) = \ln \left( \frac{\Lambda^3(\sigma) \rho f(\sigma)}{E[f]} \right) - \frac{\rho}{E[f]} \frac{\delta E[f]}{\delta \rho f(\sigma)} + \int d\sigma' \varphi(\sigma, \sigma') \rho f(\sigma'). \quad (4.5)$$

From the Maxwell relations (3.16) and (3.19) we calculate the pressure

$$\begin{aligned} \beta p &= \rho \left( \frac{\partial A^+}{\partial \rho} \right)_{T, N} - A^+ \\ &= \int_0^\infty \mu(\sigma, [f]) \rho f(\sigma) d\sigma - A^+ \end{aligned}$$

and obtain for the pressure within the vdW approximation [19]

$$\beta p([f]) = \rho \left( 1 - \frac{\rho}{E[f]} \int_0^\infty f(\sigma) \frac{\delta E[f]}{\delta \rho f(\sigma)} \right) + \frac{1}{2} \beta \int_0^\infty d\sigma \int_0^\infty d\sigma' \varphi(\sigma, \sigma') \rho f(\sigma) \rho f(\sigma'), \quad (4.6)$$

where we have kept the expressions for the chemical potential (4.5) and the pressure (4.6) in a general form, what means we have not used explicitly (4.2).

We have extended the vdW approach to the case of a HS system with a vdW attraction by substituting the excluded volume correction  $E[f]$  by

$$E[f] = e^{-\frac{\beta A_{ex}^{HS}[f]}{N}}, \quad (4.7)$$

where  $A_{ex}^{HS}[f]$  is the excess Helmholtz free energy of the HS system [12].

## 4.2 Thermodynamic perturbation theories

The intermolecular pair potential can in many cases be separated in a natural way into a hard, short-range repulsion  $\phi_0(r, \sigma_i, \sigma_j)$  and a smoothly varying long-range attraction  $\phi_1(r, \sigma_i, \sigma_j)$

$$\phi(r, \sigma_i, \sigma_j) = \phi_0(r, \sigma_i, \sigma_j) + \phi_1(r, \sigma_i, \sigma_j). \quad (4.8)$$

This separation expresses the influence of the respective contribution of the potential to the structure: it is now generally accepted that the structure of simple liquids, at least at high density, is largely determined by geometric factors associated with the packing of the particles; in contrast, the attractive interactions may, in a first approximation, be regarded as giving rise to a uniform background potential, that provides the cohesive energy of the liquid, but has little effects on its structure. In this way, the properties of a given liquid can be related (in good approximation) to those of a HS reference system, the attractive part of the potential being treated as a perturbation to the former.

The thermodynamic perturbation theory approach has its basis in the vdW equation, where we consider liquids as systems of HS moving in a uniform, attractive potential well. The vdW equation of state (4.6), proposed in the last section, is not a very exact approximation, especially for higher densities. Below we shortly discuss some perturbation theory methods (see [26]) that may be regarded as attempts to improve the theory of van der Waals in a systematic fashion. The methods we describe have as a main ingredient the assumption that the structure of a dense, polydisperse fluid resembles that of a polydisperse assembly of hard spheres. For many simple liquids this restriction is a good approximation, but particularly in the critical region the perturbation theory fails, because the role of the attractive forces gets more important due to the critical fluctuations of the system at all length scales, and the simple vdW model no longer has a sound physical basis.

If the potential (4.8) splits in two parts, the calculation then proceeds as follows, if the reference system is a HS system. One computes the effect of the perturbation (quantities characterized with index 1) on the thermodynamic properties and pair distribution functions of the reference system (index 0). This can be done systematically via an ex-

pansion in powers, either of inverse temperature (the ' $\lambda$ -expansion'), or of a parameter that measures the range of the perturbation (the ' $\gamma$ -expansion').

### 4.2.1 The $\lambda$ -expansion

In the  $\lambda$ -expansion one introduces

$$\phi_\lambda(r, \sigma_i, \sigma_j) = \phi_0(r, \sigma_i, \sigma_j) + \lambda\phi_1(r, \sigma_i, \sigma_j), \quad (4.9)$$

where  $\lambda$  is a parameter that varies between 0 and 1 and  $\phi_0(r, \sigma_i, \sigma_j)$  will be throughout a HS potential. When  $\lambda = 0$ ,  $\phi_\lambda(r, \sigma_i, \sigma_j)$  reduces to the potential of a reference system whose properties are known, whereas for  $\lambda = 1$  the potential is the one that characterizes the system of interest. The quantity  $\lambda$  has the meaning of a *coupling* parameter: the effect of varying  $\lambda$  continuously from 0 to 1 is that of gradually 'switching on' the perturbation  $\phi_1(r, \sigma_i, \sigma_j)$ . With (4.9) the total potential energy is given as

$$V_N(\lambda, r_1, \dots, r_N, \sigma_1, \dots, \sigma_N) = \frac{1}{2} \sum_{i=1}^N \sum_{j \neq i}^N \phi_\lambda(r_{ij}, \sigma_i, \sigma_j), \quad (4.10)$$

where the indices  $i, j$  denote the interacting particle pair with particle diameters  $\sigma_i, \sigma_j$ . Using the configurational integral (3.6) together with the definition of the excess free energy (3.14), we can calculate the derivative of  $A_{ex}(\lambda)$  with respect to the coupling parameter  $\lambda$

$$\frac{\partial A_{ex}}{\partial \lambda} = \langle V'_N(\lambda) \rangle_\lambda,$$

where  $V'_N(\lambda) = \frac{\partial V_N(\lambda)}{\partial \lambda}$ , and the brackets denote the canonical ensemble average for a system characterized by the potential (4.9). By integration of the last expression with respect to  $\lambda$ , one can write for the excess free energy

$$\begin{aligned} \frac{\beta A_{ex}(\lambda = 1)}{N} &= \frac{\beta A_{0;ex}}{N} + \frac{\beta}{N} \int_0^1 \langle V'_N(\lambda) \rangle_\lambda d\lambda \\ &= \frac{\beta A_{0;ex}}{N} + \frac{\beta}{2N} \int_0^\infty d\sigma_i f(\sigma_i) \int_0^\infty d\sigma_j f(\sigma_j) \times \\ &\quad \int_0^1 d\lambda \int g_\lambda(r, \sigma_i, \sigma_j) \phi_1(r, \sigma_i, \sigma_j) d^3r, \end{aligned} \quad (4.11)$$

where  $A_{0;ex} = A_{ex}(\lambda = 0)$  is the excess free energy of the HS reference system, and  $g_\lambda(r, \sigma_i, \sigma_j)$  is the radial pair distribution function of the system with the pair potential  $\phi_\lambda(r, \sigma_i, \sigma_j)$ . Since  $g_\lambda(r, \sigma_i, \sigma_j)$  cannot be calculated directly, we have to make an approximation. We make a Taylor series expansion of  $\langle V'_N(\lambda) \rangle_\lambda$  around  $\lambda = 0$  and insert the

result of this expansion in (4.11). Then we obtain, together with

$$\phi_N(r_1, \dots, r_N; \sigma_1, \dots, \sigma_N) = \frac{1}{2} \sum_{i=1}^N \sum_{j \neq i}^N \phi_1(r_{ij}, \sigma_i, \sigma_j),$$

a Taylor expansion of (4.11) in terms of  $\lambda$  (if the reference system is a HS system the expansion reduces to a Taylor series in  $\beta$  [26])

$$\begin{aligned} \beta A_{ex} &= \beta A_{0;ex} + \beta \langle \phi_N \rangle_0 - \frac{1}{2} \beta^2 (\langle \phi_N^2 \rangle_0 - \langle \phi_N \rangle_0^2) + O(\beta^3) \\ &= \beta A_{0;ex} + \beta \frac{N\rho}{2} \int_0^\infty d\sigma_i f(\sigma_i) \int_0^\infty d\sigma_j f(\sigma_j) \int g_0(r, \sigma_i, \sigma_j) \phi_1(r, \sigma_i, \sigma_j) d^3r \\ &\quad + O(\beta^2), \end{aligned} \tag{4.12}$$

where  $\phi_N$  is the total perturbation energy, and  $g_0(r, \sigma_i, \sigma_j)$  is the radial pair distribution function of the HS reference system. The brackets denote a statistical average evaluated in the reference-system ensemble. It can be shown [26], that already the second order term in  $\beta$  in (4.12) requires a knowledge of the three and four-particle distribution functions of the reference system. Hence in general expansion (4.12) is truncated after the first order term in  $\beta$  (high temperature approximation (HTA)), that means no correction of the structure of the fluid due to the perturbation are made in this approximation.

## 4.2.2 The $\gamma$ -expansion

Situations in which the influence of the attractive forces on the structure cannot be ignored may be treated by methods similar to those used when the perturbation is both weak and very long ranged relative to the reference potential. In such cases, the natural expansion parameter for the free energy  $A$  is the inverse range rather than the strength of the perturbation potential. This leads to the so called  $\gamma$  expansion [26].

As a consequence of the separation of the pair potential  $\phi(r, \sigma_i, \sigma_j)$  in (4.8), we can split the free energy  $A$  into a reference-part ( $A_0$ ) and into a perturbation-part ( $A_1$ ). The perturbation-part of the free energy depends on the direct correlation function  $c_1(r, \sigma_i, \sigma_j)$ , where we have assumed the approximation

$$c(r, \sigma_i, \sigma_j) = c_0(r, \sigma_i, \sigma_j) + c_1(r, \sigma_i, \sigma_j) \sim c_0(r, \sigma_i, \sigma_j) - \beta \phi_1(r, \sigma_i, \sigma_j). \tag{4.13}$$

After some simplifying approximations [26] and the restriction to certain terms within the  $\gamma$  expansion, we arrive at the following expression for the free energy

$$A \simeq A_0 + A_{HTA} + A_{RPA}. \tag{4.14}$$

Equation (4.14) gives the approximation for the free energy within the so called random phase approximation (RPA);  $A_{RPA}$  is the energy correction, which in addition to  $A_{HTA}$ ,

occurs in presence of the perturbation potential  $\phi_1(r, \sigma_i, \sigma_j)$ . As we can see from (4.14) the free energy within the RPA goes one step behind the HTA (4.12) in accuracy. The corresponding approximation of the radial pair distribution functions  $g(r, \sigma_i, \sigma_j)$  can be obtained from (3.6) together with (3.14) as the functional derivatives of  $A$  with respect to  $\phi_1(r, \sigma_i, \sigma_j)$

$$-\frac{\delta \ln Z_N(V, T)}{\beta \delta \phi_1(r, \sigma_i, \sigma_j)} = \frac{\delta A[\phi_1]}{\delta \phi_1(r, \sigma_i, \sigma_j)} = \frac{1}{2} \rho^2 g(r, \sigma_i, \sigma_j), \quad (4.15)$$

where  $A$  is a functional of  $\phi_1(r, \sigma_i, \sigma_j)$ . The functional derivative of  $A_{HTA}$  with respect to the perturbation potential  $\phi_1(r, \sigma_i, \sigma_j)$  gives the radial pair distribution function of the reference system, while the functional derivative of  $A_{RPA}$  gives the correction  $g_1(r, \sigma_i, \sigma_j)$  of the radial pair distribution function caused by the perturbation potential. So we can write the approximation for the radial pair distribution function within the RPA as

$$g(r, \sigma_i, \sigma_j) \simeq g_0(r, \sigma_i, \sigma_j) + g_1(r, \sigma_i, \sigma_j). \quad (4.16)$$

As we will show in one of the following sections one can find closed expressions for  $A_{RPA}$ , and  $\tilde{g}(k, \sigma_i, \sigma_j)$ .

The structure functions of the system within the RPA are, in comparison to the HTA, changed in presence of the perturbation, i.e., they are different from the structure functions of the HS reference system. But the RPA has a fundamental drawback: Due to the presence of hard cores,  $g(r, \sigma_i, \sigma_j)$  has to vanish for  $r < \hat{\sigma}$ ; in the approximation (4.13) there is no guarantee that this will be the case, since in general  $g_1(r, \sigma_i, \sigma_j)$  will be non-zero in that range. This means, that geometrical exclusion effects are not treated correctly. On the other hand, in this framework, there is a flexibility in the choice of  $\phi_1(r, \sigma_i, \sigma_j)$ , that can be usefully exploited. For the physically inaccessible region for  $r < \hat{\sigma}$ , the perturbation of the pair potential can be chosen to have any finite functional form. Thus the perturbing potential  $\phi_1(r, \sigma_i, \sigma_j)$  inside the core ( $r < \hat{\sigma}$ ) can be varied without changing the properties of the fluid, to obtain the so called optimized potential. That means that the unphysical behavior of the RPA can be eliminated by choosing  $\phi_1(r, \sigma_i, \sigma_j)$ , respectively  $c_1(r, \sigma_i, \sigma_j)$  for  $r < \hat{\sigma}$  in such a way, that

$$g_1(r, \sigma_i, \sigma_j) = 0, \quad r < \hat{\sigma}.$$

One can show, that this condition is equivalent to the functional derivative (4.15)

$$\frac{\delta A_{RPA}[\phi_1]}{\delta \phi_1(r, \sigma_i, \sigma_j)} = \frac{1}{2} \rho^2 g_1(r, \sigma_i, \sigma_j) = 0, \quad r < \hat{\sigma}. \quad (4.17)$$

In other words, the core condition is equivalent to the requirement that the RPA free energy is stationary with respect to variations in the perturbing potential inside the core.

The RPA together with the condition (4.17) is called the “optimized” random-phase approximation (ORPA). The ORPA may equally well be viewed as a solution to the Ornstein-Zernike relation, that satisfies both, the closure approximation (4.13) and the core condition  $g(r, \sigma_i, \sigma_j) = 0$  for  $r < \hat{\sigma}$ .

### 4.2.3 ORPA, mean spherical approximation for a polydisperse system

There are a variety of model fluids of interest in the theory of liquids for which the pair potential consists of a HS interaction plus an attractive tail, because the mathematical and numerical methods for hard core systems are easier to implement as compared for example with soft core systems (see for instance [40]). Hard core systems, which include both the ‘square-well’ and dipolar HS fluids, have been widely studied in the mean field-spherical approximation (MSA). The name has its origin in the fact that the approximation was first proposed by Lebowitz and Percus [39] as a generalization of the mean-spherical model for Ising spin systems, although the MSA is distinct from the Ising model.

The MSA, applied to systems with a hard core and an adjacent attractive potential, is given in terms of the radial pair distribution functions and direct correlation functions by

$$\begin{aligned} g(r, \sigma_i, \sigma_j) &= 0 && ; r < \hat{\sigma} \\ c(r, \sigma_i, \sigma_j) &= -\beta\phi_1(r, \sigma_i, \sigma_j) && ; r \geq \hat{\sigma}. \end{aligned} \quad (4.18)$$

Together with the OZ relation these expressions yield an integral equation for  $g(r, \sigma_i, \sigma_j)$  respectively for  $c(r, \sigma_i, \sigma_j)$ . The first expression in (4.18) is exact, while the second extends the asymptotic behavior of  $c(r, \sigma_i, \sigma_j)$  to all  $r \geq \hat{\sigma}$  and is clearly an approximation. Despite the approximation for the direct correlation functions the MSA gives good results in many cases [26]. For example, it provides a much better description of the properties of the square-well fluid than is given by the Percus Yevick (PY) approximation

$$c(r, \sigma_i, \sigma_j) = f(r, \sigma_i, \sigma_j) + f(r, \sigma_i, \sigma_j)[h(r, \sigma_i, \sigma_j) - c(r, \sigma_i, \sigma_j)], \quad (4.19)$$

although the MSA closure is obtained by linearization of (4.19). However, the most attractive feature of the MSA is the fact that the integral equations can be solved analytically for a number of potential models of physical interest including simple models of electrolyte solutions and of polar fluids [26]. The PY equation for hard spheres is a special case of the MSA when the tail in the potential is absent. The MSA was extended to the binary HS system by Lebowitz [31] and then to the polydisperse HS system by Blum and Stell [3].

The MSA can also be extended to a more general class of pair potentials of the form given by (4.8), where the reference potential is conventionally the HS potential. For this potentials the solution of the OZ equation together with the relations (4.18) become formally identical to the ORPA. For the reference system one then uses the PY solution for HS [3], whereas the second expression of equation (4.18) is the ansatz of the ORPA for  $c_1(r, \sigma_i, \sigma_j)$  outside the core. To improve the quality of the solution, thermodynamic properties for the reference HS system are being calculated using the Mansoori, Carnahan, Starling and Leland [35] equation of state.

#### 4.2.3.1 Structure of a polydisperse system

In application of the last section, we develop now the structure and thermodynamic quantities for a polydisperse system within the ORPA (see [12, 18]). We start with the separation of the correlation functions into reference and perturbation part as proposed in (4.16) and (4.13). The two sets of correlation functions have to fulfill the OZ equations (3.2)

$$\tilde{h}_0(k, \sigma_i, \sigma_j) = \tilde{c}_0(k, \sigma_i, \sigma_j) + \rho \int_0^\infty f(\sigma_l) d\sigma_l \tilde{h}_0(k, \sigma_i, \sigma_l) \tilde{c}_0(k, \sigma_l, \sigma_j) \quad (4.20)$$

$$\tilde{h}(k, \sigma_i, \sigma_j) = \tilde{c}(k, \sigma_i, \sigma_j) + \rho \int_0^\infty f(\sigma_l) d\sigma_l \tilde{h}(k, \sigma_i, \sigma_l) \tilde{c}(k, \sigma_l, \sigma_j). \quad (4.21)$$

Since the reference system are HS, the  $g(r, \sigma_i, \sigma_j)$  have to be zero inside the core:

$$g_0(r, \sigma_i, \sigma_j) = 0 \quad \text{and} \quad g_1(r, \sigma_i, \sigma_j) = 0 \quad \text{for} \quad r < \hat{\sigma}.$$

The closure relation for the (O)RPA (4.13) reads

$$c_1(r, \sigma_i, \sigma_j) = -\beta\phi_1(r, \sigma_i, \sigma_j) \quad \forall r. \quad (4.22)$$

As we have already discussed in the last section, equation (4.22) together with the OZ equations (4.21), do not lead to the correct behavior of  $g(r, \sigma_i, \sigma_j)$  inside the core region  $r < \hat{\sigma}$ . To avoid this problem, we solve the OZ equations (4.21) within the ORPA by use of the functional derivative (4.17), where we have to rewrite the closure relation (4.22) and the core condition as

$$\begin{aligned} c_1(r, \sigma_i, \sigma_j) &= \begin{cases} ? & ; r < \hat{\sigma} \\ -\beta\phi_1(r, \sigma_i, \sigma_j) & ; r \geq \hat{\sigma} \end{cases} \\ g_1(r, \sigma_i, \sigma_j) &= \begin{cases} 0 & ; r < \hat{\sigma} \\ ? & ; r \geq \hat{\sigma} \end{cases}. \end{aligned} \quad (4.23)$$

### 4.2.3.1.1 Solution of the OZ equations using orthogonal polynomials

To solve the OZ equations (4.20) and (4.21) for the direct correlation functions  $\tilde{c}(k, \sigma_i, \sigma_j)$ , we have to calculate the integral over  $\sigma$ . This can for instance be done by introducing orthogonal polynomials, which are associated to the distribution function  $f(\sigma)$  [9]:

$$\int_0^\infty d\sigma f(\sigma) p_i(\sigma) p_j(\sigma) = \delta_{ij},$$

where  $\delta_{ij}$  is the Kronecker delta function and  $p_0(\sigma) = 1$ . For some choices of  $f(\sigma)$ , such as the Schulz (or  $\Gamma$ ) distribution used below,  $p_i(\sigma)$  are known explicitly. In other cases, these polynomials must be constructed numerically; this can be done using the Gram-Schmidt algorithm, starting from  $p_0(\sigma) = 1$ . Now all  $\sigma$ -dependant functions can be expanded in such a way that [9]

$$\begin{aligned} x(r; \sigma) &= \sum_{j=0}^{\infty} x_j(r) p_j(\sigma); \\ y(r, \sigma_1, \sigma_2) &= \sum_{i,j=0}^{\infty} y_{ij}(r) p_i(\sigma_1) p_j(\sigma_2), \end{aligned} \quad (4.24)$$

where the coefficients are given by

$$\begin{aligned} x_i(r) &= \int_0^\infty d\sigma f(\sigma) x(r, \sigma) p_i(\sigma) \\ y_{ij}(r) &= \int_0^\infty d\sigma_1 f(\sigma_1) \int_0^\infty d\sigma_2 f(\sigma_2) y(r, \sigma_1, \sigma_2) p_i(\sigma_1) p_j(\sigma_2). \end{aligned} \quad (4.25)$$

There are analogous relations valid in  $k$  space. If we use the OZ equations (4.21) together with (4.24) in  $k$  space and the orthogonality relation, we obtain [12]

$$\tilde{h}_{lm}(k) = \tilde{c}_{lm}(k) + \rho \sum_t \tilde{h}_{lt}(k) \tilde{c}_{tm}(k), \quad (4.26)$$

where this can be written as a matrix equation for the expansion coefficients

$$\begin{aligned} \tilde{H}(k) &= \tilde{C}(k) + \rho \tilde{H}(k) \tilde{C}(k) \\ (\mathbb{I} + \rho \tilde{H}(k)) &= (\mathbb{I} - \rho \tilde{C}(k))^{-1}. \end{aligned} \quad (4.27)$$

We have denoted the coefficients for the orthogonal polynomial expansion of the direct and total correlation functions  $c(r, \sigma_i, \sigma_j)$  and  $h(r, \sigma_i, \sigma_j)$  by  $c_{lm}(r)$  and  $h_{lm}(r)$  (and similarly for their Fourier transforms, with an additional tilde). The uppercase  $\tilde{C}(k)$  and  $\tilde{H}(k)$  in (4.27) characterize matrices with the elements  $\tilde{c}_{lm}(k)$  and  $\tilde{h}_{lm}(k)$ ;  $\mathbb{I}$  stands for the unity matrix.

Equivalent relations, as in (4.27), are valid for the reference OZ equation (4.20)

$$\begin{aligned}\tilde{H}_0(k) &= \tilde{C}_0(k) + \rho \tilde{H}_0(k) \tilde{C}_0(k) \\ (\mathbb{I} + \rho \tilde{H}_0(k)) &= (\mathbb{I} - \rho \tilde{C}_0(k))^{-1}.\end{aligned}\quad (4.28)$$

We take now the OZ equation (4.26) and split the coefficients  $\tilde{c}_{lm}(k)$  and  $\tilde{h}_{lm}(k)$ , as proposed in (4.16) and (4.13), into reference (index 0) and perturbation (index 1) part. We then obtain [12]

$$\tilde{h}_{lm;1}(k) = \tilde{c}_{lm;1} + \rho \sum_t \left( \tilde{h}_{lt;1}(k) \tilde{c}_{tm;1}(k) + \tilde{h}_{lt;1}(k) \tilde{c}_{tm;0}(k) + \tilde{h}_{lt;0}(k) \tilde{c}_{tm;1}(k) \right) \quad (4.29)$$

which corresponds to the matrix relation

$$\tilde{H}_1(k) = \tilde{C}_1(k) + \rho \left( \tilde{H}_1(k) \tilde{C}_1(k) + \tilde{H}_1(k) \tilde{C}_0(k) + \tilde{H}_0(k) \tilde{C}_1(k) \right), \quad (4.30)$$

where  $\tilde{H}_1(k)$ ,  $\tilde{H}_0(k)$ ,  $\tilde{C}_0(k)$  and  $\tilde{C}_1(k)$  are matrices with the elements  $\tilde{h}_{lm;1}(k)$ ,  $\tilde{h}_{lm;0}(k)$ ,  $\tilde{c}_{lm;0}(k)$  and  $\tilde{c}_{lm;1}(k)$ . If we solve equation (4.30) for the correction of the total correlation functions,  $\tilde{h}_{lm;1}(k)$ , occurring in presence of a perturbation potential,  $\phi_{lm;1}(r)$ , we arrive at the so called residual OZ equation

$$\tilde{H}_1(k) = \tilde{G}_1(k) = \left[ \mathbb{I} + \rho \tilde{H}_0(k) \right] \tilde{C}_1(k) \left( \left[ \mathbb{I} + \rho \tilde{H}_0(k) \right]^{-1} - \rho \tilde{C}_1(k) \right)^{-1}. \quad (4.31)$$

With the help of the orthogonal polynomial expansion the number-number structure-factor  $S(k)$  (3.10) can now be rewritten as follows [9]

$$\begin{aligned}S(k) &= 1 + \rho \int_0^\infty d\sigma_i f(\sigma_i) \int_0^\infty d\sigma_j f(\sigma_j) \tilde{h}(k, \sigma_i, \sigma_j) \\ &= 1 + \rho \tilde{h}_{00}(k) = S_0(k) + \rho \tilde{h}_{00;1}(k),\end{aligned}\quad (4.32)$$

where  $S_0(k)$  is the number-number structure factor of the reference system and the perturbation  $\tilde{h}_{00;1}(k)$  has to be calculated numerically within the ORPA.

#### 4.2.3.1.2 Functional of the polydisperse fluid

The core condition and the closure relation (4.23) can now be extended to the coefficients  $c_{lm;1}(r)$  and  $g_{lm;1}(r)$  as follows [18]

$$\begin{aligned}g_{lm}(r) = g_{lm;1}(r) &= 0 & r < \hat{\sigma} \\ c_{lm;1}(r) &= -\beta \phi_{lm;1}(r) & r \geq \hat{\sigma}.\end{aligned}\quad (4.33)$$

Within the RPA one can calculate the functional  $-\frac{\beta A_{RPA}}{V} = F[\tilde{C}_1]$ , which is defined as [18]

$$F[\tilde{C}_1] = -\frac{1}{2} \left( \frac{1}{2\pi} \right)^3 \int d^3k \left\{ \text{Tr} \left( \{ \mathbb{I} + \rho \tilde{H}_0(k) \} \rho \tilde{C}_1(k) \right) + \ln \left[ \det \left( \mathbb{I} - \{ \mathbb{I} + \rho \tilde{H}_0(k) \} \rho \tilde{C}_1(k) \right) \right] \right\}, \quad (4.34)$$

where Tr denotes the trace of a matrix and det its determinant. Using the ORPA, the correlation functions  $\tilde{c}_{lm;1}(k)$  in  $F[\tilde{C}_1]$  have to be fitted in such a way, as to fulfill the core condition in (4.33). This means, in generalization of (4.17) to the coefficients, that the functional  $F[C_1]$  has to be an extremum with respect to variations of  $-\beta\phi_{lm;1}(r) = c_{lm;1}(r)$  inside the core

$$\frac{\delta F[C_1]}{\delta c_{lm;1}(r)} = \frac{\rho^2}{2} g_{lm;1}(r) = 0 \quad r < \hat{\sigma}. \quad (4.35)$$

This reads in  $k$ -space

$$\frac{\delta F[\tilde{C}_1]}{\delta \tilde{c}_{lm;1}(k)} = \frac{\rho^2}{2(2\pi)^3} \tilde{g}_{lm;1}(k). \quad (4.36)$$

One can show that the functional  $F[C_1]$  is a convex functional of  $c_{lm;1}(r)$  i.e., it has exactly one extremum, which represents its unique solution [15].

### 4.2.3.2 Thermodynamics of a polydisperse system

In chapter 3 we have already developed thermodynamic expressions for the internal energy, the free energy, the pressure, the chemical potential and the isothermal compressibility for a polydisperse system. While for the expressions of the internal energy  $U$  and the isothermal compressibility  $\chi_T$  we have only to evaluate the integrals in (3.11) and (3.22) by use of (4.24), the expressions for the pressure  $p$ , the free energy  $A$  and the chemical potential  $\mu(\sigma)$ , based on the ORPA formalism, will be derived in the following subsections.

#### 4.2.3.2.1 Internal energy $U$

For the internal energy we have obtained equation (3.11)

$$\beta U_{ex} = \frac{N\rho}{2} \int d^3r \int_0^\infty d\sigma_1 f(\sigma_1) \int_0^\infty d\sigma_2 f(\sigma_2) \beta \phi(r, \sigma_1, \sigma_2) g(r, \sigma_1, \sigma_2).$$

With the help of the orthogonal polynomial expansion we can now eliminate the integrals over  $\sigma$  to get [18]

$$\beta U_{ex} = 2\pi N\rho \int_0^\infty dr r^2 \sum_{l,m} \beta \phi_{lm;1}(r) g_{lm}(r). \quad (4.37)$$

### 4.2.3.2.2 Virial pressure $P$

The calculation of the virial pressure (3.13) requires derivatives of the potential  $\phi(r, \sigma_i, \sigma_j)$  with respect to  $r$ , - for the case of the HS reference potential - the problems with the jumps in  $g(r, \sigma_i, \sigma_j)$  and in  $\phi'(r, \sigma_i, \sigma_j)$  can be circumvented by introducing the function  $y(r, \sigma_i, \sigma_j)$  (we have done this in chapter 3), which must be a continuous function. The ORPA violates this condition and  $y(r, \sigma_i, \sigma_j)$  is never a continuous function, it turns out that  $y(r, \sigma_i, \sigma_j)$  is discontinuous where the potential  $\phi(r, \sigma_i, \sigma_j)$  contains discontinuities [40]. In the following we will derive an expression, which can cope with such a discontinuity in general (see [40]).

At first we have to rewrite those parts of the integral (3.13), which are concerned. Let us assume, that  $y(r, \sigma_i, \sigma_j)$  (and hence  $\phi(r, \sigma_i, \sigma_j)$ ) have discontinuities at  $r = \gamma_m$  ( $m = 1, \dots, p$ ) outside the core region ( $r > \hat{\sigma}$ ) and that these functions are continuous elsewhere. We start from equation (3.13)

$$\begin{aligned} p_{ex} &= \frac{2\pi}{3} \frac{\rho^2}{\beta} \underbrace{\int_0^\infty dr r^3 \int_0^\infty d\sigma_i f(\sigma_i) \int_0^\infty d\sigma_j f(\sigma_j) \frac{d}{dr} e^{-\beta\phi(r, \sigma_i, \sigma_j)} y(r, \sigma_i, \sigma_j)}_I \\ &= \frac{2\pi}{3} \frac{\rho^2}{\beta} (I^S + I^D), \end{aligned}$$

where the integral  $I$  splits into two parts,  $I^S$  and  $I^D$ . The integral  $I^S$  consists of all the continuous parts of  $I$  and is defined as [12]

$$I^S = \int_0^\infty d\sigma_i f(\sigma_i) \int_0^\infty d\sigma_j f(\sigma_j) \hat{\sigma}^3 g(\hat{\sigma}^+, \sigma_i, \sigma_j), \quad (4.38)$$

whereas, the integral  $I^D$  takes into account the  $p$  jumps contained in the integrand of  $I$ :

$$I^D = \sum_{m=1}^p I_m^D,$$

where  $I_m^D$  is the integral across the  $m$ th discontinuity

$$\begin{aligned} I_m^D &= \int_{\gamma_m^-}^{\gamma_m^+} dr r^3 \int_0^\infty d\sigma_i f(\sigma_i) \int_0^\infty d\sigma_j f(\sigma_j) y(r, \sigma_i, \sigma_j) \frac{de(r, \sigma_i, \sigma_j)}{dr} \\ &= \int_{\gamma_m^-}^{\gamma_m^+} dr r^3 \int_0^\infty d\sigma_i f(\sigma_i) \int_0^\infty d\sigma_j f(\sigma_j) g(r, \sigma_i, \sigma_j) \frac{d \ln e(r, \sigma_i, \sigma_j)}{dr} \\ &= \int_{\gamma_m^-}^{\gamma_m^+} dr r^3 \int_0^\infty d\sigma_i f(\sigma_i) \int_0^\infty d\sigma_j f(\sigma_j) g(r, \sigma_i, \sigma_j) \frac{dc_1(r, \sigma_i, \sigma_j)}{dr}, \quad (4.39) \end{aligned}$$

where we have used the ORPA closure and introduced

$$e^{-\beta\phi(r, \sigma_i, \sigma_j)} = e(r, \sigma_i, \sigma_j).$$

Now we define  $c_1(r, \sigma_i, \sigma_j)$  near the discontinuity [40]

$$c_1(r, \sigma_i, \sigma_j) = \epsilon_0(\sigma_i, \sigma_j) + \Delta\epsilon(\sigma_i, \sigma_j)\Theta(r - x),$$

where  $\epsilon_0(\sigma_i, \sigma_j) = c_1(\gamma_m^-, \sigma_i, \sigma_j)$  and  $\epsilon_1(\sigma_i, \sigma_j) = \epsilon_0(\sigma_i, \sigma_j) + \Delta\epsilon(\sigma_i, \sigma_j) = c_1(\gamma_m^+, \sigma_i, \sigma_j)$ . Using this ansatz for  $c_1(r, \sigma_i, \sigma_j)$ , we introduce a continuous function  $\hat{g}(r, \sigma_i, \sigma_j)$  at  $\gamma_m$ : from the OZ equation we know that  $g(r, \sigma_i, \sigma_j) - c(r, \sigma_i, \sigma_j)$  is a convolution and therefore continuous:

$$\hat{g}(r, \sigma_i, \sigma_j) = g(r, \sigma_i, \sigma_j) - c_1(r, \sigma_i, \sigma_j). \quad (4.40)$$

Inserting (4.40) into equation (4.39) leads to

$$\begin{aligned} I_m^D &= \int_{\gamma_m^-}^{\gamma_m^+} dr r^3 \int_0^\infty d\sigma_i f(\sigma_i) \int_0^\infty d\sigma_j f(\sigma_j) [\hat{g}(r, \sigma_i, \sigma_j) + c_1(r, \sigma_i, \sigma_j)] \frac{dc_1(r, \sigma_i, \sigma_j)}{dr} \\ &= \int_0^\infty d\sigma_i f(\sigma_i) \int_0^\infty d\sigma_j f(\sigma_j) \left( \int_{\gamma_m^-}^{\gamma_m^+} dr r^3 \hat{g}(r, \sigma_i, \sigma_j) \frac{dc_1(r, \sigma_i, \sigma_j)}{dr} \right. \\ &\quad \left. + \frac{1}{2} \int_{\gamma_m^-}^{\gamma_m^+} dr r^3 \frac{dc_1^2(r, \sigma_i, \sigma_j)}{dr} \right). \end{aligned}$$

Now we can integrate over  $r$  and use  $\Theta^2(r - x) = \Theta(r - x)$  to get

$$I_m^D = \gamma_m^3 \left( \hat{g}(\gamma_m, \sigma_i, \sigma_j) + \frac{2\epsilon_0(\sigma_i, \sigma_j)\Delta\epsilon + \Delta\epsilon^2(\sigma_i, \sigma_j)}{2} \right). \quad (4.41)$$

We can replace  $\hat{g}(r, \sigma_i, \sigma_j)$  with the left- and right-side limit of  $g(r, \sigma_i, \sigma_j)$

$$\begin{aligned} g(\gamma_m^-, \sigma_i, \sigma_j) &= \hat{g}(\gamma_m, \sigma_i, \sigma_j) + \epsilon_0(\sigma_i, \sigma_j) \\ g(\gamma_m^+, \sigma_i, \sigma_j) &= \hat{g}(\gamma_m, \sigma_i, \sigma_j) + \epsilon_0(\sigma_i, \sigma_j) + \Delta\epsilon(\sigma_i, \sigma_j), \end{aligned}$$

to eliminate  $\epsilon_0(\sigma_i, \sigma_j)$  from equation (4.41)

$$\hat{g}(\gamma_m^+, \sigma_i, \sigma_j) = \frac{g(\gamma_m^-, \sigma_i, \sigma_j) - \epsilon_0(\sigma_i, \sigma_j) + g(\gamma_m^+, \sigma_i, \sigma_j) - \epsilon_0(\sigma_i, \sigma_j) - \Delta\epsilon(\sigma_i, \sigma_j)}{2},$$

so finally the integral  $I_m^D$  evaluates to

$$I_m^D = \frac{1}{2} \int_0^\infty d\sigma_i f(\sigma_i) \int_0^\infty d\sigma_j f(\sigma_j) \gamma_m^3 \Delta\epsilon(\sigma_i, \sigma_j) [g(\gamma_m^-, \sigma_i, \sigma_j) + g(\gamma_m^+, \sigma_i, \sigma_j)].$$

Together with the integral  $I^S$  the virial pressure then becomes [12, 18]

$$\begin{aligned} \frac{\beta p^v}{\rho} &= 1 + \frac{2\pi}{3} \rho \int_0^\infty d\sigma_i f(\sigma_i) \int_0^\infty d\sigma_j f(\sigma_j) \times \\ &\quad \left( \hat{\sigma}^3 g(\hat{\sigma}^+, \sigma_i, \sigma_j) + \frac{1}{2} \sum_{m=1}^p \gamma_m^3 \Delta\epsilon(\sigma_i, \sigma_j) [g(\gamma_m^-, \sigma_i, \sigma_j) + g(\gamma_m^+, \sigma_i, \sigma_j)] \right), \end{aligned} \quad (4.42)$$

where the location of the jumps  $\gamma_m$  are depending on the perturbation potential  $\phi_1(r; \sigma_i, \sigma_j)$ . For the square well potential ( $p = 1$ ) we obtain

$$\gamma_1 = \lambda(\sigma_i, \sigma_j) \hat{\sigma}$$

and for the potential depth

$$\Delta\epsilon(\sigma_i, \sigma_j) = -\beta\epsilon(\sigma_i, \sigma_j),$$

whereas for the Yukawa potential ( $p = 1$ ) the jump is located at

$$\gamma_1 = \hat{\sigma}.$$

with the jump height

$$\Delta\epsilon(\sigma_i, \sigma_j) = c_1(\hat{\sigma}^+, \sigma_i, \sigma_j) - c_1(\hat{\sigma}^-, \sigma_i, \sigma_j),$$

which can be calculated only numerically.

#### 4.2.3.2.3 Helmholtz free energy $A$

The free energy  $A$  is calculated from

$$A = A_0 + A_1,$$

where  $A_0$  is the free energy of the reference system, and  $A_1$  is the free energy due to the perturbation. We assume that the free energy of the reference system (in our case a hard-sphere system) is known [4]. The perturbation free energy  $A_1$  is calculated using equation (3.18):

$$\frac{A_1(T_1)}{T_1} - \frac{A_1(T_0)}{T_0} = \int_{\frac{1}{T_0}}^1 T_1 d\frac{1}{T} U_p(T),$$

where  $U_p$  is the internal energy due to the perturbation potential. By setting  $T_0$  to  $\infty$  (ideal gas),  $T_1$  to the actual temperature and substituting  $\lambda = \frac{T_1}{T}$ , we get [40]

$$\frac{A_1}{T_1} = \frac{1}{T} \int_0^1 d\lambda U_p(\lambda),$$

where  $U_p(\lambda)$  corresponds to (3.11) except, that the  $g(r, \sigma_i, \sigma_j)$  are now depending on the coupling parameter  $\lambda$ :

$$A_1 = \frac{\rho N}{2} \int_0^\infty d\sigma_i f(\sigma_i) \int_0^\infty d\sigma_j f(\sigma_j) \int_0^1 d\lambda \int d^3r g_\lambda(r, \sigma_i, \sigma_j) \phi_1(r, \sigma_i, \sigma_j). \quad (4.43)$$

This equation corresponds to the expression for  $A_1$  already found in the  $\lambda$  expansion (4.11), where  $g_\lambda(r, \sigma_i, \sigma_j)$  is the radial pair distribution function for a system that is

characterized by a potential  $\phi_\lambda(r, \sigma_i, \sigma_j)$  (4.9). Within the (O)RPA we split the radial pair distribution function  $g_\lambda(r, \sigma_i, \sigma_j)$  into

$$g_\lambda(r, \sigma_i, \sigma_j) = g_0(r, \sigma_i, \sigma_j) + g_{1;\lambda}(r, \sigma_i, \sigma_j).$$

Inserting this expression into (4.43) leads to

$$\begin{aligned} A_1 &= \frac{N\rho}{2} \int_0^\infty d\sigma_i f(\sigma_i) \int_0^\infty d\sigma_j f(\sigma_j) \left( \int d^3r \phi_1(r, \sigma_i, \sigma_j) g_0(r, \sigma_i, \sigma_j) \right. \\ &\quad \left. + \int_0^1 d\lambda \int d^3r \phi_1(r, \sigma_i, \sigma_j) g_{1;\lambda}(r, \sigma_i, \sigma_j) \right). \end{aligned} \quad (4.44)$$

The first term of this equation corresponds to the HTA (4.12). Using orthogonal polynomials this term can be rewritten as

$$A_{HTA} = 2\pi N\rho \int_0^\infty dr r^2 \sum_{l,m} \phi_{lm;1}(r) g_{lm;0}(r).$$

The second term in (4.44) can be simplified further, in the framework of the (O)RPA, by using the residual OZ equation (4.31). By use of the orthogonal polynomials we obtain for the second term, [12]

$$\begin{aligned} A_{RPA} &= \frac{\rho N}{2} \int d^3r \int_0^\infty d\sigma_i f(\sigma_i) \int_0^\infty d\sigma_j f(\sigma_j) \phi_1(r, \sigma_i, \sigma_j) \int_0^1 d\lambda g_{1;\lambda}(r, \sigma_i, \sigma_j) \\ &= \frac{N\rho}{2} \int d^3r \int_0^1 d\lambda \sum_{l,m} \phi_{lm;1}(r) g_{lm;1}(r, \lambda). \end{aligned} \quad (4.45)$$

With the closure  $\beta\phi_{lm;1}(r) = -c_{lm;1}(r)$  and Parseval's theorem, we get

$$A_{RPA} = -\frac{N\rho}{2\beta} \frac{1}{(2\pi)^3} \int d^3k \int_0^1 d\lambda \sum_{l,m} \tilde{g}_{lm;1}(k, \lambda) \tilde{c}_{lm;1}(k) \quad (4.46)$$

$$= -\frac{N\rho}{2\beta} \frac{1}{(2\pi)^3} \int d^3k \int_0^1 d\lambda \text{Tr} \left( \tilde{G}_1(k, \lambda) \tilde{C}_1(k) \right). \quad (4.47)$$

Using the residual OZ equation (4.31) in the form

$$\tilde{G}_{1,\lambda}(k) = [\mathbb{I} + \rho\tilde{H}_0(k)]\lambda\tilde{C}_1(k) \left( [\mathbb{I} + \rho\tilde{H}_0(k)]^{-1} - \rho\lambda\tilde{C}_1(k) \right)^{-1},$$

we can integrate (4.47) with respect to  $\lambda$  and finally obtain for  $A_{RPA}$  [18, 12]

$$\begin{aligned} A_{RPA} &= \frac{1}{2(2\pi)^3} \frac{N}{\rho\beta} \int d^3k \left\{ \text{Tr} \left( [\mathbb{I} + \rho\tilde{H}_0(k)]\rho\tilde{C}_1(k) \right) \right. \\ &\quad \left. + \ln \left[ \det \left( \mathbb{I} - [\mathbb{I} + \rho\tilde{H}_0(k)]\rho\tilde{C}_1(k) \right) \right] \right\}. \end{aligned} \quad (4.48)$$

The result for  $A_{RPA}$  is, as already proposed in the last chapter, proportional to the functional  $F$  (4.34). If we use for  $c_1(r, \sigma_i, \sigma_j)$  the optimized direct correlation functions, (4.48) is the ORPA contribution of the Helmholtz free energy. Hence, we can write for the Helmholtz free energy within the ORPA

$$\begin{aligned} A &= A_0 + A_{HTA} - \frac{V}{\beta} F[\tilde{C}_1] \\ A &= A_{id} + A_{0;ex} + A_{HTA} + A_{ORPA}. \end{aligned} \quad (4.49)$$

Using the definition of  $A$ , given by Hoye and Stell [42] for the monodisperse and binary case, we can rewrite the Helmholtz free energy  $A_1 = A_{HTA} + A_{ORPA}$  for the polydisperse fluid as

$$\begin{aligned} A_1^+ &= -\frac{N\rho}{2\beta} \int_0^\infty d^3r \sum_{l,m} [c_{lm}(r) - c_{lm;0}(r)][h_{lm;0}(r) + 1] \\ &\quad + \frac{N}{2\beta} \frac{1}{(2\pi)^3} \int d^3k \sum_{l,m} [\delta_{lm} + \rho \tilde{h}_{lm;0}(k)][\tilde{c}_{lm}(k) - \tilde{c}_{lm;0}(k)] \\ &\quad + \frac{N}{2\rho\beta} \frac{1}{(2\pi)^3} \int d^3k \ln \left[ \det \left( \mathbb{I} - [\mathbb{I} + \rho \tilde{H}_0(k)] \rho \tilde{C}_1(k) \right) \right] \\ &= \frac{\rho^2}{2} \sum_{l,m} \tilde{c}_{lm;1}(0) + \frac{\rho}{2} \sum_l c_{l;1}(0) \\ &\quad + \frac{1}{2(2\pi)^3} \int d^3k \left( \text{Tr} \left[ \ln \left\{ \mathbb{I} - \rho \tilde{C}(k) \right\} \right] - \text{Tr} \left[ \ln \left\{ \mathbb{I} - \rho \tilde{C}_0(k) \right\} \right] \right), \end{aligned} \quad (4.50)$$

where we have used Parseval's theorem and the relations (see also appendix C)

$$\begin{aligned} \mathbb{I} - \rho \tilde{C}_1(k) [\mathbb{I} + \rho \tilde{H}_0(k)] &= \mathbb{I} - \rho \tilde{C}_1(k) (\mathbb{I} - \rho \tilde{C}_0(k))^{-1} \\ &= [\mathbb{I} - \rho \tilde{C}_0(k) - \rho \tilde{C}_1(k)] (\mathbb{I} - \rho \tilde{C}_0(k))^{-1} \\ &= (\mathbb{I} - \rho \tilde{C}(k)) (\mathbb{I} - \rho \tilde{C}_0(k))^{-1} \\ \ln [\det (X)] &= \text{Tr} [\ln (X)] \end{aligned} \quad (4.51)$$

and  $X$  denotes a matrix. Expression (4.50) will be used in the next subsection to calculate the chemical potential of the polydisperse system within the MSA.

#### 4.2.3.2.4 Chemical potential $\mu(\sigma)$

Hoye and Stell [42] have calculated a closed expression for the chemical potential within the ORPA for the one-component and the binary fluid. We want to extend this approach to a polydisperse fluid. To calculate the functional derivative (3.19) of the free energy (4.50) we would need the free energy in dependence of the direct correlation functions and not in dependence of their coefficients, in addition the number densities and sums must

be substituted by integrals over one-particle density distribution functions. Otherwise we do not obtain  $\sigma$  dependent functions by the functional derivation (3.19). To avoid the problems occurring by rewriting the free energy (4.50) in appropriate form to take the functional derivative with respect to the one-particle density distribution function  $\rho(\sigma)$ , we calculate the discrete chemical potentials  $\mu_i$  of species  $i$  for the corresponding  $n$ -component system and take then the limit  $n \rightarrow \infty$  to obtain the chemical potential  $\mu(\sigma)$  for the polydisperse fluid. For this purpose we have to rewrite equation (4.50) for a discrete system as [12]

$$A_1^+ = -\frac{1}{2} \sum_{l,m} \rho_l \rho_m \tilde{c}_{lm}^1(0) + \frac{1}{2} \sum_l \rho_l c_{ll}^1(0) \quad (4.52)$$

$$+ \frac{1}{2(2\pi)^3} \int d^3k \left( \text{Tr} \left[ \ln \left\{ \mathbb{I} - \tilde{C}(k) \right\} \right] - \text{Tr} \left[ \ln \left\{ \mathbb{I} - \tilde{C}^0(k) \right\} \right] \right),$$

where we have substituted the number densities in (4.50) by the one-particle densities  $\rho_l$  of species  $l$ , and the coefficients of the direct correlation function by the direct correlation functions  $c_{lm}$  concerning particles of species  $l$  and  $m$  of a discrete  $n$  component mixture. The matrices  $\tilde{C}$  and  $\tilde{C}^0$  in (4.52) consists of the matrix elements  $\sqrt{\rho_l \rho_m} \tilde{c}_{lm}$  and  $\sqrt{\rho_l \rho_m} \tilde{c}_{lm}^0$ . To make it easier to distinguish between the correlation functions of the discrete  $n$ -component system and the expansion coefficients of the continuous correlation functions of the polydisperse system, we have chosen another font and in addition high indices to indicate the reference and the perturbation part of a discrete correlation functions.

For the chemical potential of a discrete system we can write

$$\beta\mu_i = \beta\mu_{idi} + \beta\mu_{exi}^0 + \frac{\partial A_1^+}{\partial \rho_i}, \quad (4.53)$$

where  $\mu_{exi}^0$  is the excess chemical potential of the HS system [12] and the chemical potential of the ideal  $n$ -component fluid is given as

$$\mu_{idi} = \ln(\rho_i \Lambda_i^3)$$

with  $\Lambda_i$  the de Broglie wavelength of species  $i$ .

To calculate the derivative of the matrix relation  $\ln[\mathbb{I} - \tilde{C}(k)]$  in (4.50), we have to expand the logarithmic function in a Taylor series

$$\ln[\mathbb{I} - \tilde{C}(k)] = \sum_n a_n [\mathbb{I} - \tilde{C}(k)]^n.$$

For the derivative it follows then

$$\begin{aligned} \frac{\partial}{\partial \rho_i} \ln[\mathbb{I} - \rho \tilde{C}(k)] &= \sum_n a_n n [\mathbb{I} - \tilde{C}(k)]^{n-1} \frac{\partial}{\partial \rho_i} [\tilde{C}(k)] \\ &= -\frac{\partial}{\partial \rho_i} [\tilde{C}(k)] [\mathbb{I} - \tilde{C}(k)]^{-1}. \end{aligned}$$

Similar relations are valid for  $\ln [\mathbb{I} - \tilde{\mathbf{C}}^0(k)]$  in (4.50). Using this relations and the OZ equations in matrix notation [12]

$$\begin{aligned} (\mathbb{I} - \tilde{\mathbf{C}}(k))^{-1} &= \mathbb{I} + \tilde{\mathbf{H}}(k) \\ (\mathbb{I} - \tilde{\mathbf{C}}^0(k))^{-1} &= \mathbb{I} + \tilde{\mathbf{H}}^0(k) \end{aligned}$$

where the matrices  $\tilde{\mathbf{H}}$  and  $\tilde{\mathbf{H}}^0$  have as elements the total correlation functions  $\sqrt{\rho_l \rho_m} \tilde{\mathbf{h}}_{lm}$  and  $\sqrt{\rho_l \rho_m} \tilde{\mathbf{h}}_{lm}^0$ . We can write for the derivatives of  $A_1$  with respect to  $\rho_i$  (4.53)

$$\begin{aligned} \frac{\partial A_1^+}{\partial \rho_i} &= - \sum_l \rho_l \tilde{c}_{li}^1(0) - \frac{1}{2} \sum_{lm} \rho_l \rho_m \frac{\partial \tilde{c}_{lm}^1(0)}{\partial \rho_i} - \frac{1}{2(2\pi)^3} \int d^3k \times \\ &\quad \left\{ \sum_l \rho_l \left( \tilde{c}_{li}(k) \tilde{\mathbf{h}}_{li}(k) - \tilde{c}_{li}^0(k) \tilde{\mathbf{h}}_{li}^0(k) \right) \right. \\ &\quad \left. + \sum_{lm} \rho_l \rho_m \left( \tilde{\mathbf{h}}_{lm}(k) \frac{\partial \tilde{c}_{lm}(k)}{\partial \rho_i} - \tilde{\mathbf{h}}_{lm}^0(k) \frac{\partial \tilde{c}_{lm}^0(k)}{\partial \rho_i} \right) \right\} \\ &= - \sum_l \rho_l \tilde{c}_{li}^1(0) - \frac{1}{2} \sum_{lm} \rho_l \rho_m \frac{\partial \tilde{c}_{lm}^1(0)}{\partial \rho_i} - \frac{1}{2} \int d^3r \times \\ &\quad \left\{ \sum_l \rho_l \left( \mathbf{c}_{li}(r) \mathbf{h}_{li}(r) - \mathbf{c}_{li}^0(r) \mathbf{h}_{li}^0(r) \right) \right. \\ &\quad \left. + \sum_{lm} \rho_l \rho_m \left( (\mathbf{g}_{lm}(r) - 1) \frac{\partial \mathbf{c}_{lm}(r)}{\partial \rho_i} - (\mathbf{g}_{lm}^0(r) - 1) \frac{\partial \mathbf{c}_{lm}^0(r)}{\partial \rho_i} \right) \right\} \\ &= - \sum_l \rho_l \tilde{c}_{li}^1(0) - \frac{1}{2} (h_{ii}(0) - c_{ii}(0)) + \frac{1}{2} (h_{ii}^0(0) - c_{ii}^0(0)) \\ &\quad - \frac{1}{2} \int d^3r \sum_{lm} \rho_l \rho_m \left( \mathbf{g}_{lm}(r) \frac{\partial \mathbf{c}_{lm}(r)}{\partial \rho_i} - \mathbf{g}_{lm}^0(r) \frac{\partial \mathbf{c}_{lm}^0(r)}{\partial \rho_i} \right), \quad (4.54) \end{aligned}$$

where we have used Parseval's theorem and for the last expression the OZ equation for the  $n$ -component fluid in the form [12]

$$\mathbf{h}_{lm}(r) - \mathbf{c}_{lm}(r) = \sum_{i=1}^n \rho_i \int d^3r' \mathbf{c}_{li}(|\vec{r} - \vec{r}'|) \mathbf{h}_{im}(r'),$$

$$\mathbf{h}_{lm}^0(r) - \mathbf{c}_{lm}^0(r) = \sum_{i=1}^n \rho_i \int d^3r' \mathbf{c}_{li}^0(|\vec{r} - \vec{r}'|) \mathbf{h}_{im}^0(r').$$

The final relation in (4.54) can be further simplified within the ORPA (4.23) to obtain for the chemical potential of a  $n$ -component mixture

$$\beta \mu_i = \beta \mu_{id_i} + \beta \mu_{ex_i}^0 - \sum_{l=1}^n \rho_l \tilde{c}_{li}^1(0) + \frac{1}{2} c_{ii}^1(0). \quad (4.55)$$

If we use the rules (2.2) and let  $n \rightarrow \infty$  in equation (4.55), then we obtain for the chemical potential  $\mu(\sigma)$  of the polydisperse fluid

$$\beta\mu(\sigma) = \beta\mu_{id}(\sigma) + \beta\mu_{0;ex}(\sigma) - \rho \int d\sigma' f(\sigma') \tilde{c}_1(0, \sigma, \sigma') + \frac{1}{2}c_1(0, \sigma, \sigma). \quad (4.56)$$

Equation (4.56) can, by use of (4.24), be rewritten in terms of the expansion coefficients of the  $\sigma$  dependent functions as

$$\beta\mu_i = \beta\mu_{id_i} + \beta\mu_{ex;0_i} - \rho\tilde{c}_{0i;1}(0) + \frac{1}{2}c_{ii;1}(0), \quad (4.57)$$

where the  $\mu_i$  are the coefficients of the chemical potential  $\mu(\sigma)$ .

#### 4.2.3.2.5 Isothermal compressibility $\chi_T$

The isothermal compressibility (3.22) can be simplified to [18]

$$\begin{aligned} \frac{1}{\rho k_B T \chi_T} &= 1 - \rho \int d^3r \int_0^\infty d\sigma_1 f(\sigma_1) \int d\sigma_2 f(\sigma_2) c(r, \sigma_1, \sigma_2) \\ &= 1 - \rho\tilde{c}_{00}(k=0) = \left\{ [\mathbb{I} + \rho\tilde{H}(k=0)]^{-1} \right\}_{00}, \end{aligned} \quad (4.58)$$

where the indices 00 in the matrix representation means the element 00 of the corresponding matrix. We can rewrite the compressibility in the following form

$$\frac{\chi_T}{\chi_{Tid}} = \frac{\det(\mathbb{I} + \rho\tilde{H}(0))}{|(\mathbb{I} + \rho\tilde{H}(0))|_{00}},$$

where  $|(\mathbb{I} + \rho\tilde{H}(0))|_{00}$  is the cofactor of the 00 element.

### 4.2.4 HS Reference system

As a reference system for the thermodynamic perturbation theory described in the preceding sections, we have used the HS system. To calculate its structure and thermodynamic properties, we have used the analytical solutions of the PY closure [3], or the semi empirical parameterization of computer simulation based on results of Verlet and Weis (VW) [33], which were extended to the polydisperse case [12].

In the PY approximation the solution for the direct correlation functions  $c(r, \sigma_i, \sigma_j)$  at given moments  $\xi_i$  ( $i = 1, 2, 3$ ) of the distribution function  $f(\sigma)$

$$\xi_i = \rho \int d\sigma f(\sigma) \sigma^i \quad i = 1, 2, 3$$

are found to be [43]-[46]:

$$c(r, \sigma_i, \sigma_j) = \begin{cases} \frac{\pi}{2} \left( \frac{1}{3}\sigma_i^3 a + \sigma_i^2 b + \sigma_i \frac{\xi_2}{(1-\eta)^2} \right) & ; r \leq \nu \\ \frac{1}{1-\eta} \Theta(\hat{\sigma} - r) + \frac{1}{r} [a(\sigma_i, \sigma_j) \\ + rb(\sigma_i, \sigma_j) + r^2 d(\sigma_i, \sigma_j) + r^4 f(\sigma_i, \sigma_j)] & ; \nu < r < \hat{\sigma}, \end{cases} \quad (4.59)$$

where

$$\nu = \frac{1}{2}(\sigma_j - \sigma_i)$$

with  $\sigma_j > \sigma_i$  and  $\Theta$  denotes the Heavyside-function. The coefficients in (4.59) are defined as

$$\begin{aligned} a &= \left( \frac{\rho}{(1-\eta)^2} + \frac{\pi^2 \xi_2^3}{4(1-\eta)^4} + \frac{\xi_1 \xi_2 \pi}{(1-\eta)^3} \right), \\ b &= \left( \frac{\xi_1}{(1-\eta)^2} + \frac{\xi_2^2 \pi}{2(1-\eta)^3} \right), \end{aligned}$$

$$\begin{aligned} a(\sigma_i, \sigma_j) &= -\frac{\pi}{16}(\sigma_i - \sigma_j)^2 \left[ \frac{1}{4}(\sigma_i + \sigma_j)^2 a + (\sigma_i + \sigma_j)b + \frac{\xi_2}{(1-\eta)^2} \right], \\ b(\sigma_i, \sigma_j) &= \frac{\pi}{4} \left[ \frac{1}{3}(\sigma_i^3 + \sigma_j^3)a + (\sigma_i^2 + \sigma_j^2)b + (\sigma_i + \sigma_j) \frac{\xi_2}{(1-\eta)^2} \right], \\ d(\sigma_i, \sigma_j) &= -\frac{\pi}{4} \left[ \frac{1}{2}(\sigma_i^2 + \sigma_j^2)a + (\sigma_i + \sigma_j)b + \frac{\xi_2}{(1-\eta)^2} \right], \\ f(\sigma_i, \sigma_j) &= \frac{\pi}{12}a \end{aligned}$$

The total correlation functions  $\tilde{h}(k, \sigma_i, \sigma_j)$  can either be calculated from  $\tilde{c}(k, \sigma_i, \sigma_j)$  via (4.28), or directly from the analytical expressions calculated by Blum and Stell within the PY approximation [3].

For the thermodynamic quantities analytical expressions can be found. The pressure calculated via the compressibility equation (3.23) is found to be [4]

$$\begin{aligned} \beta p^c &= \rho - \rho^2 \int_0^\infty d\sigma_i f(\sigma_i) \int_0^\infty d\sigma_j f(\sigma_j) \int c(r, \sigma_i, \sigma_j) d^3r \\ &= \frac{\rho}{(1-\eta)} + \frac{\xi_1 \xi_2 \pi}{2(1-\eta)^2} + \frac{\xi_2^3 \pi^2}{12(1-\eta)^3}. \end{aligned} \quad (4.60)$$

For the pressure via the virial equation (3.13) we obtain [4]

$$\begin{aligned} \beta p^v &= \rho + \frac{2\pi}{3} \rho^2 \int_0^\infty d\sigma_i f(\sigma_i) \int_0^\infty d\sigma_j f(\sigma_j) \hat{\sigma}^3 g(\hat{\sigma}, \sigma_i, \sigma_j) \\ &= \frac{\rho}{1-\eta} + \frac{\pi \xi_2 (6\xi_1 + \pi \xi_2^2)}{12(1-\eta)^2}, \end{aligned} \quad (4.61)$$

where the contact values  $g(\hat{\sigma}, \sigma_i, \sigma_j)$  are obtained from [47] and [12]. Calculating the Helmholtz free energy from these two expressions for the pressure by use of equation (3.17) yields [4]

$$\begin{aligned} \beta \frac{A_{ex}^c}{V} &= -\rho \ln(1-\eta) + \frac{\xi_1 \xi_2 \pi}{2(1-\eta)} + \frac{\xi_2^3 \pi^2}{24(1-\eta)^2} \\ \beta \frac{A_{ex}^v}{V} &= \beta \frac{A_{ex}^c}{V} + \frac{\xi_2^3 \pi^2}{12\eta} \left[ \frac{(1-\frac{3}{2}\eta)}{(1-\eta)^2} + \frac{\ln(1-\eta)}{\eta} \right]. \end{aligned} \quad (4.62)$$

From the expressions for free energies and pressures it is obvious, that the PY solution is thermodynamically inconsistent. The analytical expressions for the chemical potential  $\mu(\sigma)^c$  respectively  $\mu(\sigma)^v$ , derived by equation (3.19), are given in [12] and [4].

The structural quantities, calculated with the PY approximation, have some fundamental shortcomings, which result in the described thermodynamic inconsistency of the thermodynamic quantities. This shortcomings are in generalization of [33, 36] to the polydisperse fluid given as follows [12]

- The contact values of the radial pair distribution functions  $g(r, \sigma_i, \sigma_j)$ , calculated using the direct correlation functions (4.59), are too low. This leads to an increasing discrepancy between the prediction from the PY solution and the results from simulations as the packing fraction  $\eta$  increases.
- The maximum of the number-number structure factor  $S(k)$  is too high, because of the oscillations of the radial pair distribution functions for larger  $r$  (these oscillations are also slightly out of phase with respect to computer simulations.)
- The cavity functions  $y(r, \sigma_i, \sigma_j)$  are too small inside the core ( $r < \hat{\sigma}$ )

To overcome these deficiencies, Verlet and Weis [33] have proposed a semi-empirical parameterization of the radial pair distribution function  $g(r)$  for the monodisperse fluid, which is used in combination with the empirical parameterization of the equation of state due to Carnahan and Starling [32]. Grundke and Henderson [36] then generalized this parameterizations to the discrete  $n$ -component case, from where the corresponding polydisperse expressions can easily be found [12].

The VW parameterization for the radial pair distribution functions  $g(r, \sigma_i, \sigma_j)$  of a polydisperse system are given by

$$g(r, \sigma_i, \sigma_j) = \begin{cases} 0 & ; r < \hat{\sigma} \\ g^{PY}(r, \sigma'_i, \sigma'_j) + \frac{A(\sigma_i, \sigma_j)}{r} e^{-b(\sigma_i, \sigma_j)(r - \hat{\sigma})} \cos [b(\sigma_i, \sigma_j)(r - \hat{\sigma})] & ; r \geq \hat{\sigma} \end{cases} ,$$

where we calculate the radial pair distribution function  $g^{PY}(r, \sigma'_i, \sigma'_j)$  (upper index PY means within the PY approximation) with respect to a smaller packing fraction  $\eta'$  as compared with the packing fraction  $\eta$  of  $g(r, \sigma_i, \sigma_j)$

$$\eta' = \eta \left(1 - \frac{\eta}{16}\right).$$

Hence we obtain for the corresponding hard sphere diameters

$$\begin{aligned} \hat{\sigma}' &= \hat{\sigma} \left(1 - \frac{\eta}{16}\right)^{\frac{1}{3}} \\ \sigma'_i &= \sigma_i \left(1 - \frac{\eta}{16}\right)^{\frac{1}{3}}. \end{aligned}$$

The parameters  $A(\sigma_i, \sigma_j)$  and  $b(\sigma_i, \sigma_j)$  are determined so that the results for the pressure from the virial and compressibility equations agree. Relations for the two parameters are derived in [12].

The expressions for the pressure proposed by Mansoori, Carnahan, Starling and Leland (MCSL) [35] is given by

$$\begin{aligned}\beta p &= \beta \frac{1}{3} p^v + \beta \frac{2}{3} p^c \\ &= \frac{\rho}{1-\eta} + \frac{\xi_1 \xi_2 \pi}{2(1-\eta)^2} - \frac{\xi_2^3 \pi^2 (\eta-3)}{36(1-\eta)^3}.\end{aligned}$$

This expression for the pressure fits the results of computer simulations nearly perfectly. For the free energy one finds then [12, 4]

$$\begin{aligned}A &= \frac{1}{3} A^v + \frac{2}{3} A^c \\ \frac{\beta A_{ex}}{V} &= \frac{\pi \xi_2}{36\eta(\eta-1)^2} (18\eta\xi_1(1-\eta) + \pi\xi_2^2) + \ln(1-\eta) \left( \frac{\xi_2^3 \pi^2}{36\eta^2} - \rho \right).\end{aligned}$$

For a more detailed description of the VW parameterization concerning polydisperse hard sphere systems see [12].

### 4.3 Integral equations

In this section we will give an overview over integral equation theories (IETs) generalized to polydisperse systems. For a general introduction in IET see, for instance, [26, 38] and [40]. IETs represent an alternative approach to perturbation theories (PTs) to calculate the structure and thermodynamic properties of a liquid. While in PTs one generally relates the properties of the system to those of a reference system and corrects for the (hopefully small) perturbations. IETs, on the other hand, are based on the Ornstein Zernike equation (3.1), which is solved along with a suitable closure relation.

These closures are derived from exact diagrammatic relations under simplifying approximations. During the past years a large number of closure relations have been developed, which in some cases were constructed in order to satisfy particular requirements of the system. The closure relation can, in the general case, be written as

$$F[c, h, \phi](r) = 0$$

i.e., a functional relation between the direct correlation function  $c(r)$ , the total correlation function  $h(r)$ , and the pair potential  $\phi(r)$ .

IETs can be generalized in a straightforward way to the case of polydisperse systems, where the OZ equation (3.1) is solved together with the closure relation

$$F[c, h, \phi](r, \sigma_i, \sigma_j) = 0.$$

For example the PY [3], hyper-netted chain (HNC) [9] or Rogers Young (RG) closure [9] in the polydisperse case reads

$$F[\gamma, \phi](r, \sigma_i, \sigma_j) = c(r, \sigma_i, \sigma_j) = [1 - e^{\beta\phi(r, \sigma_i, \sigma_j)}]g(r, \sigma_i, \sigma_j) = f(r, \sigma_i, \sigma_j)y(r, \sigma_i, \sigma_j) \quad (4.63)$$

$$F[\gamma, \phi](r, \sigma_i, \sigma_j) = c(r, \sigma_i, \sigma_j) = e^{-\beta\phi(r, \sigma_i, \sigma_j) + \gamma(r, \sigma_i, \sigma_j)} - \gamma(r, \sigma_i, \sigma_j) - 1, \quad (4.64)$$

$$F[\gamma, \phi](r, \sigma_i, \sigma_j) = c(r, \sigma_i, \sigma_j) = e^{-\beta\phi(r, \sigma_i, \sigma_j)} \left\{ 1 + \frac{\exp[\gamma(r, \sigma_i, \sigma_j)f(\alpha; r)] - 1}{f(\alpha; r)} \right\} - \gamma(r, \sigma_i, \sigma_j) - 1, \quad (4.65)$$

where  $\gamma(r, \sigma_i, \sigma_j) = h(r, \sigma_i, \sigma_j) - c(r, \sigma_i, \sigma_j)$  and the mixing function  $f(\alpha; r)$  in the RY closure interpolates between the PY and the HNC approximation.

The integral, occurring in the OZ equation (3.1), is in general only numerical solvable. This was done for example by D'Aguanno et al. [8] and by Lado [9]. They have calculated structure and thermodynamic properties of a polydisperse system, using the HNC or RY closure, where the particles of the system were interacting via a Yukawa potential. The RY closure has as a built-in requirement the fulfillment of thermodynamically self-consistency between virial and compressibility route.

Similar as in the one component or  $n$ -component case, a few model systems can be treated, within suitable closure relations, analytically. Blum and Stell [3] for example have used the PY closure relation to calculate the analytical expressions for the correlation functions in  $k$ -space of the HS reference system. The solutions of this IETs approach have already been discussed in the previous section.



# Chapter 5

## Phase equilibria of a polydisperse system

To understand why the prediction of phase equilibria in polydisperse systems is a challenging problem, it is useful to recall first the procedure for a monodisperse system. In a suspension of identical particles, for example, the experimentally controlled variables would be the temperature  $T$ , the suspension volume  $V$ , and the number  $N$  of particles; the appropriate thermodynamic ensemble is therefore the canonical one, and the thermodynamic potential the Helmholtz free energy  $A(N, V, T)$ . The suspension will separate into two phases with particle numbers  $N^{(\alpha)}$  and volume,  $V^{(\alpha)}$  ( $\alpha = 1, 2$ ) if it can thereby lower its total free energy  $\sum_{\alpha} A(N^{(\alpha)}, V^{(\alpha)}, T)$  below the value  $A(N, V, T)$ . The  $N^{(\alpha)}$  and  $V^{(\alpha)}$  adopt the values which minimize this total free energy, subject to conservation of volume and particle number. Introducing Lagrange multipliers for this constraints then gives the familiar coexistence conditions of equal chemical potential and pressure in the two phases [20]. In terms of the free energy density  $A^+$ , the coexistence condition has a simple geometrical interpretation. The number densities  $\rho^{(1)}$  and  $\rho^{(2)}$  of two coexisting phases are determined by constructing the well known double tangent to  $A^+$  [20].

Before we move now to the polydisperse case, we regard first the phase equilibria of a discrete  $n$ -component system, where we assume that there are  $n$  different species of colloid particles, each with its own particle number  $N_i$  and corresponding one-particle density of species  $i$   $\rho_i = \frac{N_i}{V}$ . The free energy density  $A^+(T, \rho_i)$  is now a function of all  $n$  one-particle densities, as well as of a fixed temperature  $T$ . A plot of  $A^+(T, \rho_i)$  versus the one-particle density distribution functions  $\rho_i$  would give a (hyper-)surface in a graph with  $n + 1$  coordinate axes, and to find phase coexistence we would have to construct multiple tangent (hyper-) planes to this surface; a procedure known as constructing the ‘convex envelope’ of the hypersurface. Where such tangent planes exist, the total free energy is lowered by phase separation into the appropriate number of phases (which from Gibbs’ phase rule, can be between two and  $n + 1$ ). The one-particle densities  $\rho_i^{(\alpha)}$  in the different

phases are given by the points where the tangent plane touches the free energy surface.

Now consider the polydisperse case. The discrete one-particle densities  $\rho_i$  are now replaced by the continuous one-particle density distribution function  $\rho(\sigma) = \rho f(\sigma)$ . Formally, this corresponds to a scenario with an infinite number of particle species, as can be seen by splitting the range of  $\sigma$  into  $n$  “bins”, defining the  $\rho_i$  to be the one-particle density within each bin, and then taking  $n \rightarrow \infty$  [4]. The tangent plane procedure for finding phase coexistence then clearly becomes unmanagable, both conceptually and numerically: one would have to work in an infinite-dimensional space, which mathematically corresponds to the fact that the free energy becomes a functional  $A^+(T, [\rho])$  of the one-particle density distribution function  $\rho(\sigma)$ , and Gibbs’ phase rule allows the coexistence of arbitrarily many thermodynamic phases.

As we will show later, there is a limited class of polydisperse systems, which can be reduced without approximation to finite dimensionality. In those cases the phase separation can be calculated via the usual common tangent construction as for a  $n$  component mixture.

In the following section we develop the phase equilibrium and stability conditions for a polydisperse system.

## 5.1 Phase coexistence conditions

### 5.1.1 Binodals

When for a given  $T$ , a parent phase of one-particle density distribution function  $\rho^{(0)} f^{(0)}(\sigma)$ , phase separates into  $m$  daughter phases of one-particle density distribution function  $\rho^{(i)}(\sigma) = \rho^{(i)} f^{(i)}(\sigma)$  ( $i = 1, \dots, m$ ), the thermodynamic conditions of phase equilibrium [19, 4] imply the equality of the pressures and of the chemical potentials

$$\begin{aligned} p(T, [\rho^{(1)}]) &= p(T, [\rho^{(2)}]) = \dots = p(T, [\rho^{(m)}]) \\ \mu(\sigma, T, [\rho^{(1)}]) &= \mu(\sigma, T, [\rho^{(2)}]) = \dots = \mu(\sigma, T, [\rho^{(m)}]) \end{aligned} \quad (5.1)$$

for each species characterized by  $\sigma$ . In addition the phase separation is constrained by the conservation of the total number of particles of each species  $\sigma$  [19, 4]

$$N^{(0)} f^{(0)}(\sigma) = \sum_{i=1}^m N^{(i)} f^{(i)}(\sigma), \quad (5.2)$$

where  $N^{(i)}$  is the particle number and  $f^{(i)}(\sigma)$  the normalized distribution function of phase  $i$ . The conservation of the total volume occupied by the parent phase can be written as,

$$\begin{aligned}
V^{(0)} &= \sum_{i=1}^m V^{(i)} \\
\frac{N^{(0)}}{\rho^{(0)}} &= \sum_{i=1}^m \frac{N^{(i)}}{\rho^{(i)}},
\end{aligned} \tag{5.3}$$

where we have assumed that a polydisperse system of  $N^{(0)}$  particles initially distributed according to  $f^{(0)}(\sigma)$ , separates into  $m$  phases which occupy the total volume  $V^{(0)}$  [4]. Finally, the normalization of the distribution functions  $f^{(i)}(\sigma)$  in (5.2) implies

$$\begin{aligned}
N^{(0)} \int f^{(0)} d\sigma &= \sum_{i=1}^m N^{(i)} \int f^{(i)}(\sigma) d\sigma \\
N^{(0)} &= \sum_{i=1}^m N^{(i)},
\end{aligned} \tag{5.4}$$

which expresses the conservation of the total number of particles.

In principle, given  $T$ ,  $\rho^{(0)}$  and  $f^{(0)}(\sigma)$ , one has to solve the system of equations (5.1) - (5.4) for the  $\rho^{(i)}$  and  $f^{(i)}(\sigma)$  ( $i = 1, 2, \dots, m$ ) to obtain the region of phase coexistences characterized by the equilibrium number densities  $\rho$  and temperature  $T$ . The curves in the  $\rho, T$ -plane along this equilibrium number densities are called binodals.

Even when starting from a relatively simple expression for  $A(T, [\rho])$  the solution to (5.1) - (5.4) turns out to be a rather formidable task because equations (5.1) - (5.4) are no longer algebraic equations (as would be the case for discrete mixtures) but become here integral equations for the  $f^{(i)}(\sigma)$ .

### 5.1.2 Cloud point and shadow

The cloud point is the point at which, for a system with given density distribution function  $\rho^{(0)}(\sigma)$ , phase separation *first* occurs as the temperature  $T$  or another external control parameter is varied. At a cloud point one has therefore phase coexistence between a slightly varied initial phase (the parent) occupying the whole volume  $V^{(0)}$  and containing all particles  $N^{(0)}$  and the corresponding incipient phases, called the ‘shadows’, which are present only in infinitesimal amounts. The cloud point curve can be obtained by diluting or concentrating the system, i.e., varying its number density  $\rho^{(0)}$  while maintaining a fixed ‘shape’ of polydispersity  $f^{(0)}(\sigma)$ . Plotting the cloud point temperature  $T$  versus number density  $\rho^{(0)}$  defines the cloud point curve (CPC), while plotting  $T$  versus the number density of the shadow gives the shadow curve (SC). These curves provide envelopes for the binodals calculated via (5.1) - (5.4). If we restrict ourselves, for the purpose of simplicity, to two phase (gas-liquid) coexistences, physically, the roles of CPC and SC

---

can be explained as follows: If the parent phase is a gas represented by the low density phase given by the left branch of the CPC then the coexisting high density phase given by the right branch of the SC represents the first occurring liquid drop; if we start with the liquid phase to be the parent, then the CPC and the incipient SC represent a liquid which is in equilibrium with the first occurring gas bubble.

The equations to calculate the CPC and the SC can be obtained from equations (5.1) - (5.4) by considering a situation of incipient phase separation whereby all phases but one are present only in infinitesimal amounts. This situation is seen to correspond to  $N^{(i)} \rightarrow 0$  respectively  $V^{(i)} \rightarrow 0$  for  $i = 1, \dots, m - 1$  or  $\rho^{(m)} \rightarrow \rho^{(0)}$  with  $\rho^{(j)}$  ( $j = 1, \dots, m$ ) finite. From equation (5.2) it is seen that this implies  $f^{(m)}(\sigma) \rightarrow f^{(0)}(\sigma)$ . The CPC and the SC are hence solutions of

$$\begin{aligned} p(T, [\rho^{(1)}]) &= p(T, [\rho^{(2)}]) = \dots = p(T, [\rho^{(0)}]) \\ \mu(\sigma, T, [\rho^{(1)}]) &= \mu(\sigma, T, [\rho^{(2)}]) = \dots = \mu(\sigma, T, [\rho^{(0)}]) \end{aligned} \quad (5.5)$$

with the additional conditions

$$\begin{aligned} N^{(0)} &= N^{(m)} \\ f^{(0)}(\sigma) &= f^{(m)}(\sigma) \\ V^{(0)} &= V^{(m)} \\ \rho^{(0)} &= \rho^{(m)}. \end{aligned} \quad (5.6)$$

In a monodisperse system, the CPC and the SC would coincide, with a critical point at their common maximum. In the polydisperse case, however, CPC and SC are different, and the critical point occurs at the crossing of the two curves. To understand this difference between monodisperse and polydisperse systems, it is useful to bear in mind, that the set of parent phases whose behavior is represented by the CPC have constant composition on the curve what means the distribution function  $f(\sigma) = f^{(0)}(\sigma)$  remains constant for every cloud point on the curve. In general, the SC does not have constant composition on the curve, because its distribution functions are given by solution of the equilibrium conditions (5.5) and (5.6) that means, in comparison to the cloud phases, the shadow phases have become enriched in one or the other of the species, a process normally referred to as ‘fractionation’. Thus, in contrast to a monodisperse system, the roles of cloud and shadow phases cannot be reversed, and CPC and SC are therefore in general different. The fact that the critical point is located at a crossing of the CPC and SC follows because at criticality cloud and shadow are by definition identical.

---

## 5.2 Thermodynamic stability conditions

Even if the solution for a phase split into  $m$  phases could be determined numerically, one would still need to verify that the calculated phase coexistence is thermodynamically stable, i.e. that it gives the lowest possible total energy; this problem is more complex in a polydisperse system than in a monodisperse one due to the potentially unlimited number of coexisting phases. In principle, the criterion for global stability is that no part of the free energy surface cuts the calculated tangent plane; equivalently, an appropriately defined tangent plane distance [48] needs to be everywhere non-negative. We can therefore define global stability for a polydisperse phase split as the property that there is no other phase split that gives a lower total free energy for the same parent one-particle density distribution function  $\rho^{(0)}(\sigma)$ . Or, in more intuitive language, this means that if we put a collection of  $m$  phases  $\rho^{(\alpha)}(\sigma)$  ( $\alpha = 1, \dots, m$ ), which satisfy the phase equilibrium conditions (5.1) - (5.4), into contact with each other, the resulting system would be globally (thermodynamically) stable; neither the composition nor the number of phases would change over time. For global stability, the free energy density  $A^+(T, [\rho])$ , must remain a convex functional of  $\rho(\sigma) = \rho^{(0)}(\sigma)$ , i.e., it must satisfy [19, 48]

$$A^+(T, [\rho + \lambda\delta\rho]) < \lambda A^+(T, [\rho + \delta(\rho)]) + (1 - \lambda)A^+(T, [\rho]) \quad (5.7)$$

for any  $\lambda$ ,  $0 < \lambda < 1$ , and for any change,  $\delta\rho(\sigma) \neq 0$ , of the functional form of  $\rho(\sigma)$ . If we consider only infinitesimal changes,  $\delta\rho(\sigma)$ , the above equation is equivalent to [19]

$$0 < \sum_{k=2}^{\infty} \frac{1}{k!} (\lambda - \lambda^k) \delta^k A^+(T, [\rho]), \quad (5.8)$$

where  $\delta^k A^+$  is the  $k$ th functional variation of  $A^+$ ,

$$\delta^k A^+ = \int d\sigma_1 \dots \int d\sigma_k \frac{\delta^k A^+(T, [\rho])}{\delta\rho(\sigma_1) \dots \delta\rho(\sigma_k)} \delta\rho(\sigma_1) \dots \delta\rho(\sigma_k). \quad (5.9)$$

Definition (5.8) characterizes the local stability, where this corresponds to the requirement that the defined tangent plane distance [48] be a local minimum at each of the  $m$  phases in the regarded solution of (5.1) - (5.4).

### 5.2.1 Spinodals and critical states

In comparison to the monodisperse case where there can exist e.g. only a critical point of order two (what means, at fixed temperature two phases with identical number densities), in the phase behavior of polydisperse systems there is the possibility of encountering critical points of arbitrary order. Such critical points are specified by a one-particle

---

density distribution function  $\rho(\sigma)$  and a temperature  $T$ ; their defining property is that, at those parameters, a single phase separates into  $m$  infinitesimally different phases. Thus  $m = 2$  is an ordinary critical point,  $m = 3$  a tricritical point and so on [49, 48, 19]. Since there is no limit on the number of coexisting phases, it is intuitively clear that there is also no upper limit on the order of critical points that occur in polydisperse systems.

The condition (5.8) for local stability reduces ( $\delta^{k+1}A^+ \ll \delta^k A^+$ ) to [19]

$$0 < \delta^2 A^+(T, [\rho]), \quad (5.10)$$

where this condition characterizes the so called ordinary stable state. In the region on the  $\rho$ - $T$  plane where the parent phase first becomes unstable to local density fluctuations, there must exist at least one density fluctuation  $\delta\rho(\sigma) \neq 0$ , such that  $\delta^2 A^+(T, [\rho]) = 0$ , or explicitly

$$\delta^2 A^+ = \int d\sigma_1 \int d\sigma_2 \frac{\delta^2 A^+(T, [\rho])}{\delta\rho(\sigma_1)\delta\rho(\sigma_2)} \delta\rho(\sigma_1)\delta\rho(\sigma_2) = 0 \quad (5.11)$$

for a given  $T$  and  $\rho(\sigma)$ , where any  $\delta\rho(\sigma)$  of equation (5.11) will be called a critical fluctuation. For the system to remain stable with respect to these critical fluctuations  $\delta\rho(\sigma)$  we must have according to (5.8),  $\delta^3 A^+ = 0$  (as  $\delta^3 A^+$  changes the sign in dependence of  $\delta\rho$ ) and  $\delta^4 A^+ > 0$  [19]

$$\delta^3 A^+ = \int d\sigma_1 \int d\sigma_2 \int d\sigma_3 \frac{\delta^3 A^+(T, [\rho])}{\delta\rho(\sigma_1)\delta\rho(\sigma_2)\delta\rho(\sigma_3)} \delta\rho(\sigma_1)\delta\rho(\sigma_2)\delta\rho(\sigma_3) = 0 \quad (5.12)$$

$$\delta^4 A^+ = \int d\sigma_1 \int d\sigma_2 \int d\sigma_3 \int d\sigma_4 \frac{\delta^4 A^+(T, [\rho])}{\delta\rho(\sigma_1)\delta\rho(\sigma_2)\delta\rho(\sigma_3)\delta\rho(\sigma_4)} \times \delta\rho(\sigma_1)\delta\rho(\sigma_2)\delta\rho(\sigma_3)\delta\rho(\sigma_4) > 0. \quad (5.13)$$

The conditions for stable and critical states initially shown by Brannock [49] can now be summarized as follows;  $\delta^2 A^+ > 0$  defines the ordinary stable state;  $\delta^2 A^+ = 0, \delta^3 A^+ = 0, \delta^4 A^+ > 0$  an ordinary critical state,  $\delta^2 A^+ = 0, \delta^3 A^+ = 0, \delta^4 A^+ = 0, \delta^5 A^+ = 0, \delta^6 A^+ > 0$  a tricritical state, etc [19].

The values of  $T$  and  $\rho(\sigma)$ , for which equation (5.11) has a solution define a spinodal, whereas those values for which relations (5.11), (5.12) and (5.13) are satisfied simultaneously correspond to the critical states of a polydisperse fluid. Note that in the present context the stability conditions (5.10) - (5.13) imply stability with respect to changes in both the number density ( $\delta\rho(\sigma) = \delta\rho f(\sigma)$ ) and the composition ( $\delta\rho(\sigma) = \rho\delta f(\sigma)$ ). The spinodals (SP) in a polydisperse system are the points where for varied temperature for example a given parent phase first becomes unstable to local density fluctuations. Determining the SP points for all parents at fixed composition gives a SP curve which can

be plotted along with the CPC and the SC. The limitation that the composition of the parent phase is kept fixed can be justified by the conservation of particles types.

The critical point always lies on the SP curve and so the SP and the CPC intersect at the critical point.

## 5.3 Methods

### 5.3.1 Truncatable free energy method

Significant progress in the solution of the non-linear set of integral equations (5.1) - (5.4), can be made for (model) systems with the so-called ‘truncatable’ free energy method [20], which can in general be solved directly by numerical methods. Truncatable systems are characterized by an excess contribution to the free energy  $A_{ex} = A_{ex}(m_i)$  that depends only on a finite number  $n$  of generalized moments

$$\bar{m}_i[f] = \int d\sigma w_i(\sigma) f(\sigma) \quad (5.14)$$

of the distribution function  $f(\sigma)$ ; for power-law weight functions  $w_i(\sigma) = \sigma^i$ , the  $\bar{m}_i = m_i$  are conventional moments. The term ‘truncatable’ emphasizes that the number of generalized moments appearing in the excess free energy of truncatable models is finite, while for none-truncatable models the excess free energy depends on all details of  $\rho(\sigma)$ , corresponding to an infinite number of generalized moments. The class of polydisperse systems whose free energies are truncatable is surprisingly large (for examples see [20]). We have chosen two example systems of this class to calculate polydisperse phase diagrams the vdW model and the HS system with an adjacent interaction (HTA-type approximation).

If the free energy is not truncatable or the numerical solution of the nonlinear equations (5.1)-(5.4) for the truncatable system is not possible (the numerical algorithm does not converge because too many degrees of freedom have to be fitted), the phase equilibrium conditions have to be substituted by suitable approximations. In the following we shortly describe some of this approximate methods to calculate polydisperse phase separations.

### 5.3.2 Moment free energy method

To address the disadvantages occurring in the solution of (5.1)-(5.4) concerning systems of truncatable free energies, one can construct a so-called ‘moment free energy’ [22, 48, 21]. The moment free energy consists of an excess free energy and of an ideal part of the free energy which is substituted by an approximation, in such a way that both depend only on a finite set of generalized moment densities  $\rho \bar{m}_i$  (5.14).

There are two approaches to constructing the moment free energy: the so called projection method proposed by Sollich and Cates [21] and the so-called combinatorial method proposed by Warren [22]. To motivate the construction of the moment free energy, one can argue that the most important moment densities to treat correctly in the calculation of phase equilibria are those actually appear in the excess free energy  $A_{ex}(\rho\overline{m}_i)$ . For the approximation of the ideal free energy the combinatorial and the projection method provide two completely different routes, surprisingly they lead to practically identical moment free energies  $A(\rho\overline{m}_i)$ , except for a term depending linearly on the number density  $\rho$ . Because the difference between the two defined moment free energies is linear in this density, the combinatorial and the projection method predict exactly the same phase behavior.

In the projection method one divides the infinite-dimensional space of one-particle distribution functions into two complementary subspaces: a ‘moment-subspace’, which contains all degrees of freedom of  $\rho(\sigma)$  that contribute to the generalized moment densities  $\rho\overline{m}_i$  and a ‘transverse subspace’, which contains all the remaining degrees of freedom (they can be varied without effecting the chosen generalized moment densities  $\rho\overline{m}_i$ ) [21]. This approach allows violations of the particle conservation laws (5.2) and (5.4) as long as these occur solely in the transverse space. The transverse degrees of freedom are then chosen so as to minimize the ideal part of the free energy over all one-particle density distribution functions  $\rho(\sigma)$  with fixed generalized moment densities  $\rho\overline{m}_i$ .

In the combinatorial approach one starts with the total free energy of the system (this means of all  $m$  coexisting phases) defined as configuration space integral. The integral over partitions with fixed particle numbers  $N^{(i)}$  of the  $m$  phases can be solved approximately by replacing it by the maximum of the integrand in the thermodynamic limit [22]. From this we obtain the ideal part of the free energy in a form that depends explicitly only on the chosen generalized moment densities. But the expression for the ideal part of the free energy is intractable in general because it still contains the full complexity of the problem [22]. Progress can be made by setting in the ideal part of the free energy  $N^{(i)} \ll N^{(0)}$  ( $i = 1, \dots, m - 1$ ), when the number of particles in the  $m - 1$  phases are much smaller than in the parent phase.

The moment free energy, obtained via the projection method in one way and the combinatorial method in the other way, can then be used to construct a finite dimensional phase diagram via the usual tangency plane rules, ignoring the underlying nature of the polydisperse system [48]. For coexistence involving finite amounts of different phases the moment free energy only gives approximate results [48], because of the violation of the particle conservation law in the projection method and the restriction  $N^{(i)} \ll N^{(0)}$  in the combinatorial approach. The calculated binodals are therefore only exact, if all but one of a set of coexisting phases are of infinitesimal volume compared to the majority phase.

This means that the CPC and SC are given exactly, the same is true for the calculated SPs and critical points. According to Gibbs' phase rule, a moment free energy depending on  $n$  moment densities will not formally predict more than  $n + 1$  coexisting phases, whereas we know that polydisperse systems can in principle separate into an arbitrary number of phases. Both of these shortcomings can be overcome by including extra moment densities within the moment free energy; this does not affect any of the exactness statements above but systematically increases the accuracy of any calculated phase splits [48].

### 5.3.3 Binning and pseudo-components

For an approximate solution of the polydisperse phase equilibrium problem, the most straightforward method is to 'bin' the full one-particle density distribution function  $\rho(\sigma)$  into a number of discrete 'pseudo-components', whose one-particle density distribution functions are given by the density of particles within the respective  $\sigma$ -ranges. This then formally reduces the problem to that of a finite mixture. The pseudo-components can be spaced evenly across the  $\sigma$ -range, or chosen according to other ad-hoc prescriptions. Whatever particular implementation is chosen (for an overview see [20]), it is clear that binning introduces uncontrolled systematic errors (mainly because of the chosen discretization) and also becomes numerically unwieldy for large numbers of pseudo-components. All approaches, discussed in [20], to allocate pseudo-components, based on the idea to reduce the equations (5.1) - (5.4) to a set of (approximate) nonlinear equations in a finite number of variables, can be used to calculate at least approximate CPC and SC.

## 5.4 Phase coexistence for truncatable free energy method

For the calculation of phase transitions we restrict ourselves in this thesis on systems with truncatable free energies. To simplify the problem we assume the parent distribution function  $f^{(0)}(\sigma)$  to be monomodal, i.e. centered around a single reference species, as suitable for the polydisperse generalization of one-component systems. This parent distribution function will further be assumed to be fixed, once and for all, by the production process of the colloid particles. As an additional restriction, we would like to stress that our study will be limited to fluid phases of the polydisperse system, leaving aside whether these phases are stable or metastable with respect to possible solid phases. In this way, we will be able to focus on the central difficulty resulting from replacement of the algebraic equations in finite dimensional space, characteristic of the phase behavior of discrete mixtures, by the integral equations in infinite dimensional space (5.1) characteristic of the

---

continuous mixtures. As final simplification we will restrict ourselves here to two-phase coexistence only, i.e., to  $m = 2$ . In practice, a polydisperse system does rarely use the infinite number of phases given by Gibbs' phase rule [19]. Since these multiple-phase coexistences are expected to occur at low temperatures, the restriction ( $m = 2$ ) implies that the value of  $T$  should be chosen high enough [19]. This is consistent to the restriction to fluid phases, because for low temperatures some of the (multiple) fluid phases could coexist with solid phases.

### 5.4.1 Binodals

For a two-phase coexistence ( $m = 2$ ) the particle numbers  $N^{(i)}$  ( $i = 1, 2$ ) can be obtained from (5.3) and (5.4) as

$$\begin{aligned} N^{(1)} &= N^{(0)} \frac{\rho^{(1)}(\rho^{(2)} - \rho^{(0)})}{\rho^{(0)}(\rho^{(2)} - \rho^{(1)})} \\ N^{(2)} &= N^{(0)} \frac{\rho^{(2)}(\rho^{(1)} - \rho^{(0)})}{\rho^{(0)}(\rho^{(1)} - \rho^{(2)})}, \end{aligned}$$

expressing the so-called lever rule [50] or particle conservation, whereas  $f^{(2)}(\sigma)$  can be eliminated by using equation (5.2)

$$\begin{aligned} f^{(2)}(\sigma) &= \frac{\rho^{(0)}(\rho^{(1)} - \rho^{(2)})}{\rho^{(2)}(\rho^{(1)} - \rho^{(0)})} f^{(0)}(\sigma) + \frac{\rho^{(1)}(\rho^{(0)} - \rho^{(2)})}{\rho^{(2)}(\rho^{(1)} - \rho^{(0)})} f^{(1)}(\sigma) \\ &= \frac{(\rho^{(1)} - \rho^{(2)})\rho^{(0)} f^{(0)}(\sigma) - (\rho^{(0)} - \rho^{(2)})\rho^{(1)} f^{(1)}(\sigma)}{(\rho^{(1)} - \rho^{(0)})\rho^{(2)}}, \end{aligned} \quad (5.15)$$

where  $\rho^{(0)}$  and  $f^{(0)}(\sigma)$  are given parent phase data. To find  $\rho^{(1)}$ ,  $\rho^{(2)}$  and  $f^{(1)}(\sigma)$  we need three relations. For this purpose we eliminate the ideal contribution to the chemical potential (3.21) from equation (5.1) for  $m = 2$  and write

$$\rho^{(1)}(\sigma) = \rho^{(2)}(\sigma) e^{\beta \Delta \mu_{ex}(\sigma, T, [\rho^{(1)}, \rho^{(2)}])},$$

where

$$\Delta \mu_{ex}(\sigma, T, [\rho^{(1)}, \rho^{(2)}]) = \mu_{ex}(\sigma, T, [\rho^{(2)}]) - \mu_{ex}(\sigma, T, [\rho^{(1)}]), \quad (5.16)$$

with  $\mu_{ex}(\sigma, T, [\rho])$  being the excess part of  $\mu(\sigma, T, [\rho])$ . In terms of  $f^{(i)}(\sigma)$ , the above equation becomes

$$f^{(1)}(\sigma) = f^{(2)}(\sigma) \frac{\rho^{(2)}}{\rho^{(1)}} e^{\beta \Delta \mu_{ex}(\sigma, T, \rho^{(1)}, \rho^{(2)}, [f^{(1)}], [f^{(2)}])}. \quad (5.17)$$

Eliminating  $f^{(2)}(\sigma)$  from equation (5.17) by use of (5.15), one obtains finally

$$f^{(1)}(\sigma) = \frac{\rho^{(0)} f^{(0)}(\sigma) (\rho^{(1)} - \rho^{(2)}) e^{\beta \Delta \mu_{ex}}}{\rho^{(1)} [\rho^{(1)} - \rho^{(0)} + (\rho^{(0)} - \rho^{(2)}) e^{\beta \Delta \mu_{ex}}]}. \quad (5.18)$$

This equation is the first relation between  $\rho^{(1)}$ ,  $\rho^{(2)}$  and  $f^{(1)}(\sigma)$ . Given  $T$ ,  $\rho^{(0)}$  and  $f^{(0)}(\sigma)$ , equation (5.18) can in principle be solved with respect to  $f^{(1)}(\sigma)$  for given  $\rho^{(1)}$  and  $\rho^{(2)}$  values. A relation between  $\rho^{(1)}$  and  $\rho^{(2)}$  can then be found by solving

$$1 = \int d\sigma f^{(1)}(\sigma) = \int d\sigma \frac{\rho^{(0)} f^{(0)}(\sigma) (\rho^{(1)} - \rho^{(2)}) e^{\beta \Delta \mu_{ex}}}{\rho^{(1)} [\rho^{(1)} - \rho^{(0)} + (\rho^{(0)} - \rho^{(2)}) e^{\beta \Delta \mu_{ex}}]}, \quad (5.19)$$

which is the normalization of the distribution function  $f^{(1)}(\sigma)$ . Finally, the system of equations is closed by equation (5.1), the equality of the pressures

$$p(T, [\rho^{(1)}]) = p(T, [\rho^{(2)}]). \quad (5.20)$$

As it depends continuously on the particle diameter  $\sigma$ , for the general case (5.18) is an equation in an infinite dimensional space, which can not be used to calculate numerically a two phase coexistence. For a system of truncatable free energies, however, the thermodynamic quantities can be rewritten as functions of a finite set of generalized moments  $\overline{m}_k[f]$  (5.14). This can be exploited to map the equation (5.18) onto a finite dimensional space.

For further considerations we suppress the functional dependence of the generalized moments  $\overline{m}_k$  on  $f(\sigma)$ . We can thus express the excess chemical potentials (5.16) by use of (5.14) in dependence of their generalized moments as

$$\Delta \mu_{ex}(\sigma, T, \rho^{(1)}, \rho^{(2)}, \overline{m}_k^{(1)}, \overline{m}_k^{(0)}) = \mu_{ex}(\sigma, T, \rho^{(2)}, \overline{m}_k^{(1)}, \overline{m}_k^{(0)}) - \mu_{ex}(\sigma, T, \rho^{(1)}, \overline{m}_k^{(1)}), \quad (5.21)$$

where the generalized moments  $\overline{m}_k^{(2)}$  have been eliminated in favor of  $\overline{m}_k^{(1)}$  and  $\overline{m}_k^{(0)}$  by using equation (5.15). The explicit dependence of the equations (5.15) and (5.18) on  $\sigma$  can be eliminated by integration to transfer them into a set of moment relations [19]

$$\overline{m}_k^{(2)} = \frac{(\rho^{(1)} - \rho^{(2)}) \rho^{(0)} \overline{m}_k^{(0)} - (\rho^{(0)} - \rho^{(2)}) \rho^{(1)} \overline{m}_k^{(1)}}{(\rho^{(1)} - \rho^{(0)}) \rho^{(2)}}, \quad (5.22)$$

$$\overline{m}_k^{(1)} = \int d\sigma w_k(\sigma) \frac{\rho^{(0)} f^{(0)}(\sigma) (\rho^{(1)} - \rho^{(2)}) e^{\beta \Delta \mu_{ex}}}{\rho^{(1)} [\rho^{(1)} - \rho^{(0)} + (\rho^{(0)} - \rho^{(2)}) e^{\beta \Delta \mu_{ex}}]}, \quad (5.23)$$

with  $\Delta \mu_{ex}$  from equation (5.21). Finally the equality of the pressures (5.20) becomes

$$p(T, \rho^{(1)}, \overline{m}_k^{(1)}) = p(T, \rho^{(2)}, \overline{m}_k^{(1)}, \overline{m}_k^{(0)}). \quad (5.24)$$

For any given  $T$ ,  $\rho^{(0)}$  and  $f^{(0)}(\sigma)$  the  $k + 2$  unknowns  $(\rho^{(1)}, \rho^{(2)}, \overline{m}_k^{(1)})$  can be obtained by solving the system of  $k + 2$  equations (5.23) and (5.24) together with the normalization relation (5.19). When this result is substituted in equation (5.18) by use of (5.21), we obtain  $f^{(1)}(\sigma)$  and from equation (5.15) finally  $f^{(2)}(\sigma)$ . This then completely solves the two-phase coexistence problem for the present model.

### 5.4.2 CPC and SC

The CPC and SC can be obtained from equations (5.23) and (5.24) by use of (5.5), (5.6) and (5.22) as [19]

$$\begin{aligned}\overline{m}_k^{(2)} &= \overline{m}_k^{(0)} \\ \overline{m}_k^{(1)} &= \int d\sigma w_k(\sigma) \frac{\rho^{(0)} f^{(0)}(\sigma) e^{\beta\Delta\mu_{ex}}}{\rho^{(1)}} \\ p^{(1)}(T, \rho^{(1)}, \overline{m}_k^{(1)}) &= p^{(2)}(T, \rho^{(0)}, \overline{m}_k^{(0)})\end{aligned}\quad (5.25)$$

with

$$\Delta\mu_{ex}(\sigma, T, \rho^{(1)}, \rho^{(0)}, \overline{m}_k^{(1)}, \overline{m}_k^{(0)}) = \mu_{ex}(\sigma, T, \rho^{(0)}, \overline{m}_k^{(0)}) - \mu_{ex}(\sigma, T, \rho^{(1)}, \overline{m}_k^{(1)}). \quad (5.26)$$

The distribution function  $f^{(1)}(\sigma)$  becomes then

$$f^{(1)}(\sigma) = f^{(0)}(\sigma) \frac{\rho^{(0)}}{\rho^{(1)}} e^{\beta\Delta\mu_{ex}} \quad (5.27)$$

with

$$\begin{aligned}f^{(2)}(\sigma) &= f^{(0)}(\sigma) \\ \rho^{(2)} &= \rho^{(0)}\end{aligned}$$

The solution of equations (5.25) - (5.27) corresponding to the majority phase 2 yields the CPC, while the solution for the minority phase 1 yields the SC.

### 5.4.3 Spinodals and ordinary critical points

Critical points can be obtained by the following different routes. The most straightforward possibilities are to look for the so called untruncated binodals or for intersections of CPC and SC. In a polydisperse phase transition untruncated binodals play an important role because the critical points are situated on their maxima. This untruncated or critical binodals are obtained by solution of (5.18) - (5.20) by the special choice of the parent number density  $\rho^{(0)} = \rho_{crit}$ , while all remaining binodals for  $\rho^{(0)} \neq \rho_{crit}$  are truncated before they approach the critical point. When the critical region is approximately known, the determination of the critical point via the untruncated binodal or the intersection of CPC and SC is easily executed but these methods become unpracticable when no a priori knowledge about their location is available, as is the case here for all the polydispersity induced critical points.

The method to be followed here will therefore be based on the stability criteria (5.11), (5.12) and (5.13). When we follow this route the critical points can be found by looking for intersections of the SP and the stability curve.

We can write the SP criterion also in the form (because along the SP curve we have stability at least against one density fluctuation  $\delta\rho(\sigma)$ )

$$0 = \int d\sigma_2 \delta\rho(\sigma_2) \left( \frac{\delta^2 A^+}{\delta\rho(\sigma_1)\delta\rho(\sigma_2)} \right), \quad (5.28)$$

where this definition corresponds to the SP criterion given by Brannock [49] in vector notation

$$0 = (\delta\vec{\rho}\nabla)\vec{\mu}[\rho^{(0)}] = (\delta\vec{\rho}\nabla)\vec{\nabla}A[\rho^{(0)}] \quad (5.29)$$

with the infinite dimensional vectors  $\vec{\rho}$  and  $\vec{\mu}$  containing the values of  $\rho(\sigma)$  and  $\mu(\sigma)$ . The SP criteria (5.28) and (5.29) for a parent phase  $\rho^{(0)}(\sigma)$  mean then, that there is an incipient instability direction  $\delta\vec{\rho}$  along which the chemical potentials do not change [48]. Equation (5.28) can be cast into an eigenvalue form for zero eigenvalue [51] by writing  $\delta\rho(\sigma)$  as  $\delta\rho(\sigma) = \rho(\sigma)e(\sigma)$ , where  $e(\sigma)$  is yet unknown. If we split the free energy in (5.28) into ideal and excess part [48, 51], we obtain

$$\begin{aligned} 0 &= \int d\sigma_2 \delta\rho(\sigma_2) \left( \frac{\delta^2 A_{id}^+}{\delta\rho(\sigma_1)\delta\rho(\sigma_2)} + \frac{\delta^2 A_{ex}^+}{\delta\rho(\sigma_1)\delta\rho(\sigma_2)} \right) \\ &= \int d\sigma_2 f(\sigma_2)e(\sigma_2) \left( \frac{\delta(\sigma_1 - \sigma_2)}{\sqrt{f(\sigma_1)f(\sigma_2)}} + C_2(\sigma_1, \sigma_2, T, \rho) \right) \end{aligned} \quad (5.30)$$

where  $C_2(\sigma_1, \sigma_2, T, \rho) = \rho \frac{\delta^2 A_{ex}^+(T, [\rho])}{\delta\rho(\sigma_1)\delta\rho(\sigma_2)}$  depends on the excess free energy of the used model. For systems of truncatable free energies we can rewrite  $C_2(\sigma_1, \sigma_2, T, \rho)$  as [51, 19]

$$\begin{aligned} C_2(\sigma_1, \sigma_2, T, \rho) &= \rho \sum_i \sum_{k, k'} \frac{\partial^2 A_{ex}^+}{\partial\bar{m}_{k,i}\partial\bar{m}'_{k',i}} \frac{\delta\bar{m}_{k,i}}{\delta\rho(\sigma_1)} \frac{\delta\bar{m}'_{k',i}}{\delta\rho(\sigma_2)} \\ &= \sum_i \sum_{k, k'} w_{k,i}(\sigma_1) c_{kk',i}(T, \rho) w_{k',i}(\sigma_2), \end{aligned} \quad (5.31)$$

where the  $\frac{\partial^2 A_{ex}^+}{\partial\bar{m}_{k,i}\partial\bar{m}'_{k',i}}$  are partial derivatives with respect to the generalized moments (5.14) and the coefficients  $c_{kk',i}(T, \rho)$  are independent of  $\sigma$  and can be deduced by comparison of the explicit expression for  $C_2(\sigma_1, \sigma_2, T, \rho)$  with definition (5.31). The index  $i$  in (5.31) was introduced to make it possible to distinguish between different generalized moment types, which are characterized each by a certain weight function  $w_{k,i}(\sigma)$ . The functional derivative  $C_2(\sigma_1, \sigma_2, T, \rho)$  depends on a finite set of generalized moments contained in  $A_{ex}^+$ ; the sums over  $k$  and  $k'$  in (5.31) are therefore finite.

A solution of the homogeneous equation (5.30) for the eigenvector  $e(\sigma)$  can by use of (5.31) be given as

$$e(\sigma) = - \sum_i \sum_{k, k'} c_{kk',i}(\rho, T) w_{k,i}(\sigma) \delta\bar{m}'_{k',i}, \quad (5.32)$$

where  $\delta\bar{m}_{k,i}$  is the variation of the  $k$ th generalized moment with respect to the weight function  $w_{k,i}(\sigma)$

$$\delta\bar{m}_{k,i} = \int d\sigma f(\sigma) e(\sigma) w_{k,i}(\sigma) = \int d\sigma \delta f(\sigma) w_{k,i}(\sigma). \quad (5.33)$$

If we take the  $l$ th generalized moment of  $e(\sigma)$ , we can rewrite (5.32)

$$\begin{aligned} 0 &= \int d\sigma f(\sigma) w_{l,j}(\sigma) \left( e(\sigma) + \sum_i \sum_{kk'} c_{k,k',i}(T, \rho) w_{k,i}(\sigma) \delta\bar{m}_{k',i} \right) \\ &= \sum_i \sum_k \delta\bar{m}_{k,i} \left( \delta_{kl,ij} + \sum_{k'} c_{k,k',i}(T, \rho) \bar{m}_{k',ij} \right) \end{aligned} \quad (5.34)$$

where we have used

$$\int d\sigma f(\sigma) w_{k,i}(\sigma) w_{l,j}(\sigma) = \bar{m}_{lk,ij}. \quad (5.35)$$

Because the variation of the eigenvector  $\delta\bar{m}$  is not zero (compare (5.29)) a solution to (5.34) will exist provided the determinant of the matrix

$$\det(\mathbb{1} + B) = 0 \quad (5.36)$$

with the matrix elements

$$B_{kl,ij} = \sum_{k'} c_{k,k',i}(\rho, T) \bar{m}_{k',ij}. \quad (5.37)$$

(5.36) is the equation to calculate the SP. In the present context this amounts to looking for thermodynamic states  $(T, \rho)$  which, for a given distribution function  $f(\sigma) = f^{(0)}(\sigma)$ , satisfy (5.36). From the eigenvector  $e(\sigma)$  we can then deduce the fluctuations in the one-particle density distribution function  $\delta\rho(\sigma) = \delta\rho^{(0)}(\sigma)$  obtained from (5.32) by inserting the solution  $\delta\bar{m}$  of (5.34).

After calculation of the SP, we turn now to the determination of the ordinary critical point, for which the SP criterion (5.36) and the criteria for the critical point (5.12) and (5.13) have to be fulfilled simultaneously. We can rewrite (5.12) for a system of truncatable free energies as

$$\begin{aligned} &\int d\sigma_1 d\sigma_2 d\sigma_3 \rho(\sigma_1) \rho(\sigma_2) \rho(\sigma_3) e(\sigma_1) e(\sigma_2) e(\sigma_3) \left( -\frac{\delta(\sigma_1 - \sigma_2) \delta(\sigma_2 - \sigma_3)}{\rho(\sigma_1) \rho(\sigma_2)} \right. \\ &\quad \left. + \frac{C_3(\sigma_1, \sigma_2, \sigma_3, T, \rho)}{\rho^2} \right) \\ &= -\int d\sigma_1 f(\sigma_1) e^3(\sigma_1) + \sum_j \sum_{k,l,o} c_{klo,j}(T, \rho) \delta\bar{m}_{k,j} \delta\bar{m}_{l,j} \delta\bar{m}_{o,j} = 0, \end{aligned} \quad (5.38)$$

where  $\frac{C_3(\sigma_1, \sigma_2, \sigma_3, T, \rho)}{\rho^2}$  is the third functional derivative of  $A_{ex}$  with respect to  $\rho(\sigma)$  and the coefficients  $c_{klo}(T, \rho)$  can be deduced from the relation

$$C_3(\sigma_1, \sigma_2, \sigma_3, \rho, T) = \sum_j \sum_{klo} c_{klo,j}(\rho, T) w_{k,j}(\sigma_1) w_{l,j}(\sigma_2) w_{o,j}(\sigma_3). \quad (5.39)$$

If we insert the definition of  $e(\sigma)$  (5.32) into (5.38), we obtain

$$\begin{aligned} & \sum_{jj'j''} \sum_{k,l,o} \delta \bar{m}_{k,j} \delta \bar{m}_{l,j'} \delta \bar{m}_{o,j''} \left( c_{klo,j}(T, \rho) \delta_{jj'} \delta_{jj''} + \right. \\ & \left. \sum_{k',l',o'} c_{kk',j}(T, \rho) c_{ll',j'}(T, \rho) c_{oo',j''}(T, \rho) \bar{m}_{k'l'o',jj'j''} \right) = 0, \end{aligned} \quad (5.40)$$

where we have used for  $\bar{m}_{k'l'o',jj'j''}$  a relation similar to (5.35). For the condition in (5.13) we get in similar manner as in (5.38) and (5.40)

$$\begin{aligned} & \int d\sigma_1 f(\sigma_1) \left[ 2e^A(\sigma_1) + \int d\sigma_2 d\sigma_3 d\sigma_4 f(\sigma_2) f(\sigma_3) f(\sigma_4) \times \right. \\ & \left. e(\sigma_1) e(\sigma_2) e(\sigma_3) e(\sigma_4) C_4(\sigma_1, \sigma_2, \sigma_3, \sigma_4, \rho, T) \right] \\ = & \sum_{jj'j''j'''} \sum_{k,l,o,p} \delta \bar{m}_{k,j} \delta \bar{m}_{l,j'} \delta \bar{m}_{o,j''} \delta \bar{m}_{p,j'''} \left( c_{klpo,j}(T, \rho) \delta_{jj'} \delta_{jj''} \delta_{jj'''} \right. \\ & \left. + 2 \sum_{k',l',o',p'} c_{kk',j}(T, \rho) c_{ll',j'}(T, \rho) c_{ii',j''}(T, \rho) c_{pp',j'''}(T, \rho) \bar{m}_{k'l'o'p',jj'j''j'''} \right) > 0, \end{aligned} \quad (5.41)$$

where  $\frac{C_4(\sigma_1, \sigma_2, \sigma_3, \sigma_4, T, \rho)}{\rho^3}$  is the fourth functional derivative of  $A_{ex}$  with respect to the one-particle density distribution function  $\rho(\sigma)$ . The coefficients  $c_{klpo,j}(\rho, T)$  are given through

$$C_4(\sigma_1, \sigma_2, \sigma_3, \sigma_4, \rho, T) = \sum_j \sum_{k,l,o,p} c_{klpo,j}(\rho, T) w_{k,j}(\sigma_1) w_{l,j}(\sigma_2) w_{o,j}(\sigma_3) w_{p,j}(\sigma_4) \quad (5.42)$$

and the  $m_{k'l'o'p',jj'j''j'''} by$

$$m_{k'l'o'p',jj'j''j'''} = \int d\sigma f(\sigma) w_{k,j}(\sigma) w_{l,j'}(\sigma) w_{o,j''}(\sigma) w_{p,j'''}(\sigma).$$

Note that equations (5.31) - (5.41) are algebraic equations involving  $T$ ,  $\rho$  and the generalized moments of type  $\bar{m}_{k,j}$ ,  $\bar{m}_{kk',jj'}$ ,  $\bar{m}_{kk'k'',jj'j''}$  and  $\bar{m}_{kk'k''k''',jj'j''j'''}$ , where  $(k, k', k'', k''')$  cover the finite set of values appearing in the excess free energy and  $(jj'j''j''')$  the set of all generalized moment types of the excess free energy.

In the following subsections we present two examples of truncatable free energies, the vdW free energy (4.1) and the free energy within the HTA approximation (4.12), for which two-phase coexistences have been calculated numerically.

### 5.4.4 Van der Waals fluid

Xu et al. [19, 52] have studied the phase behavior of a system within a vdW approximation, first at the level of two-phase coexistence and later for three-phase coexistence. It was shown there [19], that the polydispersity can have profound influence on the binodals of this system as compared with their monodisperse counterparts. In [52] they show that, as a consequence of the Gibbs phase rule, a polydisperse system can also phase separate or ‘fractionate’ into more than two fluid phases, each phase differing both on number density and in size distribution.

In [19] Xu et al. have studied the influence of amplitude polydispersity and (or) size polydispersity on a polydisperse phase separation process. With size polydispersity we mean that the amplitude of the attractions ( $\nu(\sigma, \sigma')$  in the vdW model) is constant for all particle type interactions, while for amplitude polydispersity it depends on the diameters  $\sigma$  of the interacting particles. The size or (and) amplitude polydispersity of the attractions can be adjusted by the special choice of parameters within the definition of the attractions. The systems with size or amplitude polydispersity only are simpler to study, because their excess free energy involves fewer moments (5.14) of the size distribution function  $f(\sigma)$ . We will therefore consider either only the size or the amplitude polydisperse model, to discuss the conclusions made already by [19] with the help of some later calculated phase diagrams.

With the attractions  $\varphi(\sigma, \sigma')$  (4.4) rewritten in more general form as [19]

$$\varphi(\sigma, \sigma') = -\bar{\nu} \frac{4\pi}{3} (\sigma\sigma')^s \left( \frac{\sigma^t + \sigma'^t}{2} \right)^3 \quad (5.43)$$

the vdW excluded volume (4.2) and the definition of the moments (5.14) characterized by the weight function  $w_k(\sigma) = \sigma^k$ , one can rewrite the equations for excess free energy (4.1), chemical potential (4.5) and pressure (4.6) of a vdW fluid [19]

$$\begin{aligned} A_{ex}^+(T, \rho, [f]) &= -\rho \ln \left( 1 - \frac{\pi}{6} \rho m_{3t} \right) - \beta \frac{\pi}{6} \rho^2 \bar{\nu} (m_s m_{3t+s} + 3m_{t+s} m_{2t+s}) \\ \beta \mu_{ex}(\sigma, T, \rho, [f]) &= -\ln \left( 1 - \frac{\pi}{6} \rho m_{3t} \right) + \frac{\frac{\pi}{6} \rho \sigma^{3t}}{1 - \frac{\pi}{6} \rho m_{3t}} \\ &\quad - \beta \frac{\pi}{6} \bar{\nu} \rho (\sigma^{3t+s} m_s + 3\sigma^{2t+s} m_{t+s} + 3\sigma^{t+s} m_{2t+s} + \sigma^s m_{3t+s}) \\ \beta p(T, \rho, [f]) &= \frac{\rho}{1 - \frac{\pi}{6} \rho m_{3t}} - \beta \frac{\pi}{6} \rho^2 \bar{\nu} (m_s m_{3t+s} + 3m_{t+s} m_{2t+s}) \end{aligned} \quad (5.44)$$

where  $\bar{\nu}$  has the dimension of an energy and gives a fixed potential depth. As we can see in (5.44) the thermodynamic properties depend only on a finite set of conventional moments. Equation (5.43) was chosen to be able to calculate independently a size or a amplitude polydisperse system by varying the parameters  $t$  and  $s$  in a suitable manner;

$\{s = 0, t = 0\}$  corresponds to the absence of polydispersity,  $\{s = 1, t = 0\}$  to a system that is polydisperse in amplitude (or interaction strength) only,  $\{s = 0, t = 1\}$  to a system that is polydisperse in size only, finally all other combination of  $s$  and  $t$  corresponds to a system that is both amplitude and size polydisperse. We restrict ourselves here to the cases  $\{s = 0, t = 1\}$  and  $\{s = 1, t = 0\}$ .

The phase equilibrium can be calculated with (5.22) - (5.24) for the unknowns  $(\rho^{(1)}, \rho^{(2)}, m_k^{(1)}, m_k^{(2)})$  by use of (5.44) and the normalization relation (5.19). The corresponding distribution functions  $f^{(1)}(\sigma)$  and  $f^{(2)}(\sigma)$  are then found with (5.18) and (5.15).

To calculate the critical behavior of the vdW fluid, we will limit ourselves to determine the ordinary critical states (5.36), (5.12) and (5.13) of the vdW free energy (4.1). The functional derivatives of the free energy (4.1) with respect to the one-particle density distribution functions need to calculate an ordinary critical state are given as [19]

$$\beta \frac{\delta^2 A^+(T, [\rho])}{\delta \rho(\sigma_1) \delta \rho(\sigma_2)} = \frac{\delta(\sigma_1 - \sigma_2)}{\rho(\sigma_1)} + \beta \varphi(\sigma_1, \sigma_2) + \frac{1}{1 - \frac{\pi}{6} \rho m_{3t}} \left[ V(\sigma_1) + V(\sigma_2) + \frac{\rho V(\sigma_1) V(\sigma_2)}{1 - \frac{\pi}{6} \rho m_{3t}} \right] \quad (5.45)$$

$$\beta \frac{\delta^3 A^+(T, [\rho])}{\delta \rho(\sigma_1) \delta \rho(\sigma_2) \delta \rho(\sigma_3)} = -\frac{\delta(\sigma_1 - \sigma_2) \delta(\sigma_2 - \sigma_3)}{\rho(\sigma_1) \rho(\sigma_2)} + \frac{2\rho}{(1 - \frac{\pi}{6} \rho m_{3t})^3} (V(\sigma_1) V(\sigma_2) V(\sigma_3) + \frac{1}{(1 - \frac{\pi}{6} \rho m_{3t})^2} [V(\sigma_1) V(\sigma_2) + V(\sigma_2) V(\sigma_3) + V(\sigma_3) V(\sigma_1)]) \quad (5.46)$$

$$\beta \frac{\delta^4 A^+(T, [\rho])}{\delta \rho(\sigma_1) \delta \rho(\sigma_2) \delta \rho(\sigma_3) \delta \rho(\sigma_4)} = 2 \frac{\delta(\sigma_1 - \sigma_2) \delta(\sigma_2 - \sigma_3) \delta(\sigma_3 - \sigma_4)}{\rho(\sigma_1) \rho(\sigma_2) \rho(\sigma_3)} + \frac{6\rho}{(1 - \frac{\pi}{6} \rho m_{3t})^4} V(\sigma_1) V(\sigma_2) V(\sigma_3) V(\sigma_4) + \frac{2}{(1 - \frac{\pi}{6} \rho m_{3t})^3} \times [V(\sigma_1) V(\sigma_2) V(\sigma_3) + V(\sigma_1) V(\sigma_2) V(\sigma_4) + V(\sigma_1) V(\sigma_3) V(\sigma_4) + V(\sigma_2) V(\sigma_3) V(\sigma_4)], \quad (5.47)$$

where it is seen that the fourth functional derivative of  $A^+$  with respect to the one-particle density distribution function  $\rho(\sigma)$  is positive definite, while the third and second functional derivative can vanish because the volume  $V(\sigma)$  of species  $\sigma$  and the excluded volume  $E = (1 - \frac{\pi}{6} \rho m_{3t})$  are positive while in the second derivative  $\varphi(\sigma_1, \sigma_2)$  is negative and in the third derivative the first term has a negative sign [19].

The equations (5.31) - (5.37) and (5.38) - (5.42) to calculate the SP and the ordinary critical state simplifies for the vdW fluid since they depend now only on one moment type (the indices  $i$  and  $j$  can be skipped). We obtain for  $C_2(\sigma_1, \sigma_2, T, \rho) = \rho \frac{\delta^2 A_x^+}{\delta \rho(\sigma_1) \delta \rho(\sigma_2)}$  in the

vdW excess free energy (4.1)

$$C_2(\sigma_1, \sigma_2, T, \rho) = \frac{\frac{\pi}{6}\rho}{1 - \frac{\pi}{6}\rho m_{3t}} [\sigma_1^{3t} + \sigma_2^{3t}] + \frac{\frac{\pi^2}{36}\rho^2}{(1 - \frac{\pi}{6}\rho m_{3t})^2} \sigma_1^{3t} \sigma_2^{3t} - \beta\varepsilon \frac{\pi}{6}\rho [\sigma_1^{3t+s} \sigma_2^s + 3\sigma_1^{2t+s} \sigma_2^{t+s} + 3\sigma_1^{t+s} \sigma_2^{2t+s} + \sigma_1^s \sigma_2^{3t+s}]. \quad (5.48)$$

For the weight function  $w_k(\sigma) = \sigma^k$ ,  $C_2(\sigma_1, \sigma_2, \rho, T)$  (5.31) becomes

$$C_2(\sigma_1, \sigma_2, \rho, T) = \sum_{kk'} \sigma^k c_{kk'}(\rho, T) \sigma^{k'} \quad (5.49)$$

and the SP criterion (5.34) can then be written as

$$\begin{aligned} 0 &= \sum_k \delta m_k \left( \delta_{ki} + \sum_{k'} c_{kk'}(T, \rho) m_{k'+i} \right) \\ &= \sum_k \delta m_k (\delta_{ki} + B_{ki}) \end{aligned} \quad (5.50)$$

with  $\delta m_k$  (5.33) given now for the weight function  $w_k(\sigma) = \sigma^k$  and  $B_{ki}$  (5.37) in dependence of the conventional moments

$$m_{ik} = m_{i+k} = \int d\sigma f(\sigma) \sigma^{i+k}.$$

Similar relations are valid for the moments in (5.40) ( $m_{ikl} = m_{i+k+l}$ ) and (5.41) ( $m_{iklj} = m_{i+k+l+j}$ ). From this we can follow, that if the excess free energy contains moments up to order  $n$ , the SP condition (5.50) involves moments up to order  $2n$  and the ordinary critical point (5.40) moments up to order  $3n$ .

From expressions (5.48) and (5.49) we can deduce the matrix elements  $c_{kk'}(T, \rho)$  for the size polydisperse case  $\{t = 1, s = 0\}$  ( $k = 0, 1, 2, 3; k' = 0, 1, 2, 3$ ) as

$$\begin{aligned} c_{03} = c_{30} &= \frac{\frac{\pi}{6}\rho}{1 - \frac{\pi}{6}\rho m_3} - \beta\bar{\nu} \frac{\pi}{6}\rho \\ c_{12} = c_{21} &= -\beta\bar{\nu} \frac{\pi}{2}\rho \\ c_{33} &= \frac{\frac{\pi^2}{36}\rho^2}{(1 - \frac{\pi}{6}\rho m_3)^2}, \end{aligned} \quad (5.51)$$

while all remaining elements vanish. The matrix  $(\mathbb{I} + B)$  obtained from (5.50) and (5.51) can then be written as

$$\begin{pmatrix} 1 + c_{03}m_3 & c_{03}m_4 & c_{03}m_5 & c_{03}m_6 \\ c_{12}m_2 & 1 + c_{12}m_3 & c_{12}m_4 & c_{12}m_5 \\ c_{12}m_1 & c_{12}m_2 & 1 + c_{12}m_3 & c_{12}m_4 \\ c_{03} + c_{33}m_3 & c_{03}m_1 + c_{33}m_4 & c_{03}m_2 + c_{33}m_5 & 1 + c_{03}m_3 + c_{33}m_6 \end{pmatrix}, \quad (5.52)$$

where we have set  $m_0 = 1$ . The determinant to calculate the SP is then given through (5.36) by use of (5.52). Where (5.36) has by use of (5.52) to be solved numerically for the unknown number densities  $\rho$  leading to the SP curve and the moments  $m_k$  ( $k = 1, \dots, 6$ ) are the moments of the parent distribution function  $f^{(0)}(\sigma)$ . Finally the eigenvector  $\delta m$  is obtained up to a constant from (5.50) and (5.52) by

$$\text{const} \begin{pmatrix} -\frac{1}{1+c_{03}m_3} \left[ c_{03}m_6 + c_{03}m_5 \frac{|\mathbb{I} + B|_{43}}{|\mathbb{I} + B|_{44}} - \frac{c_{03}m_4}{a} \left( b - c \frac{|\mathbb{I} + B|_{43}}{|\mathbb{I} + B|_{44}} \right) \right] \\ -\frac{1}{a} \left[ b - c \frac{|\mathbb{I} + B|_{43}}{|\mathbb{I} + B|_{44}} \right] \\ \frac{|\mathbb{I} + B|_{43}}{|\mathbb{I} + B|_{44}} \\ 1 \end{pmatrix} = \begin{pmatrix} \delta m_0 \\ \delta m_1 \\ \delta m_2 \\ \delta m_3 \end{pmatrix}, \quad (5.53)$$

where  $|\mathbb{I} + B|_{kk'}$  denotes a cofactor and the expressions for  $a$ ,  $b$  and  $c$  are given by

$$\begin{aligned} a &= (1 + c_{03}m_3)(1 + c_{12}m_3) - c_{03}m_4c_{12}m_2 \\ b &= -c_{03}m_6c_{12}m_2 + (1 + c_{03}m_3)c_{12}m_5 \\ c &= c_{03}m_5(1 + c_{12}m_3) - (1 + c_{03}m_3)c_{12}m_4. \end{aligned}$$

For the amplitude polydisperse case  $\{t = 0, s = 1\}$  ( $k = 0, 1; k' = 0, 1$ ) we obtain with (5.48) and (5.49) the coefficients for  $C_2$

$$\begin{aligned} c_{00} &= \frac{\frac{\pi^2}{36}\rho^2\bar{\sigma}^6}{\left(1 - \frac{\pi}{6}\rho\bar{\sigma}^3\right)^2} + \frac{\frac{\pi}{3}\rho\bar{\sigma}^3}{\left(1 - \frac{\pi}{6}\rho\bar{\sigma}^3\right)} \\ c_{11} &= -\frac{4\pi}{3}\rho\bar{\sigma}^3\beta, \end{aligned} \quad (5.54)$$

where all other coefficients vanish and  $\bar{\sigma} = 1$  is the average hard core diameter given by the parent distribution function  $f^{(0)}(\sigma)$ . With the coefficients (5.54) we can write the determinant of the  $2 \times 2$  matrix, which gives the SP criterion

$$(1 + c_{00})(1 + c_{11}m_2) - c_{00}c_{11}m_1^2 = 0. \quad (5.55)$$

The eigenvector  $\delta m$  in (5.50) is then given through

$$\begin{pmatrix} \delta m_0 \\ \delta m_1 \end{pmatrix} = \text{const} \begin{pmatrix} -\frac{c_{00}m_1}{1+c_{00}} \\ 1 \end{pmatrix}. \quad (5.56)$$

Having found the SP and the eigenvector  $\delta m$  for the two considered cases, we now turn to the stability condition (ST), equation (5.38). Inserting (5.46) into (5.38) we obtain in the general case [19]

$$\begin{aligned} \int d\sigma f(\sigma) e^3(\sigma) &= 3 \left( \frac{\rho}{1 - \frac{\pi}{6}\rho m_{3t}} \right)^2 \left\{ \int d\sigma f(\sigma) e(\sigma) \right\} \left\{ \int d\sigma f(\sigma) e(\sigma) V(\sigma) \right\}^2 \\ &+ 2 \left( \frac{\rho}{1 - \frac{\pi}{6}\rho m_{3t}} \right)^3 \left\{ \int d\sigma f(\sigma) e(\sigma) V(\sigma) \right\}^3. \end{aligned}$$

Substitution of

$$e(\sigma) = \sum_k a_{0k} \sigma^k$$

with

$$a_{0k} = - \sum_{k'} c_{kk'} \delta m_{k'}$$

into the above equation yields finally

$$\begin{aligned} \sum_{k,k',k''} a_{0k} a_{0k'} a_{0k''} m_{k+k'+k''} &= 3 \left( \frac{\frac{\pi}{6} \rho}{1 - \frac{\pi}{6} \rho m_{3t}} \right)^2 \left( \sum_k a_{0k} m_k \right) \left( \sum_{k'} a_{0k'} m_{k'+3t} \right)^2 \\ &+ 2 \left( \frac{\frac{\pi}{6} \rho}{1 - \frac{\pi}{6} \rho m_{3t}} \right)^3 \left( \sum_k a_{0k} m_{k+3t} \right)^3, \end{aligned} \quad (5.57)$$

where the coefficients  $a_{0k}$  for size polydispersity only ( $s = 0, t = 1$ ) are given as

$$\begin{aligned} a_{00} &= -c_{03} \delta m_3 \\ a_{01} &= -c_{12} \delta m_2 \\ a_{02} &= -c_{12} \delta m_1 \\ a_{03} &= -c_{03} \delta m_0 - c_{33} \delta m_3, \end{aligned}$$

whereas for amplitude polydispersity only ( $s = 1, t = 0$ ) one obtains

$$\begin{aligned} a_{00} &= -c_{00} \delta m_0 \\ a_{01} &= -c_{11} \delta m_1. \end{aligned}$$

Equations (5.50) and (5.57) have to be solved simultaneously to get the critical point using (5.52) and (5.53) for the size polydisperse case and using (5.55) and (5.56) for the amplitude polydisperse case. In the present context this amounts to look for thermodynamic states  $(T, \rho)$  which, for a given distribution function  $f(\sigma) = f^{(0)}(\sigma)$ , satisfy both (5.50) and the stability criteria (5.57). In the vdW model the relation  $\delta^4 A^+ > 0$  is always satisfied because equation (5.47) is positive definite.

### 5.4.5 HS fluid with attractive tail

The free energy (4.50) calculated within the ORPA does not belong to the class of truncatable free energies. We restrict ourselves therefore to the free energy within the HTA (4.12). Here we have to make in addition the approximation that the radial pair distribution function of the HS system takes its long distance value, what means  $g_0(r, \sigma_i, \sigma_j) = 1$ .

With this approximation we obtain the free energy

$$\begin{aligned} A^+ &= A_{id}^+ + A_{ex,0}^+ + \beta \frac{\rho^2}{2} \int d\sigma_i f(\sigma_i) \int d\sigma_j f(\sigma_j) \int d^3r \phi(r, \sigma_i, \sigma_j) \\ &= A_{id}^+ + A_{ex,0}^+ + \beta \frac{\rho^2}{2} \int d\sigma_i f(\sigma_i) \int d\sigma_j f(\sigma_j) \varphi(\sigma_i, \sigma_j), \end{aligned} \quad (5.58)$$

where  $A_{ex,0}^+$  is the excess free energy (4.62) of the HS system and  $\varphi(\sigma, \sigma')$  is the average potential. For the square-well potential (2.8) we obtain [18]

$$\varphi(\sigma, \sigma') = -\frac{4\pi}{3} \hat{\sigma}^3 (\lambda^3(\sigma, \sigma') - 1) \varepsilon(\sigma, \sigma') = -\frac{4\pi}{3} \hat{\sigma}^3 [\lambda^3(\sigma, \sigma') - 1] e^{z(\hat{\sigma} - \bar{\sigma})} \bar{\varepsilon}, \quad (5.59)$$

and for the Yukawa potential (2.9) we find [53]

$$\varphi(\sigma, \sigma') = -\gamma(\sigma, \sigma') \frac{4\pi}{\kappa(\sigma, \sigma')} \left( \hat{\sigma} + \frac{1}{\kappa(\sigma, \sigma')} \right) = -4\pi \bar{\gamma} \frac{\sigma^a \sigma'^a}{\bar{\sigma}^{2(a-1)}} \left( \hat{\sigma} + \frac{1}{\kappa(\sigma, \sigma')} \right), \quad (5.60)$$

where  $\bar{\sigma}$  is the average hard core diameter given as

$$\bar{\sigma} = m_1 = \int d\sigma f(\sigma) \sigma,$$

$\bar{\varepsilon}$  and  $\bar{\gamma}$  have the dimension of an energy,  $a$  is a positive integer, which models the charge in the Yukawa potential and  $z$  is a parameter (with dimension of an inverse length) modeling the depth of the square well. Both expressions (5.59) and (5.60) are size and amplitude polydisperse. If we set  $\kappa(\sigma, \sigma')$  and  $\lambda(\sigma, \sigma')$  to constant values and in addition  $a = 0$  and  $z = 0$  then we obtain potentials which are size polydisperse only.

In the above equations (5.59) and (5.60), we have used the Berthelot rule [26]

$$\begin{aligned} \epsilon(\sigma, \sigma') &= \sqrt{\epsilon(\sigma, \sigma) \epsilon(\sigma', \sigma')} = \bar{\varepsilon} e^{\frac{z}{2}(\sigma - \bar{\sigma})} e^{\frac{z}{2}(\sigma' - \bar{\sigma})} \\ \gamma(\sigma, \sigma') &= \sqrt{\gamma(\sigma, \sigma) \gamma(\sigma', \sigma')} = \bar{\gamma} \frac{\sigma^a}{\bar{\sigma}^{a-1}} \frac{\sigma'^a}{\bar{\sigma}^{a-1}} \sqrt{\kappa(\sigma, \sigma) \kappa(\sigma', \sigma')} \\ \kappa(\sigma, \sigma') &= \sqrt{\kappa(\sigma, \sigma) \kappa(\sigma', \sigma')}. \end{aligned} \quad (5.61)$$

As we can see in (5.59) and (5.60) the potentials depend now not only on the sphere diameters, but also on the first moment  $m_1$  of the distribution function  $f(\sigma)$ . This has to be taken into account in the calculation of the chemical potential  $\mu(\sigma)$ . For the excess chemical potential (3.19) and for the pressure (4.6), one obtains then by use of (4.7)

$$\begin{aligned} \beta \mu_{ex}(\sigma, T, \rho, [f]) &= \beta \mu_{ex,0}(\sigma, T, \rho, [f]) + \beta \rho \int d\sigma' f(\sigma') \varphi(\sigma, \sigma', m_1) + \\ &\quad \beta \frac{\rho^2}{2} \int d\sigma' f(\sigma') \int d\sigma'' f(\sigma'') \frac{\delta \varphi(\sigma', \sigma'', m_1)}{\delta \rho(\sigma)} \end{aligned} \quad (5.62)$$

$$\beta p(T, \rho, [f]) = \beta p_0(T, \rho, [f]) + \frac{\beta \rho^2}{2} \int d\sigma f(\sigma) \int d\sigma' f(\sigma') \varphi(\sigma, \sigma', m_1), \quad (5.63)$$

where  $p_0$  is the pressure (4.61) and  $\mu_{ex,0}$  the excess chemical potential of polydisperse HS are given by [12]

$$\begin{aligned} \beta \mu_{ex,0}(\sigma, T, \rho, [f]) = & -\ln \left( 1 - \frac{\pi}{6} \rho m_3 \right) + \frac{\sigma^3 + \frac{\pi}{2} \rho \sigma (\sigma m_1 + m_2)}{1 - \frac{\pi}{6} \rho m_3} + \\ & \frac{\pi^2 \rho^2 \sigma^2 m_2 (\frac{1}{3} \sigma m_1 + \frac{1}{2} m_2)}{4(1 - \frac{\pi}{6} \rho m_3)^2} + \frac{(\pi \rho \sigma m_2)^3}{72(1 - \frac{\pi}{6} \rho m_3)^3} \\ & + \frac{2\pi \rho (\sigma m_2)^2}{m_3} \left( 3 \left[ \frac{1 - \frac{\pi}{4} \rho m_3}{(1 - \frac{\pi}{6} \rho m_3)^2} + \frac{6 \ln(1 - \frac{\pi}{6} \rho m_3)}{\pi \rho m_3} \right] \right. \\ & \left. - \frac{\sigma m_2}{m_3} \left[ \frac{1 - \frac{\pi}{6} \rho m_3 + (1 - \frac{\pi}{3} \rho m_3)^2}{(1 - \frac{\pi}{6} \rho m_3)^3} + \frac{12}{\pi \rho m_3} \ln \left( 1 - \frac{\pi}{6} \rho m_3 \right) \right] \right). \end{aligned} \quad (5.64)$$

The last term in (5.62) vanishes only in the limit  $z = 0$  for the square-well potential and  $a = 1$  for the Yukawa potential. From definition (5.64) we can calculate  $C_2(\rho, T, \sigma, \sigma')$  (5.49) for the HS system, for which the non-vanishing coefficients  $c_{kk'}^{HS}(\rho, T)$  ( $k, k' = 0, 1, 2, 3$ ) are given as

$$\begin{aligned} c_{03}^{HS} &= c_{30}^{HS} = \frac{\frac{\pi}{6} \rho}{(1 - \frac{\pi}{6} \rho m_3)} \\ c_{12}^{HS} &= c_{21}^{HS} = \frac{\frac{\pi}{2} \rho}{1 - \frac{\pi}{6} \rho m_3} \\ c_{13}^{HS} &= c_{31}^{HS} = \frac{\frac{\pi^2}{12} \rho^2 m_2}{(1 - \frac{\pi}{6} \rho m_3)^2} \\ c_{23}^{HS} &= c_{32}^{HS} = \frac{1}{12 m_3^3 (1 - \frac{\pi}{6} \rho m_3)^2} \left[ \pi^2 \rho^2 m_1 m_3^3 - 3 m_2^2 \left( 72 \ln \left[ 1 - \frac{\pi}{6} \rho m_3 \right] \right. \right. \\ & \left. \left. + 12\pi \left( 1 - 2 \ln \left[ 1 - \frac{\pi}{6} \rho m_3 \right] \right) \rho m_3 + \pi^2 \left( -3 + 2 \ln \left[ 1 - \frac{\pi}{6} \rho m_3 \right] \right) \rho^2 m_3^2 \right] \\ c_{33}^{HS} &= \frac{-1}{216 m_3^4 (1 - \frac{\pi}{6} \rho m_3)^3} \left[ -6\pi^3 \rho^3 m_1 m_2 m_3^4 - 6\pi^2 \rho^2 m_3^4 \left( 1 - \frac{\pi}{6} \rho m_3 \right) + \right. \\ & \left. 3m_2^3 \left( -1296 \ln \left[ 1 - \frac{\pi}{6} \rho m_3 \right] + 216\pi \left( -1 + 3 \ln \left[ 1 - \frac{\pi}{6} \rho m_3 \right] \right) \rho m_3 - \right. \right. \\ & \left. \left. 18\pi^2 \left( -5 + 6 \ln \left[ 1 - \frac{\pi}{6} \rho m_3 \right] \right) \rho^2 m_3^2 + \pi^3 \left( -11 + 6 \ln \left[ 1 - \frac{\pi}{6} \rho m_3 \right] \right) \rho^3 m_3^3 \right] \\ c_{22}^{HS} &= \frac{m_2}{4m_3^2 (1 - \frac{\pi}{6} \rho m_3)^2} \left[ 72 \ln \left[ 1 - \frac{\pi}{6} \rho m_3 \right] + 12\pi \left( 1 - 2 \ln \left[ 1 - \frac{\pi}{6} \rho m_3 \right] \right) \rho m_3 \right. \\ & \left. + 2\pi^2 \left( -1 + \ln \left[ 1 - \frac{\pi}{6} \rho m_3 \right] \right) \rho^2 m_3^2 \right]. \end{aligned} \quad (5.65)$$

### 5.4.5.1 Square-well fluid

The expressions in equation (5.62) and (5.63) become for the square-well potential (5.59)

$$\begin{aligned}\mu_{ex}(\sigma) &= \mu_{ex,0} - \rho \frac{\pi}{6} \bar{\varepsilon} (\lambda^3 - 1) e^{-zm_1} \left[ e^{\frac{z}{2}\sigma} (\bar{m}_3(z) + \sigma^3 \bar{m}_0(z) + 3\sigma \bar{m}_2(z) + 3\sigma^2 \bar{m}_1(z)) \right. \\ &\quad \left. - z(\sigma - m_1) [\bar{m}_3(z) \bar{m}_0(z) + 3\bar{m}_1(z) \bar{m}_2(z)] \right] \\ p &= p_0 - \frac{\pi}{6} \rho^2 \bar{\varepsilon} (\lambda^3 - 1) e^{-zm_1} (\bar{m}_0(z) \bar{m}_3(z) + 3\bar{m}_1(z) \bar{m}_2(z)),\end{aligned}\quad (5.66)$$

where we have used for  $\lambda(\sigma, \sigma')$  the constant value  $\lambda$  and the generalized moments  $\bar{m}_k(z)$  ( $k = 0, 1, 2, 3$ ) are calculated from (5.14) with  $w_k(\sigma) = \sigma^k e^{\frac{z}{2}\sigma}$ .

The chemical potential and the pressure in (5.66) involves two types of moments; conventional moments  $m_k$  via the HS contribution and generalized moments  $\bar{m}_k$  via the potential contribution. The phase equilibrium conditions are then given by the equations (5.23) and (5.24) for the unknown moments  $m_k^{(1)}$  ( $w_k(\sigma) = \sigma^k$ ), generalized moments  $\bar{m}_k^{(1)}$  ( $w_k(\sigma) = \sigma^k e^{\frac{z}{2}\sigma}$ ) and the number densities  $\rho^{(1)}$  and  $\rho^{(2)}$ . Together with the normalization relation (5.19) this provides 9 equations for the 9 unknowns. The distribution functions of the two phases are obtained by the equations (5.18) and (5.15).

The CPC and the SC are obtained from equations (5.25) - (5.27) by use of equation (5.66).

To simplify the equations for the spinodal criterion (5.31) - (5.37) we will restrict ourselves with the calculation of the spinodal to the size polydisperse case ( $z = 0$ ): equations (5.66) depend then only on one moment type - the conventional moments  $m_k$  ( $k = 1, 2, 3$ ) - and we can use (5.50) to calculate the number densities characterizing the region of local stability. The non-zero coefficients  $c_{kk'}(\rho, T)$  in (5.49) for the square-well fluid are then given with (5.65) as

$$\begin{aligned}c_{03} &= c_{30} = c_{03}^{HS} - \beta \bar{\varepsilon} \frac{\pi}{6} \rho (\lambda^3 - 1) \\ c_{12} &= c_{21} = c_{12}^{HS} - \beta \bar{\varepsilon} \frac{\pi}{2} \rho (\lambda^3 - 1) \\ c_{13} &= c_{31} = c_{13}^{HS} \\ c_{22} &= c_{22}^{HS} \\ c_{23} &= c_{32} = c_{23}^{HS} \\ c_{33} &= c_{33}^{HS}\end{aligned}\quad (5.67)$$

with the corresponding determinant (5.36)

$$\begin{vmatrix} a_{11} & a_{12} & a_{13} & a_{14} \\ a_{21} & a_{22} & a_{23} & a_{24} \\ a_{31} & a_{32} & a_{33} & a_{34} \\ a_{41} & a_{42} & a_{43} & a_{44} \end{vmatrix} = 0,\quad (5.68)$$

and the matrix elements in the general case

$$\begin{aligned}
a_{11} &= 1 + c_{00} + c_{01}m_1 + c_{02}m_2 + c_{03}m_3 \\
a_{12} &= c_{00}m_1 + c_{01}m_2 + c_{02}m_3 + c_{03}m_4 \\
a_{13} &= c_{00}m_2 + c_{01}m_3 + c_{02}m_4 + c_{03}m_5 \\
a_{14} &= c_{00}m_3 + c_{01}m_4 + c_{02}m_5 + c_{03}m_6 \\
a_{21} &= c_{01} + c_{11}m_1 + c_{12}m_2 + c_{13}m_3 \\
a_{22} &= 1 + c_{01}m_1 + c_{11}m_2 + c_{12}m_3 + c_{13}m_4 \\
a_{23} &= c_{01}m_2 + c_{11}m_3 + c_{12}m_4 + c_{13}m_5 \\
a_{24} &= c_{01}m_3 + c_{11}m_4 + c_{12}m_5 + c_{13}m_6 \\
a_{31} &= c_{02} + c_{12}m_1 + c_{22}m_2 + c_{23}m_3 \\
a_{32} &= c_{02}m_1 + c_{12}m_2 + c_{22}m_3 + c_{23}m_4 \\
a_{33} &= 1 + c_{02}m_2 + c_{12}m_3 + c_{22}m_4 + c_{23}m_5 \\
a_{34} &= c_{02}m_3 + c_{12}m_4 + c_{22}m_5 + c_{23}m_6 \\
a_{41} &= c_{03} + c_{13}m_1 + c_{23}m_2 + c_{33}m_3 \\
a_{42} &= c_{03}m_1 + c_{13}m_2 + c_{23}m_3 + c_{33}m_4 \\
a_{43} &= c_{03}m_2 + c_{13}m_3 + c_{23}m_4 + c_{33}m_5 \\
a_{44} &= 1 + c_{03}m_3 + c_{13}m_4 + c_{23}m_5 + c_{33}m_6
\end{aligned} \tag{5.69}$$

to calculate the number densities  $\rho^{(0)}$  for the SP criterion (5.50). The eigenvector  $\delta m$  in (5.50) of a  $4 \times 4$  matrix can be written in general form as

$$const \begin{pmatrix} -\frac{1}{a_{11}} \left[ a_{14} + a_{13} \frac{|\mathbb{I} + B|_{43}}{|\mathbb{I} + B|_{44}} - \frac{a_{12}}{a} \left( b - c \frac{|\mathbb{I} + B|_{43}}{|\mathbb{I} + B|_{44}} \right) \right] \\ -\frac{1}{a} \left[ b - c \frac{|\mathbb{I} + B|_{43}}{|\mathbb{I} + B|_{44}} \right] \\ \frac{|\mathbb{I} + B|_{43}}{|\mathbb{I} + B|_{44}} \\ 1 \end{pmatrix} = \begin{pmatrix} \delta m_0 \\ \delta m_1 \\ \delta m_2 \\ \delta m_3 \end{pmatrix}, \tag{5.70}$$

with  $B$  from (5.50) and the expressions

$$\begin{aligned}
a &= a_{11}a_{22} - a_{21}a_{12} \\
b &= a_{11}a_{24} - a_{14}a_{21} \\
c &= a_{13}a_{21} - a_{11}a_{23}.
\end{aligned} \tag{5.71}$$

### 5.4.5.2 Yukawa fluid

For the Yukawa potential the expressions (5.62) and (5.63) become

$$\begin{aligned}\mu_{ex}(\sigma) &= \mu_{ex,0} - 4\pi\rho\bar{\gamma}\frac{\sigma^a}{m_1^{2(a-1)}}\left(\frac{m_{a+1}}{2} + \left[\frac{\sigma}{2} + \frac{1}{\kappa}\right]m_a\right) \\ &\quad + 4\pi\rho\bar{\gamma}\frac{(a-1)}{m_1^{2a-1}}(\sigma - m_1)\left[m_{a+1}m_a + \frac{m_a^2}{\kappa}\right] \\ p &= p_0 - 2\pi\bar{\gamma}\frac{\rho^2}{m_1^{2(a-1)}}\left(m_a m_{a+1} + \frac{m_a^2}{\kappa}\right),\end{aligned}\tag{5.72}$$

where we have set  $\kappa(\sigma, \sigma')$  to the constant value  $\kappa$ ;  $m_a$  and  $m_{a+1}$  are conventional moments. The phase coexistence conditions (5.23) and (5.24) ( $w_k(\sigma) = \sigma^k$ ) and (5.19) are then solved by use of (5.72) to get the unknowns  $(\rho^{(1)}, \rho^{(2)}, m_k^{(1)})$  where  $k = 1, 2, 3$  if  $a \leq 2$  (5 unknowns) otherwise  $k = 1, \dots, a + 1$  ( $a + 3$  unknowns). The distribution functions of the two phases are again obtained from the equations (5.18) and (5.15).

The CPC and the SC are obtained from equations (5.25) - (5.27) by use of equation (5.72).

The coefficients  $c_{kk'}(\rho, T)$  for the SP criterion (5.50) depend on  $a$ . We have restricted ourselves to the cases  $a = 0$  (size polydisperse),  $a = 1$  and  $a = 2$ . For the size polydisperse case only ( $a = 0$ ) we obtain the non- vanishing coefficients

$$\begin{aligned}c_{00} &= -\beta\bar{\gamma}4\pi\rho m_1^3 \\ c_{01} &= c_{10} = \beta\bar{\gamma}6\pi\rho m_1^2 \\ c_{03} &= c_{30} = c_{03}^{HS} \\ c_{11} &= -\frac{4\pi}{\kappa}\rho(1 + 3\kappa m_1) \\ c_{12} &= c_{21} = c_{12}^{HS} - 2\beta\bar{\gamma}\pi\rho \\ c_{13} &= c_{31} = c_{13}^{HS} \\ c_{22} &= c_{22}^{HS} \\ c_{23} &= c_{32} = c_{23}^{HS} \\ c_{33} &= c_{33}^{HS}\end{aligned}\tag{5.73}$$

with the elements (5.69) of the determinant (5.68).

For  $a = 1$  the non-zero coefficients in (5.49) read

$$\begin{aligned}
c_{03} &= c_{30} = c_{03}^{HS} \\
c_{11} &= -\frac{4\pi}{\kappa}\rho \\
c_{12} &= c_{21} = c_{12}^{HS} - 2\beta\bar{\gamma}\pi\rho \\
c_{13} &= c_{31} = c_{13}^{HS} \\
c_{22} &= c_{22}^{HS} \\
c_{23} &= c_{32} = c_{23}^{HS} \\
c_{33} &= c_{33}^{HS}
\end{aligned} \tag{5.74}$$

with the elements (5.69) of the determinant (5.68). For  $a = 2$  we get the non-zero coefficients

$$\begin{aligned}
c_{00} &= -\beta\bar{\gamma}4\pi\rho\frac{m_2(m_2 + \kappa m_3)}{\kappa m_1^2} \\
c_{01} &= c_{10} = \beta\bar{\gamma}8\pi\rho\frac{m_2(m_2 + \kappa m_3)}{\kappa m_1^3} \\
c_{02} &= c_{20} = -\beta\bar{\gamma}4\pi\rho\frac{2m_2 + \kappa m_3}{\kappa m_1^2} \\
c_{03} &= c_{30} = c_{03}^{HS} - \beta\bar{\gamma}4\pi\rho\frac{m_2}{m_1^2} \\
c_{11} &= -\beta\bar{\gamma}12\pi\rho\frac{m_2(m_2 + \kappa m_3)}{\kappa m_1^4} \\
c_{12} &= c_{21} = c_{12}^{HS} + \beta\bar{\gamma}4\pi\rho\frac{2m_2 + \kappa m_3}{\kappa m_1^3} \\
c_{13} &= c_{31} = c_{13}^{HS} + \beta\bar{\gamma}4\pi\rho\frac{m_2}{m_1^3} \\
c_{22} &= c_{22}^{HS} - \beta\bar{\gamma}4\pi\frac{\rho}{\kappa m_1^2} \\
c_{23} &= c_{32} = c_{23}^{HS} - \beta\bar{\gamma}2\pi\frac{\rho}{m_1^2} \\
c_{33} &= c_{33}^{HS}
\end{aligned} \tag{5.75}$$

to calculate the matrix elements (5.69) for the SP criterion.

The eigenvectors  $\delta m$  for the three different cases can be obtained by the use of (5.70) together with (5.73) - (5.75).

# Chapter 6

## Results

### 6.1 Parent phase distribution

We now specify,  $\rho^{(0)}(\sigma) = \rho^{(0)} f^{(0)}(\sigma)$ , the distribution of the parent phases to be considered here. Very large values of  $\sigma$  are unphysical but these will be given a very small weight by requiring that  $f^{(0)}(\sigma)$  decays with  $\sigma$  in a manner which is sufficiently rapid for all the moments of  $f^{(0)}(\sigma)$ ,  $m_k^{(0)}$ , to exist. In addition, we restrict ourselves to monomodal distributions so that the systems considered here are polydisperse generalizations of single component systems. We have limited ourselves in this work to the Schulz-Zimm (SZ) distribution

$$f^{(0)}(\sigma) = \frac{\alpha^\alpha}{\Gamma(\alpha)} \sigma^{\alpha-1} e^{-\alpha\sigma}, \quad (6.1)$$

where  $\Gamma(\alpha)$  is the Euler gamma function of argument  $0 < \alpha < \infty$ , where  $\alpha$  is a parameter which determines the inverse width of the SZ distribution, or equivalently, its polydispersity index,  $I = 1 + \frac{1}{\alpha}$  [19]; the average hard core diameter was set to  $\bar{\sigma} = m_1^{(0)} = 1$ . The conventional moments of (6.1) are given by

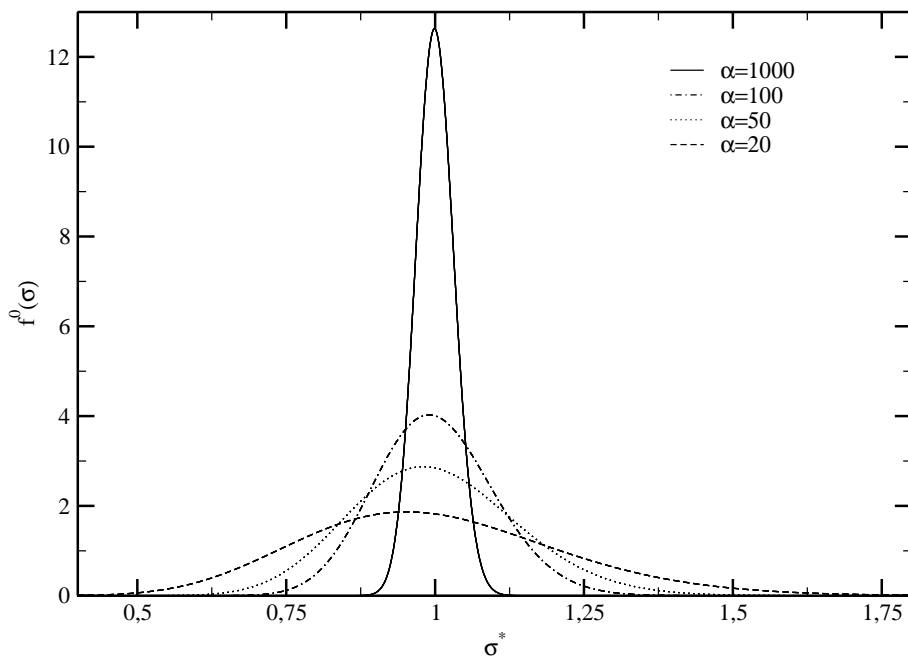
$$m_k = \frac{1}{\alpha^k} \frac{\Gamma(\alpha + k)}{\Gamma(\alpha)}, \quad (6.2)$$

whereas the generalized moments  $\bar{m}_k$  (5.14) of the square-well fluid ( $w_k(\sigma) = \sigma^k e^{-\frac{z}{2}\sigma}$ ) are defined by use of the SZ distribution as

$$\bar{m}_k = \frac{\alpha^{\alpha-1}}{(\alpha - \frac{z}{2})^{\alpha-1+k}} \frac{\Gamma(\alpha + k)}{\Gamma(\alpha)}. \quad (6.3)$$

As we can see from (6.2) the conditions (2.1) are fulfilled.

In the monodisperse limit ( $I \rightarrow 1, \alpha \rightarrow \infty$ ) the SZ distribution reduces to the Dirac distribution,  $\delta(\sigma - 1)$ , centered around the average species diameter  $\bar{\sigma} = 1$ . On the contrary, when  $I$  becomes very large ( $\alpha$  is small) the above distribution becomes very

Figure 6.1: Schulz distributions for different values of inverse width  $\alpha$ 

wide, increasing hereby the importance of the particles which are not only centered around  $\bar{\sigma}$ . In figure 6.1, we have plotted the SZ distribution functions versus reduced hard core diameter  $\sigma^* = \frac{\sigma}{\bar{\sigma}}$  for the four  $\alpha$  values used in this chapter. Note, that the average value  $\bar{\sigma}$  does not coincide with the value of  $\sigma$  for which  $f^{(0)}(\sigma)$  reaches its maximum: the maximum is shifted to lower  $\sigma$  when the polydispersity increases.

## 6.2 Thermodynamics

We have examined the behavior of the thermodynamic quantities within the ORPA for the polydisperse square-well (2.8) and for the Yukawa potential (2.9) by use of the relations (5.61). We have calculated four thermodynamic quantities, the isothermal compressibility (4.58), the Helmholtz free energy (4.49), the virial pressure (4.42) as well as the pressure obtained by derivation of the Helmholtz free energy with respect to the volume (3.16) to check the self-consistency of the ORPA method introduced in chapter 4; we have used the PY solution for the reference HS systems. We have chosen the reduced temperatures  $t = \frac{k_B T}{\epsilon}$  (SW);  $t = \frac{k_B T}{\gamma}$  (HSY) to be below the critical temperature of the corresponding monodisperse system since we want to study the influence of polydispersity on the thermodynamic properties. We have examined the behavior of the thermodynamic quantities for different polydispersity indices  $I$  and have compared these results with the monodisperse case.

The following figures, are arranged as follows: for each of the four thermodynamic quantities mentioned above we display on one page three plots, where each of them shows the results for a different potential parameter ( $z = 0, 1$  or  $2$  for the square-well potential and  $a = 0, 1$ , or  $2$  for the Yukawa potential), in addition each of this single plots shows this thermodynamic quantity as function of  $\rho^* = \rho\bar{\sigma}^3$  for three  $\alpha$  values ( $\alpha = 1000; \alpha = 50; \alpha = 20$ ), where for  $\alpha = 1000$  we produce the monodisperse case. As shown in the following figures the convergence of the ORPA algorithm is good for small  $z$  or  $a$ , large temperature  $t$  and small polydispersity index  $I$ . In regions where the ORPA fails the curves for the corresponding thermodynamic quantities are interrupted. The vertical lines in the plots mark for the given temperature  $t$  the  $\rho$ -values of the spinodal belonging to the monodisperse fluid.

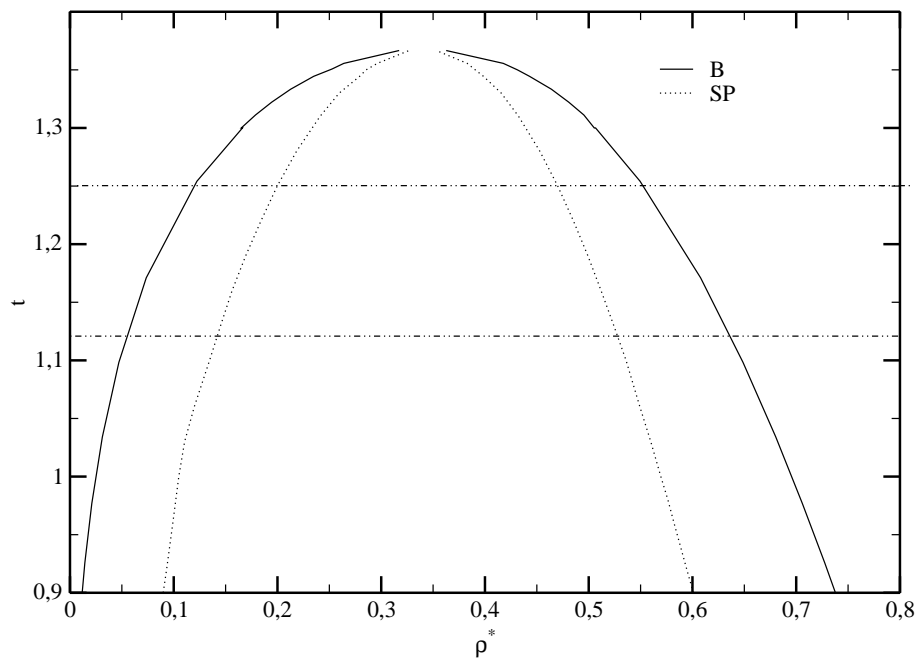
### 6.2.1 Square-well fluid

In figure 6.2 we have plotted the gas-liquid coexistence curve together with the SP curve for the monodisperse square-well system for  $\lambda = 1.5$  within the ORPA. The binodals were calculated via the common tangent construction what means by the derivation of the free energy with respect to the volume and with respect to the particle number to obtain the equilibrium conditions given by the equality of pressures and chemical potentials. The horizontal lines indicate the two temperatures ( $t = 1.25, t = 1.12$ ) for which we have calculated the thermodynamic quantities discussed below.

The parameter  $z$  within the square-well potential (5.61) has the task to vary the potential strength in dependence of the particle sizes; for size polydispersity  $z = 0$  all particles are attracted, irrespective of the particle diameters, by the same pair potential depending only on the inverse temperature, whereas for  $z \neq 0$  (size and amplitude polydispersity) the potential depth becomes  $\sigma$  dependent.

In figures 6.3 and 6.4 we show the reduced (with respect to the ideal gas) isothermal compressibility (4.58) ( $\chi_T^* = \frac{\chi_T}{\chi_{Tid}}$ ) of the polydisperse square-well fluid, for  $t = 1.25$  and  $t = 1.12$ . We observe that in all cases the maximum of the peak in the isothermal compressibility moves to lower densities as the polydispersity is increased. According to this remarks we can observe for increasing  $z$  and  $I$  that the isothermal compressibilities belonging to the gas phases (for densities lower than the densities on the left branch of the monodisperse spinodal) split more and more off, while for the liquid phase (densities higher than the densities on the right branch of the monodisperse spinodal) we can observe the opposite effect but much weaker.

Due to physical reasons the isothermal compressibility should diverge within the region of instability characterized in figures 6.3 and 6.4 for the monodisperse case by vertical lines. The ORPA does not lead to the expected divergence of the compressibility, neither for the

Figure 6.2: Phase coexistence region of a monodisperse square-well fluid with  $\lambda = 1.5$ 

monodisperse nor for the polydisperse case. This can be explained by the thermodynamic inconsistency of the ORPA. The spinodal curve in figure 6.2 was calculated from the free energy (4.49) obtained via the virial route, while the region where the compressibility diverges should be determined from the free energy (3.24) obtained via the compressibility route.

Figure 6.3: Reduced dimensionless isothermal compressibilities of a polydisperse square-well system with  $\lambda = 1.5$  reduced temperature  $t = 0.8$  for different  $\alpha$ -values, where each single plot represents a different value  $z$  (from top to the bottom  $z = 0, z = 1, z = 2$ ).

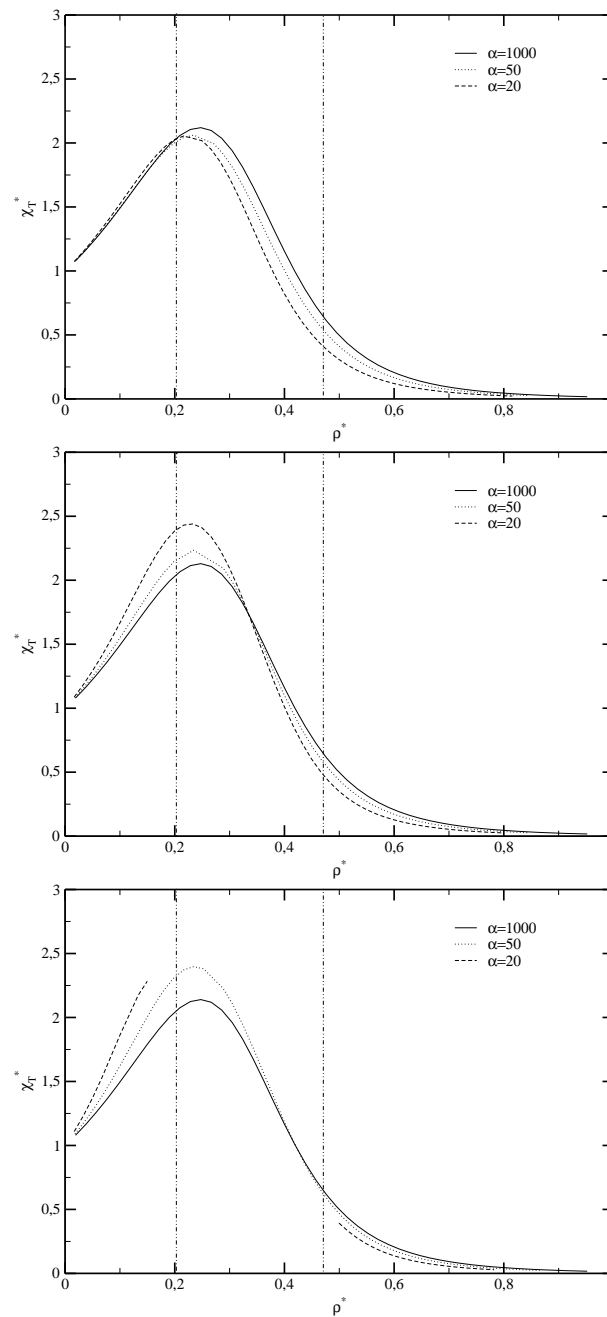
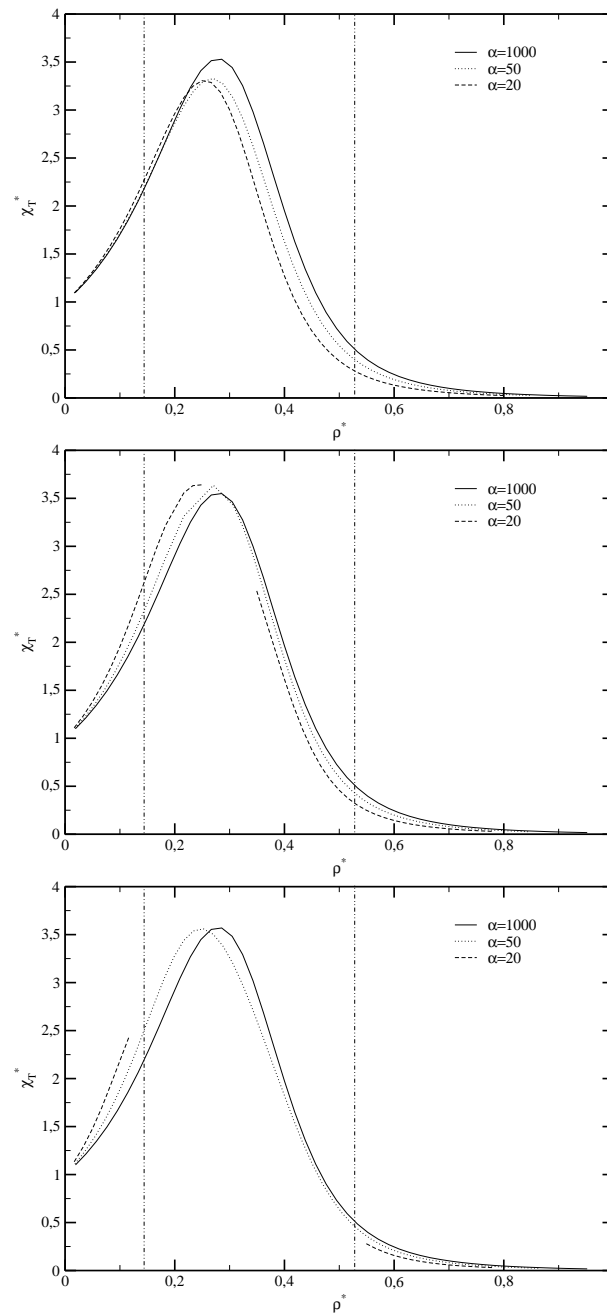


Figure 6.4: Reduced dimensionless isothermal compressibilities of a polydisperse square-well system with  $\lambda = 1.5$  and reduced temperature  $t = 1.12$  for different  $\alpha$ -values, where each single plot represents a different value  $z$  (from top to the bottom  $z = 0, z = 1, z = 2$ ).



In figures 6.5 and 6.6 we have plotted the free energy density  $A^+$  (4.49) for  $t = 1.25$  and  $t = 1.12$ . For fixed temperature and fixed  $z$  one can observe that the minimum in the free energy density is shifted to lower densities as the polydispersity increases. For increasing  $z$  the minimum of the free energy density moves to smaller values because the attractions become more important as compared with the size polydisperse and the monodisperse case. In addition we can see that the free energies on the liquid phase side split off in dependence of  $I$ . If we let the composition of the system unaltered by the phase transition process as it is the case along the CPC we can expect, that for the size polydisperse free energies ( $z = 0$ ) in figures 6.5 and 6.6, the densities representing the high density phase corresponding to the right branch of the CPC will lie at lower densities than the corresponding high density phase given by the monodisperse phase coexistence curve. For size and amplitude polydispersity ( $z = 1, z = 2$ ) the high density phase on the CPC has moved towards higher densities than the high density phase of the monodisperse case. This can be checked by making the common tangent construction to the free energies in figures 6.5 and 6.6 for fixed  $I$ . We will see the effects discussed above more evidently by looking at the phase diagrams of the next section.

Figures 6.8 and 6.10 show the virial pressure (4.42)  $\frac{p^v}{t}$  for  $t = 1.25$  and  $t = 1.12$ . As we can see in each single plot the minimum of the virial pressure moves to lower densities as the polydispersity increases and with increasing  $z$  the values for the virial pressures decrease. As we increase the amplitude polydispersity, the virial pressure tends to have negative values (i.e. unphysical) in an increasingly large  $\rho$ -range. As long as this happens in the region of instability where the values of the thermodynamic quantities are not defined the unphysical results play no role. If the ORPA leads to negative pressures in the region of local stability, one has to check that the equilibrium densities for the gas-liquid coexistences are not represented by negative pressures, to avoid unphysical phase transitions. The pressure  $\frac{p^A}{t}$  (3.16) plotted in figures 6.7 and 6.9 is calculated from the virial free energy, it shows qualitatively the same behavior as  $p^v$  and should by comparison with  $p^v$  give some insight into the degree of thermodynamic inconsistency of the ORPA. Results from  $p^v$  and  $p^A$  agree rather well for small and intermediate values of  $\rho^*$ , while for larger number densities the self consistency is worse. As we can see in figures 6.7 - 6.10 the self consistency is independent of the polydispersity  $I$  and of the potential parameter  $z$ .

Figure 6.5: Free energy densities of a polydisperse square-well system with  $\lambda = 1.5$  and reduced temperature  $t = 1.25$  for different  $\alpha$ -values, where each single plot represents a different value  $z$  (from top to the bottom  $z = 0, z = 1, z = 2$ ).

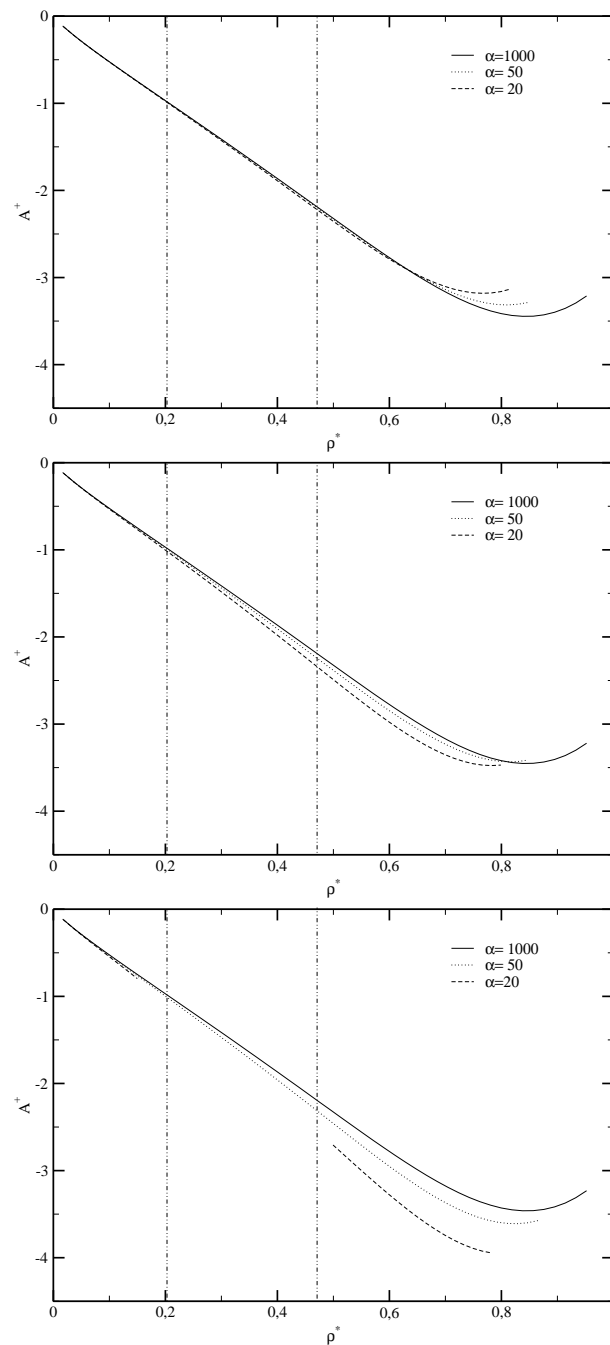


Figure 6.6: Free energy densities of a polydisperse square-well system with  $\lambda = 1.5$  and reduced temperature  $t = 1.12$  for different  $\alpha$ -values, where each single plot represents a different value  $z$  (from top to the bottom  $z = 0, z = 1, z = 2$ ).

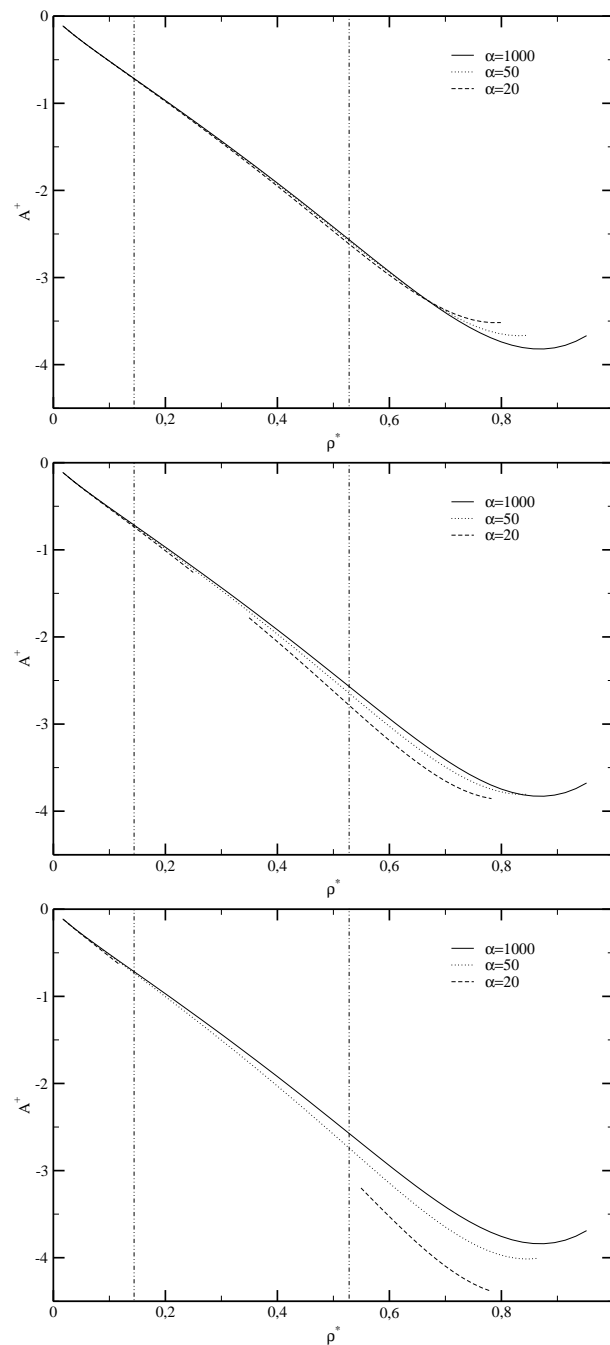


Figure 6.7: Pressures calculated from the free energy of a polydisperse square-well system with  $\lambda = 1.5$  and reduced temperature  $t = 1.25$  for different  $\alpha$ -values, where each single plot represents a different value  $z$  (from top to the bottom  $z = 0, z = 1, z = 2$ ).

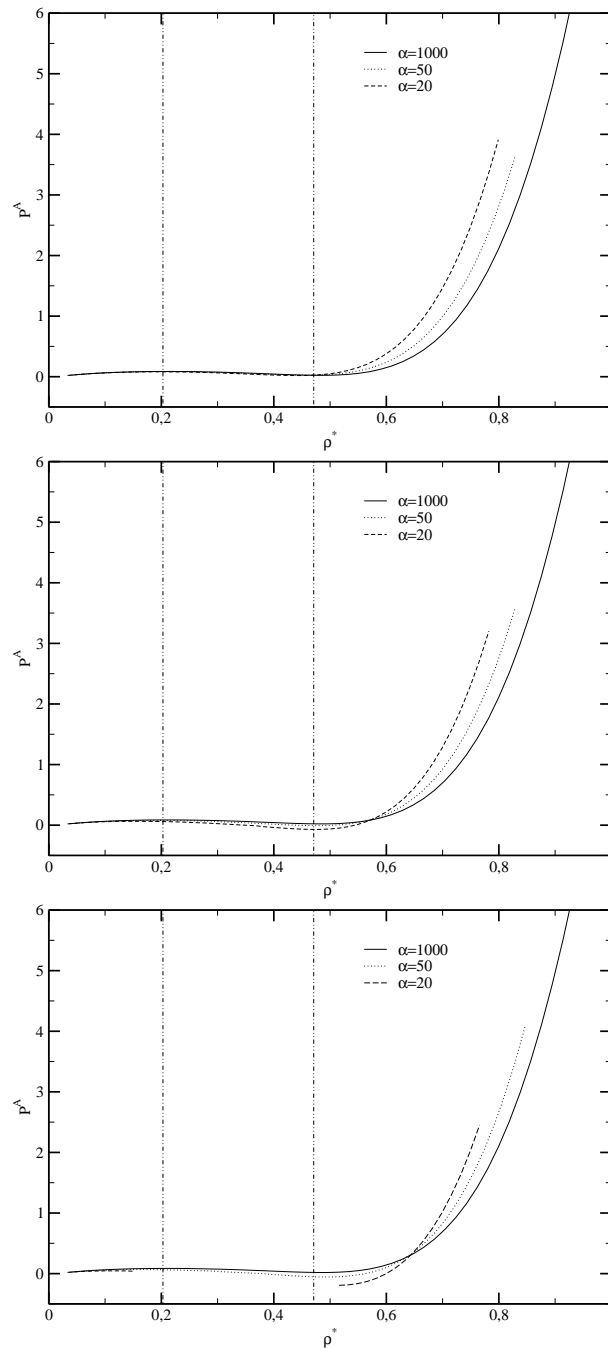


Figure 6.8: Virial pressures of a polydisperse square-well system with  $\lambda = 1.5$  and reduced temperature  $t = 1.25$  for different  $\alpha$ -values, where each single plot represents a different value  $z$  (from top to the bottom  $z = 0, z = 1, z = 2$ ).

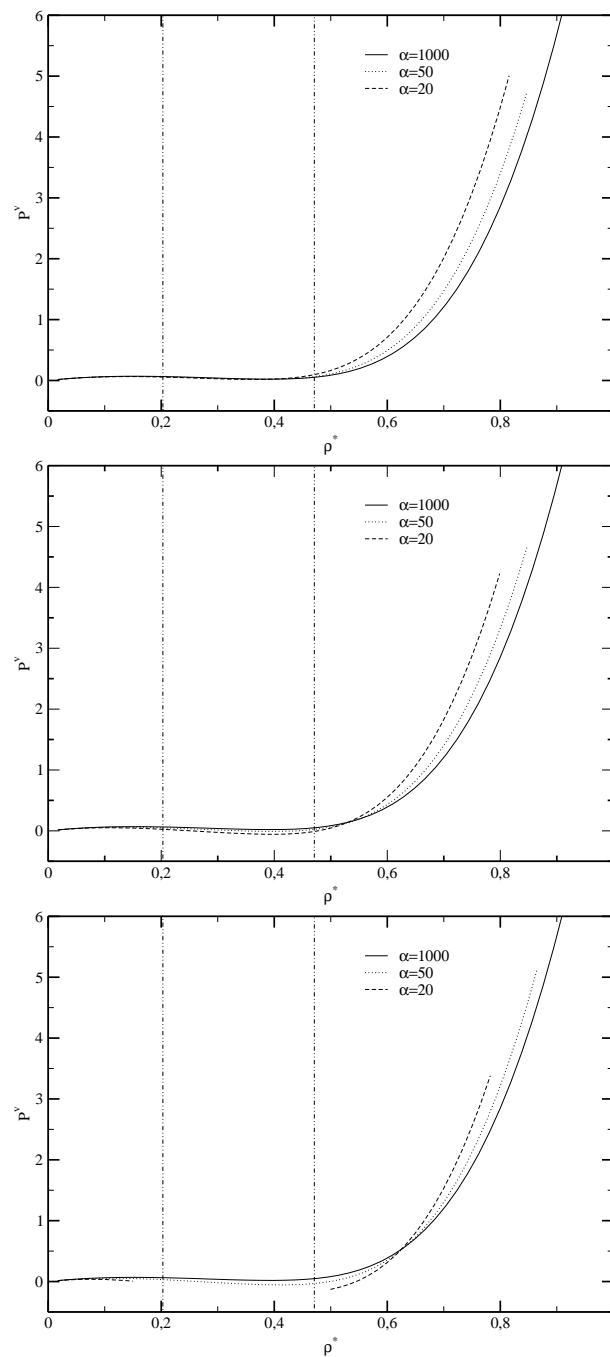


Figure 6.9: Pressures calculated from the free energy of a polydisperse square-well system with  $\lambda = 1.5$  and reduced temperature  $t = 1.12$  for different  $\alpha$ -values, where each single plot represents a different value  $z$  (from top to the bottom  $z = 0, z = 1, z = 2$ ).

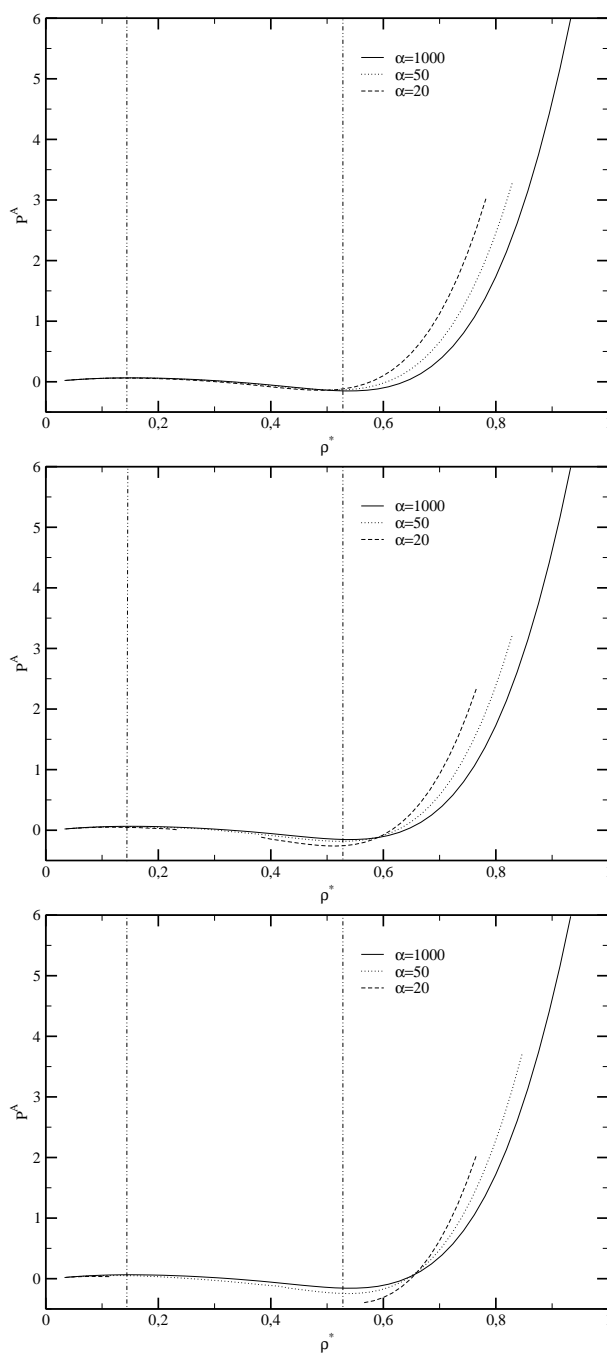
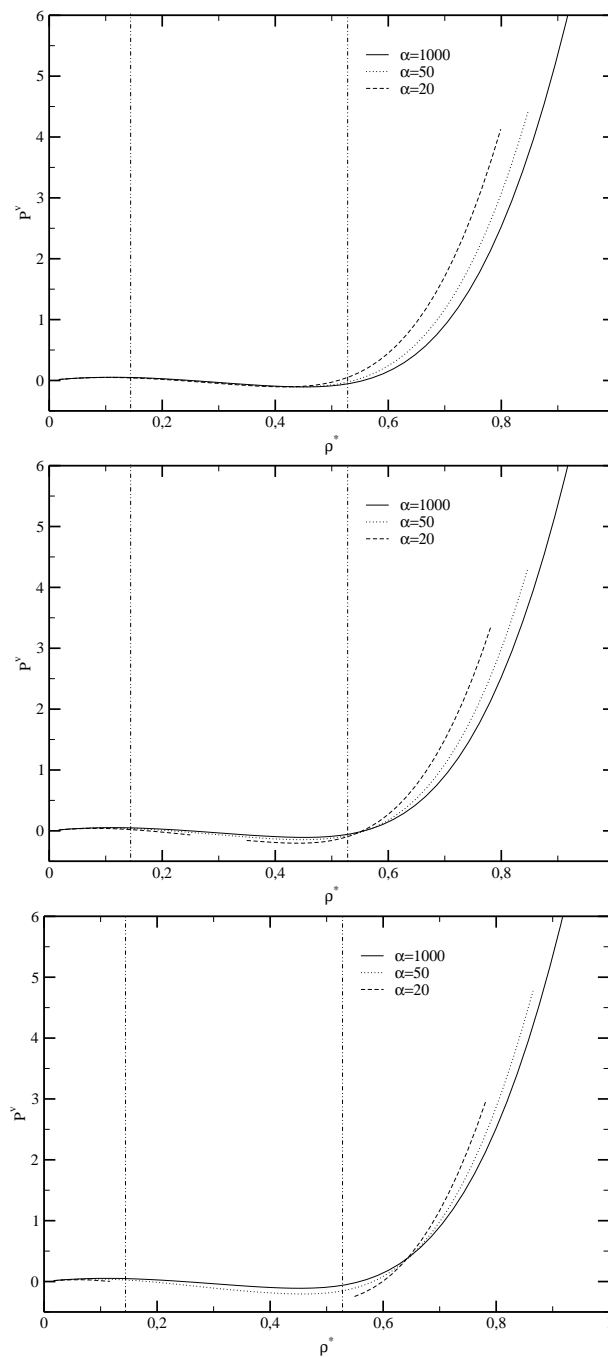


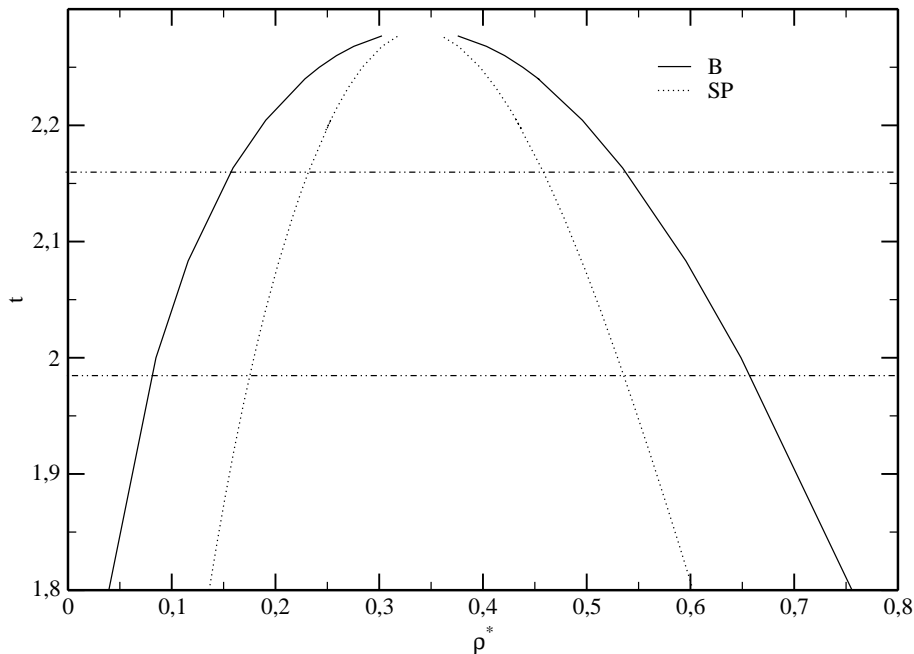
Figure 6.10: Virial pressures of a polydisperse square-well system with  $\lambda = 1.5$  and reduced temperature  $t = 1.12$  for different  $\alpha$ -values, where each single plot represents a different value  $z$  (from top to the bottom  $z = 0, z = 1, z = 2$ ).



### 6.2.2 Yukawa fluid

In figure 6.11 we have plotted the phase coexistence curve and the SP curve calculated within the ORPA for a monodisperse Yukawa-fluid with  $\kappa = 1.8$ . The horizontal lines indicate again the temperatures ( $t = 2.16, t = 1.98$ ) used for the calculation of the thermodynamic quantities.

Figure 6.11: Phase coexistence curve of a monodisperse Yukawa fluid with  $\kappa = 1.8$



The depth of the polydisperse Yukawa potential (2.9) is via the exponential term always depending on the particle diameters, in addition we can vary the potential depth with the help of the prefactor (5.61) given in dependence of  $a$ ; for  $a = 0$  the prefactor is constant for all particle type interactions (size polydispersity) whereas for  $a \neq 0$  the prefactor becomes  $\sigma$  dependent (size and amplitude polydispersity).

The reduced isothermal compressibility (4.58) shown in figures 6.12 and 6.13 show in many aspects different behavior as the ones calculated for the square-well fluid (figures 6.3, 6.4). One difference between the two models is that the split off in the compressibility of the gas phase for increasing  $I$  is stronger for  $a = 0$  than for  $a = 1$ . For  $a = 2$  finally the compressibility of the Yukawa fluid shows common behavior in comparison to the monodisperse case like the compressibility of the square-well fluid. Another difference between the square-well and the Yukawa model is, that the maximum of the polydisperse isothermal compressibility in the Yukawa model increases much slower with growing importance of the attractions (with growing  $a$ ) than in the square-well model (for growing  $z$ ) with respect to the corresponding monodisperse case. The effect of the

amplitude polydispersity dominates the one of the size polydispersity for values  $a \geq 2$  an effect which can also be observed in the phase diagrams of the following section.

Figure 6.12: Reduced isothermal compressibilities for a polydisperse Yukawa system with  $\kappa = 1.8$  and reduced temperature  $t = 2.16$  for different values of  $\alpha$ , where each single plot corresponds to a different value of  $a$  (from top to the bottom  $a = 0, a = 1, a = 2$ ).

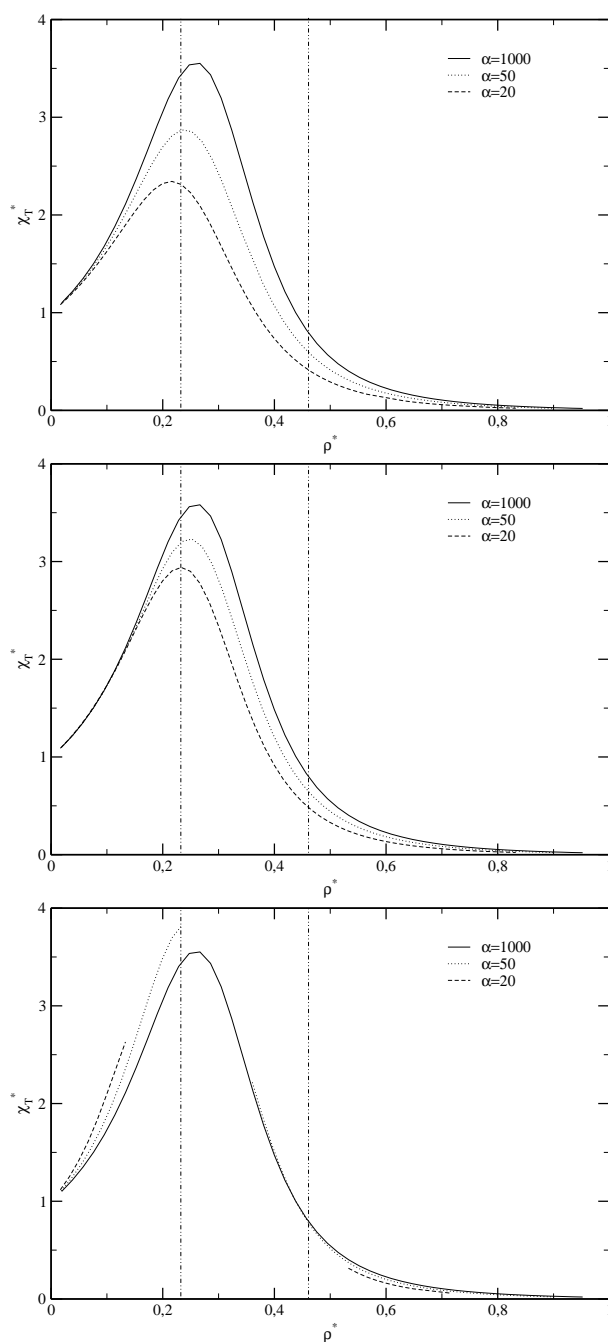
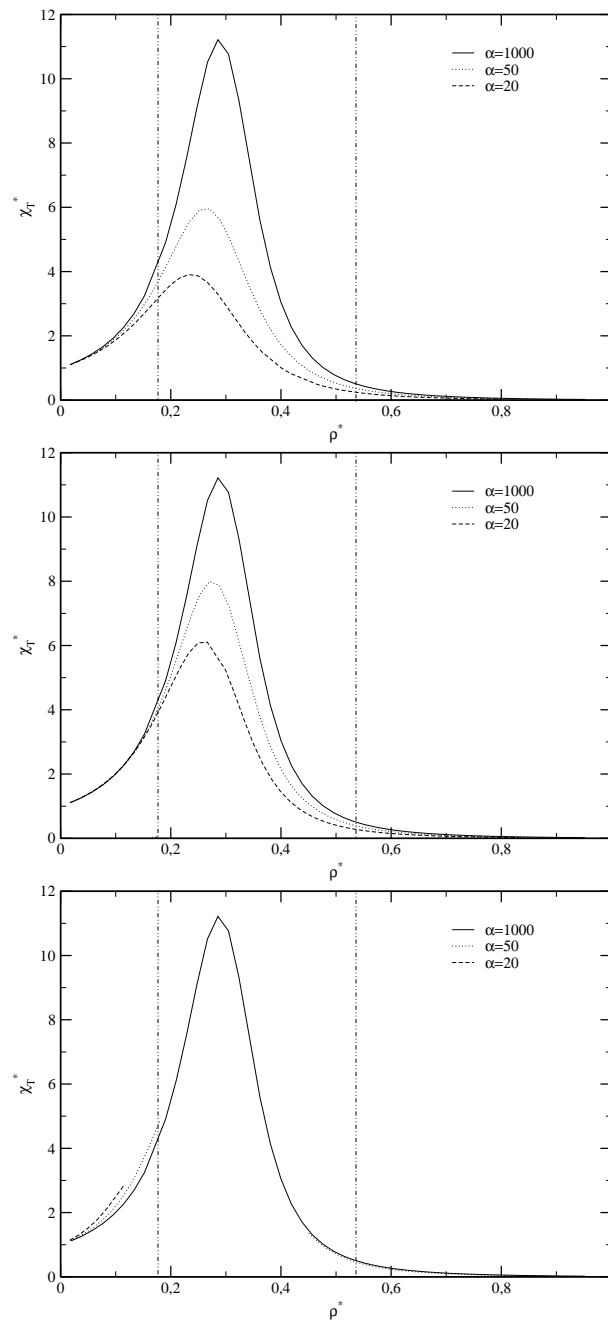


Figure 6.13: Reduced isothermal compressibilities for a polydisperse Yukawa system with  $\kappa = 1.8$  and reduced temperature  $t = 1.98$  for different values of  $\alpha$ , where each single plot corresponds to a different value of  $a$  (from top to the bottom  $a = 0, a = 1, a = 2$ ).



In figures 6.14 and 6.15 one can see the free energy densities (4.49) for the temperatures  $t = 2.16$  and  $t = 1.98$ . The split off in the free energies corresponding to the high density phase is weaker with growing  $a$  as the one in the square-well model for growing  $z$ , in addition the split off for  $a = 0$  is stronger than the one for  $a = 1$  in the Yukawa fluid. Further we can observe by common tangent construction that the high density phase represented by the right branch of the CPC is shifted to higher densities for increasing amplitude polydispersity (increasing  $a$  and  $I$ ) as compared to the monodisperse case. For  $a = 2$  finally we can see by common tangent construction (for fixed  $I$ ) that the high density phase on the CPC is lying at higher values than the corresponding high density phase of the monodisperse fluid. See for instance the phase diagrams of the following section.

The virial pressures (4.42) in figure 6.17 and 6.19 as well as the pressures (3.16) calculated from the free energy in figures 6.16 and 6.18 show a behavior similar to the corresponding pressures of the square-well fluid. Apart from this we can observe that the region where the pressures become negative is larger for the Yukawa fluid and the self-consistency is worse as compared to the square-well model. In addition for  $a = 2$  the self-consistency seems to depend on the polydispersity  $I$  (see figures 6.16 and 6.17). For  $\kappa = 4$  the self-consistency becomes even worse than for  $\kappa = 1.8$  because the ORPA is not suited for short ranged interactions [26, 54].

Figure 6.14: Free energy density for a polydisperse Yukawa system with  $\kappa = 1.8$  and reduced temperature  $t = 2.16$  for different values of  $\alpha$ , where each single plot corresponds to a different value of  $a$  (from top to the bottom  $a = 0, a = 1, a = 2$ ).

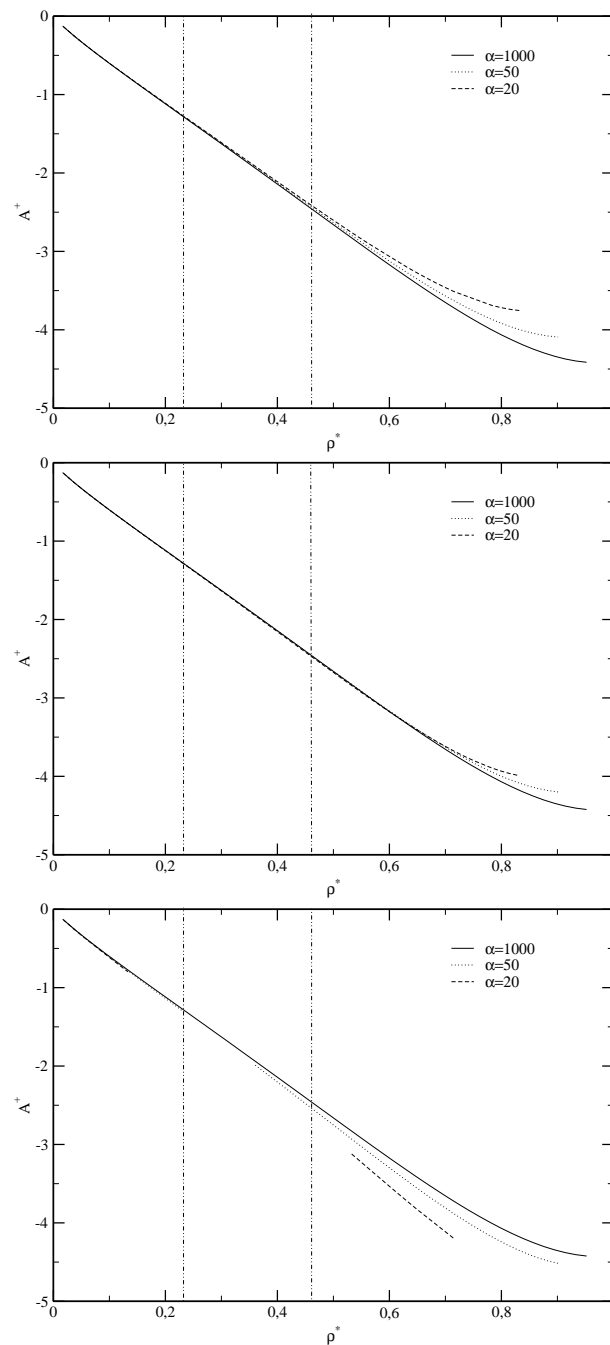


Figure 6.15: Free energy density for a polydisperse Yukawa system with  $\kappa = 1.8$  and reduced temperature  $t = 1.98$  for different values of  $\alpha$ , where each single plot corresponds to a different value of  $a$  (from top to the bottom  $a = 0, a = 1, a = 2$ ).

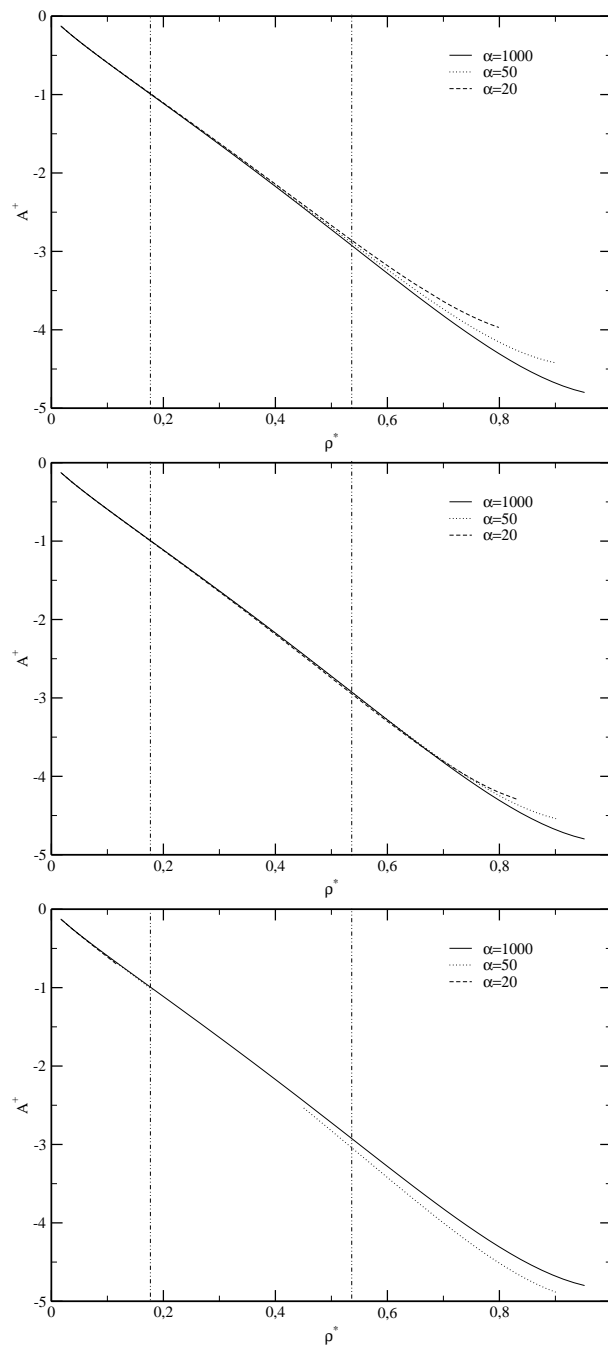


Figure 6.16: Pressures calculated from the free energy for a polydisperse Yukawa system with  $\kappa = 1.8$  and reduced temperature  $t = 2.16$  for different values of  $\alpha$ , where each single plot corresponds to a different value of  $a$  (from top to the bottom  $a = 0, a = 1, a = 2$ ).

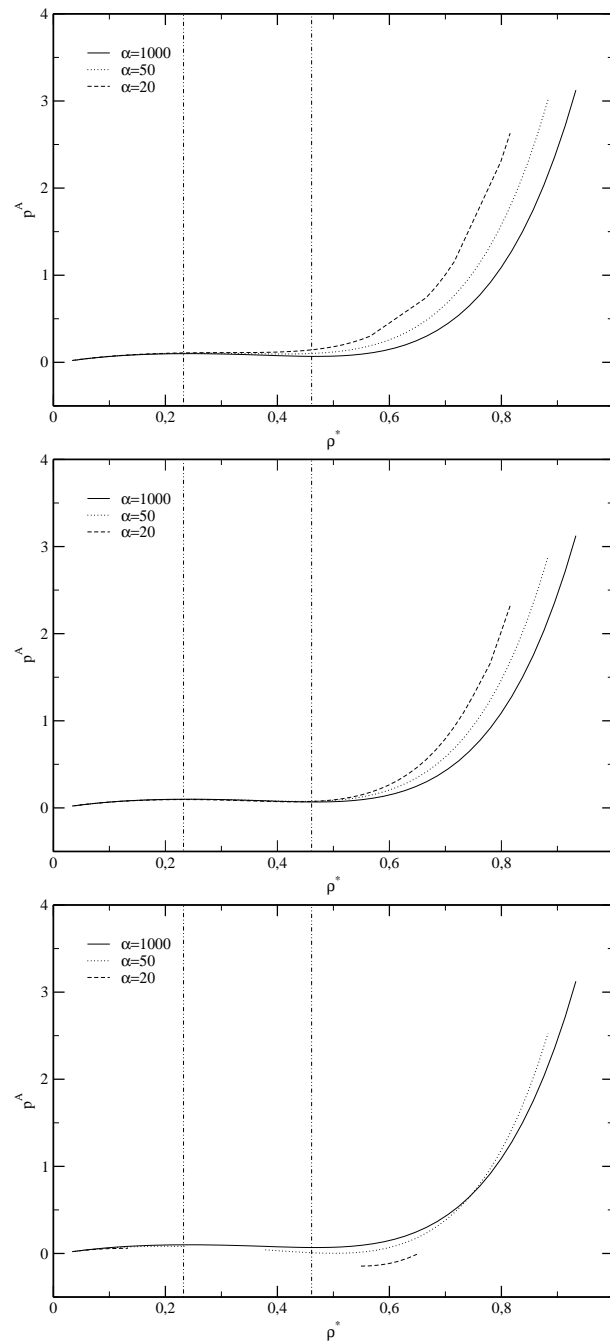


Figure 6.17: Virial pressures for a polydisperse Yukawa system with  $\kappa = 1.8$  and reduced temperature  $t = 2.16$  for different values of  $\alpha$ , where each single plot corresponds to a different value of  $a$  (from top to the bottom  $a = 0, a = 1, a = 2$ ).

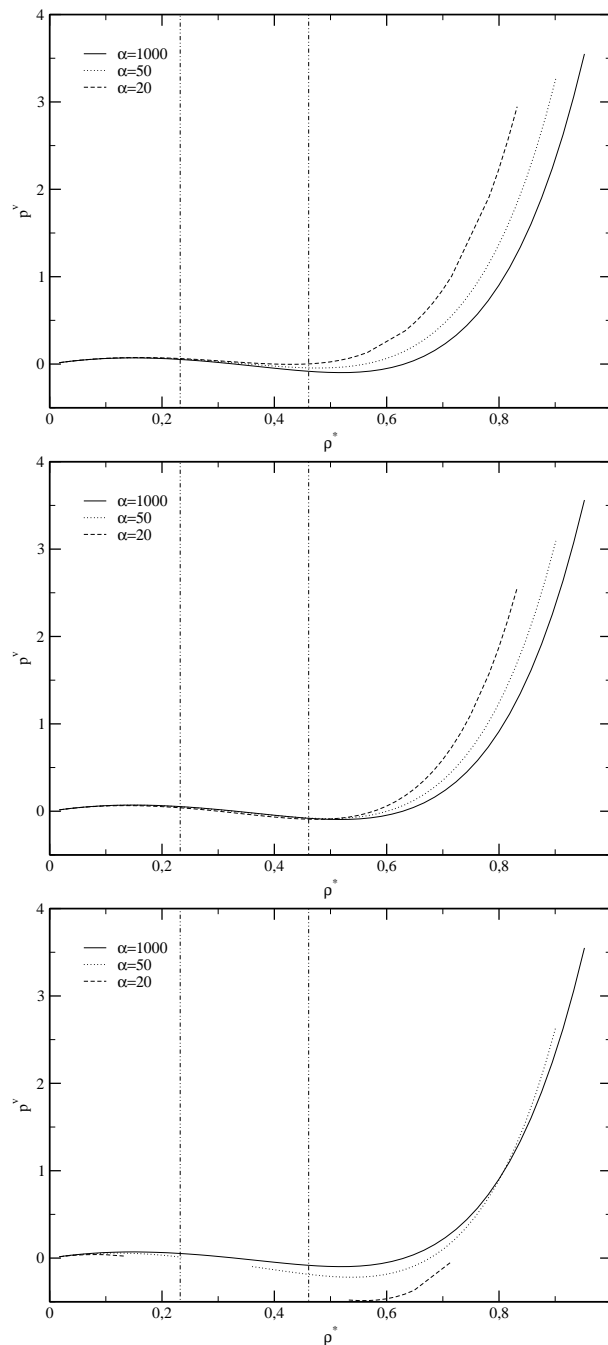


Figure 6.18: Pressures calculated from the free energy for a polydisperse Yukawa system with  $\kappa = 1.8$  and reduced temperature  $t = 1.98$  for different values of  $\alpha$ , where each single plot corresponds to a different value of  $a$  (from top to the bottom  $a = 0, a = 1, a = 2$ ).

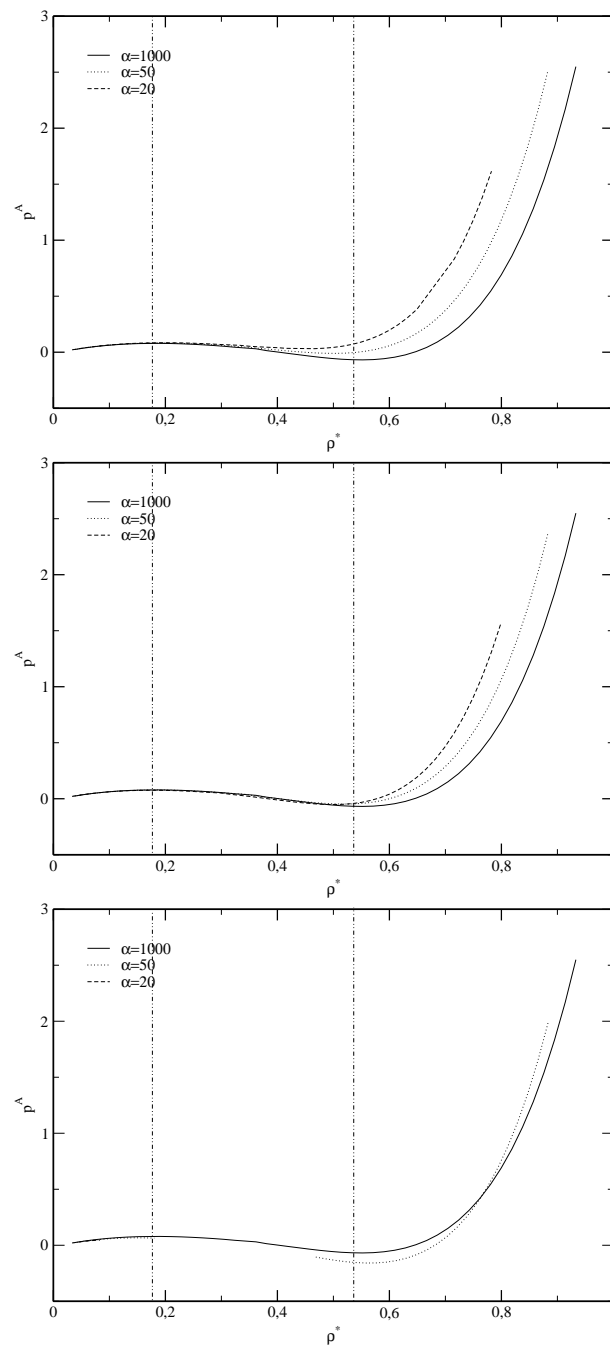
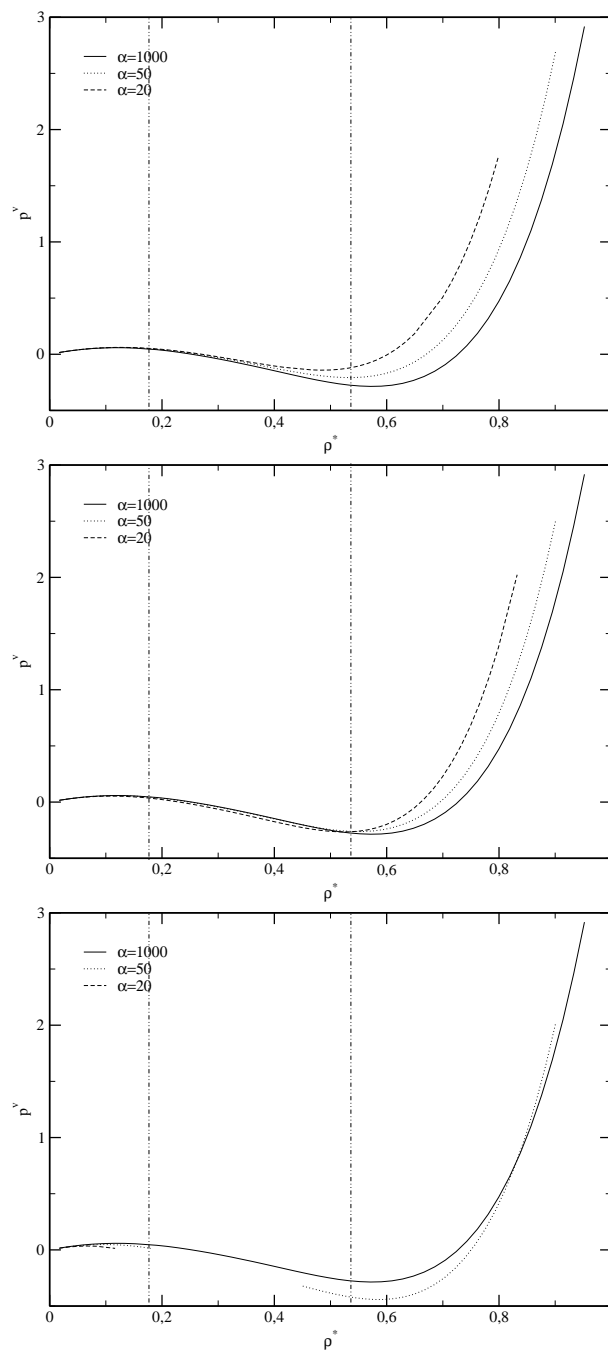


Figure 6.19: Virial pressures for a polydisperse Yukawa system with  $\kappa = 1.8$  and reduced temperature  $t = 1.98$  for different values of  $\alpha$ , where each single plot corresponds to a different value of  $a$  (from top to the bottom  $a = 0, a = 1, a = 2$ ).



## 6.3 Phase Diagrams

In chapter 5 we have developed the mathematical expressions to calculate phase separation processes for three different model systems: a vdW system and a HS system with attractive tail which is in one case given by a square-well and in the other case by a Yukawa potential. Although the thermodynamic quantities of the three model systems are rather different from each other, as we will show later, the phase diagrams show common behavior in many aspects.

As already mentioned in chapter 5, in the polydisperse system there exists a binodal for each chosen  $\rho^{(0)}$ , where only the binodal (B) calculated at the critical number density  $\rho_{crit} = \rho^{(0)}$ , the so called untruncated or critical binodal ( $B_c$ ), reaches the critical point (c. p.). The other binodals are truncated as soon as they touch the CPC on the high temperature side. Or in more intuitive language; if  $\rho^{(0)} < \rho_{crit}$ , then the binodal is truncated when it touches the low density phase which is represented by the left branch of the CPC; for  $\rho^{(0)} > \rho_{crit}$  the binodal is truncated by cutting the high density phase given by the right branch of the CPC and for  $\rho^{(0)} = \rho_{crit}$  it reaches the critical point. The truncated binodals fill the space between the CPC and the SC. This can be explained by the fact that the left branch of the CPC together with the coexisting right branch of the SC provide envelopes for the binodals, where the set of parent densities on the left branch of the CPC representing the low density phase and the set of densities on the right branch of the SC representing the high density phase are phase equilibrium-densities. (the same is valid for reversed roles of CPC and SC), and from that it follows that at the truncation temperature and for the temperatures above the truncated binodal coincides with the left branch of the CPC and the right branch of the incipient SC. The statements above will be demonstrated by some binodals calculated for different  $\rho^{(0)}$ , where the truncated binodals are indicated by horizontal lines along the truncation temperature.

Although the distribution function (6.1) is monomodal, we will see that the phase diagrams are considerable modified by the polydispersity, in particular in the region of the critical point. When the temperature is lowered, starting from the critical temperature, one expects to encounter a region where three, four etc. phases coexist. Because only fluid phases are involved we expect a transition from the two-phase to the three-phase region to proceed through a second critical point. Xu et al. [19, 52] have shown this for the vdW fluid using a log-normal distribution function and found out that when  $I$  increases the number of critical points increases while at the same time the SP invades the high density region of the temperature- ( $t$ -) packing fraction ( $\eta$ ) plane. Since such a second critical point is absent from the ordinary monodisperse vdW fluid it must be polydispersity induced [19].

As we will see also in the following phase diagrams the maxima of the CPC and the

SC in general do not correspond to the critical point (lying always at the intersection of CPC and SC); for typical polydisperse mixtures the critical point lies below the maxima. In the following plots the temperature  $t_m$  corresponding to the maxima of CPC and SC is indicated by a dashed-dotted horizontal line. While for the vdW fluid we have calculated the critical points via the intersection of SP and stability curve the critical points for the HTA of square-well and Yukawa fluids are obtained only via the intersections of CPC and SC and by the maxima of the critical binodals which can be calculated near to the critical point. The critical points for the HTA-systems are therefore only approximately given.

In the following sections we show  $t - \rho^*$  plots of the phase diagrams (two coexisting phases). The corresponding distribution functions are shown in additional plots.

### 6.3.1 Van der Waals fluid

Xu et al. [19] have already examined phase transitions for the vdW fluid, taking into account size polydispersity only, amplitude polydispersity only, and size and amplitude polydispersity. We discuss here the qualitative conclusions made in [19] and complement them by some phase plots calculated for different polydispersity indices  $I$  than the ones used in [19].

#### 6.3.1.1 Size polydispersity only

For the size polydisperse system  $\{s = 0, t = 1\}$  we have chosen two polydispersity indices  $I = 1.05$ , ( $\alpha = 20$ ) (figure 6.20), and  $I = 1.066$ , ( $\alpha = 15$ ) (figure 6.21). We have calculated the SP as well as the  $B_c$ , the CPC and SC. As reference we have in addition plotted the corresponding monodisperse binodal ( $B_m$ ). We have shown in figure 6.20 three examples of truncated binodals for  $\rho^{(0)} = 0.3055 < \rho_{crit}$ ,  $\rho^{(0)} = 0.4202 < \rho_{crit}$  and  $\rho^{(0)} = 0.7066 > \rho_{crit}$ . For the size polydisperse vdW fluid the SC is situated entirely in the interior of the CPC and is tangent to the later at the common maximum, corresponding to the critical point, of both curves (see figure 6.20 and figure 6.21) [19].

If we look at the pressure (5.44) then we can see as compared to the corresponding monodisperse case that for size polydispersity the effect of the polydispersity on the repulsions is stronger,

$$\frac{\frac{\pi}{6}\rho}{1 - \frac{\pi}{6}\rho} \rightarrow \frac{\frac{\pi}{6}\rho}{1 - \frac{\pi}{6}\rho m_3}$$

than its effect on the attractions

$$\frac{2\pi}{3}\rho^2 \rightarrow \frac{\pi}{6}\rho^2(m_3 + 3m_1m_2),$$

because the moments  $m_k$  are increasing functions of  $I$ . This growing importance of the repulsions with increasing  $I$  leads to a shift in the phase coexistence region to lower

---

temperatures as compared to the corresponding monodisperse phase diagram ( $I = 1$ ). Because the relative increase of the repulsions (as compared to the increase in the attractions) for size polydisperse vdW fluids demand, if we start with high temperatures, a stronger decrease in the temperature to invade the gas-liquid coexistence region as it would be the case for a monodisperse vdW fluid. This situation is demonstrated in figures 6.20 and 6.21: for size polydispersity the critical temperature and the critical density are lowered with increasing  $I$  (see also table (6.1)), in addition the high density branch of the binodal moves towards lower densities, whereas the low density branch is only slightly shifted towards higher densities. When increasing the value of  $I$  all these shifts increase monotonically without modifying the overall aspect of the phase diagram [19].

---

Figure 6.20: SC, CPC, SP curve, critical binodal and some truncated binodals for the size polydisperse vdW fluid with  $I = 1.05$ , ( $\alpha = 20$ )

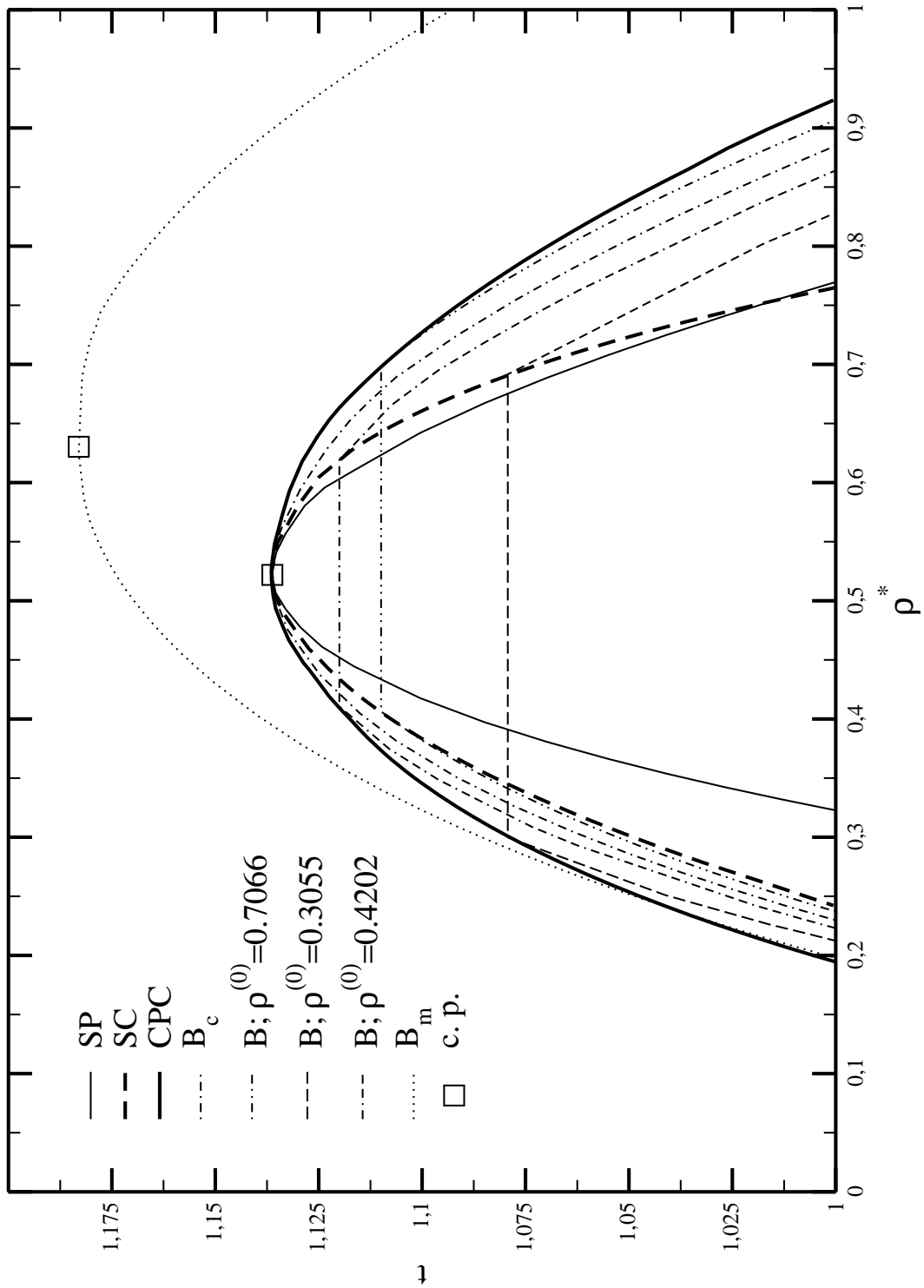
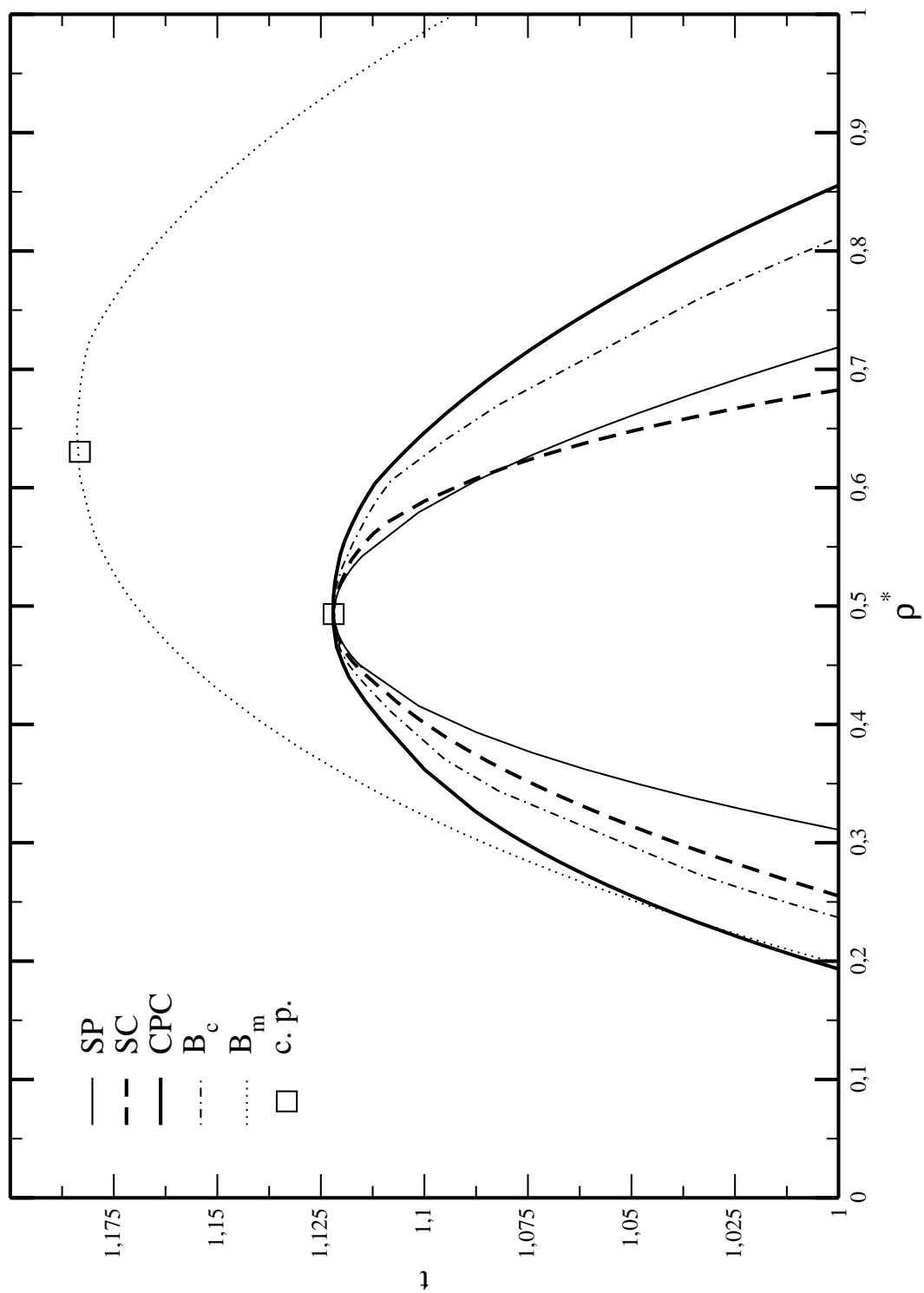


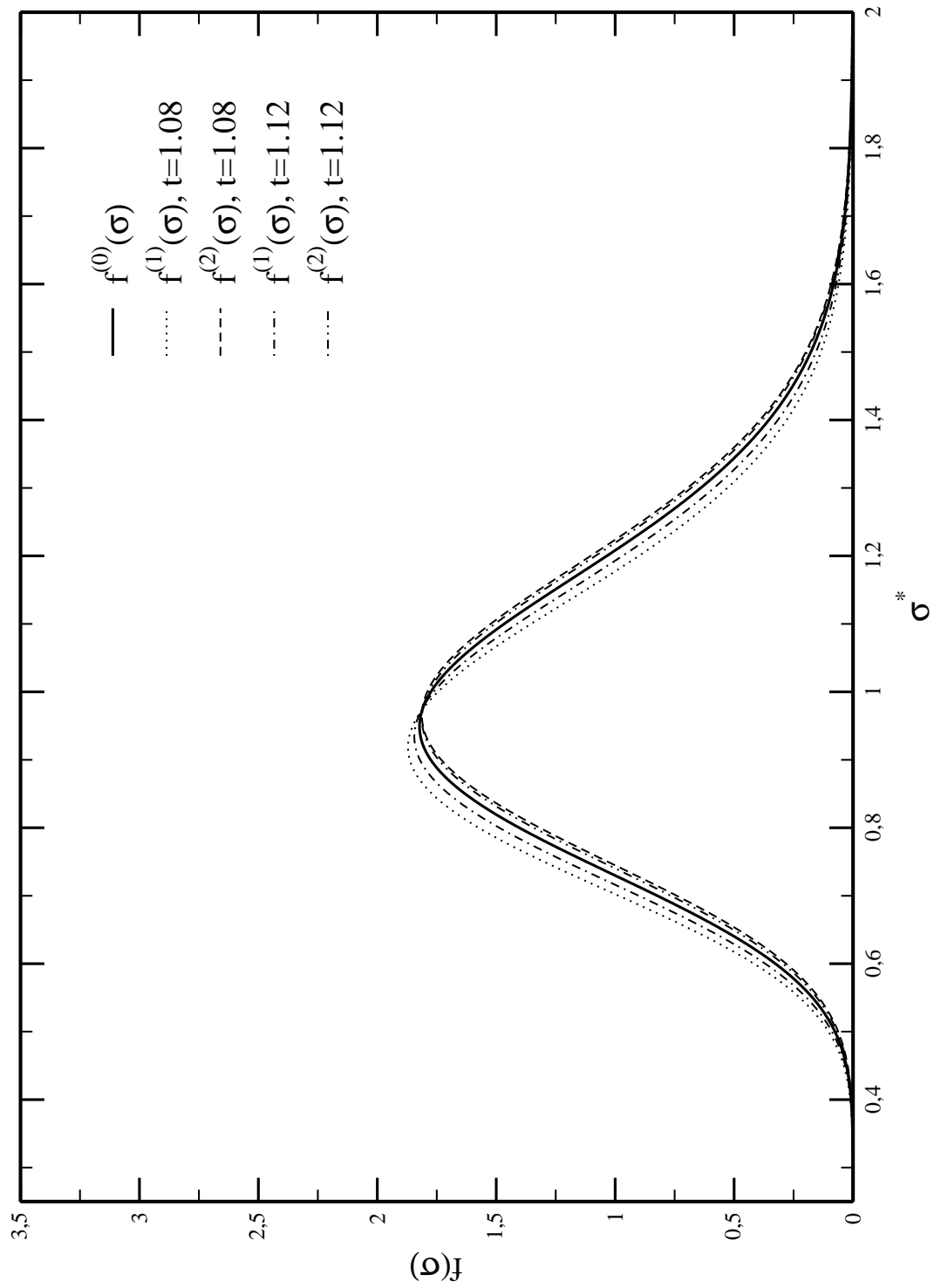
Figure 6.21: SC, CPC, SP curve, and the critical binodal for the size polydisperse vdW fluid with  $I = 1.066$ , ( $\alpha = 15$ )



In figure 6.22 we have plotted the distribution functions  $f^{(1)}(\sigma)$  and  $f^{(2)}(\sigma)$  on the critical binodal of the system in figure 6.20 together with the parent distribution: we have chosen the reduced temperatures  $t = 1.08$  and  $t = 1.12$ . The distribution function  $f^{(1)}(\sigma)$  belongs to the equilibrium density of the low density phase and  $f^{(2)}(\sigma)$  to the one of the high density phase of the critical binodal. As we can see in figure 6.22 the distribution functions of the low density phase are shifted to lower particle diameters and are slightly narrower as compared with the parent distribution independent of the temperature. The maximum of the distribution functions belonging to the high density phase of  $B_c$  are slightly shifted to higher particle diameters and slightly become wider as compared to the parent distribution. From this we can conclude that smaller particles prefer to move to the less dense phase while the bigger particles move to the denser phase. In addition we can see that the low density phase must have a smaller polydispersity than the coexisting high density phase.

---

Figure 6.22: Low and high density distributions  $f^{(1)}(\sigma)$  and  $f^{(2)}(\sigma)$  calculated for two different temperatures on the critical binodal of the system in figure 6.20



### 6.3.1.2 Amplitude polydispersity only

In the amplitude polydisperse case ( $t = 0, s = 1$ ) the polydispersity does only affect the attractions in the expression for the pressure (5.44)

$$\frac{2\pi}{3}\rho^2 \rightarrow \frac{2\pi}{3}\rho^2 m_1^2,$$

a situation which is favorable to phase separation as compared to the monodisperse case [19]. Where with favorable we mean that the amplitude polydisperse phase separation occurs already at higher temperatures than the corresponding monodisperse one. This is shown in figure 6.23, for  $I = 1.018, (\alpha = 55)$  where the phase coexistence region of the amplitude polydisperse system is shifted to higher temperatures in addition the coexistence densities of the binodals are shifted for the low density phase to lower values and for the high density phase toward higher densities in comparison to the monodisperse case, so that finally the monodisperse binodal is entirely situated inside the polydisperse binodals. In comparison to the size polydisperse case (figures 6.20, 6.21) the SC has moved to higher densities and also moved partly outside of the interior of the CPC. While the CPC is tangent to the SP curve at the critical point the SC cuts the SP curve at the critical point and is then continued within the region of instability. That means the coexistence of a parent liquid phase with a gas bubble is physically not possible for temperatures below  $t_{crit}$ . Similar conclusions as for the SC are valid for the low density phase given by the truncated and untruncated binodals which invade the region of instability for temperatures near  $t_{crit}$ . As a result of the shift in the SC the intersection of the CPC and the SC, i.e., the critical point  $\{\rho_{crit} = 0.654, t_{crit} = 1.2341\}$ , is situated now below the temperature  $t_m = 1.2415$  (dashed-dotted line), i.e., the common maximum of the CPC and the SC. This allows for a re-entrant behavior of the low density phase [19]. The expression re-entrant behavior of the low density phase means that at temperatures above the critical temperature we still have the coexistence between a parent gas phase and a liquid drop and in addition for a special choice of  $\rho^{(0)}$  coexistence between gas and liquid phases present in finite amounts which are given by the corresponding truncated binodals. The same behavior with respect to the critical point and to the region of re-entrant behavior is found for any amplitude polydisperse vdW system ( $s > 0$ ), where Xu et al. [19] found out that for the present vdW model also for  $t \neq 0, s = 1$  the attractions are always more affected by the polydispersity than the repulsions, this means that systems that are both size and amplitude polydisperse show a similar behavior with respect to the SC, CPC and critical point as the discussed amplitude polydisperse vdW fluid. Qualitatively equivalent CPC and SC as those in figure 6.23 were found by Gualtieri et al. [55] for a vdW model similar to one used here. Apart from the CPC and SC we have plotted the SP and three different binodals: the critical binodal having its maximum at the critical point, as well

as the truncated binodals for  $\rho^{(0)} = 0.5198 < \rho_{crit}$  and  $\rho^{(0)} = 0.8498 > \rho_{crit}$ . As we can see in figure 6.23 the binodal for  $\rho^{(0)} = 0.5198$  has its maximum above the critical point. In addition we have plotted the binodal corresponding to the monodisperse system. As we can see by comparison with the monodisperse binodal and the binodals shown in [19] (figure 4a) for increasing  $I$  the critical point moves to higher temperatures, because the attractions become stronger.

---

Figure 6.23: SC, CPC, SP curve, critical binodal and same truncated binodals calculated for the amplitude polydisperse vdW with  $I = 1.018$ , ( $\alpha = 55$ )

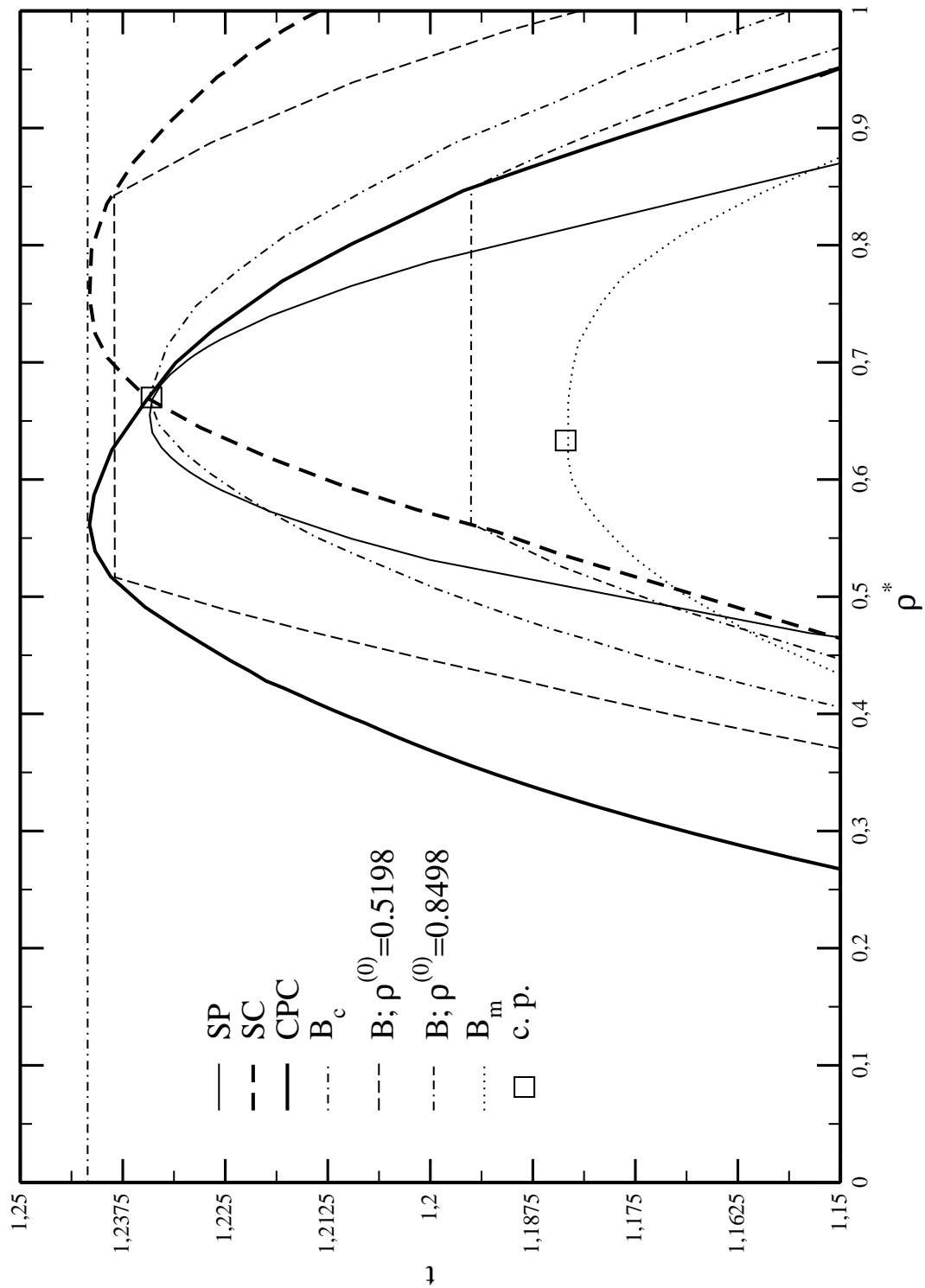
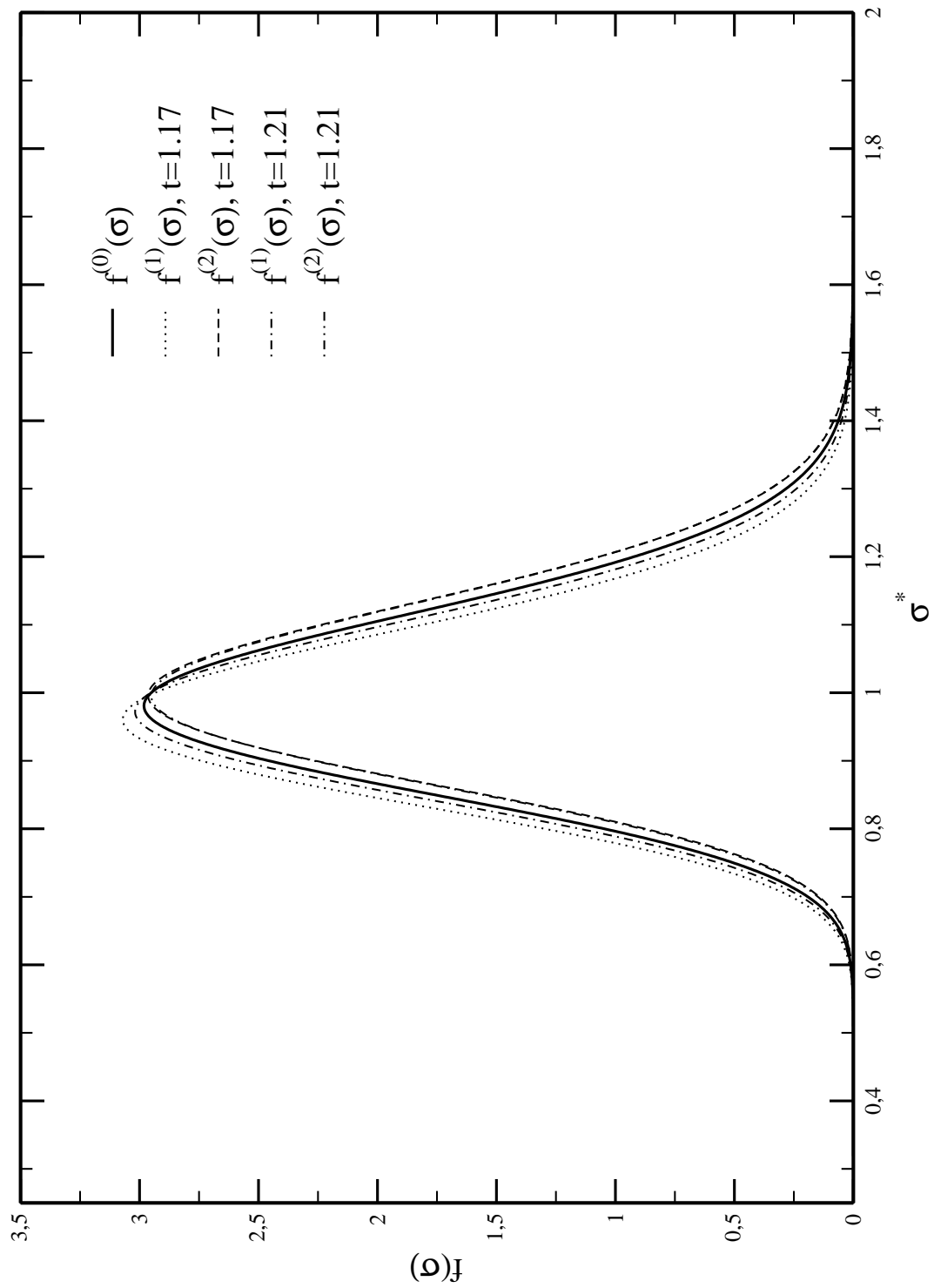


Table 6.1: Critical points for the vdW-model

I	$\rho_{crit}$	$t_{crit}$
1	0.6303	1.1831
1.018	0.6426	1.2341
1.05	0.5219	1.1362
1.066	0.4932	1.1219

In figure 6.24 we can see the distribution functions  $f^{(1)}(\sigma)$  and  $f^{(2)}(\sigma)$  belonging to the low and high density phase of the critical binodal for the temperatures  $t = 1.17$  and  $t = 1.21$ . The behavior is qualitatively the same as for the size polydisperse case (figure 6.22).

Figure 6.24: Low and high density distributions  $f^{(1)}(\sigma)$  and  $f^{(2)}(\sigma)$  calculated for two different temperatures on the critical binodal of the system in figure 6.23



## 6.3.2 Square-well fluid

A very similar behavior of the SC and CPC as in the polydisperse vdW fluid can be observed for the polydisperse square-well fluid. We have calculated phase diagrams for the size polydisperse square-well potential ( $z = 0$ ) as well as for size and amplitude polydispersity.

### 6.3.2.1 Size polydispersity

In figure 6.25 we show a phase diagram for a size polydisperse ( $z = 0$ ) square-well fluid. The potential width is  $\lambda = 1.25$  and the polydispersity index is  $I = 1.05$ , ( $\alpha = 20$ ), the thermodynamic properties (5.66) depend now only on the moments  $m_k$ . We have plotted the SP, the CPC with the incipient SC, as well as the critical binodal and two truncated binodals at  $\rho^{(0)} = 0.15 < \rho_{crit}$  and  $\rho^{(0)} = 0.4 > \rho_{crit}$ . In addition we have drawn the corresponding binodal of the monodisperse case.

If we substitute the excluded volume term in the free energy of the size polydisperse vdW ( $s = 0, t = 1$ ) fluid by the HS free energy

$$\frac{\frac{\pi}{6}\rho}{1 - \frac{\pi}{6}\rho m_3} \rightarrow A_{ex}^{HS},$$

we obtain a free energy which is practically identical to the free energy of the size polydisperse square-well ( $z = 0$ ) fluid. Where the attractions of the two models are then given by use of (5.44) and (5.66) as

$$\begin{aligned} A_{att}^{vdW} &= -\frac{1}{t} \frac{4\pi}{3} \hat{\sigma}^3 \\ A_{att}^{SW} &= -\frac{1}{t} \frac{4\pi}{3} \hat{\sigma}^3 (\lambda^3 - 1) \end{aligned}$$

with  $A_{att}$  giving the attractive part of the free energy. If  $\lambda$  in the square-well model is chosen to be 1.26 then the two considered models coincide for other values the phase coexistence region is only shifted to higher or lower temperatures in dependence of  $(\lambda^3 - 1)$ . After this considerations we can conclude that the size polydisperse vdW model (5.44) and the size polydisperse square-well model (5.66) are only different in their repulsions given by the excluded volume term in the vdW and by the HS contribution in the square-well fluid. This leads to a differing behavior in the phase equilibrium curves, mainly with respect to the temperatures where the phase split occurs. The size polydispersity in the square-well system has less influence on the phase coexistence curves than in the vdW fluid; the influence of the size polydispersity on the repulsions caused by the HS contribution in (5.66) seems to be compensated by its effects on the attractions (2.8) at least in this way as the phase coexistence region is not shifted to lower temperatures for increasing

I. This means while the size polydispersity is not favorable for the phase transition in the vdW fluid (with not favorable we mean that the phase coexistence region of the size polydisperse fluid is shifted to lower temperatures in comparison to the phase coexistence region of the monodisperse fluid) in the square-well fluid it plays only a negligible role as far as the shift in the critical temperature is concerned. As we can see in figure 6.25 the critical temperature ( $t_{crit} \simeq 0.364$ ) is only slightly shifted to lower values as compared to the monodisperse case  $\{t_{crit} \simeq 0.3645, \rho_{crit} \simeq 0.2657\}$  when the polydispersity is increased, whereas the critical density ( $\rho_{crit} \simeq 0.217$ ) as well as the densities on the high density phase of the critical binodal moves definitely to lower values similar as observed for the size polydisperse vdW fluid.

In figure 6.26 we show the distribution functions on the critical binodal for the temperatures  $t = 0.32$  and  $t = 0.35$ . Although the qualitative behavior is similar as for the vdW fluid (see figure 6.22), the shift in the low and high density phase distributions with respect to the parent distribution are stronger. In addition the low density phase distributions  $f^{(1)}(\sigma)$  become smaller and their maxima have higher values, as a consequence the high density phase distributions  $f^{(2)}(\sigma)$  become broader and their maxima decrease as compared to the parent (the effect is stronger for lower temperature), what means the two phases demix stronger than in the vdW fluid.

Figure 6.25: SC, CPC, SP curve, critical binodal and same truncated binodals calculated for the size polydisperse square-well fluid with  $I = 1.05$ ,  $(\alpha = 20)$ ,  $\lambda = 1.25$ ,  $z = 0$ .

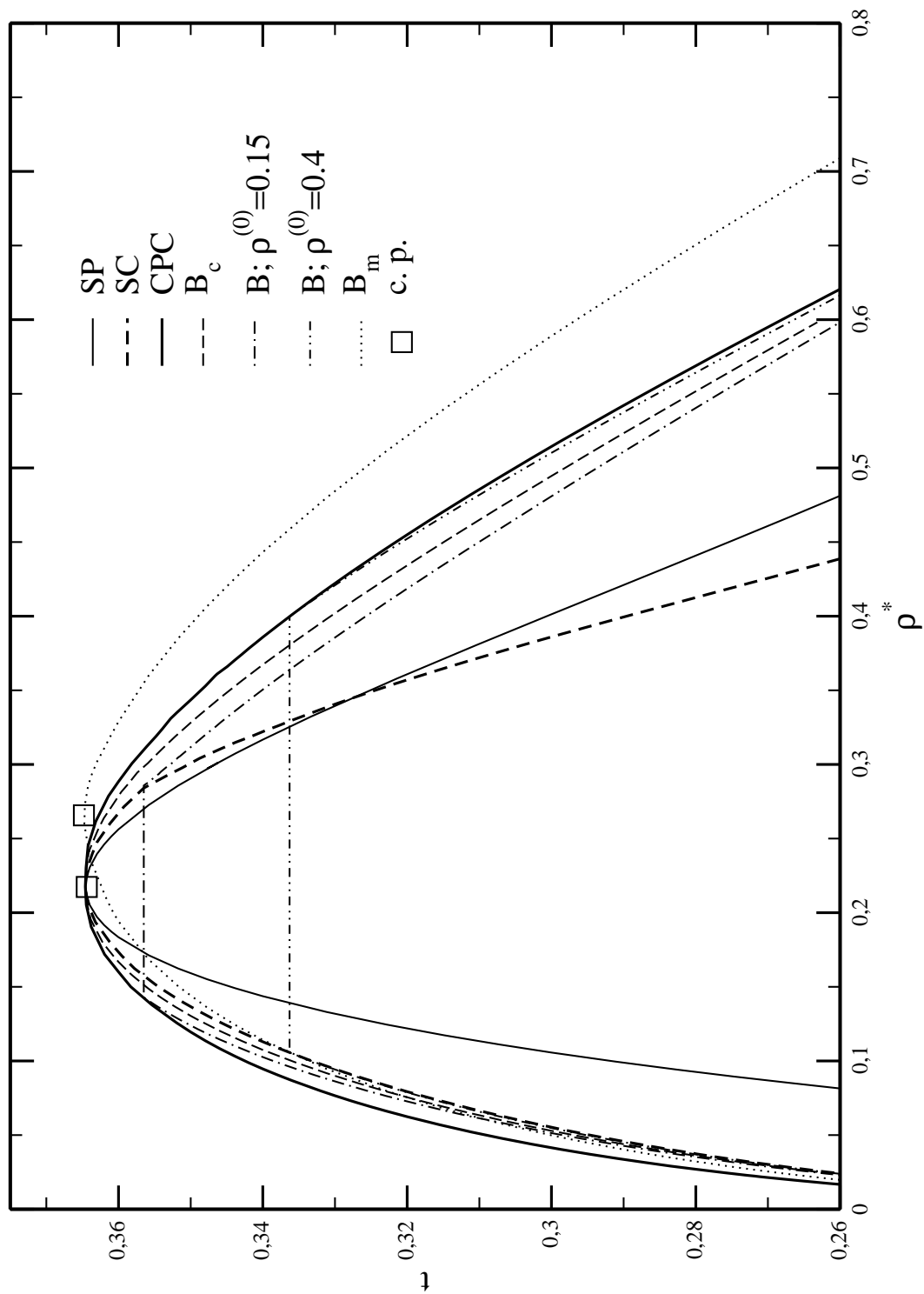
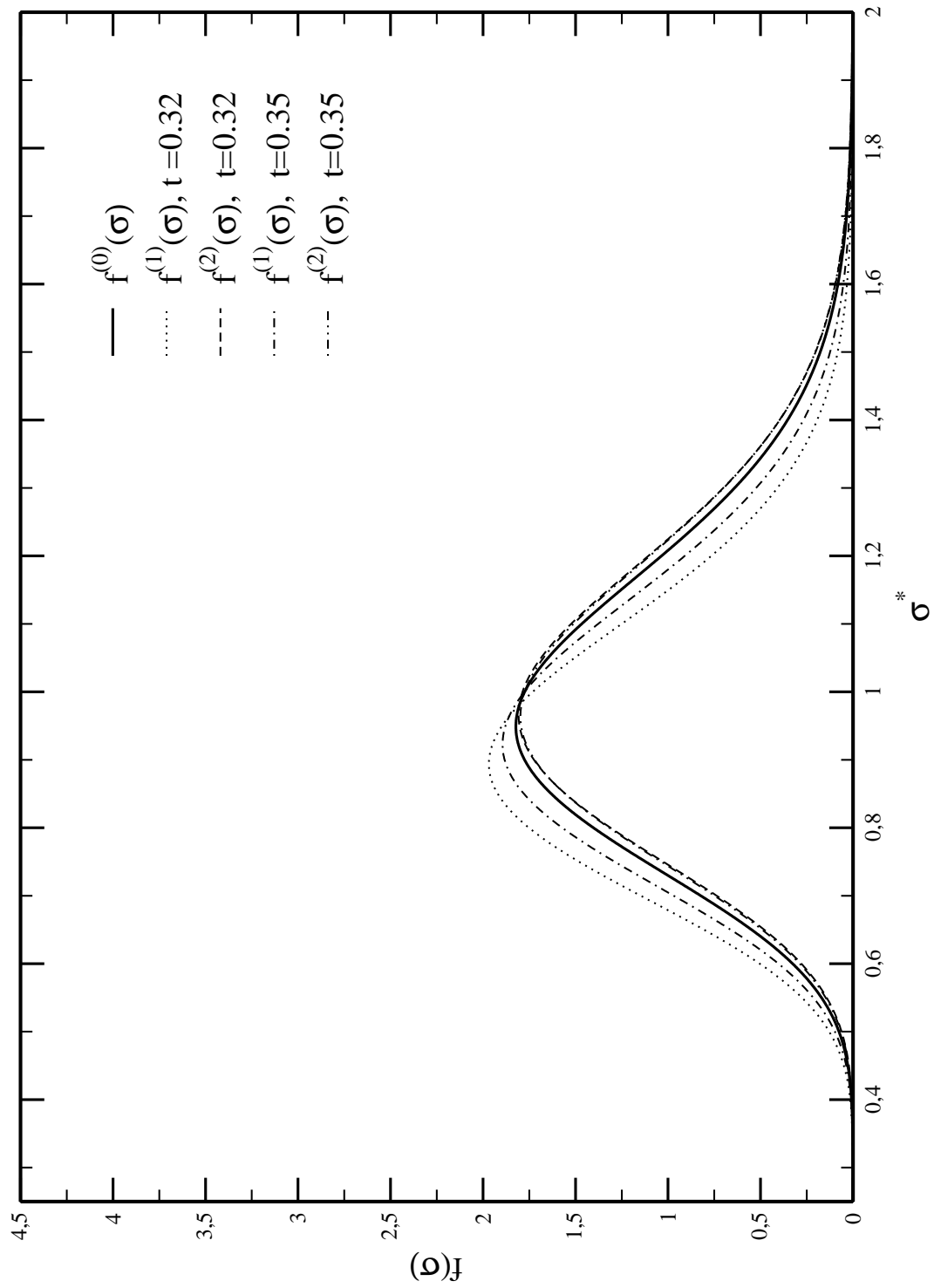


Figure 6.26: Low and high density distributions  $f^{(1)}(\sigma)$  and  $f^{(2)}(\sigma)$  calculated for two different temperatures on the critical binodal of the system in figure 6.25



### 6.3.2.2 Size and amplitude polydispersity

Now we have considered the more realistic case where the square-well potential with  $\lambda = 1.25$  is both size and amplitude polydisperse, where the thermodynamic properties now depend on the generalized moments  $\overline{m}_k$ ; results are shown in figures 6.27 - 6.29 for potential strength  $z = 0.1, z = 0.5$  and  $z = 1$  and polydispersity indices  $I = 1.018; (\alpha = 55)$  and  $I = 1.01; (\alpha = 100)$ . In figures 6.27 - 6.29 we have plotted the CPC, the SC and the critical binodal. We start in figure 6.27 with a system which is besides the size polydispersity only weakly polydisperse in amplitude ( $z = 0.1$ ). Although  $z$  is very small the phase diagram has changed with respect to the pure size polydisperse case (figure 6.25); the SC and with it the critical density is shifted to higher densities and has partly moved out of the interior of the CPC. In addition the phase coexistence region is shifted slightly to higher temperatures and the densities on the high density phase of the binodals definitely to higher values as the increasing  $z$  only affects the attractions in (5.66). The shift of the SC out of the interior of the CPC and the re-entrant behavior of the low density phase was already observed at the amplitude polydisperse vdW fluid figure 6.23. For  $z = 0.5$  (figure 6.28) and  $z = 1$  (figure 6.29) the influence of the attractions compared to the repulsions becomes stronger when compared to the monodisperse case and the shift of the SC to higher densities is further increased. At the same time the temperature  $t_m$  or the region of re-entrant behavior becomes larger as compared to the system in figure 6.27 ( $z = 0.1$ ). The critical point hardly moves to higher densities and temperature as compared to the systems in figures 6.25 and 6.27 (see table (6.2)).

We can conclude here that in the size and amplitude polydisperse square-well fluid the effects of amplitude polydispersity (which leads to an increase of the attractions when compared to the monodisperse case) dominates over the ones of the size polydispersity even for small values of  $z$  ( $z \geq 0.5$ ) (because even for small values of  $z$  (weak amplitude polydispersity) the phase coexistence region is shifted to higher temperatures and the high density phase to higher densities). As in the vdW fluid the presence of amplitude polydispersity is favorable to the phase transition process because of the shift of the phase coexistence region as compared to the monodisperse case.

Table 6.2: Critical points for the square-well systems with  $\lambda = 1.25$

I	z	$\rho_{crit}$	$t_{crit}$
1	-	0.2657	0.3645
1.05	0	0.217	0.364
1.018	0.1	0.237	0.365
1.018	0.5	0.239	0.367
1.01	1	0.241	0.368

Figure 6.27: SC, CPC and critical binodal calculated for the size and amplitude polydisperse square-well fluid with  $I = 1.018$ ,  $(\alpha = 55)$ ,  $\lambda = 1.25$ ,  $z = 0.1$

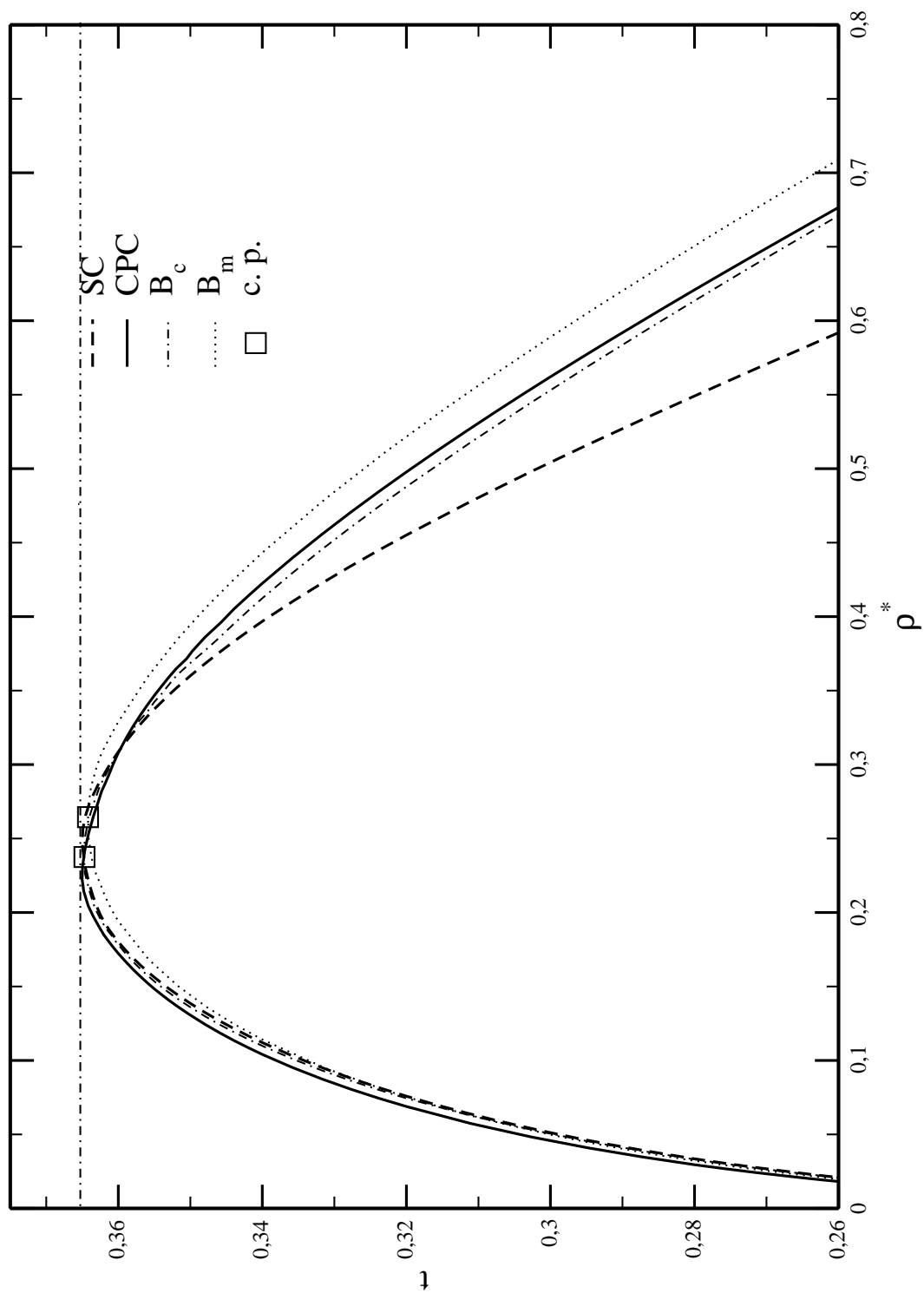


Figure 6.28: SC, CPC and critical binodal calculated for the size and amplitude polydisperse square-well fluid with  $I = 1.018$ ,  $(\alpha = 55)$ ,  $\lambda = 1.25$ ,  $z = 0.5$ ; the dashed-dotted line indicates the temperature  $t_m$

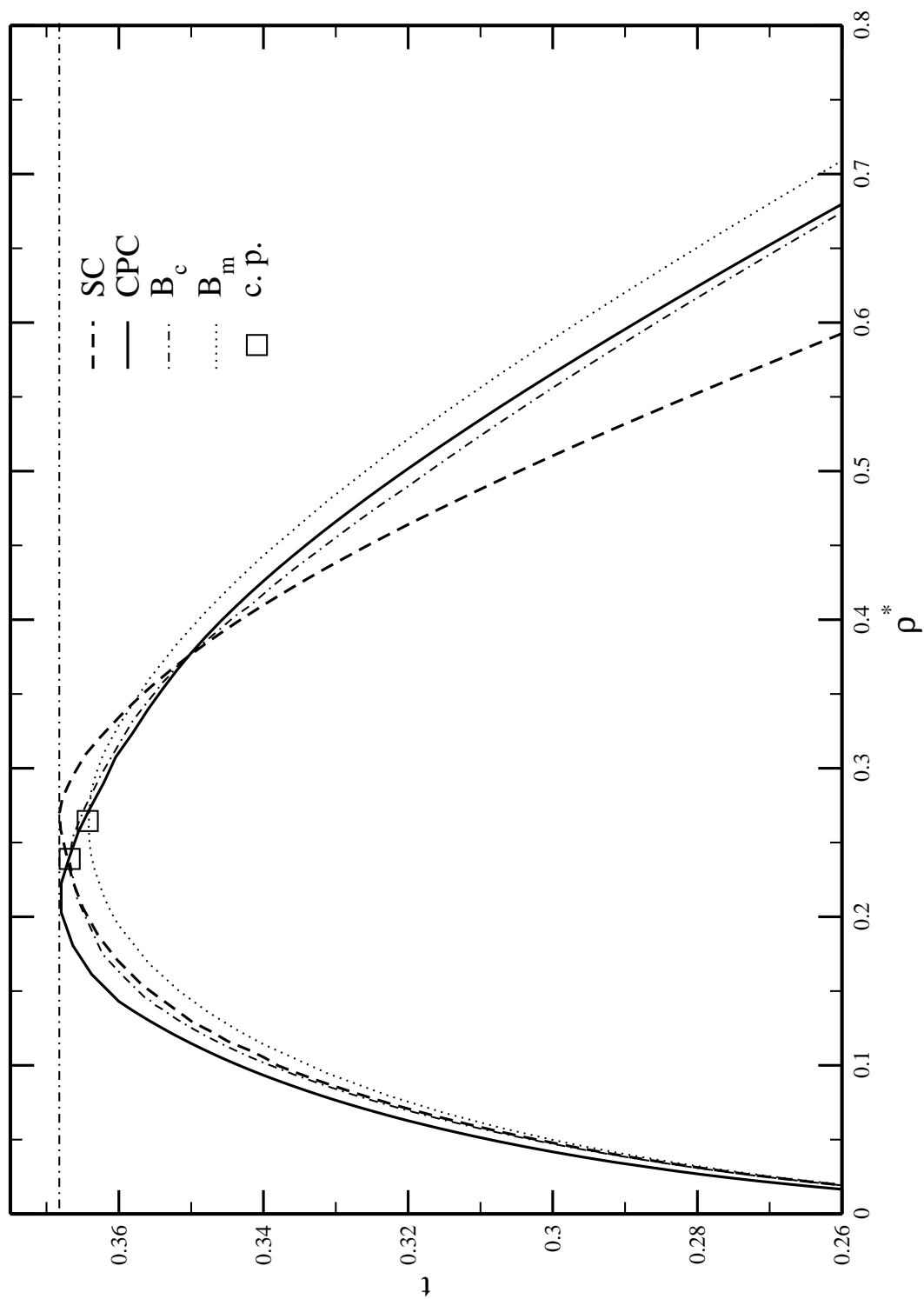
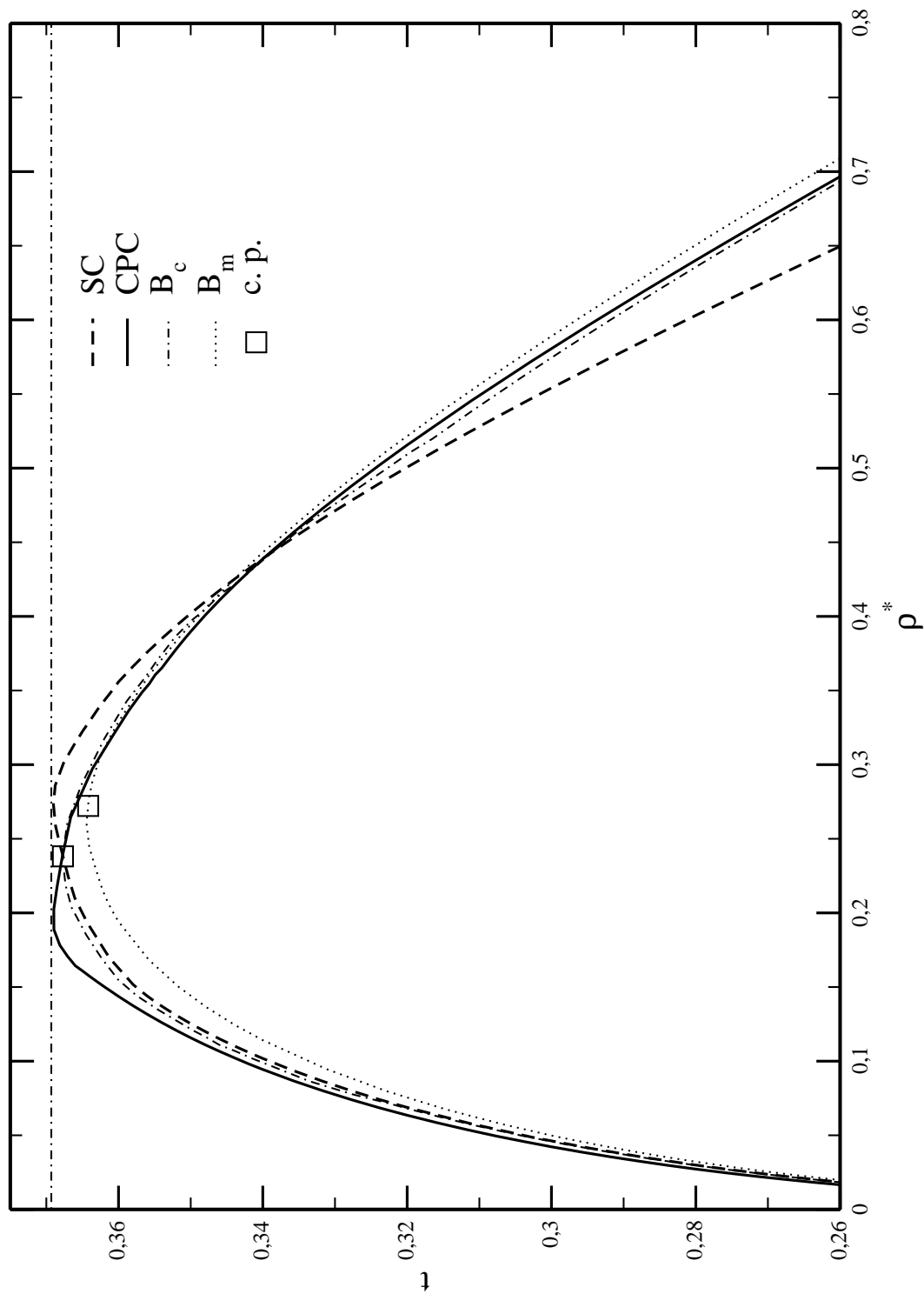


Figure 6.29: SC, CPC and critical binodal calculated for the size and amplitude polydisperse square-well fluid with  $I = 1.01$ ,  $(\alpha = 100)$ ,  $\lambda = 1.25$ ,  $z = 1$ ; the dashed-dotted line indicates the temperature  $t_m$



In figure 6.30 and 6.31 we have plotted the parent and daughter distribution functions of the systems studied in figures 6.28 and 6.29 for  $t = 0.33$ ; we can see that the smaller particles enrich the low density phase and the larger particles the high density phase.

---

Figure 6.30: Low and high density distributions  $f^{(1)}(\sigma)$  and  $f^{(2)}(\sigma)$  calculated for one temperature on the critical binodal of the system in figure 6.28

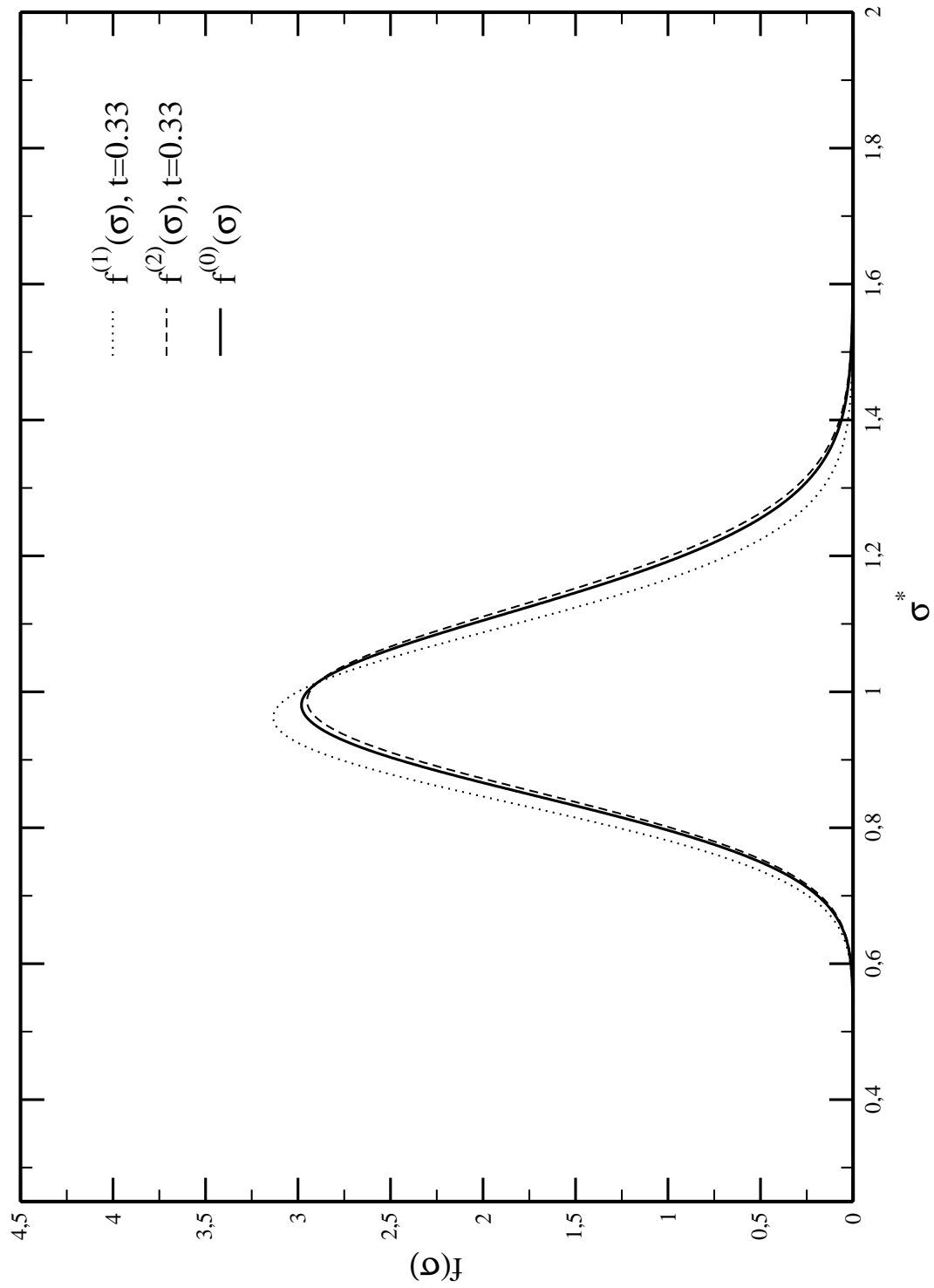
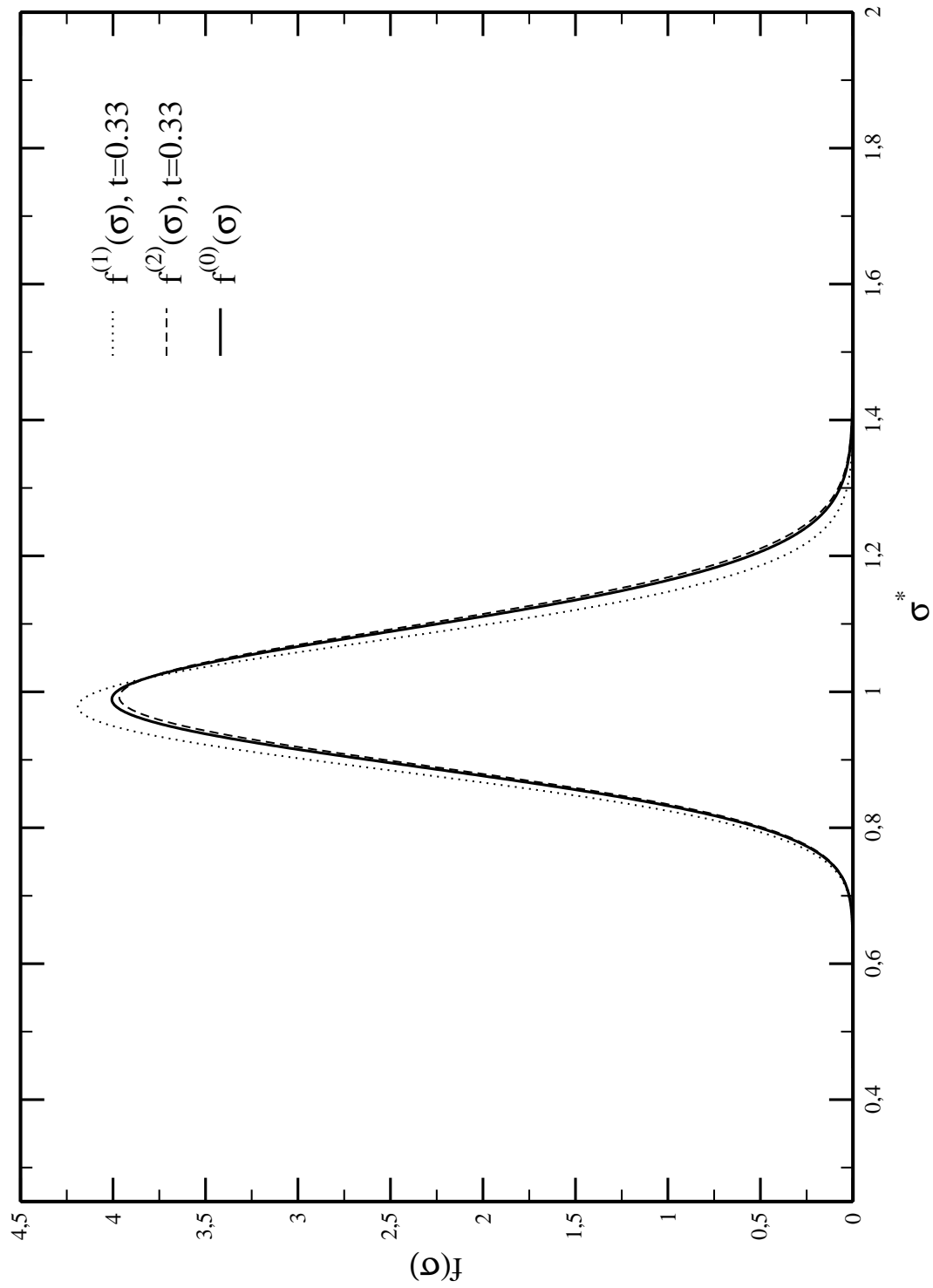


Figure 6.31: Low and high density distributions  $f^{(1)}(\sigma)$  and  $f^{(2)}(\sigma)$  calculated for one temperature on the critical binodal of the system in figure 6.29



### 6.3.3 Yukawa fluid

The Yukawa potential (5.60) is rather different from the attractions (5.43) given by the vdW model, this is also expressed by the phase diagrams of the Yukawa system. We have studied phase transitions for polydisperse Yukawa fluids for three different values of parameter  $a$  ( $a = 0, a = 1, a = 2$ ); the cases for  $a = 0$  and  $a = 1$  are special cases:  $a = 0$  represents size polydispersity only and for  $a = 1$  the potential (5.60) becomes independent of  $m_1$  and the additional term in the chemical potential (5.72) vanishes.

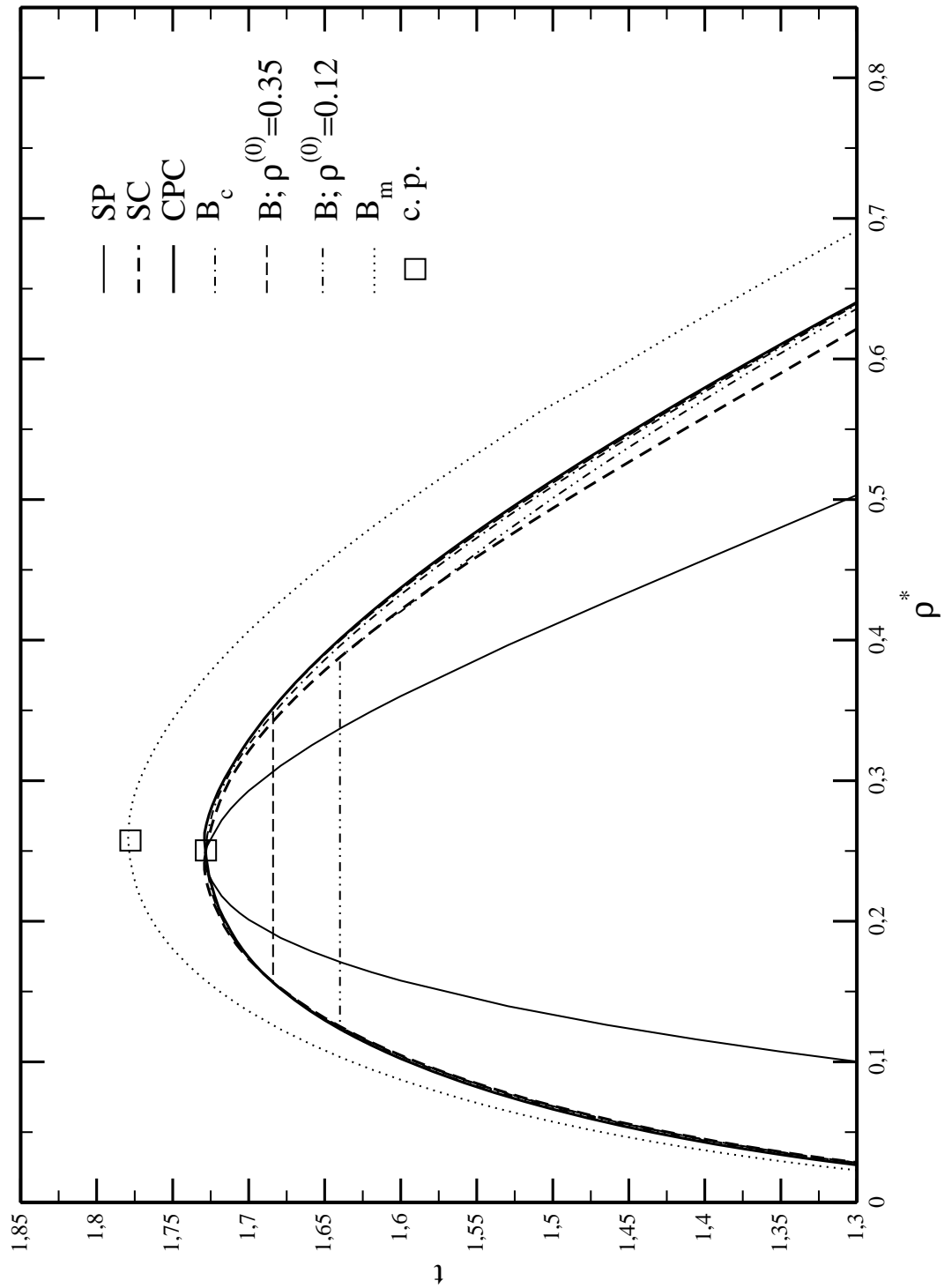
#### 6.3.3.1 Size polydispersity

For the purely size polydisperse case we have used the following system parameters:  $I = 1.018, (\alpha = 55); \kappa = 1.8$ . In figure 6.32 we have plotted the SP, the CPC, the SC and the critical binodal together with two truncated binodals for  $\rho^{(0)} = 0.12 < \rho_{crit}$  and  $\rho^{(0)} = 0.35 > \rho_{crit}$ . In addition we have drawn the binodal for the corresponding monodisperse case with the critical point at  $\{\rho_{crit} \simeq 0.258, t_{crit} \simeq 1.778\}$ . For the size polydisperse Yukawa fluid the effects on the repulsions seem to be stronger than the ones on the attractions in (5.72) when compared to the monodisperse case; like for the size polydisperse vdW fluid the critical point  $\{\rho_{crit} \simeq 0.250, t_{crit} \simeq 1.728\}$  for the system in figure 6.32 moves to lower densities and temperatures as  $I$  increases. While the low density phase on the critical binodal moves only slightly to higher densities the high density phase is definitely shifted towards lower densities. From that it follows that the size polydispersity is not favorable to the phase transition process of the Yukawa fluid, where the size polydispersity in the Yukawa fluid has more influence on the phase coexistence region than in the size polydisperse square-well fluid as the phase coexistence region for the size polydisperse Yukawa fluid is shifted definitely to lower temperatures in comparison to the monodisperse Yukawa system.

The CPC and SC show a different behavior as compared with the size polydisperse vdW or square-well fluid. The SC is never entirely situated in the interior of the CPC, because the CPC is slightly shifted to higher densities. The roles of SC and CPC seem to be exchanged in the polydisperse Yukawa fluid as the SC is now tangent to the SP curve at the critical point and the CPC cuts the SP curve at the critical point so that the low density phase represented by the left branch of the CPC invades a region of instability near criticality. Physically this means that the coexistence of a parent gas phase with an incipient liquid drop near the critical point is not possible. The maxima of CPC and SC are lying slightly above the critical temperature and we can already observe re-entrant behavior now for the high density phase near the critical point for size polydispersity only.

In figure 6.33 we can see the distribution functions along the critical binodal for  $t = 1.4$  and  $t = 1.6$ . Here we can also observe a difference in the behavior compared with the

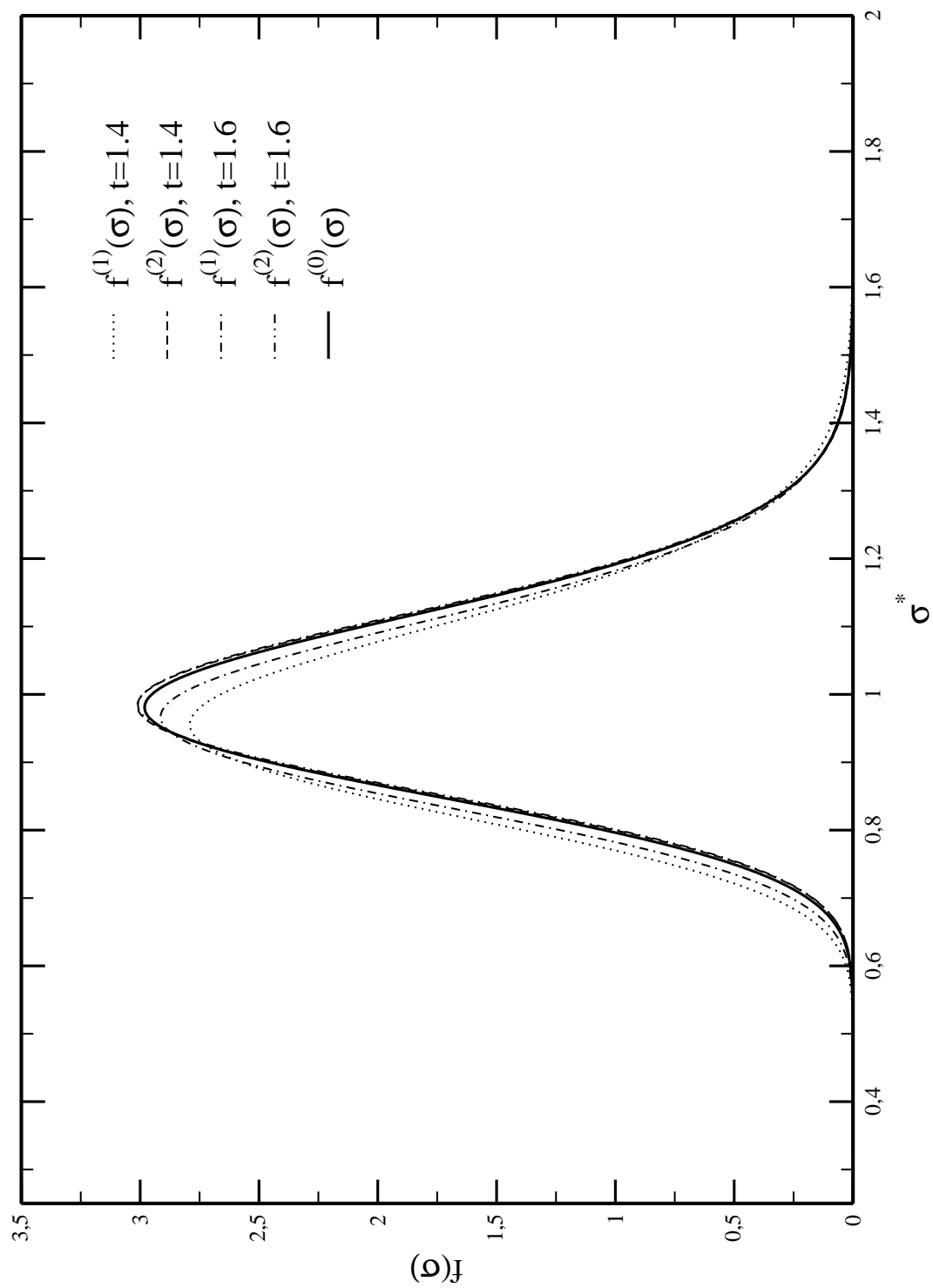
Figure 6.32: SC, CPC, SP curve, critical binodal and same truncated binodals calculated for the size polydisperse Yukawa fluid with  $I = 1.018$ ,  $(\alpha = 55)$ ,  $\kappa = 1.8$ ,  $a = 0$



distribution functions for the polydisperse vdW and the polydisperse square-well fluid. The distribution functions for the low density phases are again shifted to lower particle diameters, but the distributions are broader now what means the polydispersity in the low density phases are now higher as compared to the parent distribution. In the same time the high density distributions are moved to higher values of  $\sigma$  and becoming narrower; the polydispersity is decreased in comparison to  $f^{(0)}(\sigma)$ .

---

Figure 6.33: Low and high density distributions  $f^{(1)}(\sigma)$  and  $f^{(2)}(\sigma)$  calculated for two different temperatures on the critical binodal of the system in figure 6.32



### 6.3.3.2 Size and amplitude polydispersity

#### 6.3.3.2.1 $a = 1$

For the case  $a = 1$  we have switched off the dependence on the moment  $m_1$  in the Yukawa potential (5.60) what means the third term in the chemical potential (5.72) which could have caused the shift of the CPC to higher densities for  $a = 0$  (see figure 6.32) vanishes. We have calculated the phase diagram for  $\kappa = 1.8$ ,  $I = 1.018$  (figure 6.34) and moreover the phase diagrams for  $\kappa = 1.8$ ,  $I = 1.05$  (figure 6.35),  $\kappa = 4$ ,  $I = 1.05$  (figure 6.36) and  $\kappa = 10$ ,  $I = 1.05$  (figure 6.37) to study the influence of  $I$  and  $\kappa$  on the phase transition process. Also if the additional term in the chemical potential (5.72) vanishes, the phase diagrams for  $\kappa = 1.8$  in figures 6.34 and 6.35 remain qualitatively the same as for  $a = 0$  (figure 6.32) with the exception that the CPC seems to be even more shifted to higher densities than in the size polydisperse case. With increasing importance of the attractions the critical point of the system in figure 6.34  $\{\rho_{crit} \simeq 0.247, t_{crit} \simeq 1.747\}$  has moved to higher temperature and slightly to lower density as compared with the system in figure 6.32 (see table (6.3)).

The polydispersity seems to affect the repulsions stronger than the attractions because we can observe like in the size polydisperse vdW fluid that for increasing  $I$  the phase coexistence region is shifted to lower temperatures and the high density phase on the critical binodal towards lower densities (compare figures 6.34 and 6.35) a behavior which is not favorable for the phase transition process. The shift in the CPC with respect to the SC seems to be weaker for higher polydispersity since the intersection in the low density branches of SC and CPC is closer to the critical point in the system of figure 6.35 than in the one of figure 6.34.

In figures 6.36 and 6.37 we can see that the phase coexistence region is shifted to lower temperatures as the inverse screening length  $\kappa$  increases, in addition we can observe that the shift in the CPC to higher densities is slightly decreased (the distance between the low density phases on the SC and CPC is increased and the intersection of the low density branches of CPC and SC moves towards the critical point for growing  $\kappa$ ) as compared to the phase diagram in figure 6.35. For  $\kappa = 10$  the re-entrant region is practically completely vanished.

While the daughter distribution functions for the systems with  $\kappa = 1.8$  (see figure 6.38) remain qualitatively the same as for the system in figure 6.33 the distributions belonging to the systems in figures 6.36 and 6.37 show a qualitative equivalent behavior as for the vdW or square-well fluid. In figure 6.39 one can see the distribution functions belonging to the system in figure (6.36) for the temperatures  $t = 1.25$ ,  $t = 1.35$ . So we conclude, that the shift in the CPC curve is mainly due to the term  $\frac{1}{\kappa}$  of the Yukawa potential (5.60), which gets less important as  $\kappa$  increases.

Figure 6.34: SC, CPC, SP curve and critical binodal calculated for the size and amplitude polydisperse Yukawa fluid with  $I = 1.018$ , ( $\alpha = 55$ ),  $\kappa = 1.8$ ,  $a = 1$

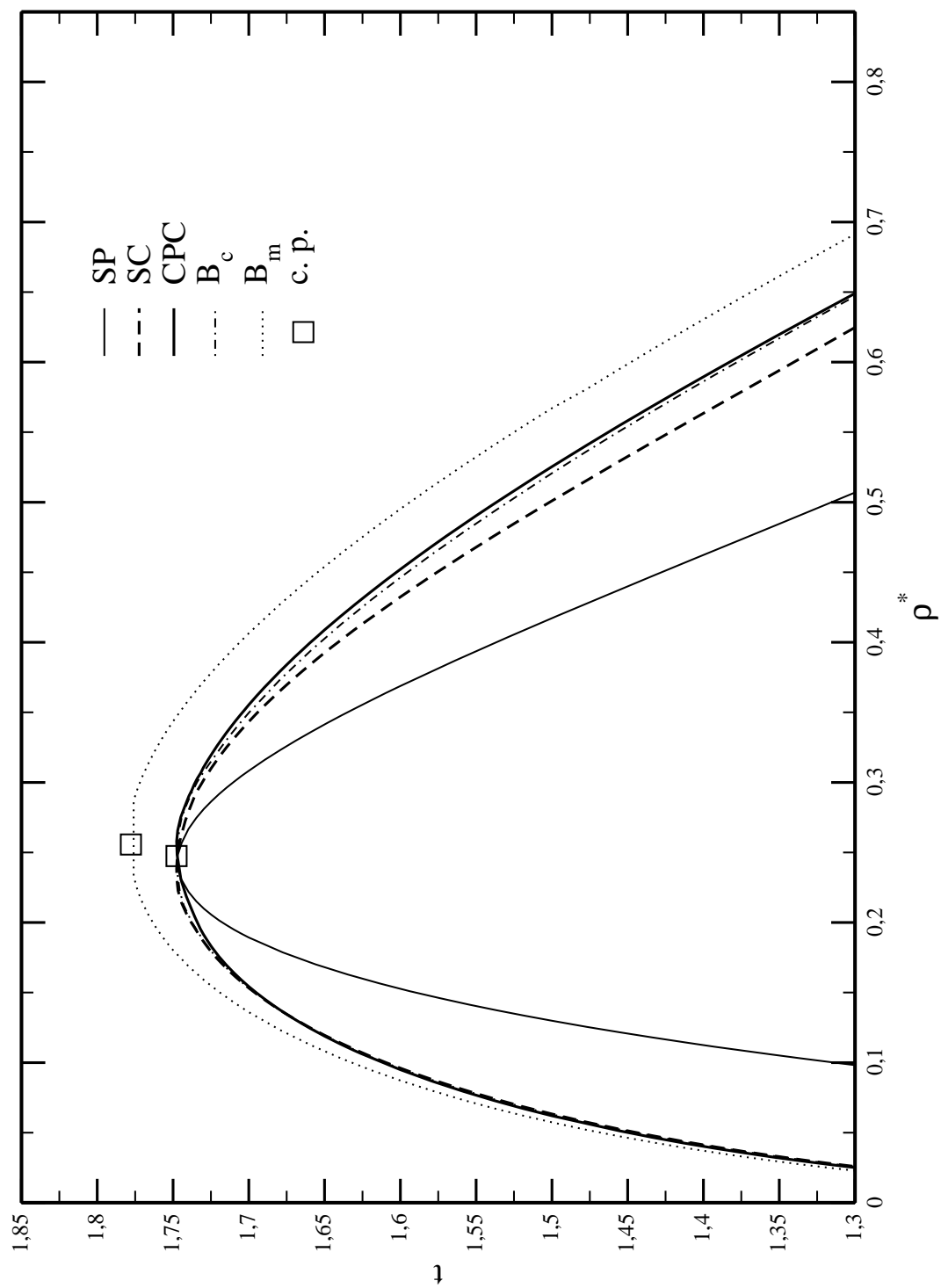


Figure 6.35: SC, CPC, SP curve and critical binodal calculated for the size and amplitude polydisperse Yukawa fluid with  $I = 1.05$ ,  $(\alpha = 20)$ ,  $\kappa = 1.8$ ,  $a = 1$

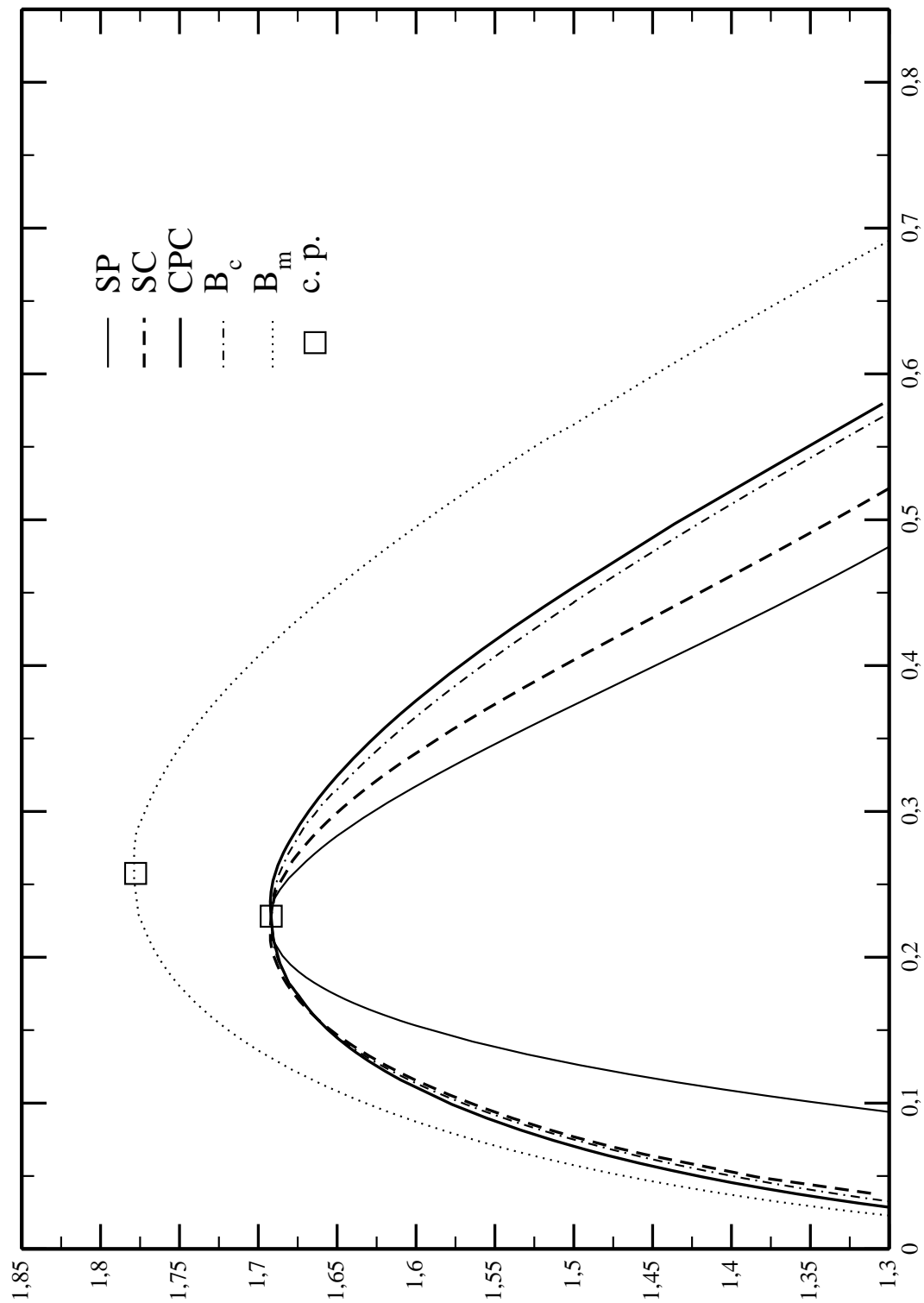


Figure 6.36: SC, CPC, SP curve and critical binodal calculated for the size and amplitude polydisperse Yukawa fluid with  $I = 1.05$ ,  $(\alpha = 20)$ ,  $\kappa = 4$ ,  $a = 1$

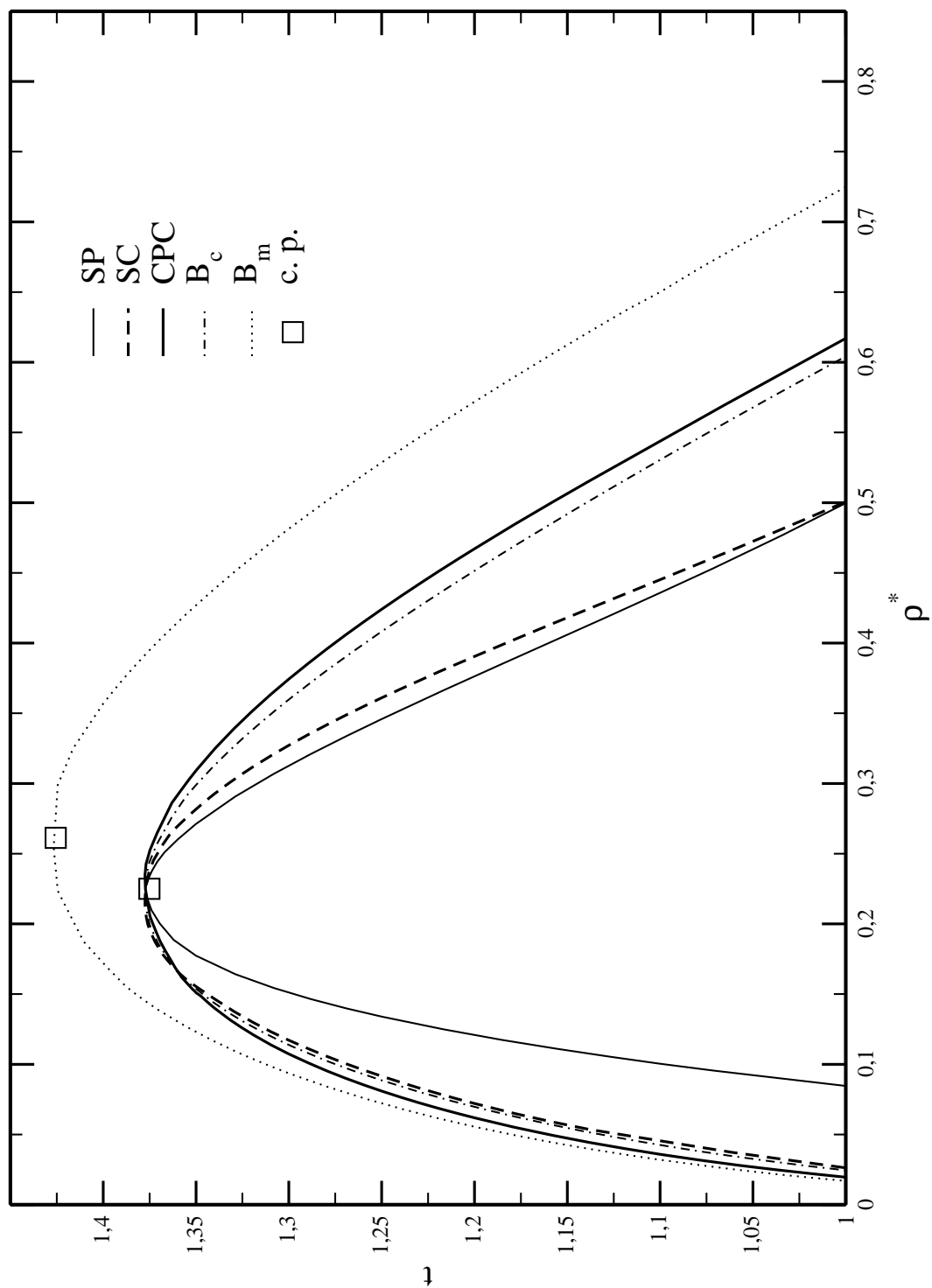


Figure 6.37: SC, CPC, SP curve and critical binodal calculated for the size and amplitude polydisperse Yukawa fluid with  $I = 1.05$ , ( $\alpha = 20$ ),  $\kappa = 10$ ,  $a = 1$

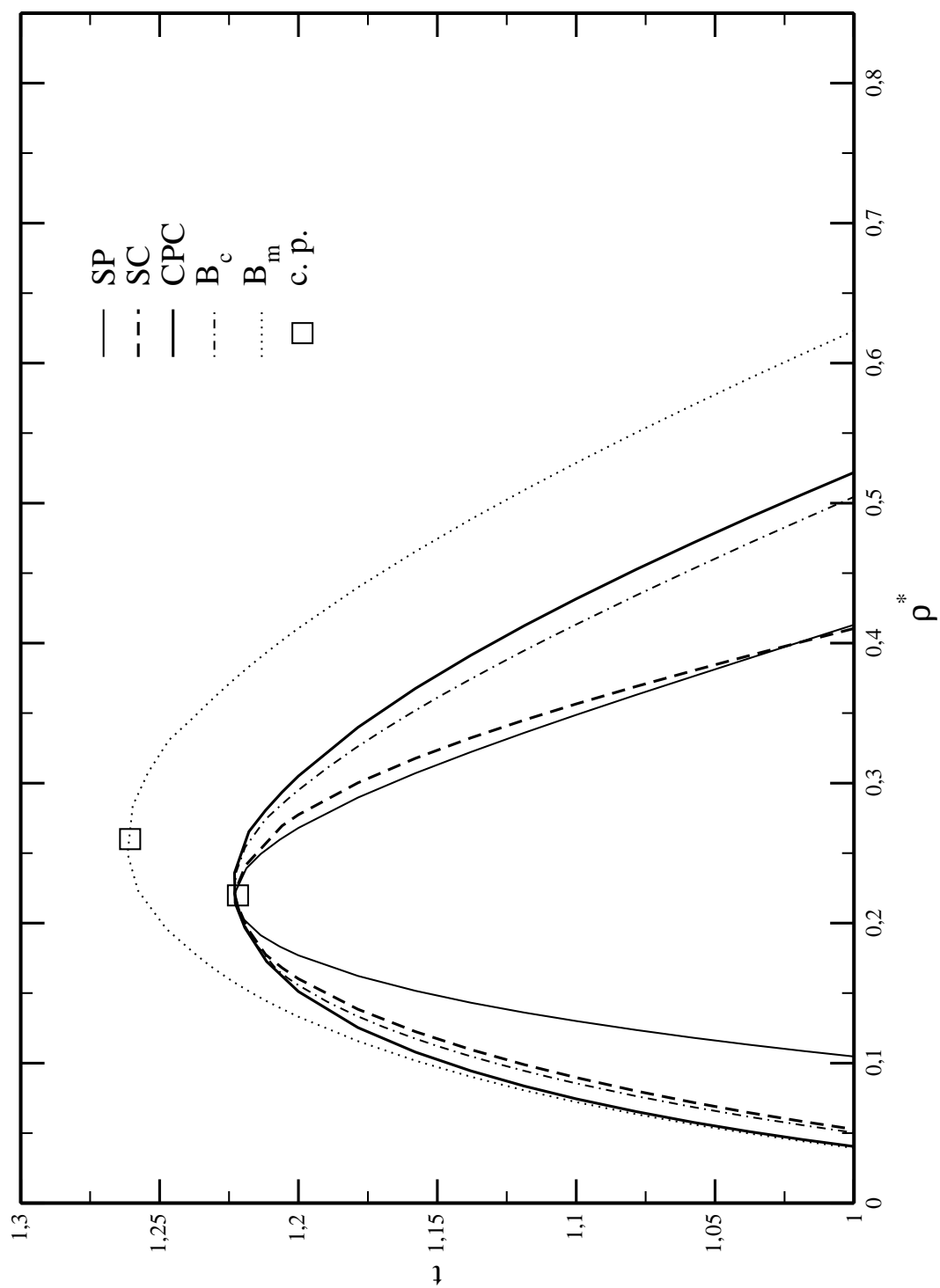


Figure 6.38: Low and high density distributions  $f^{(1)}(\sigma)$  and  $f^{(2)}(\sigma)$  calculated for one temperature on the critical binodal of the system in figure 6.34

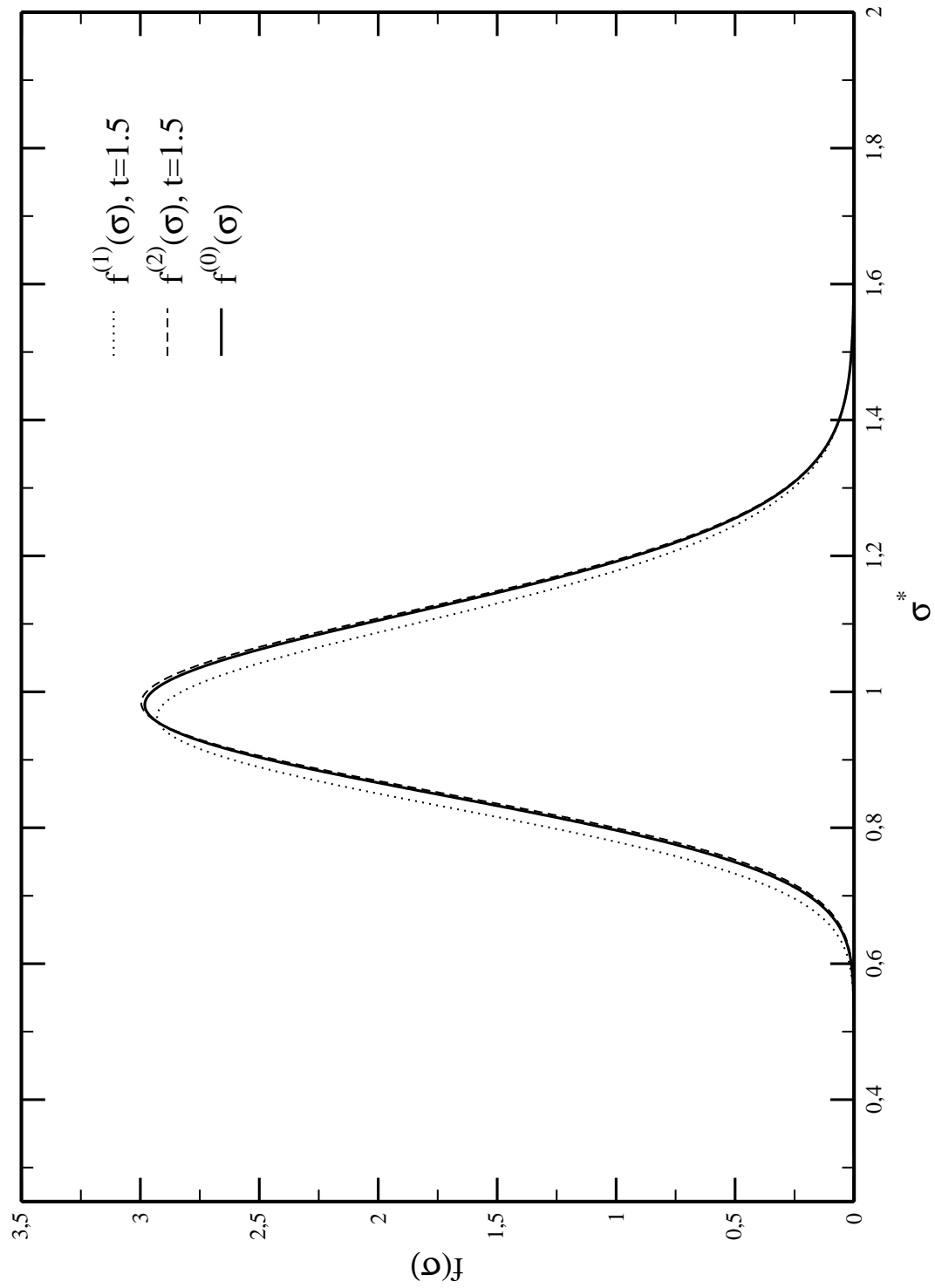
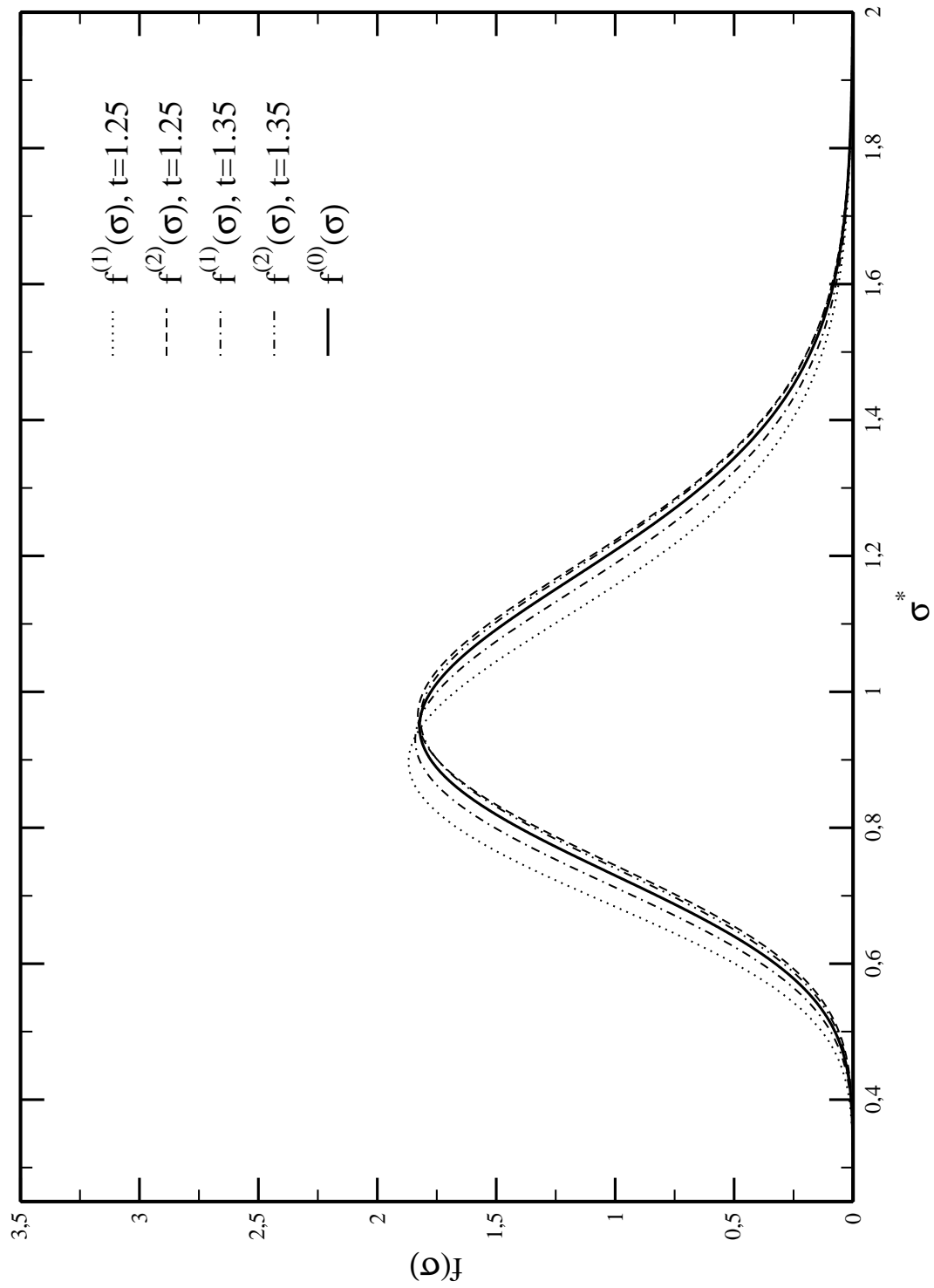


Figure 6.39: Low and high density distributions  $f^{(1)}(\sigma)$  and  $f^{(2)}(\sigma)$  calculated for two different temperatures on the critical binodal of the system in figure 6.36



**6.3.3.2.2**  $a = 2$ 

For  $a = 2, \kappa = 1.8, I = 1.018, (\alpha = 55)$  (figure 6.40) the SC is almost entirely situated inside the CPC only for temperatures near the critical point  $\{\rho_{crit} \simeq 0.246, t_{crit} \simeq 1.833\}$  the CPC is already lying at higher densities as the low density phase on the SC. Like for the polydisperse vdW and the square-well fluid the SC seems to shift to higher densities with respect to the CPC as  $a$  respectively the strength of the potential is increased. The shift in the CPC to higher densities caused by the  $\frac{1}{\kappa}$ -term is then compensated by the shift in the SC as the potential parameter  $a$  increases. If  $a$  is chosen high enough, we expect therefore a similar behavior with respect to CPC and SC as in the phase diagrams for the size and amplitude polydisperse square-well fluid. The critical temperature has now moved to higher values as compared to the cases for  $a = 0$  and  $a = 1$  ( $I = 1.018, \kappa = 1.8$ ) because the attractions become more importance with increasing  $a$  (see table (6.3)).

We can conclude now for the Yukawa model as far as the phase coexistence region is concerned that the phase transition is favored if the effects of the size polydispersity are dominated by the ones of amplitude polydispersity that is the case for potential parameters  $a \geq 2$ ; then the critical temperature is lying above the critical temperature of the monodisperse system.

Table 6.3: Critical points for the Yukawa systems

I	a	$\kappa$	$\rho_{crit}$	$t_{crit}$
1	-	1.8	0.258	1.778
	-	4	0.264	1.426
	-	10	0.261	1.261
1.018	0	1.8	0.252	1.728
1.018	1	1.8	0.249	1.747
1.018	2	1.8	0.247	1.833
1.05	1	1.8	0.228	1.689
1.05	1	4	0.225	1.375
1.05	1	10	0.221	1.221

The distribution functions calculated along the critical binodal for  $t = 1.6$  (figure 6.41) show qualitative the same behavior as for the polydisperse square-well model where the coexisting phases demix stronger than in the square-well fluid. This can be seen by comparison of low and high density distributions  $f^{(1)}(\sigma)$  and  $f^{(2)}(\sigma)$  for the system in figure 6.41.

Figure 6.40: SC, CPC, SP curve and critical binodal calculated for the size and amplitude polydisperse Yukawa fluid with  $I = 1.018$ , ( $\alpha = 55$ ),  $\kappa = 1.8$ ,  $a = 2$

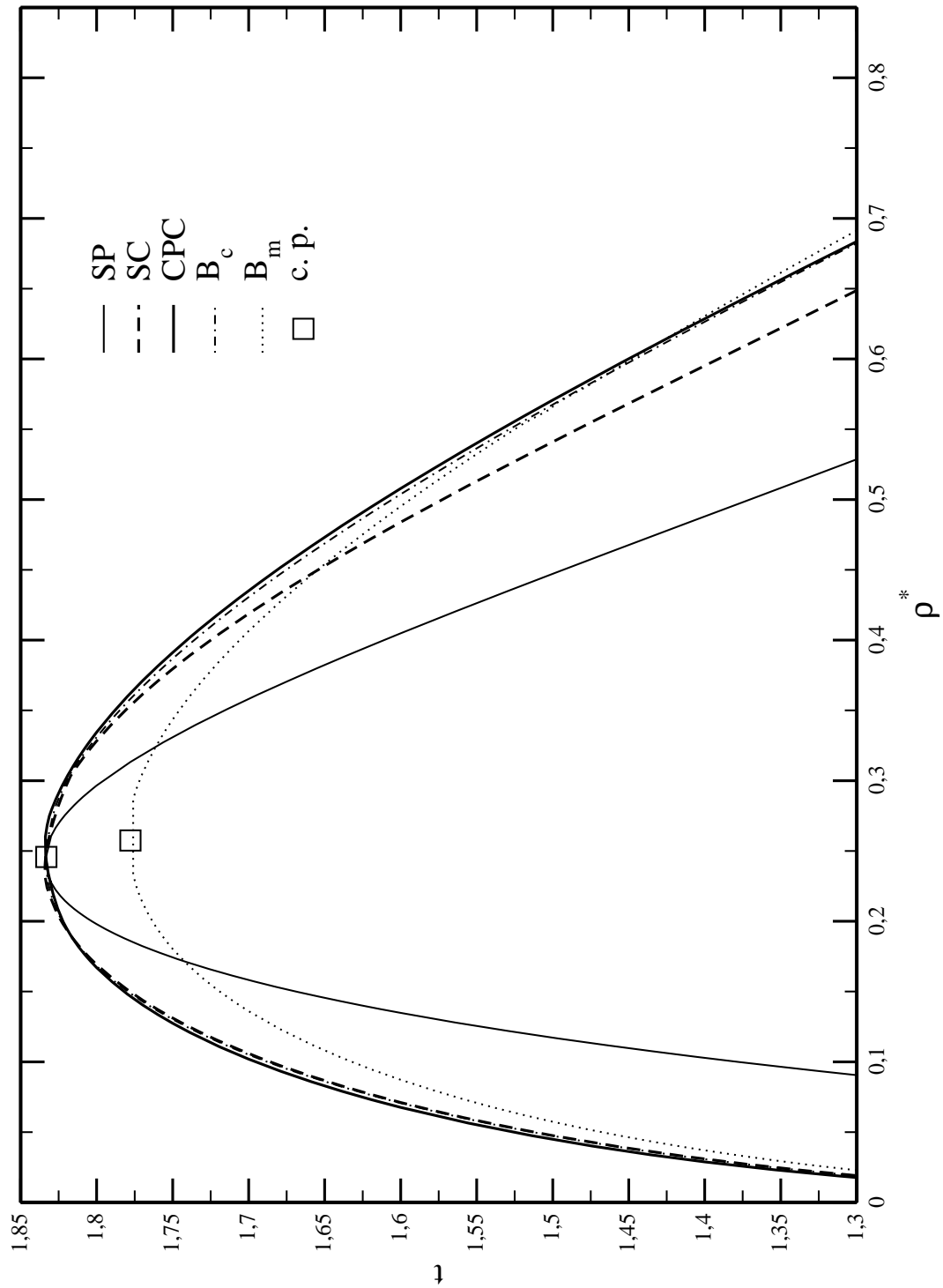
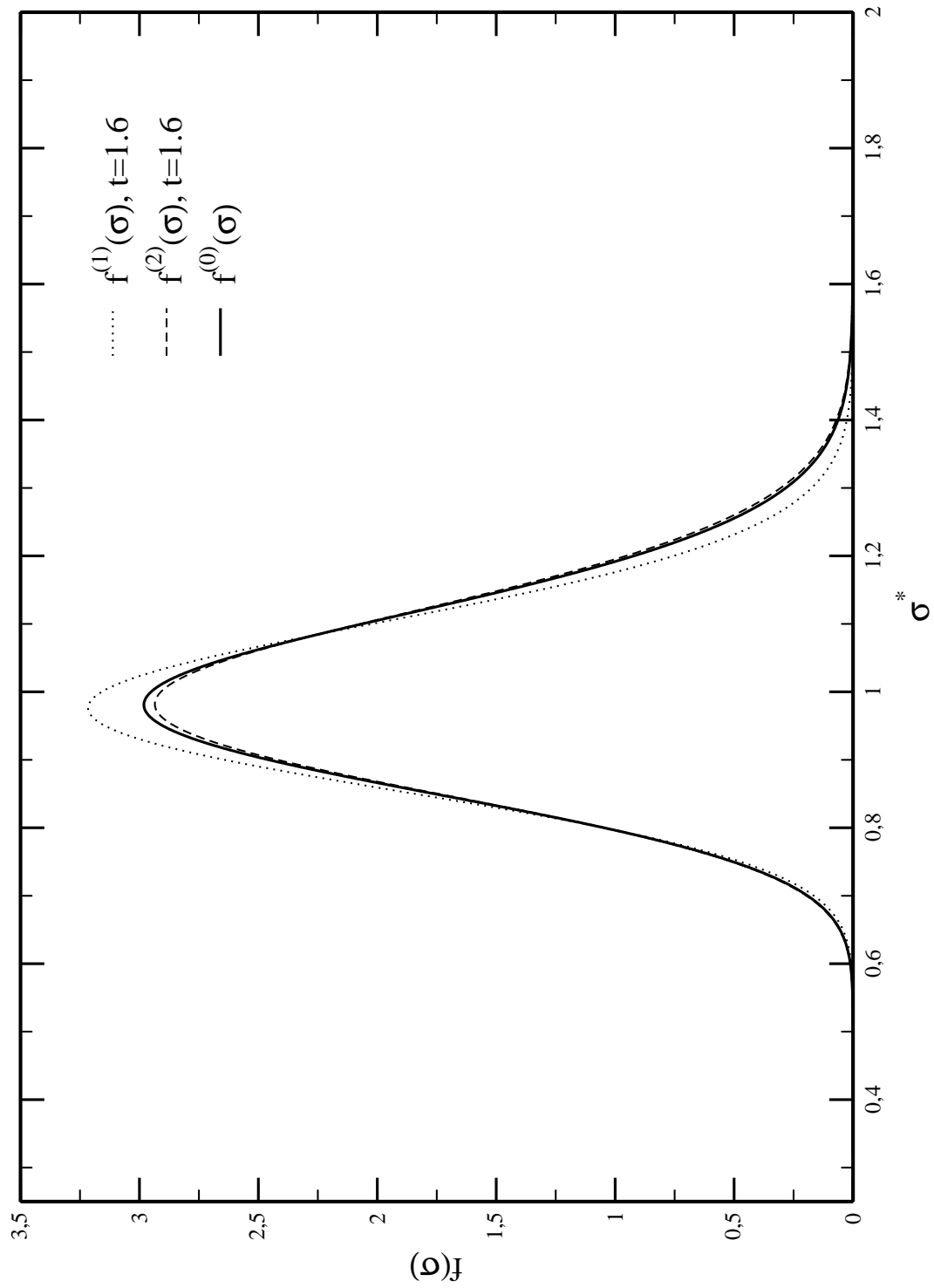


Figure 6.41: Low and high density distributions  $f^{(1)}(\sigma)$  and  $f^{(2)}(\sigma)$  calculated for one temperature on the critical binodal of the system in figure 6.40



# Conclusion

In this thesis we have calculated structure functions, thermodynamic properties and phase diagrams for polydisperse fluid mixtures. The effective interactions mediated between the colloid particles were chosen to be the HSY or the HS with attractive SW potential, in addition we have studied the vdW model.

To produce structure functions and thermodynamic quantities we have used a perturbation theory - the ORPA - to solve the OZ equations of a polydisperse fluid by introducing orthogonal polynomials associated to the distribution function  $f(\sigma)$ .

We have studied the influence of temperature, potential depth and polydispersity (characterized by an index  $I$ ) on four different thermodynamic quantities, where we have made a difference between size and amplitude polydispersity. With size polydispersity we mean that the amplitude of the attractions is constant for all particle type interactions, while for amplitude polydispersity it depends on the diameters  $\sigma$  of the interacting particles. The size or (and) amplitude polydispersity of the potential can be adjusted by the special choice of potential parameters ( $z$  for the square-well model and  $a$  for the Yukawa model). We have shown that the SW and HSY model have in many aspects similar behavior with respect to the monodisperse case when the polydispersity is increased. The most evident difference between the SW and the HSY model turned out to be the thermodynamic self-consistency of the pressures calculated either via the energy route and or via the virial route. While for the SW potential the ORPA is self-consistent to a high degree even for larger number densities, the self-consistency for the HSY potential is not satisfying (mainly for large screening length  $\kappa = 4$ ). This might be explained by the fact, that the ORPA is made for long ranged potentials (like the SW potential) as it takes only the asymptotic limit of the attractions into account.

We have calculated the polydisperse phase transitions using truncatable free energy methods, throughout in such a calculation the free energy of a polydisperse system can be expressed in dependence of the finite set of moments of a distribution function  $f(\sigma)$ . The truncatable free energy method is an exact method, however it is limited to a rather small class of model systems [20]. We restrict ourselves in this work to rather simple models: a vdW free energy and a HTA like approximation for the free energy of a HS system with

attractive tail (either SW or Yukawa potential). Although these models are rather simple we have found several interesting aspects concerning the influence of polydispersity on the phase coexistences.

While for monodisperse systems there exists only one binodal, for polydisperse systems one can calculate an arbitrary number of binodals one for each choice of parent number density  $\rho^{(0)}$ , where only the binodal calculated for  $\rho^{(0)} = \rho_{crit}$  approaches the critical point; all other binodals are truncated at a certain temperature below or above the critical point. If we let the composition of the parent phase unaltered and calculate for fixed temperature the phase coexistence densities of the parent- (corresponds to the special choice that  $\rho^{(0)}$  is equal to the equilibrium number density of the majority phase) and incipient minority-phase which is present in infinitesimal amounts only, we obtain a cloud point with coexisting shadow. The resulting CPC (given by the number densities of the parent phases versus temperature) and SC (number densities of the incipient phases versus temperature) provide then envelopes for the various binodals.

Also for the critical point an evident difference between monodisperse and polydisperse system can be observed: while the critical point in the monodisperse case is always situated at the maximum of binodal or spinodal, in the polydisperse case it can be obtained from the intersection of CPC and SC which have in general no common maximum (only for special choices of potential parameters). In most cases the maxima of CPC and SC are at temperature  $t_m$  above the critical point; this allows for a re-entrant behavior of the high or low density phase: with re-entrant behavior we mean that for a special choice of  $\rho^{(0)}$  one can observe also by restriction to two-phase coexistences phase equilibria above the critical point.

We have studied the influence of the size polydispersity, the amplitude polydispersity and the combination of size and amplitude polydispersity on the phase separation process. If we compare the results obtained via the three model systems (vdW, SW and HSY system) we can observe the following: With respect to the phase coexistence region we could observe for the vdW and HSY fluid by comparison with the monodisperse case that size polydispersity leads to a reduction in the critical temperature and in the coexistence densities mainly of the high density phase (because the repulsions of the studied systems are affected stronger by the size polydispersity than the attractions when compared to the monodisperse case). In the square-well fluid the size polydispersity has less influence, it causes only a shift in the coexistence densities to lower values but the critical temperature remains practically unaltered as in the monodisperse case. If the studied systems are both size and amplitude polydisperse we can observe that the phase coexistence region is shifted to higher temperatures and the densities on the high density phase moves to higher values when compared to the monodisperse case. With increasing potential pa-

parameter ( $z \neq 0$  for square-well and  $a \geq 2$  for Yukawa) and polydispersity index  $I$  the monodisperse phase coexistence curve is finally situated entirely within the phase coexistence region of the polydisperse system. We can conclude now that size polydisperse fluids need lower temperatures to phase separate than the corresponding monodisperse fluid while amplitude polydisperse fluids phase separate already at higher temperatures than the monodisperse fluid. One can also say amplitude polydispersity favors the phase transition process while size polydispersity is not favorable to it.

The size and (or) amplitude polydispersity has also differing influence on the CPC and SC of the regarded model systems. While for size polydispersity only in the vdW and SW fluid the SC is entirely situated inside the CPC, the CPC curve in the HSY system was shifted to higher densities; thus the maxima of CPC and SC never coincide and the system shows re-entrant behavior near the critical point. If we introduce in addition amplitude polydispersity by a suitable choice of the potential parameters, the SC for the vdW and SW system moves partly out of the interior of the CPC and the region of re-entrant behavior of the low density phase increases with growing amplitude polydispersity. In the HSY system which is both size and amplitude polydisperse we can observe a very similar behavior as for the pure size polydisperse HSY system at least as it concerns the positions of the CPC and the SC to each other; it seems to be that for the chosen parameter  $a \leq 2$  the effects of the size polydispersity dominate over the ones of the amplitude polydispersity.

The chosen model systems gave us a good insight into phase transition processes of simple polydisperse fluids. They can be used as basis for future work on this topic.



# Appendix A

## A.1 Abbreviations

Table A.1: List of abbreviations

Abbreviation	Meaning	section
B	Binodal	6.3
$B_c$	Critical binodal	6.3
c. p.	Critical point	6.3
CPC	Cloud point curve	5.1.2
HNC	Hyper-netted chain	4.3
HS	Hard sphere	2.2.1
HSY	Hard-sphere Yukawa	2.2.3
HTA	High temperature approximation	4.2.1
IET	Integral equation theories	4.3
MCSL	Mansoori-Carnahan-Starling-Leland	4.2.4
MSA	mean spherical approximation	4.2.3
ORPA	Optimized random phase approximation	4.2.2
OZ	Ornstein-Zernike	3.1
pdf	Probability density function	2.1
PY	Percus-Yevick	2.2.1
RPA	Random phase approximation	4.2.2
RY	Rogers-Young	4.3
SC	Shadow curve	5.1.2
SP	Spinodal	5.2.1
SW	Square-well	2.2.2
SZ	Schulz-Zimm	6.1
vdW	van der Waals	4.1
VW	Verlet-Weis	4.2.4



# Appendix B

## B.1 Numerical methods

### B.1.1 Numerical solution of the ORPA

For numerical purposes, we have to find approximate expressions for the sums and integrals in (4.24) and (4.25). This can be done by Gaussian quadrature. The Gaussian quadrature uses for an approximate integral or sum the  $n$  roots  $\sigma_k$  of the polynomial  $p_n(\sigma)$  to discretize the infinite sums and integrals over  $\sigma$  on a grid with  $n$  points. When  $y(\sigma)$  is a  $\sigma$  dependent function, then we can write the approximation [9] using the  $n$  roots  $\sigma_k$

$$\int_0^\infty d\sigma f(\sigma)y(\sigma) \simeq \sum_{k=1}^n w_k y(\sigma_k) \quad (\text{B.1})$$

with the weights

$$w_k = \frac{1}{\sum_{l=0}^{n-1} p_l^2(\sigma_k)}.$$

The above expressions are exact, if  $y(\sigma)$  is a polynomial of degree  $2n - 1$  or smaller. If we use a value  $n$  to truncate the series in (4.25), then the polydisperse system is mapped onto a discrete  $n$  component system, which is characterized by the particle diameters (the roots)  $\sigma_k$  and concentrations (weights)  $w_k$ . The matrices in (4.27), (4.28), (4.30) and (4.31) become now  $n \times n$  matrices, where  $n$  is the (chosen) parameter of discretization; the actual value for  $n$ , required for a sufficient level of accuracy, are discussed later in this work. With the use of the Gaussian quadrature the equations (4.24) and (4.25) read

$$\begin{aligned} y(r, \sigma_k, \sigma_l) &\simeq \sum_{i,j=0}^{n-1} y_{ij}(r) p_i(\sigma_k) p_j(\sigma_l) \\ y_{ij}(r) &\simeq \sum_{k,l=1}^n w_k w_l y(r, \sigma_k, \sigma_l) p_i(\sigma_k) p_j(\sigma_l). \end{aligned} \quad (\text{B.2})$$

Now we have developed the theoretical framework and the numerical concepts to calculate numerically the structure and thermodynamics of a polydisperse system within the ORPA.

From a numerical point of view, the ORPA reduces to a search of the minimum of the functional  $F$  [16]. Its gradient (4.35) with respect to the coefficients of the direct correlation functions can easily be evaluated via the residual OZ equation (4.31). For the numerical solution of the ORPA one proceeds as follows [12]:

1. Define a starting value for  $c_1(r, \sigma_1, \sigma_2) = c_1^{(i)}(r, \sigma_1, \sigma_2)$  inside the core ( $i$  denotes the iteration step).
2. Fourier transformation of  $c_1^{(i)}(r, \sigma_1, \sigma_2)$  to get  $\tilde{c}_1^{(i)}(k, \sigma_1, \sigma_2)$ .
3. Decomposition of the direct correlation functions with respect to their expansion coefficients  $\tilde{c}_{lm;1}^{(i)}(k)$  by use of (B.2).
4. Insert this  $\tilde{c}_{lm;1}^{(i)}(k)$  into the residual OZ equation (4.31) to get  $\tilde{h}_{lm;1}^{(i)}(k)$ .
5. Calculation of the Fourier transform  $h_{lm;1}^{(i)}(r)$ .
6. Compose the total correlation functions  $h^{(i)}(r, \sigma_1, \sigma_2)$  with (B.2).
7. Check if  $g^{(i)}(r, \sigma_i, \sigma_j)$  satisfies the core condition which corresponds to the minimum of  $F$ . For application it is sufficient to stop this iteration as soon as the maximum average of  $g_1^{(i)}(r, \sigma_1, \sigma_2)$  with respect to all grid points  $m$  inside the core is below a given threshold:

$$\max_{r < \hat{\sigma}} |g_1^{(i)}(r, \sigma_1, \sigma_2)| < \epsilon,$$

where  $|g_1^{(i)}(r, \sigma_1, \sigma_2)|_{r < \hat{\sigma}}$  is the average value of  $g_1^{(i)}(r, \sigma_1, \sigma_2)$  defined as

$$|g_1^{(i)}(r, \sigma_1, \sigma_2)|_{r < \hat{\sigma}} = \frac{1}{m} \sum_k g_1^{(i)}(r_k, \sigma_1, \sigma_2)_{r_k < \hat{\sigma}},$$

and  $\max$  denotes a maximum value. The parameter  $\epsilon$  is typically of the size  $10^{-5}$ .

8. Use this  $g_1^{(i)}(r, \sigma_1, \sigma_j)$  to correct  $c_1^{(i)}(r, \sigma_1, \sigma_2)$  inside the core. This can be done using various techniques, the simplest and most common one is the method of steepest descents [46].
9. Take the new  $c_1^{(i+1)}(r, \sigma_1, \sigma_2)$  and go back to step (2).

One has to be careful with the numerical implementation of this algorithm: especially the Fourier transform of  $\tilde{g}_{lm;1}(k)$  from  $k$  to  $r$  space can cause some problems, because the resulting  $g_{lm;1}(r)$  is discontinuous at contact. The solution of this problem requires a little trick [40]. Obviously, the expression  $g_{lm}(r) - c_{lm}(r)$  is a convolution and therefore a continuous function. The same is valid for the expression  $g_{lm;1}(r) - c_{lm;1}(r)$ . Before

Fourier transformation of  $\tilde{g}_{lm;1}(k)$ , we simply subtract  $\tilde{c}_{lm;1}(k)$  from  $\tilde{g}_{lm;1}(k)$ , after Fourier transformation we add  $c_{lm;1}(r)$ , obtaining thus  $g_{lm;1}(r)$ :

$$g_{lm;1}(r) = \frac{1}{(2\pi)^3} \int d^3k e^{-i\vec{k}\vec{r}} (\tilde{g}_{lm;1}(k) - \tilde{c}_{lm;1}(k)) + c_{lm;1}(r).$$

## B.1.2 Numerical solution of the phase equilibrium conditions

To solve the phase equilibrium conditions (5.23), (5.24) and (5.19) for the truncated free energy method we have used a globally convergent Newton-Raphson algorithm [56].

### B.1.2.1 Globally convergent Newton-Raphson Algorithm

The Newton-Raphson algorithm is one of the simplest multidimensional root finding methods. If the solution is approximately known the convergence is very good, for other initial guesses in the most cases the simple Newton Raphson fails. An improvement to the simple Newton Raphson can be find by use of the so called globally convergent Newton-Raphson method, which, as the name means, converges also for initial guesses far away from the solution.

A typical problem gives  $n$  in general nonlinear functional relations to be zeroed, involving variables  $x_i, i = 1, 2, \dots, n$ :

$$F_i(x_1, x_2, \dots, x_n) = 0 \quad i = 1, 2, \dots, n,$$

where the functions  $F_i$  are given with (5.23), (5.24) and (5.19) as

$$\begin{aligned} m_k^{(1)} - \int f^{(1)}(\sigma) \sigma^k d\sigma &= 0 \\ p^{(1)} - p^{(2)} &= 0 \end{aligned} \tag{B.3}$$

with  $k = 0, 1, \dots, n - 2$  and the unknowns  $x_i$  corresponding to  $m_k^{(1)}, \rho^{(1)}$  and  $\rho^{(2)}$ . The moment  $m_0^{(1)}$  is no unknown variable, it is in all relations set to 1. We let  $\vec{x}$  denote the entire vector of values  $x_i$  and  $\vec{F}$  denote the entire vector of functions  $F_i$ . In the neighborhood of  $\vec{x}$ , each of the functions  $F_i$  can be expanded in Taylor series

$$F_i(\vec{x} + \delta\vec{x}) = F_i(\vec{x}) + \sum_{j=1}^n \frac{\partial F_i}{\partial x_j} \delta x_j + O(\delta\vec{x}^2).$$

which can be written in matrix notation as

$$\vec{F}(\vec{x} + \delta\vec{x}) = \vec{F}(\vec{x}) + J\delta\vec{x} + O(\delta\vec{x}^2), \tag{B.4}$$

where  $J$  is the Jacobi matrix

$$J_{ij} = \frac{\partial F_i}{\partial x_j}. \tag{B.5}$$

By neglecting terms of order  $\delta\vec{x}^2$  and higher and by setting  $\vec{F}(\vec{x} + \delta\vec{x}) = 0$ , we obtain a set of linear equations for the corrections  $\delta\vec{x}$  that move each function closer to zero simultaneously, namely

$$\begin{aligned} J\delta\vec{x} &= -\vec{F} \\ \delta\vec{x} &= -J^{-1}\vec{F} \end{aligned} \quad (\text{B.6})$$

The corrections  $\delta\vec{x}$  are then added to the solution vector to obtain the new values

$$\vec{x}_{new} = \vec{x}_{old} + \delta\vec{x} \quad (\text{B.7})$$

The equations (B.4) - (B.7) define the simple Newton-Raphson algorithm which provides a good convergence for initial values near the solution. To obtain a globally convergent Newton-Raphson algorithm we define a function [56]

$$f = \frac{1}{2}\vec{F}\vec{F} \quad (\text{B.8})$$

so that we can write

$$\vec{\nabla}f\delta\vec{x} = (J\vec{F})(-J^{-1}\vec{F}) = -\vec{F}\vec{F} < 0 \quad (\text{B.9})$$

and  $\delta\vec{x}$  is a descent direction of  $f$ . We always try the full Newton step (B.7), because once we are close enough to the solution we will get quadratic convergence. We check at each iteration that the proposed step reduces  $f$

$$f_{new} \leq f_{old} + \alpha\vec{\nabla}f(\vec{x}_{new} - \vec{x}_{old}), \quad (\text{B.10})$$

where  $\alpha = 10^{-4}$  [56]. If (B.10) is not fulfilled then we have to reduce the correction  $\delta\vec{x}$  along the Newton direction until we have an acceptable step. For this purpose we introduce a variable  $\lambda$  ( $0 < \lambda \leq 1$ ) into (B.7) to obtain

$$\vec{x}_{new} = \vec{x}_{old} + \lambda\delta\vec{x}. \quad (\text{B.11})$$

The Newton step is a descent direction for  $f$  because initially  $f$  decreases as we move in the Newton direction, so we are guaranteed to find an acceptable step with (B.11). The globally convergent Newton-Raphson algorithm is a method which minimizes  $f$  by taking Newton steps designated to bring  $\vec{F}$  to zero.

To calculate the constant  $\lambda$  in (B.11) we define the function [56]

$$g(\lambda) = f(\vec{x}_{old} + \lambda\delta\vec{x}) \quad (\text{B.12})$$

so that

$$g'(\lambda) = \vec{\nabla}f\delta\vec{x}.$$


---

We expand now  $g(\lambda)$  in a Taylor series around  $\lambda$  and truncate it at the second order term

$$g(\lambda) \simeq (g(1) - g(0) - g'(0))\lambda^2 + g'(0)\lambda + g(0),$$

where  $g(1)$  is the value in the full Newton step,  $g(0)$  corresponds to the unaltered initial value and  $g'(0)$  is its gradient. The value  $\lambda$  is determined in that way as  $g(\lambda)$  should have its minimum there

$$\lambda = -\frac{g'(0)}{2(g(1) - g(0) - g'(0))}. \quad (\text{B.13})$$

For small  $\alpha$ , it can be shown [56] that  $\lambda$  should be in the range of  $0.1 \leq \lambda \leq 0.5$ . If the Newton step (B.12) calculated with this  $\lambda$  does not fulfill the condition (B.10) then we have to calculate a further  $\lambda$  given now through a cubic equation

$$g(\lambda) = a\lambda^3 + b\lambda^2 + g'(0)\lambda + g(0), \quad (\text{B.14})$$

where we use the values  $g(\lambda_1)$  from the previous step and the value  $g(\lambda_2)$  from the step before the previous one. Requiring that equation (B.14) gives the correct values for  $g(\lambda_1)$  and  $g(\lambda_2)$  leads to the determining equations for the coefficients  $a$  and  $b$ :

$$\frac{1}{\lambda_1 - \lambda_2} \begin{pmatrix} \frac{1}{\lambda_1^2} & -\frac{1}{\lambda_2} \\ -\frac{\lambda_2}{\lambda_1^2} & \frac{\lambda_1}{\lambda_2^2} \end{pmatrix} \begin{pmatrix} g(\lambda_1) - g'(0)\lambda_1 - g(0) \\ g(\lambda_2) - g'(0)\lambda_2 - g(0) \end{pmatrix} = \begin{pmatrix} a \\ b \end{pmatrix}, \quad (\text{B.15})$$

The minimum of the cubic equation (B.14) is then at

$$\lambda = \frac{-b + \sqrt{b^2 - 3ag'(0)}}{3a}, \quad (\text{B.16})$$

with  $0.1\lambda_1 \leq \lambda \leq 0.5\lambda_1$ .

We summarize the steps of the globally convergent Newton algorithm as follows:

1. The initial guess for the moments  $m_k^{(1)}$  is given by the moments of the parent by  $m_k^1 = m_k^0$ , the number densities  $\rho^{(1)}$  and  $\rho^{(2)}$  are chosen to be those of the corresponding monodisperse phase coexistence. Where the moments  $m_k^{(1)}$  and the number densities are represented by the solution vector  $\vec{x}_{old}$ .
2. Calculation of the functions  $F_i$  and  $f(\vec{x}_{old}) = f_{old}$  by use of (B.3) and (B.8).
3. Check whether the  $\vec{F}_i$  are in good approximation equal to zero. The iteration is stopped as soon as the largest  $F_i$  is below a constant  $\varepsilon$

$$\max|F_i| < \varepsilon,$$

where we have chosen  $\varepsilon = 10^{-10}$ .

4. If the condition of point 3 is not fulfilled we continue with the calculation of the Jacobi matrix (B.5).
  5. Determination of the corrections  $\delta\vec{x}$  with (B.6).
  6. Calculation of the full Newton step (B.7) to obtain  $\vec{x}_{new}$  and  $f(\vec{x}_{new}) = f_{new}$ .
  7. Check whether condition (B.10) is fulfilled. If this is the case we accept the calculated Newton step and set  $\vec{x}_{new} \rightarrow \vec{x}_{old}$  to continue with point 2.
  8. If (B.10) is not fulfilled we have to calculate an appropriate  $\lambda = \lambda_1$  for (B.11) by use of (B.13) to get  $\vec{x}_{new}$ .
  9. If condition (B.10) is still not fulfilled we calculate a further  $\lambda$  with (B.16) by use of  $\lambda_1$  and  $\lambda_2 = 1$  of the two previous Newton steps. Finally we set  $\lambda_1 \rightarrow \lambda_2$  and  $\lambda \rightarrow \lambda_1$  and continue to calculate values for  $\lambda$  by use of equation (B.16) until we obtain a  $\vec{x}_{new}$  for which the interruption criterion (B.10) is reached and we can return by setting  $\vec{x}_{new} \rightarrow \vec{x}_{old}$  to 2.
-

# Appendix C

## C.1 Mathematical Expressions

### C.1.1 Trace of a symmetric matrix

We will now proof the last equation in (4.51) which where used to calculate the free energy within the MSA (4.50). We have to show now that

$$\text{Tr}(\ln A) = \ln(\det A)$$

or equivalently

$$\det A = e^{\text{Tr}(\ln A)}, \quad (\text{C.1})$$

where the matrix  $A$  is symmetric. There exists a diagonal matrix  $D$  to  $A$  so that we can write

$$A = TDT^{-1},$$

with  $T$  the transformation matrices. The determinant of  $A$  and of the corresponding diagonal matrix are identical and defined as

$$\det A = \det D = \prod_{i=1}^n \lambda_i \quad (\text{C.2})$$

where the  $\lambda_i$  are the eigenvalues of the diagonal matrix  $D$ . Equation (C.1) we can now be written as

$$e^{\text{Tr}(\ln A)} = e^{\text{Tr}(T \ln(D) T^{-1})} = e^{\text{Tr}(\ln D)} = e^{\ln \lambda_1 + \dots + \ln \lambda_n} = \prod_{i=1}^n \lambda_i, \quad (\text{C.3})$$

where we have used the relations

$$\text{Tr}(TDT^{-1}) = \text{Tr}(T^{-1}TD) = \text{Tr}(D)$$

$$\ln(TDT^{-1}) = T \ln(D) T^{-1},$$

for the last relation we have expanded the logarithm into a Taylor series. The equations (C.2) and (C.3) lead to the same result, so that we have proofed the equality (C.1).



# Bibliography

- [1] W. Poon, P. N. Pusey and H. N. W. Lekkerkerker, *Phys. World* **9**, 27 (1996).
- [2] A. Vrij, *J. Chem. Phys.* **69**, 1742 (1978).
- [3] L. Blum and G. Stell, *J. Chem. Phys.* **71**, 42 (1979); **72**, 2212 (1980).
- [4] J. J. Salacuse and G. Stell, *J. Chem. Phys.* **77**, 3714 (1982); J. J. Salacuse, *ibid.* **81**, 2468 (1984); Ph D. thesis, State University of New York, Stony Brook, 1987.
- [5] J. G. Briano and E. D. Glandt, *J. Chem. Phys.* **80**, 3336 (1984).
- [6] C. Robertus, W. H. Philipse, J. G. H. Joosten and Y. K. Levine, *J. Chem. Phys.* **90**, 4482 (1989).
- [7] C. Tutschka and G. Kahl, *J. Chem. Phys.* **108**, 9498 (1998).
- [8] B. D'Aguanno and R. Klein, *Phys. Rev. A* **46**, 7652 (1992).
- [9] F. Lado, *Phys. Rev. E* **54**, 4411 (1996).
- [10] F. Lado, *Phys. E* **55**, 426 (1997); F. Lado, E. Lomba and M. Lombardero, *J. Chem. Phys.* **108**, 4530 (1998).
- [11] F. Lado and E. Lomba, *Phys. Rev. Lett.* **80**, 3535 (1998).
- [12] S. Leroch, *Diploma thesis TU Wien 1998 (unpublished)*.
- [13] H. C. Anderson and D. Chandler, *J. Chem. Phys.* **57**, 1918 (1972); H. C. Anderson, D. Chandler and J. D. Weeks, *ibid.* **56**, 3812 (1972).
- [14] H. C. Anderson, D. Chandler and J. D. Weeks, *Adv. Chem. Phys.* **34**, 105 (1976).
- [15] G. Pastore, F. Matthews, O. Akinlade and Z. Badirkhan, *Mol. Phys.* **84**, 653 (1995).
- [16] G. Pastore, O. Akinlade, F. Matthews and Z. Badirkhan, *Phys. Rev. E* **57**, 460 (1998).

- 
- [17] A. Lang, C. N. Likos, A. R. Denton, G. Kahl and H. Löwen (unpublished).
- [18] S. Leroch, G. Kahl and F. Lado, *Phys. Rev. E* **59**, 6937 (1999).
- [19] L. Bellier-Castella, H. Xu and M. Baus, *J. Chem. Phys.* **113**, 8337 (2000).
- [20] P. Sollich, *J. Phys. Condens. Matter* unpublished (2001).
- [21] P. Sollich and M. E. Cates, *Phys. Rev. Lett.* **80(7)**, 1365 (1998).
- [22] P. B. Warren, *Phys. Rev. Lett.* **80(7)**, 1369 (1998).
- [23] R. Lovett and M. Baus, *J. Chem. Phys.* **111**, 5544 (1999), A. Daanoun, C. F. Tejero and M. Baus *Phys. Rev. E* **50**, 2913 (1994).
- [24] J.J. Salacuse, *J. Chem. Phys.* **81**, 2468 (1984).
- [25] C.N. Likos, *Effective interactions in soft condensed matter physics*, *Phys. Rep.* (in press).
- [26] J. P. Hansen and J. R. McDonald, *Theory of simple liquids* (1986).
- [27] V. Degiorgio, R. Piazza, M. Corti, and J. Stavans, *J. Chem. Soc. Faraday Trans.* **87**, 431 (1991).
- [28] J.C. Crocker and D.G. Grier, *Phys. Rev. Lett.* **73**, 352 (1994).
- [29] J.C. Crocker and D.G. Grier, *Phys. Rev. Lett.* **77**, 352 (1996).
- [30] J.K. Percus and G.L. Yevick, *Phys. Rev.* **110**, 1 (1958).
- [31] J. L. Lebowitz, *Phys. Rev.* **133**, 895 (1964).
- [32] N.F. Carnahan and K.E. Starling, *J. Chem. Phys.* **51**, 635 (1969).
- [33] L. Verlet and J.J. Weis, *Phys. Rev.* **A5**, 939 (1972).
- [34] D. Henderson and E.W. Grundke, *J. Chem. Phys.* **63**, 601 (1975).
- [35] G. A. Mansoori, N. F. Carnahan, K. E. Starling and T. W. Leland, *J. Chem. Phys.* **54**, 1523 (1971).
- [36] E. W. Grundke and D. Henderson, *Mol. Phys.* **24**, 269 (1972).
- [37] H. Löwen, *Phys. Rep.* **237**, 249 (1994).
- [38] C. Caccamo, *Phys. Rep.* **274**, 1 (1996).
-

- 
- [39] J. L. Lebowitz and J. K. Percus, *Phys. Rev* **144**, 251 (1966).
- [40] A. Lang *Dissertation TU-Wien 2001 (unpublished)*.
- [41] P. Bartlett, *J. Mol. Phys.* **97**, 685 (1999).
- [42] J. S. Hoye and G. Stell, *J. Chem. Phys.* **67**, 439 (1977).
- [43] R. J. Baxter, *Austral. J. Phys.* **21**, 563 (1968).
- [44] R. J. Baxter, *J. Chem. Phys.* **52**, 4559 (1970).
- [45] M. Cehn, *J. Math. Phys.* **16**, 1150 (1975).
- [46] G. Pastore, *J. Mol. Phys.* **63**, 731 (1988).
- [47] J. L. Lebowitz and J. S. Rowlinson, *J. Chem. Phys.* **41**, 133 (1964).
- [48] P. Solloich, P. B. Warren and M. E. Cates, *Adv. Chem. Phys.* **116**, 265 (2001).
- [49] G. R. Brannock, *J. Chem. Phys.* **95(1)**, 612 (1991).
- [50] R. T. DeHoff, *Thermodynamics in Materials Sciences (McGraw-Hill, New York)*, (1993).
- [51] J. A. Cuesta, *Europhys. Lett.* **46**, 197 (1999).
- [52] L. Bellier-Castella, M. Baus and H. Xu, *J. Chem. Phys.* (unpublished).
- [53] D. Gazzillo and A. Giacometti, *J. Chem. Phys.* **113**, 9837 (2000).
- [54] D. Pini, A. Parola and L. Reatto *J. Phys. Condens. Matter* (unpublished).
- [55] J. A. Gualtieri, J. M. Kincaid and G. Morrison, *J. Chem. Phys.* **77(1)**, 521 (1982).
- [56] W. H. Press, S. A. Teukolsky, W. T. Vetterling and B. P. Flannery *Numerical Recipes sec. Edition*
-



# Acknowledgment

This work was supported by the Österreichische Forschungsfond under the Project No. P11194-PHY and by the Fond zur Förderung der wissenschaftlichen Forschung (FWF) under the Project No. P14371-TPH. For the financial support during the last month of my work a thanks goes moreover to enterprise init.at.

During the last three years I was supported by many people and I want to express my thanks to them here. First of all I would like to thank Elisabeth Maria Schöll-Paschinger for many hints concerning the solution of mathematical problems and for fruitful discussions. A big thanks goes also to Christos Likos who instructed me to put the necessary emphasis on Physics in my phd. Further I want to thank my colleagues Dieter Gottwald and Hans Renezeder who are becoming very good friends of mine during the past years.

Beside this persons my work was only made possible by the following people: First of all by Gerhard Kahl, because he gave me the opportunity to work in his group and because he used all possible (legal) means to provide the necessary financial support to me. After all by my closest friends (including Hans and Dieter) and my family who gave me the strength and support which drives me through the last three years. My biggest thanks goes here to my parents and of course to my boyfriend Andreas who were accompanying me through the ups and downs of the last years.

In memory of my grandfather Josef Leroch (\*24.05.1923 †14.08.1985).



# Curriculum Vitae

- Personal:

- Name: Sabine Leroch
- Date of Birth: June 18th 1973
- Place of Birth: Vienna
- Address: Bendlgasse 24/3, 1120 Vienna, Austria

- Education:

- 4 years primary school (September 1979 - June 1983)
- 4 years secondary school (September 1983 - June 1987)
- 5 years economical high-school (HBLA) (September 1987 - June 1992)
- 12 terms Technical Physics at the Technical University of Vienna (October 1992 - September 1998)
- 3 years PhD at the Technical University of Vienna (October 1998 - March 2002)